THE ROLE OF SHANK3 AT THE SYNAPSE AND ITS IMPLICATIONS IN AUTISM-ASSOCIATED BEHAVIORS AND SYNAPTIC TRANSMISSION

APPROVED BY

Craig M. Powell, M.D., Ph.D. (Supervisor)

Adrian Rothenfluh, Ph.D.

Kimberly Huber, Ph.D.

James A. Bibb, Ph.D.

DEDICATION

First and foremost, I would like to thank my mentor, Dr. Craig M. Powell. Without his support and guidance, both personally and professionally, I would not have been able to accomplish this. I would also like thank the members of my Graduate Committee and Dr. Nancy Street for their invaluable advice throughout this journey. I would like to thank all past and present members of Powell lab, who have become my dearest friends, for their technical assistance and contributions to this work. I would also like to thank my husband, my sister and my brother in law for their love and support. Last but certainly not the least; I would love to thank my mother who has been a constant source of inspiration and motivation in my life.

THE ROLE OF SHANK3 AT THE SYNAPSE AND ITS IMPLICATIONS IN AUTISM-ASSOCIATED BEHAVIORS AND SYNAPTIC TRANSMISSION

by

MEHREEN KOUSER

DISSERTATION / THESIS

Presented to the Faculty of the Graduate School of Biomedical Sciences

The University of Texas Southwestern Medical Center at Dallas

In Partial Fulfillment of the Requirements

For the Degree of

DOCTOR OF PHILOSOPHY

The University of Texas Southwestern Medical Center at Dallas

Dallas, Texas

May, 2015

THE ROLE OF SHANK3 AT THE SYNAPSE AND ITS IMPLICATIONS IN AUTISM-ASSOCIATED BEHAVIORS AND SYNAPTIC TRANSMISSION

Mehreen Kouser, Ph.D.

The University of Texas Southwestern Medical Center at Dallas, 2015

Craig M. Powell, M.D., Ph.D.

Autism is a neurodevelopmental disorder characterized by an increase in repetitive behaviors and impairments in social interaction and communication. Since its discovery, a multitude of studies have linked *SHANK3* to autism. Moreover, deletion of *SHANK3* has been shown to cause Phelan McDermid Syndrome (22q13 Deletion Syndrome) by several human studies. Shank3 is a multi domain post-synaptic scaffolding proteins that is found in excitatory synapses and plays a critical role in forming the post-synaptic density by connecting the necessary machinery together.

In this study, I have characterized a homozygous *Shank3* mutation in mice that deletes exon 21(*Shank3*$^{\Delta C}$) including the Homer binding domain. In the homozygous state, deletion of exon 21 results in loss of the major, naturally occurring Shank3 protein bands. *Shank3*$^{\Delta C/\Delta C}$ mice exhibit an increased localization of mGluR5 to the synapses in the hippocampus, a decrease in NMDA/AMPA excitatory postsynaptic current ratio in area CA1 of hippocampus, reduced long-term potentiation in area CA1, and deficits in hippocampus-dependent spatial learning and memory. In addition, these mice also exhibit motor-coordination deficits, hypersensitivity to heat, novelty avoidance, altered locomotor response to novelty, and minimal social abnormalities.

I also report on a novel mouse model of human autism caused by the insertion of a single guanine nucleotide into exon 21 (*Shank3*^{G}*)* which causes a premature STOP codon and loss of major higher molecular weight Shank3 isoforms at the synapse like the *Shank3*$^{\Delta C/\Delta C}$ mice. *Shank3*$^{G/G}$ mice exhibit deficits in hippocampus-dependent spatial learning, impaired motor coordination, and altered response to novelty. *Shank3*$^{G/G}$ mice also exhibit impaired hippocampal excitatory transmission and plasticity.

Finally, *Shank3*$^{G/G}$ mice were designed to be genetically rescued to wild-type at various times during development. In this study, I also report on the biochemical and behavioral results of the genetic rescue in *Shank3*$^{G/G}$ mice after the completion of neurodevelopment. I was able to achieve a biochemical rescue in the *Shank3*$^{G/G}$ mice. Interestingly, not all the behavioral impairments observed in *Shank3*$^{G/G}$ mice were

replicated in the *Reversible-Shank3*$^{G/G}$ mutation mice making the interpretation of the data more challenging which is discussed in detail in this thesis.

TABLE OF CONTENTS

PRIOR PUBLICATIONS

Blundell, J., **Kouser, M.,** & Powell, C.M. (2008) Systemic Inhibition of Mammalian Target of Rapamycin Inhibits Fear Memory Reconsolidation. ***Neurobiology of Learning and Memory***, 90, 28-35.

Kouser, M., Speed, H.E., Dewey, C.M., Reimers, J.M., Widman, A.J., Gupta, N., Liu, S., Jaramillo, T.C., Bangash, M., Xiao, B., Worley, P., Powell, C.M. (2013) Loss of Predominant Shank3 Isoforms Results in Hippocampus-dependent Impairments in Behavior and Synaptic Transmission. ***Journal of Neuroscience*** *33*, 18448-18468

Speed, H.E., **Kouser, M.,** Xuan, Z., Reimers, J.M., Ochoa, C.F., Gupta, N., Liu, S., Powell, C.M. (2015) Autism-associated Insertion Mutation (InsG) of *Shank3* Exon 21 Causes Impaired Synaptic Transmission and Behavioral Deficits. ***Journal of Neuroscience*** (In Review)

LIST OF FIGURES

LIST OF TABLES

LIST OF DEFINITIONS

ADHD – Attention Deficit/Hyperactivity Disorder

AMPA – α-Amino-3-hydroxy-5-methyl-4-isoxazolepropionic acid

ANK – Ankyrin repeat domain

ANOVA – Analysis of variance

ASD – Autism Sprectrum Disorder

CNV – Copy number variant

DIC – Differential interference contrast microscopy

DNA – Deoxyribonucleic acid

DSM V – Diagnostic and Statistical Manual of Mental Disorders. Fifth Edition

EPSC – Excitatory postsynaptic current

GKAP - Guanylate kinase-associated protein

HBD – Homer binding domain

HOTAM – 4-Hydroxytamoxifen

I/O – Input/Output curves

LTD – Long term depression

LTP – Long term potentiation

mGluR – Metabotropic glutamate receptors

NMDA – N-methyl-D-aspartic acid

PCR – Polymerase chain reaction

PDD-NOS – Pervasive Developmental Disorder – Not Otherwise Specified

PDZ – Postsynaptic density protein/Drosophila disc large tumor suppressor/zonula occludens-1 protein (zo-1)

PMS – Phelan McDermid Syndrome

PPI – Paired pulse inhibition

PSD – Postsynaptic density

RNA – Ribonucleic Acid

SAM – Sterile alpha motif

SH3 – Src homology domain

TAM – Tamoxifen

CHAPTER ONE
Introduction

Autism Spectrum Disorders

Autism was first described clinically in a seminal case study of 11 children by an American physician Leo Kanner as "children's inability to relate themselves in the ordinary way to people and situations from the beginning of life" (Kanner, 1943). Since then there have been millions of children diagnosed with what Kanner called autism. Particularly in the past two decades the number of children diagnosed with autism spectrum disorders (ASD) have risen exponentially (Hansen et al., 2015), and it is currently estimated that 1 in 68 children will be diagnosed with ASD (Baio, 2014). This rise in observed prevalence of ASD can be attributed to increased awareness, well defined diagnostic criteria and better reporting practices (Hansen et al., 2015). According to the current prevalence estimates, more than 2 million individuals live with ASD in the US (Thurm and Swedo, 2012) and it is more prevalent in males vs. females compared to other neurodevelopmental disorders (Fombonne, 2005). It costs an estimated $2.4 to $1.4 million to support an individual with ASD during their life span in the United States alone (Buescher et al., 2014). This includes the special education services, parental productivity loss and medical costs during childhood and residential care, individual productivity loss and medical costs in the adulthood. In addition to the economic costs, ASD take a toll on the emotional well being of the families of the individuals with autism (Samadi et al., 2014; Wisessathorn et al., 2013). Therefore it is important to discover the etiology of

ASD and perhaps more importantly find clinically relevant treatments as there is no known cure for ASD.

The term "autism spectrum disorders" (ASD) was established to cover the phenotypic breadth and high variability in symptom presentation in this disorder. This spectrum encompasses autism, Asperger's disorder, and pervasive developmental disorder not otherwise specified (PDD-NOS). Additionally, ASD can be either idiopathic (unknown cause) or syndromic (associated with a known genetic syndrome) (Bishop et al., 2014). Syndromic forms of ASD include but are not limited to tuberous sclerosis complex disorder, fragile-X syndrome, Turner syndrome, neurofibromatosis, and 16p11.2 syndrome (Bishop et al., 2014). The symptoms for ASD typically become noticeable before the age of three and impact the normal development of the brain. Therefore it is considered a neurodevelopmental disorder and is mainly diagnosed behaviorally. According to the latest diagnostic criteria in DSM-V, ASD are characterized by an increase in repetitive behaviors, restricted interests and impairments in social interaction and communication. To add to the complexity, there are several comorbidities associated with ASD such as intellectual disability, motor incoordination, anxiety disorders, aberrant responses to sensory stimuli, sleep disorders, and seizures (Accardo and Malow, 2014; Kim et al., 2011; Moruzzi et al., 2011; Rogers and Ozonoff, 2005; Sappok et al., 2010; White et al., 2009b).

ASD are a very heterogeneous disorders as symptoms can vary greatly not only in the severity of the core diagnostic features but also in the combination of

comorbidities associated with ASD presented in a patient. The repetitive behaviors can range from simple motor stereotypies such as hand flapping to complex rituals and restricted interests (Bodfish et al., 2000; Lam et al., 2008). Impairments in social behavior and communication manifest as impaired eye-contact, facial expressions, complete lack of or unresponsiveness to verbal communication, or impaired responses to emotions (Grossman et al., 2013; Hazlett et al., 2009; Lord, 1995). Cognitive ability in ASD is also highly variable and can range from severe mental retardation to above average intelligence (Hazlett et al., 2009). Another source for heterogeneity in autism is the onset of symptoms. Symptoms of ASD may appear anytime from the first year to third year of life. (Palomo et al., 2006; Werner et al., 2000). Regression also introduces variability in ASD. Regression occurs when children may develop typically and acquire particular verbal and/or social skills but then lose it (Goldberg et al., 2003; Ozonoff et al., 2010).

Genetics Risk Factors of Autism Spectrum Disorders

Several twin and family studies have conclusively recognized ASD as highly heritable (Bailey et al., 1995; Folstein and Rutter, 1977; Lichtenstein et al., 2010; Taniai et al., 2008). These studies reveal the strong genetic basis of ASD by significantly increased pairwise concordance rates between monozygotic twins (80-92%) as compared to dizygotic twins (1-10%), and sibling recurrence risk of 6-20% and make it one of the most heritable of psychiatric disorders (Abrahams and Geschwind, 2008; Ey et al., 2011; Freitag, 2007; Toro et al., 2010). With the

advancement of high-throughput genetic research tools and well characterized patient cohorts, considerable breakthroughs have been made in identification of genetic risk factors for ASD and it is now well understood that ASD can be caused either by genetic mutations or by chromosomal aberrations (Murdoch and State, 2013; Pinto et al., 2010).

Genetic syndromes including but not limited to Fragile-X, tuberous sclerosis, Rett syndrome, neurofibromatosis with an identifiable genetic condition account for about 10% of individuals with ASD (Devlin and Scherer, 2012). Another review has identified more than a hundred genes and 44 genomic loci implicated in rare cases of ASD (Betancur, 2011). Using cytogenetic tools, chromosomal rearrangements have been in observed in approximately 5% of idiopathic cases of autism (Marshall et al., 2008). Three larger genome wide association studies (GWAS) have been conducted to find common genetic variants in ASD but no significantly consistent common variant has been reported (Devlin et al., 2011). Using microarray platforms, as many as 10% of ASD cases have been attributed to copy number variations (CNV) which may involve from one to several genes (Scherer and Dawson, 2011). A large number of genes have been identified in ASD as a result of CNV screening and direct sequencing of candidate genes (Devlin and Scherer, 2012). Key themes to emerge from these studies are that although rare mutations have been identified in ASD as a genetic risk factor, the effect sizes are very small and there is substantial overlap between syndromic and non-syndromic forms of ASD.

Despite of the fact that a large number of ASD risk genes remain unknown, two major biological mechanisms for ASD are emerging as points of convergence in this heterogeneous disorder. One pathway is the abnormal cellular and synaptic growth in ASD and the other is abnormal balance between inhibitory and excitatory currents in ASD (Bourgeron, 2009). Abnormal cellular and synaptic growth has been linked to ASD with the overgrowth of the brain in 10-30% of patients (Sacco et al., 2007). This has been observed in patients diagnosed with neurofibromatosis, tuberous sclerosis, and Cowden/Lhermitte-Duclos syndromes caused by tumor suppressor genes, *NF1, TSC1/TSC2,* and *PTEN,* respectively(Williams et al., 2008). These genes are negative regulators of the major regulator of the cell growth, rapamycin-sensitive mTOR-raptor complex (Kelleher and Bear, 2008). Thus mutations in these genes will increase mTOR activity, activating the phosphoinositede-3 kinase (PI3K) pathway which will cause an increase in protein synthesis at the synapse causing abnormal synaptic function (Kelleher and Bear, 2008).

The other point of convergence in ASD is the abnormal balance between inhibitory and excitatory currents in the brain. This inhibitory/excitatory balance theory was first supported by the observation of epilepsy in about 30-40% of patients diagnosed with ASD (Jensen, 2011). This was further confirmed by the discovery of mutations affecting cell adhesion molecules Neuroligin and Neurexins in individuals with ASD (Jamain et al., 2003; Kim et al., 2008). Along with these discoveries, an excitatory post-synaptic density scaffolding protein Shank3that binds to Neuroligins and is known to regulate the shape and size of dendritic spines, became implicated in

ASD (Durand et al., 2007; Roussignol et al., 2005). Also, Neuroligin and Neurexin are emerging as the organizing molecules for the excitatory and inhibitory synapses in the mammalian brain (Craig and Kang, 2007).

These findings suggest that there are core principles underlying the heterogeneity of ASD and they need to be further elucidated so that effective treatments can be developed to improve the quality of life of the individuals and families suffering from ASD.

Phelan-McDermid Syndrome, ASD, and *SHANK3*

Phelan-McDermid Syndrome (PMS) is caused by deletions or translocations in chromosome 22 and is also called 22q13 Deletion Syndrome. Symptoms of PMS include low muscle tone, moderate to profound intellectual disability, normal to accelerated growth, absent to severely delayed speech, and minor dysmorphic features (Phelan and Rogers, 1993; Verhoeven et al., 2012). About 80% of children diagnosed with PMS also exhibit autistic behavior and are diagnosed with ASD (Phelan and Rogers, 1993). In individuals affected with PMS, *SHANK3* deletions of varying sizes have been reported in all but one case (Boccuto et al., 2012; Bonaglia et al., 2001; Bonaglia et al., 2006; Dhar et al., 2010; Wilson et al., 2008; Wilson et al., 2003) (Table 1). In that particular case, the deletions were proximal to *SHANK3* but exon dosage or mutations in *SHANK3* were not tested (Wilson et al., 2008). Therefore we cannot conclusively say that *SHANK3* was unaffected. These studies strongly implicate *SHANK3* as a candidate gene in PMS.

Deletions and point mutations in *SHANK3* have also been linked to ASD by several studies (Boccuto et al., 2012; Durand et al., 2007; Gauthier et al., 2009; Moessner et al., 2007). In their study, Durand et al. (2007) report genetic analysis of three separate probands from three families. The first proband carried a breakpoint deletion in intron 8 of *SHANK3* which removed 142kb of the terminal 22q13. This patient was diagnosed with ASD, absent language and moderate mental retardation. In the second family, two brothers with severely impaired speech and mental retardation carried a heterozygous insertion of guanine nucleotide in exon 21 of *SHANK3*. This mutation was absent in the unaffected sibling or parents and was transmitted via *de novo* mutation on the maternal chromosome 22. In the third family, a girl with a terminal 22q deletion affecting 25 genes had ASD and severe language delay whereas her brother who carried a 22qter partial trisomy (duplication) affecting the same 25 genes had Asperger syndrome, precocious language development and fluent speech. In this case, the genetic abnormalities were inherited from a paternal translocation (Durand et al., 2007).

The next study to examine the role of *SHANK3* in ASD was conducted by Moessner et al. (2007). Through DNA sequencing they identified a *de novo* mutation in *SHANK3* in exon 8 of a girl which led to a heterozygous Q321R substitution. This mutation was absent in the parents, unaffected sibling and the 372 control chromosomes. She has narrow interests, verbal repetitive behaviors, establishes no eye contact, however she exceeds the autism cutoff in Autism Diagnostic Interview which is a test for ASD diagnosis. This group also conducted a copy number variant

(CNV) screen and found a ~277kb deletion including *MAPK8192, ARSA,* and *SHANK3* genes in a female proband. This deletion was absent in the parents and two unaffected brothers. The proband has ASD associated with severe intellectual disability. In another family, the female proband inherited an unbalanced translocation from the father, leading to a 3.2Mb heterozygous deletion including *SHANK3* of chromosome 22q13.31-33. Her sister has a partial trisomy of the same region and was diagnosed with attention-deficit/hyperactivity disorder (ADHD) suggesting a gene dosage dependent effect of *SHANK3.* Another male proband maternally inherited a 4.4Mb deletion including *SHANK3* and exhibits profound social impairment and no speech. Same deletion was also present in the affected sister (Moessner et al., 2007). Another group also sequenced the *SHANK3* gene and identified a *de novo* G-residue deletion at an intron 19 splice donor site (Gauthier et al., 2009). This mutation was not found in the proband's parents or any of the controls.

Boccuto et al. (2012) screened two cohorts of ASD patients for *SHANK3* mutations and found several potentially pathogenic alterations. They reported a *de novo* loss of 106kb on chromosome 22q13.33 encompassing the whole *SHANK3* gene. Along with ASD, this patient also had speech delay. They also found two frameshift alterations causing premature stop codons. The first frameshift mutation patient with c.3931delG had a diagnosis of pervasive developmental disorder not otherwise specified (PDD-NOS) and severe intellectual disability. Similarly, the other frameshift mutation case, the patient also had ASD and speech delay and carried a

c.13391340insG mutation. The mutation was inherited from the mother who also had speech delay.

After studying 1000 human patients, six different types of molecular defects have been documented in the *SHANK3* gene (Jiang and Ehlers, 2013). These are: 1) Cytogenetically visible terminal deletion of 22q13.3 or ring chromosome of 22 (Jeffries et al., 2005; Wilson et al., 2003), 2) a microdeletion which is not visible under a microscope and has to be detected by an array based method (Boccuto et al., 2012, 2013; Dhar et al., 2010), 3) microduplications (Okamoto et al., 2007), 4) translocations caused by rearrangement of parts with nonhomologous chromosomes with breakpoints in *SHANK3* gene (Bonaglia et al., 2006), 5) small intragenic deletions within the *SHANK3*gene (Bonaglia et al., 2011), and 6) point mutations (Boccuto et al., 2012; Durand et al., 2007; Moessner et al., 2007). Overall, these studies strongly implicate *SHANK3* gene in the neurological and behavioral features of ASD and PMS. Thus our understanding of the role of *SHANK3* in the brain and how disruptions in *SHANK3* function might be responsible for ASD and PMS is a critical piece of the puzzle in solving the mystery of this disorder.

Shank3 Function

Shank3 was discovered in yeast two-hybrid screens as a binding partner of guanylate kinase-associated protein (GKAP) and post synaptic density protein 95 (PSD-95) (Naisbitt et al., 1999). Shank3 along with Shank1 and Shank2 is a member of the shank/ProSAP family of postsynaptic scaffolding proteins enriched in

postsynaptic densities (PSDs). PSDs are a protein rich specialized zone on the post synaptic neuron. Shank3 binds to the machinery at the PSD through its several functional domains which include cytoskeletal proteins, ionotropic and metabotropic receptors, ion channels, signaling molecules, and scaffolding proteins (Grabrucker et al., 2011; Sheng and Kim, 2000)). Shank3 interacts with the PSD with its five functional domains which are an ankyrin repeat (ANK) domain, Src homology (SH3) domain, postsynaptic density protein/Drosophila disc large tumor suppressor/zonula occludens-1 protein (zo-1) (PDZ) domain, the homer binding domain (HBD) which is also a proline rich region, and a sterile alpha motif (SAM) domain (Figure 1.1). The ANK domain of shank3 mainly interacts with cytoskeletal proteins such as α-Fodrin and sharpin (Bockers et al., 2001; Lim et al., 1999). The SH3 domain helps mediate formation of protein complexes (Sheng and Kim, 2000). Its PDZ domain interacts with AMPA or NMDA receptors either directly or indirectly via GKAP and PSD-95 (Garner et al., 2000; Uchino et al., 2006). The HBD region of Shank3 binds to Homer which then binds to the group 1 metabotropic glutamate receptors such as mGluR1/5 (Tu et al., 1999). The HBD region also contains the binding site for F-actin associated cytoskeletal proteins named cortactin and Abp1 (Bockers et al., 2001; Naisbitt et al., 1999; Qualmann et al., 2004). The SAM domain is involved in self-multimerization of Shank3 with the help of Zn^{2+} binding (Boeckers et al., 2005; Naisbitt et al., 1999). These interactions make shank3 a critical part of the postsynaptic density.

Since Shank3 is found at the glutamatergic synapses and interacts with several PSD proteins, Roussignol et al. (2005) examined the role of Shank3 in synapse

formation and maturation in cultured neurons from mice. They found that over expression of Shank3 leads to recruitment of AMPA receptors, increase in synaptogenesis and maturation of spines. Consistently, mutation of the AMPA receptor interacting PDZ domain of Shank3 led to a decrease in synaptogenesis. Interestingly, they also report that the cortactin binding site of Shank3 controls retraction and head enlargement of spines whereas the ANK-SH3 domains only control spine head size (Roussignol et al., 2005). Knockdown of Shank3 expression using RNAi targeted towards exon 21 in rat neuronal cultures selectively reduced the synaptic expression of mGluR5 and impaired mGluR5 dependant signaling and plasticity (Verpelli et al., 2011). This knockdown of Shank3 also significantly reduced spine number and led to an increase in spine length and decrease spine width suggesting a shift towards more immature spines (Verpelli et al., 2011). These studies of *Shank3* mutations in spine formation and maturation signify the different functions of Shank3 domains at the synapses.

Another layer of complexity is added to studying the role of Shank3 at the synapse, when considering the various isoforms of Shank3 resulting from a complex transcriptional regulation of the gene and alternative splicing (Wang et al., 2011b). There have been five intragenic promoters identified in *Shank3* which taken along with the alternative splice variants lead to several mRNA and protein isoforms (Figure 1). Exact numbers of isoforms are not yet determined but Wang et al. (2011) identified Shank3 a-f isoforms and report that each isoform has a unique combination of different functional domains. Perhaps each isoform has its own specific function at

the synapse resulting in a unique biochemical and behavioral phenotype. Epigenetic mechanisms such as DNA methylation and histone deacetylation of the CpG islands found in *SHANK3,* also control Shank3 expression in an isoform specific manner (Beri et al., 2007). These findings make a strong case for isoform specific functions of Shank3 at the synapse and may contribute to the heterogeneity of molecular and behavioral phenotypes observed in patients carrying *SHANK3* deletions and mutations.

Shank3 Animal Models

In an attempt to study the role of each functional domain of *SHANK3, s*everal labs have made *Shank3* mouse models targeting different regions of the *SHANK3* gene (Bozdagi et al., 2010; Peca et al., 2011; Wang et al., 2011b; Yang et al., 2012). Detailed summary of the biochemical, synaptic, and behavioral phenotypes can be found in Table 2. These studies were critical in enhancing our understanding of the functions of the three targeted Shank3 domains. Bozdagi et al. (2010) and Yang et al. (2012) studied a novel mouse model made by Joe Buxbaum's group deleting exons$^{4-9}$ which affected the ANK domain of Shank3 (Buxbaum-Δexon$^{4-9}$). This mouse model resulted in loss of only the higher molecular weight isoforms of Shank3 by Westrern blot analysis. These mice exhibited increased self grooming behavior, decreased ultrasonic vocalizations, mild social interaction deficits and impaired novel object recognition (Bozdagi et al., 2010; Peca et al., 2011; Wang et al., 2011b; Yang et al., 2012). These mice showed deficits in basal synaptic transmission and plasticity in the

hippocampus (Bozdagi et al., 2010; Peca et al., 2011; Wang et al., 2011b; Yang et al., 2012). The same exons$^{4-9}$ region of *Shank3* affecting the ANK domain was also targeted by Yong Hui Jiang's group albeit in a different genetic background which may affect the observed phenotype (Jiang-Δexon$^{4-9}$) (Wang et al., 2011b). Like the Buxbaum-Δexon$^{4-9}$ mouse model, the Jiang-Δexon$^{4-9}$ mouse model exhibited loss of only the higher molecular weight isoform of Shank3. Behaviorally, these mice also exhibited increased self grooming behavior, impaired social interaction behavior, altered ultrasonic vocalizations, and impaired memory in Morris watermaze task. These mice also exhibited impaired synaptic plasticity but basal synaptic transmission was unaffected in the hippocampus of Jiang-Δexon$^{4-9}$ mice (Wang et al., 2011b).

Guoping Feng's group created two novel mouse models: one deleting exons$^{4-7}$(Feng-Δexon$^{4-7}$) affecting the ANK domain and the other deleting exons$^{13-16}$ (Feng-Δexon$^{13-16}$) affecting the PDZ domain. Deleting exons$^{4-7}$ also resulted in loss of only the higher molecular weight isoform of Shank3. These mice displayed impaired social novelty recognition and slight reduction in corticostriatal synaptic transmission. Feng-Δexon$^{13-16}$ mouse model affecting the PDZ domain led to the loss of two of the highest molecular weight isoforms of Shank3. These mice also have increased self grooming behavior and impairments in social interactions. Feng-Δexon$^{13-16}$ mice appear to have normal synaptic transmission in the hippocampus. Interestingly, these mice show do synaptic transmission deficits in the striatum (Peca et al., 2011). Despite the heterogeneity, there are certain commonalities such as increased grooming, social deficits, and synaptic transmission impairments among these mouse

models suggest that there may be shared underlying mechanisms that can be targeted for treatments.

My thesis focuses on mutations in the Homer binding domain (exon 21) of the *Shank3* gene that mimic a particular autism-associated mutation in the humans. This mutation is an insertion of guanine nucleotide in exon 21 causing a frameshift resulting in a premature stop codon that produces a truncated SHANK3 protein (Durand et al., 2007). This mutation is present in the child diagnosed with autism and not present in the unaffected siblings, suggesting an important role of mutations in Homer binding domain of *SHANK3*. Deletion of *Shank3* exon 21 in a mouse model *(Shank3*$^{\Delta C}$*)* and inserting the guanine nucleotide in exon 21 (*Shank3*^{G}), both result in loss of all major higher molecular weight isoforms of Shank3 in the homozygous state. This provides the best model to study the function of Shank3 protein so far as it results in the loss of most isoforms of Shank3 than any other mouse model. Behaviorally, these mouse models also show impairments in spatial memory, impairments in motor coordination, novelty avoidance, and impairments in hippocampal synaptic transmission and plasticity. We focused on the hippocampus physiology as both *Shank3*$^{\Delta C}$ and *Shank3*^{G} mice show deficits in spatial learning in the hippocampal dependent Morris watermaze task. Just as expected, both *Shank3*$^{\Delta C}$ and *Shank3*^{G} mice show significant impairment in hippocampus dependent synaptic transmission.

Another question addressed in this thesis is the neurodevelopmental basis of autism. *Shank3*^{G} is a mutant mouse model that can be genetically reversed to wild-

type using inducible or brain-region-specific cre-recombinase lines giving us temporal and spatial control over the mutation. A recent study has shown the feasibility of rescue of Rett Syndrome phenotype after neurodevelopment (Guy et al., 2007). Using the same principle, we were able to achieve biochemical rescue of the Shank3 protein. However, the rescue of behavioral phenotype observed in *Shank3*^{G} mice proved inconclusive which may signify persistence of the behavioral phenotypes observed in the *Shank3*^{G} mice.

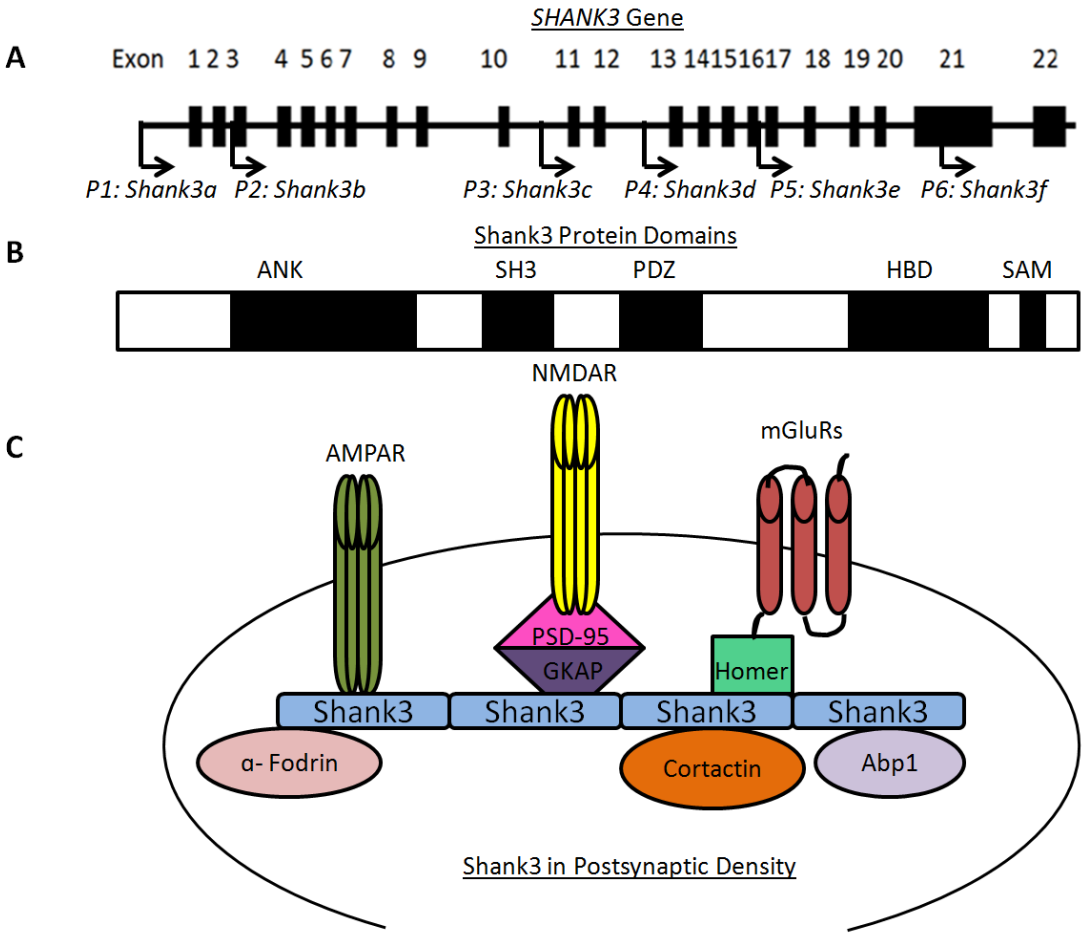

Figure 1.1: Schematic of *Shank3* Gene, Shank3 Protein and its Functional Domains A) *SHANK3* gene with the 6 promoters (P) shown by arrows and expected isoforms a -f. B) Functional domains of Shank3 protein. ANK: Ankyrin repeat domain, SH3: Src homology domain, PDZ: postsynaptic density protein/Drosophila disc large tumor suppressor/zonula occludens-1 protein (zo-1) domain, HBD: Homer binding domain also known as the Proline rich domain, and SAM: Sterile alpha motif domain. C) A schematic of Shank3 at the postsynaptic density.

Table 1: Genotype/Phenotype Correlation of Human *SHANK3* Mutations – Modified from (Jiang and Ehlers, 2013)

Genetic Defect		No. of Cases	SHANK3 Isoforms Affected	Other Genes Disrupted	ASD-Related Diagnosis	Intellectual Disability (ID)	Other Clinical Features
22q13.3 deletion (including SHANK3) (0.1-10Mb)		>1000	All isoforms disrupted	From 2-30 other genes	ASD diagnosis in >75% of cases	>95% cases with developmental delay, moderate to severe ID, absent speech, or severe speech delay	Hypotonia, seizure, motor development delay, facial dysmorphism, increased pain threshold, bipolar disorder, mild congenital anomaly
Microdeletion of SHANK3		3	All isoforms disrupted	None or /ACR	ASD	Speech delay and mild ID	Hyperactivity, hypospadias, behavioral issues, seizure/regression
Intragenic deletion							
Deletion size	Exons/domain deleted						

38 kb	exon 1–9 ANK	1	SHANK3a/b	none	Not mentioned	Moderate ID, profound delay in language acquisition	Microcephaly, astigmatism
74 kb	exon 1–17 ANK/SH3/PDZ	1	SHANK3a-e	none	Not evaluated	Profound ID	Mild congenital anomalies
44 kb	Exon 19–23 Homer binding/SAM	1	SHANK3f	ACR	ASD	Moderate ID/hyperactivity disorder	Short stature, facial dysmorphism, astigmatism
27 kb	exon 20–23 Homer binding/SAM	1	SHANK3f	ACRa	Classical autism	Not mentioned	ADHD, no facial dysmorphism
17 kb	Exon 23SAM	1	SHANK3f	ACR	No ASD	Mild ID, severe delay in language acquisition	Mild facial dysmorphism, mild motor delay
Point mutation/Small deletion							
Mutation	Exon/protein domain	1					

c.601-1G > A	ANK	1	SHANK3a-b	None	No ASD	Mild ID, severe language impairment	
p.Q312Rb	Exon 8ANK	1	SHANK3a-b	None	ASD	language delay	Abnormal EEG but no seizures; has self-injurious behavior
p.A447fsc	Exon 11SH3	1	SHANK3a-c	None	Borderline score for ASD evaluation	Language delay	No facial dysmorphism
p.G440_P446del	Exon 11SH3	1	SHANK3a-c	None	ASD	Severe ID	Delayed psychomotor development
c.1820-4G > A	PDZ	1	SHANK3a-d	None	Asperger's syndrome	Normal speech and some behavioral problems	Facial dysmorphism/mild congenital anomaly
p.R656Hd	Exon 16PDZ	1	SHANK3a-d	None	ASD	Mild ID, development delay	
c.2265+1 del G		1	SHANK3a-e	None	ASD	Not mentioned	

p.R1117X	Exon 21Homer binding	1	SHANK3f	None	No evidence for ASD	Mild to moderate ID	Schizophrenia, hyperactivity/no facial dysmorphism
p.A1227fs	Exon 21Homer-binding	1	SHANK3f	None	ASD	Severe ID and impaired speech	
p.E1311fs	Exon 21Homer-binding	1	SHANK3f	None	PDD-NOS	Severe ID and absent speech	Seizure, facial dysmorphism, motor development delay

Table 2: Biochemical, Synaptic, and Behavioral Summary of *Shank3* Mutant Mice. Modified from (Jiang and Ehlers, 2013)

Reference	**Bozdagi et al., 2010; Yang et al., 2012**	**Wang et al., 2011**	**Peça et al., 2011**	**Peça et al., 2011**	**Kouser et al., 2013**	**Speed et al (In Review)**
Exons/domain targeted	Exons 4–9B/ANK repeat (Δex4–9B)	Exons 4–9J/ANK repeat (Δex4–9J)	Exons 4–7/ANK repeat (Δex4–7)	Exons 13–16/PDZ (Δex13–16)	Exon 21/ HBD (ΔC)	Exon 21/ HBD (InsG)
Strain/background	Bruce4 C57BL/6 ES cell and maintain on C57BL/6	129SvEv ES cell backcrossing to C57BL/6J for more than 6 generations	129SvR1 ES cell and backcrossing to C57BL/6J for one generation	129 SvR1 ES cells and backcrossing to C57BL/6J for more than 1 generations	129 SvEv ES cells and backcrossing to C57BL/6J for more than 1 generations	129 SvEv ES cells and backcrossing to C57BL/6J for more than 4 generations
Age of mouse	Biochemistry: 3 months; Morphology: 3 months; Electrophysiology:3 months; Behaviors: P21 days to 16 weeks	Biochemistry: 3–4 months; Morphology: P1 neuron culture and 1–3 months; Electrophysiology: 4–6 weeks; Behaviors: 3–8 months	Biochemistry: not stated; Electrophysiology: 6–7 weeks; Behaviors: 5–6 weeks	Biochemistry: not stated; Morphology: 5 weeks; Electrophysiology: 5–7 weeks; Behaviors: 5–6 weeks	Biochemistry: 5-6 months; Morphology: 6-8 weeks; Electrophysiology: 13-16 days, 3-4weeks, 6-8 weeks; Behaviors: 2-6 months	Biochemistry: 5-6 months; Electrophysiology: 4-6 weeks; Behaviors: 2-6 months

Transcripts not disrupted	Shank3c,d,e, f	Shank3c,d,e,f	Shank3c,d,e,f	Shank3e, f		
Genotype of mice analyzed	Heterozygous/homozygous	Homozygous	Homozygous	Homozygous	Homozygous	Heterozygous/ Homozygous
Altered synaptic proteins	Reduction of GluA1	Reduction of GKAP, Homer1b/c, GluA1, GluN2A	N/A	Reduction of SAPAP3/GKAP3, Homer1, PSD-93, GluA2, GluN2A, GluN2B	Increased mGLuR5	No change
Brain and synaptic morphology	CA1 HippocampusActivity-dependent spine remodeling was affected,	CA1 HippocampusLonger dendritic spines.Decreased spine density.No change in length and thickness of PSD.	N/A	StriatumIncrease in striatal volume, dendritic length, and surface area.Decreased spine density, length, and thickness of PSD.	CA1 hippocampus - No defect identified.	N/A

Synaptic physiology	CA1 HippocampusReduced AMPAR-mediated basal transmission.Decreased mEPSC amplitude.Increased mEPSC frequency.Decrease in paired-pulse ratio.Reduced LTP.No change in NMDAR- or mGluR-mediated LTD.	CA1 Hippocampus No change in basal synaptic transmission.No change in amplitude or frequency of mEPSCs or mIPSCs.No change in paired-pulse ratio, I/O, fiber volley.Reduced LTP.	Striatum: Slight reduction in corticostriatal synaptic transmission.	CA1 Hippocampus: No change in field recordings of population spikes, paired-pulse ratio, mEPSC frequency and amplitude.StriatumNo change in paired-pulse ratio.Reduced field population spikes.Reduced mEPSC frequency and amplitude.	CA1 Hippocampus: No change in paired-pulse ratio, mEPSC amplitude, mGluR-LTD. Decrease in Input/Output Curves, LTP, mEPSC Frequency, NMDA/AMPA Ratio	CA1 Hippocampus: No change in paired-pulse ratio, mEPSC amplitude, LTP. Decrease in Input/Output Curves, mGluR-LTD, mEPSC Frequency, NMDA/AMPA Ratio

Social behaviors	Reduced social sniffing by males in male-female interactions, mild social impairment in reciprocal interactions in juveniles.Normal three chamber test for adult mice.	Reduced interest in novel mice in nonsocial versus novel social pairing in three chamber test, females performed better than males.Decreased bidirectional social interactions in dyadic test.	Normal initiation of social interaction. Perturbed recognition of social novelty during three chamber test.	Perturbed recognition of social novelty during three chamber test.Decreased reciprocal interactions in dyadic test.Decreased frequency of nose-to-nose interaction.Decreased anogenital sniffing.	Normal initiation of social interaction. Perturbed recognition of social novelty during three chamber test.	No change
USV calls	Reduced calls observed in some cohorts of adult mice during social interaction but no difference in newborn pups.	Males made more calls, while females made fewer calls.Altered frequency, complexity, and duration of calls.	Not mentioned	N/A	No change	No change

Repetitive behaviors	Increased self-grooming.Inflexible behavior in reversal of water maze observed in some cohorts.	Increased head pokes in hole-board test, increased self-grooming. Stereotypic object manipulation in novel object test.	No increase in self-injurious grooming.	Self-injurious grooming, causing skin lesions.	No change	No change
Learning and memory	Impaired novel object recognition. Normal Morris water maze, normal fear conditioning.	Impaired in acquisition and reversal in Morris water maze.Impaired short- and long-term memory	N/A	No difference observed in Morris water maze.	Impaired acquisition and recall in Morris Watermaze	Impaired acquisition in Morris Watermaze
Schizophrenia-related behaviors	Normal sensory gating and startle reflex.	No difference in PPI.Not hyperactive in the open field.	N/A	N/A	No change	No change

CHAPTER TWO
Results

Loss of Predominant Shank3 Isoforms Results in Hippocampus-dependent Impairments in Behavior and Synaptic Transmission

Previously Published: Kouser, M., Speed, H.E., Dewey, C.M., Reimers, J.M., Widman, A.J., Gupta, N., Liu, S., Jaramillo, T.C., Bangash, M., Xiao, B., Worley, P.F., Powell, C.M. (2013). Loss of predominant shank3 isoforms results in hippocampus-dependent impairments in behavior and synaptic transmission. J Neurosci *33*, 18448-18468.

Introduction

Autism is characterized by differences in three major behavioral domains: social behavior, language, and restricted and repetitive behaviors (Schreibman, 1988). Deletions and other loss-of-function mutations of the gene encoding the synaptic scaffolding protein shank3 have been strongly implicated in human autism (Boccuto et al., 2012; Durand et al., 2007; Gauthier et al., 2009; Moessner et al., 2007). Furthermore, there are hundreds of children with Phelan-McDermid Syndrome (22q13 Deletion Syndrome, intellectual disability with autism or autistic features) in which SHANK3 is strongly implicated in the autistic features and broader neurodevelopmental phenotype (Boccuto et al., 2012; Bonaglia et al., 2001; Bonaglia et al., 2006; Dhar et al., 2010; Wilson et al., 2003), making hemizygous *SHANK3* deletion the most common *SHANK3* mutation associated with autistic features. Thus, a complete understanding of SHANK3 function in the central nervous system is

critical to understand a subset of autism spectrum disorders caused by *SHANK3* deletion or mutation.

Shank3 is a member of the Shank family of postsynaptic scaffolding proteins enriched in postsynaptic densities (PSDs) and was discovered in yeast two-hybrid screens as a binding partner of guanylate kinase-associated protein (GKAP) and post synaptic density protein 95 (PSD-95) (Naisbitt et al., 1999). Shank3 binds to the integral machinery of post synaptic densities through its several functional domains. The ankyrin repeat domain of Shank3 mainly interacts with cytoskeletal proteins (Bockers et al., 2001). Its postsynaptic density protein/Drosophila disc large tumor suppressor/zonula occludens-1 protein (zo-1) (PDZ) domain interacts with ionotropic glutamate receptors either directly or indirectly via GKAP and PSD-95 (Garner et al., 2000; Uchino et al., 2006). The Homer binding domain of Shank3 binds to Homer which then binds to the group 1 metabotropic glutamate receptors such as mGluR1/5 (Tu et al., 1999).

Initial attempts to create mouse models lacking all Shank3 isoforms were unsuccessful, although they added important information of potential relevance to autism caused by *Shank3* mutations. Exon 4-9 or 4-7 deletion, coding for the ankyrin repeat domain, mouse models led to loss of only one of three major protein isoforms of Shank3 by Western blot analysis (Bozdagi et al., 2010; Peca et al., 2011; Wang et al., 2011b). A deletion model encompassing exons 13-16 (coding for the PDZ domain) led to loss of only two of the three major protein isoforms of Shank3 (Peca et al., 2011) using a single antibody.

Interestingly, an exon 21 deletion (coding for the homer binding domain) mouse model results in loss of the predominant naturally occurring isoforms of Shank3 in the homozygous state, providing the best model in which to understand the effects of loss of naturally occurring Shank3 isoforms. This exon 21 deletion mouse model is based on a particular autism-associated mutation in humans that involves a guanine nucleotide insertion in exon 21 creating a frameshift and premature stop codon near the Homer binding domain. In the hemizygous state (*Shank3*$^{+/\Delta C}$) this model results in only partial loss of the major, naturally occurring Shank3 proteins (not shown). However in the homozygous state (*Shank3*$^{\Delta C/\Delta C}$), this model results in loss of major naturally occurring isoforms of Shank3 detected by N-terminal and C-terminal antibodies. Therefore, we believe that the homozygous mutation will be more informative of the function of Shank3 even though only hemizygous mutation in exon 21 of the *Shank3* gene has been linked to autism. This is the first such model in which we can understand the effects of loss of major naturally occurring Shank3 isoforms. In this study, we examine the biochemical, behavioral, and electrophysiological consequences of homozygous loss of major naturally occurring Shank3 isoforms in the exon 21 deletion mouse model. We find that *Shank3*$^{\Delta C/\Delta C}$ mice show deficits in spatial learning and memory, motor coordination, sensitivity to sensory stimuli, and responses to novelty. To begin to understand the underlying mechanisms of these deficits we examine synaptic physiology in area CA1 of the hippocampus of these mice and find impairments in hippocampal synaptic transmission and plasticity. These findings highlight the importance of Shank3 in

normal synaptic function and behavior and provide further evidence of potential treatment targets for autism and intellectual disability associated with *Shank3* deletion/mutation.

Methods*:*

Generation of Shank3$^{\Delta C/\Delta C}$ *mice:*

The *Shank3* targeting construct was designed to delete exon 21 with Cre-mediated excision. To "flox" exon 21, *Shank3* BAC DNA clone (Geneservice, UK) was modified using standard recombineering technology (Liu P et al., 2003). The final targeting construct had two homology arms of 6.0 and 1.7 kb, respectively. To identify targeted ES cells by PCR screen, a PCR control vector was constructed, which retains the Neo-cassette and the short homology arm present in the targeting vector and additional *Shank3* genomic sequence contiguous to the short arm. The targeting construct was electroporated into ES cells (129 s6 SvEv Tac background) and ES clones were selected for G418 resistance. The ES clones with targeted homologous recombination were identified by PCR with two sets of primers (forward: 50-TCGCCTTCTTGACGAGTTCT; reverse: 50-ACACGCTTTGGACACTTCTC). The authenticity of desired homologous recombination in the ES clones was confirmed by sequencing the PCR products. The positive ES clones were then injected into blastocysts (C57/BL6 strain) to generate chimera at the Transgenic Facility of Johns Hopkins University School of Medicine. The chimeric mice were bred with C57/BL6 mice to confirm germline transmission

of floxed *shank3*, which was identified by PCR with primers as follows: Forward: 50-ACTTCGTATAATGTATGCTATACGAAG; Reverse: 50-GGCCATTGAATGGCTTCTCTGG. The floxed *shank3* mice were then mated with mice expressing actin-cre to excise exon 21. The resulting progeny were genotyped using a combination of three primers. The primer sequences were as follows: 50-TCCTGTGTCCCCTCATTGATGTT, 50-CTCTGCCACCTTCTGCCTACAAA, 50-TGTCCTGTTGCAGGTAGGGAGAG). After confirming excision, the *Shank3* $^{+/\Delta C}$ mice were mated with WT C57/BL6 mice to cross-out the cre allele and the progeny were further backcrossed with C57/BL6 mice for at least 5 generations. All mice tested were sex-matched, littermate progeny of matings between heterozygous *Shank3* mutant mice. Overall, the *Shank3*$^{\Delta C/\Delta C}$ mutant mice appeared healthy except for their smaller body weight (see Table 3).

Western Blot:

Synaptic protein levels from 7 pairs (WT/ *Shank3*$^{\Delta C/\Delta C}$, 5-6 months old) were determined by immunoblotting whole hippocampal tissue homogenized in artificial cerebrospinal fluid, 5mM EDTA, and 1X Halt protease and phosphatase inhibitor cocktail (Thermo Scientific) diluted from 100X stock solution. 10µg protein were loaded per lane and blotted with antibodies for synaptic proteins and internal loading controls (β-actin). An Image Works film processor was used to develop films and the chemiluminescence signals were quantified, normalized, and statistically analyzed using ImageJ, Image Studio and Microsoft Excel.

Synaptosome Preparation

All steps were performed at 4 C° or on ice; all buffers contained protease and phosphatase inhibitors (Thermo Scientific). Mice were sacrificed by live decapitation and rapidly dissected hippocampi were homogenized in Syn-Per (Thermo Scientific), ~1 mL/100 mg tissue. Samples were centrifuged at 1,200 x g for 10 min. The resulting supernatant was then centrifuged at 15,000 x g for 20 min. Pellets (synaptosomes) were resuspended in buffer B (3 mM sucrose in 6 mM Tris pH 8.0) with 1% SDS, briefly sonicated and flash frozen in liquid nitrogen. Samples were stored long-term at -80° and quantified by DC Protein Assay (Bio-Rad).

PSDII preparation

Synaptosome pellets were isolated as described above, resuspended in 1 mL Buffer B and homogenized. Homogenates were overlayed on sucrose density gradients,1.15 M, 1 M, and 0.85 M sucrose and centrifuged at 82,500 x g. The fraction between 1.15 M and 1 M sucrose layer was isolated, resuspended inBuffer C (6 mM Tris, pH 8.0, 1% TritonX-100) and incubated for 15 minutes before centrifugation at 32,800 x g for 20 minutes. The pellets were resuspended in Buffer D (6 mM Tris, pH 8.0, 0.5% TritonX-100), and incubated for 15 minutes. After centrifugation for 1 hr at 201,800 x g, the resulting pellets (PSD-II) were resuspended in a minimal volume of Buffer D and flash frozen in liquid nitrogen.

Behavioral Overview:

Behavioral tests were performed on a cohort of 9 female and 10 male, age- and sex-matched littermate pairs (N=19 WT and N=19 homozygous mutant) during the light cycle of the mice. All mice were born within 10 weeks of each other. Behaviors were tested at 2-6 months of age by an experimenter blind to genotype in the following order: elevated plus maze, dark/light, open field, locomotor, grooming, 3 box social interaction test, marble burying, rotorod, social interaction with a juvenile, nesting behavior, Morris water maze, visible water maze, paired-pulse inhibition, startle threshold, footshock sensitivity, hot plate sensitivity. One littermate pair was excluded from the analysis of elevated plus maze and social interaction with a juvenile as one littermate jumped out of the apparatus. Similarly, two littermate pairs were excluded from the 3 box social interaction test as the mice climbed out and started circling the outer edge of the apparatus. Also, one mouse was found dead in its home cage in the morning after nesting behavior was done so its littermate pair was also excluded from the study after nesting behavior. The ultrasonic vocalizations emitted by male with a free roaming estrous female were recorded in 8 male, age and sex-matched littermate pairs with at 10-13 months of age. One male mouse was found dead the next day so its littermate pair was also excluded from future behaviors. Afterwards, grooming behavior was repeated in the same cohort of 7 male and an addition of 9 female littermate pairs (N=16 WT and N=16 homozygous mutant). Behavioral results are described out of the order they were tested in to ease the interpretation of the data. All statistical analysis of behavioral data were

conducted using Statistica software (Version 5.5, Statsoft) using either two-way ANOVAs or three-way repeated measures ANOVA using genotype and sex as the main variables and trial as the repeated measure where applicable. Post-hoc planned comparisons were applied for significant effects and interactions. For detailed information and numerical statistical results see Table 3.

Morris Water Maze

The Morris water maze task was conducted essentially as previously described (Powell et al., 2004; Tabuchi et al., 2007). Briefly, a white, circular pool 1.2 m in diameter was filled with water ($22^{o}C \pm 1^{o}C$) made opaque with non-toxic, "gothic white" liquid tempera paint, and a circular platform (10 cm in diameter) was submerged ~1 cm beneath the surface of the water. The testing room was well lit and filled with a number of extra-maze cues. Training was conducted over 9 consecutive days, 4 trials/day with an inter-trial interval of 1-1.5 min. Mice were placed pseudo-randomly into each of 4 starting locations for each of 4 daily training trials. In each trial, mice swam until they found the hidden platform or were guided to it by the experimenter if not found within 60 s. Mice remained on the platform for 15 s before being removed to home cage. Daily data were averaged across the 4 trials. A probe trial was conducted on day 10; the hidden platform was removed, and mice were placed in the pool and allowed to swim for 60 seconds. For reversal water maze training, training resumed the next day following the probe trial for 5 days with the platform in the opposite quadrant of the maze; on the sixth day, a second probe trial

was administered. Data were analyzed using three-way repeated measures ANOVA with genotype and sex as between-subject factors and trial days as a within-subject factor for training. For probe trials, quadrant or platform location was used as the within-subject factor.

Accelerating Rotarod:

Coordination and motor learning were tested using a rotarod essentially as previously described (Powell et al., 2004). Mice were placed on a stationary rotarod in a well lit room (IITC Life Sciences) which was then activated and accelerated from 0-45 revolutions per min over 5 min. The latency for mice to fall off the rod or take one revolution was measured. Trials were repeated 4 times with inter-trial intervals of 30 min over a single day. Data were analyzed using three-way repeated measures ANOVA with genotype and sex as between-subject factors and trials as a within-subject factor.

Hot Plate Sensitivity:

This test was performed as described (Blundell et al., 2010a; Powell et al., 2004). Mice were placed on a black, anodized plate which was held at a constant temperature of 52^{o}C (IITC Model 39 Hot Plate) covered with a Plexiglas enclosure. Mice were removed after the first hind-paw lick or after 30 s if no response was elicited. The plate was cleaned with water between mice and allowed to return to

temperature. Data were analyzed using two-way ANOVA with genotype and sex as between-subject factors.

Nesting:

Nesting behavior was performed in a well-lit (~80 lux) room by first habituating the mouse to a novel home cage with approximately 1.5 cm of bedding for 15 min, and then a cotton nestlet (5.5 x5.5 x 0.5 cm) was put in the cage. Height and Width of the nests were measured at 30 min, 60 min and 90 min (Etherton et al., 2009). Data were analyzed using two-way ANOVA with genotype and sex as between-subject factors.

Marble Burying:

As previously described (Blundell et al., 2010a), twenty marbles were evenly placed around the edges of a novel home cage with 5 cm of bedding and mice were given 30 min in the cage. After 30 min the number of marbles buried was recorded. A marble was defined as buried when less than 25%of the marble was visible. The test room was well lit (~80 lux). Data were analyzed using two-way ANOVA with genotype and sex as between-subject factors.

Dark-Light:

Dark/light test was performed as described previously (Powell et al., 2004). Briefly, the dark/light apparatus consisted of two chambers (each chamber 25 cm x 26

cm), one brightly lit (~1700 lux) and the other kept dark with a small door (7 x 7 cm) separating the two. Mice were habituated for two min in the dark side, the door was opened, and then mice were allowed to move freely between the two sides for 10 min. Time spent in and the number of entries into each side was measured along with locomotor activity using photobeams monitored by Med PC IV data acquisition software. Data were analyzed using two-way ANOVA with genotype and sex as between-subject factors.

Elevated Plus Maze:

Mice were placed in the center of a white Plexiglas elevated plus maze (each arm 33 cm long and 5 cm wide with 15 cm high black Plexiglas walls on closed arms) and allowed to explore for 5 min (Powell et al., 2004). The test was conducted in dim white light (~7 lux). Mice were monitored using CleverSys TopScan Software and time spent in and entries into the open and closed arms were measured. Data were analyzed using two-way ANOVA with genotype and sex as between-subject factors.

Open Field:

The open field test was performed as described (Blundell et al., 2009; Powell et al., 2004) with the exception of the data acquisition software. Mice were monitored using CleverSys TopScan Software after being placed in a white plastic arena (48x48x48cm) for 10 min. Time spent in and number of entries into the center of the arena (15 x15 cm) as well as locomotor activity. The test was conducted in dim white

light (~7 lux). Data were analyzed using two-way ANOVA with genotype and sex as between-subject factors.

Locomotor:

Locomotor activity was tested by placing the mice in a fresh home cage with minimal bedding and monitoring their activity for two hours using photobeams linked to a computer data acquisition software (San Diego Instruments) (Powell et al., 2004). The test was conducted in the dark. Three-way repeated measures ANOVA was used to analyze the data with genotype and sex as between-subject factors and time as a within-subject factor.

Three Chambered Social Approach:

Social vs. inanimate object preference and preference for social novelty analyses were performed in a three chambered box with small openings connecting the chambers as described (Blundell et al., 2009) and based to a large extent on the original descriptions (Moy et al., 2004; Nadler et al., 2004) . The test was conducted in dim white light (~7 lux). The mouse behavior was monitored using CleverSys TopScan Software. This test consisted of three 10 min trials. During the first trial, the mouse was allowed to explore the entire apparatus with empty cages in each end chamber. In the second trial, the mouse was given a choice between an inanimate cage or a caged, social target. For the third trial, the mouse was given a choice between a caged, novel social target vs. a caged, familiar social target. Locations of

empty cages and social targets were counterbalanced., and mice were placed back into their home cage for very brief intervals between trials. Data were analyzed using three-way mixed ANOVA with genotype and sex as between-subject factors and target as a within-subject factor.

Social Learning:

Social learning was performed as described (Kwon et al., 2006). Mice were first habituated to a dimly lit testing room (~7 lux) for 20 minutes. After the habituation period, an experimental adult mouse and a juvenile were placed together in a fresh home cage with no bedding. Time spent interacting with the juvenile was recorded live by an observer blind to genotype for 2 minutes. After three days, the above procedure was repeated to assess social learning. Data were analyzed using three-way mixed ANOVA with genotype and sex as between-subject factors and test session as a within-subject factor.

Prepulse Inhibition and Startle:

As previously described (Blundell et al., 2010b), startle chambers (San Diego Instruments) were modified for mice and mounted atop a piezoelectric accelerometer that detected and transduced animal movements. Acoustic stimuli were delivered by high-frequency speakers mounted 33 cm above the cylinders. Animal movements were digitized and stored using computer software supplied by San Diego Instruments. From the onset of startle stimuli, 65, 1 ms readings were recorded, and

the amplitude of the startle responses was obtained in arbitrary units. Chambers were calibrated before each set of mice, and sound levels were monitored using a sound meter (Tandy). For pre-pulse inhibition, mice were subjected to five trial types in a 22 min session: pulse alone (40 ms, 120 dB, white noise pulse), three different prepulse/pulse trials (20 ms prepulse of 4, 8, or 16 dB above background noise level of 70 dB preceded the 120 dB pulse by 100 ms onset-onset interval), and no stimulus. All trials were presented pseudo-randomly with an average of 15 s (7–23 s) between the 62 trials. Testing began with a 5 min acclimation to the cylinders followed by four blocks of test trials. The first and last blocks consisted of six, pulse-alone trials. Blocks 2 and 3 each contained six pulse-alone trials, five of each level of prepulse/pulse trials, and five no -stimulus trials. Data were analyzed for baseline startle amplitude (initial pulse-alone trials) and prepulse inhibition (percentage decrease in startle amplitude for prepulse/pulse trials compared to pulse-alone trials).
For the Startle reactivity test, 8 presentations of 6 trial types were given in a pseudorandom order: No stimulus, 80, 90, 100, 110 or 120 dB pulses. Mean startle amplitudes for each condition were calculated. Data were analyzed using three-way mixed ANOVA with genotype and sex as between-subject factors and trial as a within-subject factor.

Grooming:

Mice were placed in a novel homecage without the bedding and time spent grooming the face, head, or body was measured for 10 minutes. Number of grooming

bouts that lasted more than 1 second were also recorded. Time per bout was calculated by dividing the total time spent grooming by the number of grooming bouts initiated. Each grooming parameter described above was then analyzed using a two-way ANOVA with genotype and sex as between-subject factors.

Ultrasonic Vocalization:

The male adult mouse was placed in a sound-attenuated (11.5x11.5x11.5 in) chamber with a estrous female mouse and allowed to freely interact for five minutes while recording (Scattoni et al., 2010). The chamber was cleaned between trials. The Ultrasound Microphone (Avisoft UltraSoundGate condenser microphone CM16/CMPA, Avisoft Bioacoustics, Berlin, Germany) was set up to record from a range of 10-200 kHz. The microphone was placed about 5 inches above the floor through a hole in the back wall of the chamber. The recording software was set at default settings with a 250 kHz sampling rate, 16 bit format with a 32 millisecond buffer. In order to analyze the calls the sound file is then converted to a spectrogram using the Avisoft-SASLab Pro software. To reduce background noise, 25 kHz was set as a lower cutoff frequency. The analysis involved only counting of calls and finding latency to first call. Data were analyzed using one-way ANOVA with genotype as a between subject factor.

Electrophysiology:

Male mice were briefly anesthetized with isoflurane (Baxter Healthcare Corporation, Deerfield, IL) and rapidly decapitated. Brains were quickly removed and submerged in ice-cold modified ACSF containing in (mM): 75 sucrose, 87 NaCl, 3 KCl, 1.25 NaH_2PO_4, 7 $MgSO_4$, 26 $NaHCO_3$, 20 dextrose, and 0.5 $CaCl_2$. Acute hippocampal slices 350-400 µm thick were made using a vibrating microtome (Vibratome, Bannockburn, IL). A cut was made between CA3 and CA1 to reduce recurrent excitation of CA3 neurons. Slices were allowed to recover at 33°C for 30 min in normal ACSF containing (in mM) 124 NaCl, 5 KCl, 1.25 NaH_2PO_4, 1 $MgCl_2$, 26 $NaHCO_3$, 10 dextrose, and 2 $CaCl_2$, and slowly cooled to room temperature over a 45-min period prior to recording. All solutions were pH 7.4 and saturated with 95% O_2/5% CO_2.

All recordings were performed at 33 ± 0.5°C, and all data were collected using Clampex (pClamp software suite version 10.2; Molecular Devices, Sunnyvale, CA). Recordings were filtered at 1 kHz and digitized at 10 kHz. CA3-CA1 synapses were stimulated by a 100 µs biphasic pulse through a monopolar tungsten microelectrode (FHC, Bowdoin, ME) placed 400–500 µm laterally from the recording electrode. The distance between the recording electrode and the stimulating electrode was kept constant within these bounds. For extracellular electrophysiology the recording electrode (1–3 MΩ) was filled with normal ACSF and placed in the *stratum radiatium* using a SZX7 dissecting microscope (Olympus, Center Valley, PA) at 35X magnification. For whole-cell electrophysiology, the recording electrode (4-6 MΩ) contained (in mM): 110 CsMethanesulfonate, 15 CsCl, 8 NaCl, 10 TEA-Cl,

2 EGTA, 10 HEPES, 3 QX 314, 2 ATP, 0.3 GTP. CA1 neurons were visually selected under 80X magnification using an AxioExaminer D1 Differential Interference Contrast (DIC) microscope (Zeiss, Thornwood, New York).

The majority of experiments were performed on male mice postnatal days 13-16, except long-term plasticity (LTP and mGluR-LTD) experiments which were evaluated in young adult male mice (3-4 or 6-8 weeks, as noted). Sample size for extracellular field recordings (I/O curve, paired-pulse ratio, long-term plasticity) represents number of slices tested with 1-2 slices used per mouse. Response size was determined by fitting a straight line to the initial slope (10–40%) of the fEPSP using automated analysis in Clampfit (pClamp software suite version 10.2; Molecular Devices). For studies of long-term potentiation (LTP) and paired-pulse ratio, stimulus intensity was set to generate approximately 50% of the maximum fEPSP, as determined by the input/output (I/O) curve. Stimulus intensity was set at 75-85% of the maximum fEPSP for mGluR-LTD experiments. I/O curves were performed in each slice immediately preceding each field recording, and stimulus intensity remained unchanged thereafter for the duration of the experiment.

Whole-cell patch clamp recordings were carried out in the presence of 100 μM picrotoxin to block fast inhibitory transmission, and began 5-10 min (NMDA/AMPA ratio) or 10-15 min (mEPSCs) following successful break-in. NMDA/AMPA ratio was measured at 0.1 Hz and elicited no short-term plasticity. For primarily AMPAR-mediated EPSCs, holding potential was -70 mV and peak amplitude was measured 10-15 ms following stimulus onset. For primarily NMDAR-

mediated EPSCs, holding potential was +40 mV and peak amplitude was measured 40-45 ms after stimulus onset. mEPSCs were recorded for five min at a holding potential of -65 mV in the presence of 1 μM TTX to block evoked transmission. Recordings were rejected if holding current or series resistance varied more than 25 % during the recording. Sample size indicates total number of cells from no less than four mice per group. Raw data were analyzed using Clampfit (pClamp software suite version 10.2; Molecular Devices, Sunnyvale, CA). GraphPad Prism was used for statistical analysis and graphing. Means are expressed as Mean ± standard error of the mean.

Histology:

For histological studies, brains were dissected from 6-8 week old mice and processed for Golgi-Cox staining with the FD Rapid GolgiStain Kit (FD Neurotechnologies, Ellicot City, MD). Following live decapitation, brains were quickly removed and rinsed in double-distilled water and then immersed into impregnation solution which was then replaced with fresh impregnation solution after 24 hours and stored in the dark at room temperature (22-25°C). After two weeks, the brains were transferred to solution C and then shipped to FD NeuroTechnologies within 48 hours. Serial 100 μm cryostat sections were cut coronally through the cerebrum containing the hippocampus and mounted on glass slides. Twenty CA1 neurons from the dorsal hippocampus were selected from 5 mice per genotype (WT and *Shank3*$^{\Delta C/\Delta C}$). Neurons were traced using NeuroLucida 3D neuron tracing

software (MicroBrightField Bioscience, Williston, VT) at X100 magnification by an experimenter blind to experimental conditions. Sholl analysis was conducted using NeuroLucida 3D software to study the branching by drawing concentric circles 30µm apart starting at 30µm from the center of the cell body. For spine density experiments, 30µm apical dendrite segments that did not have any interfering crossings were chosen at the defined distances from the cell body (0-30, 30-60, 60-90 and 90-120). Data from the 4 neurons from each mouse was averaged together before statistical analysis. Data were analyzed using two-way mixed ANOVA with genotype as between-subject factor and distance from the cell body as a within-subject factor.

Drugs:

Octahydro-12-(hydroxymethyl)-2-imino-5,9:7,10a-dimethano-10aH[1,3]dioxocino[6,5-d]pyrimidine-4,7,10,11,12-pentolTetrodotoxin (TTX, Tetrodotoxin), picrotoxin, *N*-(2,6-Dimethylphenylcarbamoylmethyl)triethylammonium chloride (QX 314), and (*RS*)-3,5-Dihydroxyphenylglycine (DHPG) were obtained from Tocris Bioscience (Minneapolis, MN). CsMethanesulfonate and CsCl were obtained from Sigma-Aldrich (St. Louis, MO). All other reagents were obtained from Fisher Scientific (Waltham, MA).

Results

Homozygous Shank3 *Mutation Results in Loss of Major Shank3 Isoforms*

To quantify the loss of Shank3 in *Shank3*$^{\Delta C/\Delta C}$ mice compared to wild-type (WT) littermate controls, we performed quantitative Western blot analysis using antibodies directed against Shank 3 C-terminus (C'), N-terminus (N') and the SH3 domain (SH3) on hippocampal lysates of 5-6 month old mice (N=7). Western blot analysis revealed that *Shank3*$^{\Delta C/\Delta C}$ mice have lost major Shank3 isoforms detected by the C-terminal, SH3 domain, and N-terminal antibodies (Figure 2.1A, Shank3(C'): $t(12) = 11.418$, $P < 0.0001$; Shank3(SH3): $t(12) = 8.524$, $P < 0.0001$; Shank3(N'): $t(12) = 5.244$, $P < 0.001$). Interestingly, however, we also observe the appearance of lower molecular weight (< 100 kD) isoforms of Shank3 detected by the SH3 domain and the N-terminal antibody in *Shank3*$^{\Delta C/\Delta C}$ hippocampus that are not substantially present in the WT controls (Figure 2.1B, Shank3(SH3 band 1): $t(12) = 8.199$, $P < 0.0001$; Shank3(SH3 band 2): $t(12) = 5.818$, $P < 0.0001$; Shank3(N' band 1): $t(12) = 11.303$, $P < 0.0001$; Shank3(N' band 2): $t(12) = 5.494$, $P < 0.001$).

In addition to Shank3, we also probed for Shank1, Shank2 and multiple other post synaptic density proteins and receptors that are either directly or indirectly linked to Shank3 to identify any compensatory effects of loss of Shank3 in hippocampal lysates. We did not observe any changes in levels of any postsynaptic density proteins or synaptic receptors in whole hippocampal homogenates (Figure 2.1D and E).

Homozygous Shank3 *Mutants Exhibit Increased mGluR5 in Synaptic Fractions*

In order to determine the effects of a complete loss of Shank3 on the subcellular distribution of synaptic proteins we isolated the synaptosome and post-

synaptic density (PSDII) fractions of the hippocampus of *Shank3*$^{\Delta C/\Delta C}$ mice compared to WT littermate controls following established methods with modifications (Cohen et al., 1977)**.** As in the whole hippocampal lysates, we found dramatic loss of all three Shank3 isoforms in both the synaptosome (Figure 2.2A, Shank3(N'): $t(12) = 5.514$, $P < 0.001$; Shank3(C'): $t(12) = 7.929$, $P < 0.001$; Shank3(SH3): $t(12) = 11.552$, $P < 0.001$) and the PSDII (Figure 2.2C, Shank3(N'): $t(4) = 9.82$, $P < 0.001$; Shank3(C'): $t(4) = 3.575$, $P = 0.023$) fractions. We also detected the presence of lower molecular weight (<100 kD) isoforms of Shank3 in the synaptosome (Figure 2.2B, Shank3(N' band 1): $t(12) = 5.417$, $P < 0.001$; Shank3(N' band 2): $t(12) = 2.81256$, $P = 0.016$) and PSDII (Figure 2.2D, Shank3(N' band 1): $t(4) = 6.594$, $P = 0.003$; Shank3(N' band 2): $t(4) = 4.114$, $P = 0.015$) fractions of the hippocampus of *Shank3*$^{\Delta C/\Delta C}$ mice using the N-terminal antibody, suggesting that these lower molecular weight isoforms are present at hippocampal synapses.

In addition to Shank3, we analyzed the levels of synaptic proteins and receptors that are either directly or indirectly bound to Shank3 in the hippocampus. Strikingly, a significant increase in mGluR5 was seen in the synaptosome fraction (Figure 2.2A, $t(12) = 5.867$, $P<0.001$) and to and even greater extent in the PSDII fraction (Figure 2.2C, $t(4) = 5.465$, $P = 0.005$), suggesting enhanced mGluR5 localization to hippocampal synapses. We found no significant differences in ionotropic glutamate receptor subunits (NMDA or AMPA) or in other scaffolding and linker proteins (Figure 2.2A & C) in the hippocampus of *Shank3*$^{\Delta C/\Delta C}$ mice.

Homozygous Shank3 *Mutants Are Impaired in Spatial Learning*

Because 40-50 % of autism patients exhibit intellectual disability (Wingate M, 2012) and a majority of patients with *SHANK3* mutation/deletion exhibit some degree of intellectual disability (Gong et al., 2012), we tested the *Shank3*$^{\Delta C/\Delta C}$ mice in the Morris water maze task, a test of spatial learning and memory. *Shank3*$^{\Delta C/\Delta C}$ mice were significantly impaired in spatial learning compared to WT littermate controls using latency to reach the hidden platform as a measure (Figure 2.3A, 3-way rmANOVA; Main effect of Genotype: $F_{1,32}$=13.55, P<0.001; Main effect of Day: $F_{7,224}$=36.47, P<0.000001; Genotype x Day Interaction: $F_{7,224}$=2.54, P<0.05; see table 3 for complete statistical results for all experiments). Even though the *Shank3*$^{\Delta C/\Delta C}$ females had significantly higher swim speed during training (See table 3), the increased latency to reach the hidden platform in *Shank3*$^{\Delta C/\Delta C}$ mice was not accounted for by overall differences in swim speed during training (Figure 2.3B, 3-way rmANOVA; Main effect of Genotype: $F_{1,32}$=0.5, P=0.48; Main effect of Day: $F_{7,224}$=2.00, P=0.05; Genotype x Day Interaction: $F_{7,224}$=0.92, P=0.48). Not surprisingly, *Shank3*$^{\Delta C/\Delta C}$ mice also exhibited significantly decreased learning using distance travelled to reach the platform, a measure that eliminates swim speed as a confound (Figure 2.3C, 3-way rmANOVA; Main effect of Genotype: $F_{1,32}$=17.41, P<0.001; Main effect of Day: $F_{7,224}$=41.61, P<0.000001; Genotype x Day Interaction: $F_{7,224}$=3.25, P<0.005). On the initial trials, *Shank3*$^{\Delta C/\Delta C}$ and WT littermates spent the same amount of time in thigmotaxis (swimming near the maze walls). As the WT mice learned, they progressed to alternative search strategies while the *Shank3*$^{\Delta C/\Delta C}$ mice were slower to

shift to alternative search strategies from the initial thigmotaxic strategy (Figure 2.3D, 3-way rmANOVA; Main effect of Genotype: $F_{1,32}$=7.62, P<0.01; Main effect of Day: $F_{7,224}$=75.09, P<0.000001; Genotype x Day Interaction: $F_{7,224}$=2.41, P<0.05). These findings are consistent with a significant decrease in spatial learning in the *Shank3*$^{\Delta C/\Delta C}$ mice.

Although *Shank3*$^{\Delta C/\Delta C}$ mice were slower to learn the water maze task, their spatial memory performance was only somewhat affected during the initial probe trial. Both WT and *Shank3*$^{\Delta C/\Delta C}$ mice showed a significant preference for the target quadrant compared to all 3 other quadrants (Figure 2.3E, 3-way rmANOVA; Main effect of Genotype: $F_{1,32}$=0.22, P=0.63; Main effect of Quadrant: $F_{3,96}$=33.49, P<0.000001; Genotype x Quadrant Interaction: $F_{3,96}$=4.21, P<0.01; Planned Comparsons for WT mice: TargetNW vs. RightNE: P<0.00001; TargetNW vs. LeftSW: P<0.00001; TargetNW vs. OppositeSE: P<0.00001; Planned Comparisons for *Shank3*$^{\Delta C/\Delta C}$ mice: TargetNW vs. RightNE: P<0.02; TargetNW vs. LeftSW: P<0.02; TargetNW vs. OppositeSE: P<0.0001), indicating that both groups were able to recall a previously learned spatial strategy. There was, however, a significant decrease in the percent time *Shank3*$^{\Delta C/\Delta C}$ mice spent in the target quadrant and a significant increase in the percent time spent in the opposite quadrant compared to WT littermates (Planned Comparisons WT vs *Shank3*$^{\Delta C/\Delta C}$ mice. : Target NW Quad: P<0.01; Opposite SE Quad: P<0.01) suggesting that *Shank3*$^{\Delta C/\Delta C}$ mutants may not have learned as efficient a spatial strategy as their WT littermate counterparts. To examine this further, we analyzed the number of times the mice crossed the exact

target platform location and corresponding locations in the other 3 quadrants. Using this measure, only the WT group demonstrated a significant preference for the target platform location compared to the 3 other corresponding locations (Figure 2.3F, 3-way rmANOVA; Main effect of Genotype: $F_{1,32}$=0.01, P=0.91; Main effect of Quadrant: $F_{3,96}$=13.00, P<0.000001; Genotype x Quadrant Interaction: $F_{3,96}$=2.13, P=0.10; Planned Comparsons for WT mice: TargetNW vs. RightNE: P<0.001; TargetNW vs. LeftSW: P<0.01; TargetNW vs. OppositeSE: P<0.0001; Planned Compairsons for *Shank3*$^{\Delta C/\Delta C}$ mice: TargetNW vs. RightNE: P=0.08; TargetNW vs. LeftSW: P=0.08; TargetNW vs. OppositeSE: P=0.052). Further analysis suggested that the inability to show a preference for target platform can be attributed to the *Shank3*$^{\Delta C/\Delta C}$ mutant males as during the probe trial they show a decrease in number of platform location crosses, decrease in average swim speed and overall distance travelled (See Table 1).Taken together, these data suggest that *Shank3*$^{\Delta C/\Delta C}$ mice are slower to learn a spatial strategy in the water maze compared to WT littermate controls.

To examine for both cognitive flexibility (Ozonoff and Jensen, 1999) and insistence on sameness (Greaves et al., 2006; Richler et al., 2007; Schreibman, 1988), we performed a reversal learning experiment using the water maze, identifying further evidence of significantly decreased spatial memory in *Shank3*$^{\Delta C/\Delta C}$ mice. The day following the first probe trial, mice were trained for 5 additional days with the hidden platform in the opposite quadrant. Interestingly, *Shank3*$^{\Delta C/\Delta C}$ mice showed no difference in acquisition of the reversal task using latency to reach the platform

(Figure 2.3G, 3-way rmANOVA; Main effect of Genotype: $F_{1,32}$=2.63, P=0.11; Main effect of Day: $F_{4,128}$=8.05, P<0.0009; Genotype x Day Interaction: $F_{4,128}$=1.69, P=0.15). Likewise, no differences were observed in swim speed (Figure 2.3H, 3-way rmANOVA; Main effect of Genotype: $F_{1,32}$=0.006, P=0.93; Main effect of Day: $F_{4,128}$=1.08, P=0.36; Sex x Genotype Interaction: $F_{1,32}$=3.05, P=0.09; Genotype x Day Interaction: $F_{4,128}$=0.68, P=0.60), distance travelled to reach the platform (Figure 2.3I, 3-way rmANOVA; Main effect of Genotype: $F_{1,32}$=2.08, P=0.15; Main effect of Day: $F_{4,128}$=4.99, P<0.0009; Genotype x Day Interaction: $F_{4,128}$=2.64, P<0.05;), or the time spent in thigmotaxis (Figure 2.3J, 3-way rmANOVA; Main effect of Genotype: $F_{1,32}$=2.29, P=0.13; Main effect of Day: $F_{4,128}$=1.50, P=0.20; Genotype x Day Interaction: $F_{4,128}$=0.57, P=0.68). On the probe trial, however, *Shank3*$^{\Delta C/\Delta C}$ mice failed to show any preference for the new target location, while WT littermates showed a clear preference for the target quadrant compared to all other quadrants (Figure 2.3K, 3-way rmANOVA; Main effect of Genotype: $F_{1,32}$=0.83, P=0.36; Main effect of Quadrant: $F_{3,96}$=5.87, P<0.01; Genotype x Quadrant Interaction: $F_{3,96}$=6.51, P<0.001; Planned Comparisons for WT mice: TargetSE vs. RightNE: P<0.001; TargetSE vs. LeftSW: P<0.001; TargetSE vs. OppositeNW: P<0.0001; Planned Comparisons for *Shank3*$^{\Delta C/\Delta C}$ mice: TargetSE vs. RightNE: P=0.55; TargetSE vs. LeftSW: P=0.32 ; TargetSE vs. OppositeNW: P=0.60). Decreased spatial memory in the reversal learning task was confirmed using number of platform location crossings as a measure with WT littermates demonstrating a clear preference for the target location over all other locations and the *Shank3*$^{\Delta C/\Delta C}$ mice showing no preference (Figure 2.3L;

3-way rmANOVA; Main effect of Genotype: $F_{1,32}$=6.11, P<0.02; Main effect of Quadrant: $F_{3,96}$=4.93, P<0.01; Genotype x Quadrant Interaction: $F_{3,96}$=1.98, P=0.12; Planned Comparisons for WT mice: TargetSE vs. RightNE: P<0.05; TargetSE vs. LeftSW: P<0.01; TargetSE vs. OppositeNW: P<0.01; Planned Comparisons for *Shank3*$^{\Delta C/\Delta C}$ mice: TargetSE vs. RightNE: P=0.66; TargetSE vs. LeftSW: P=0.20; TargetSE vs. OppositeNW: P=0.68). These data are consistent with decreased spatial learning and memory and may or may not represent additional difficulties with cognitive flexibility or behavioral inflexibility. In order to test basic visual function and comprehension of the task, we measured latency and distance travelled to reach a visible cue atop the platform in the watermaze pool. No significant differences were observed but there was a trend towards increased latency and distance travelled to reach the visible cue. See Table 3 for detailed results.

Homozygous Shank3 *Mutants Have Impaired Motor Coordination*

Shank3$^{\Delta C/\Delta C}$ mice exhibit impaired coordination on the accelerating rotarod. *Shank3*$^{\Delta C/\Delta C}$ mice had consistently decreased latencies to fall from the rotarod apparatus, although they demonstrated the same rate of motor learning indicated by improvement in their ability over subsequent trials (Figure 2.4A, 3-way rmANOVA; Main effect of Sex: $F_{1,34}$=7.17,P<0.02; Main effect of Genotype: $F_{1,34}$=6.95, P<0.02; Main effect of Trial: F(7,238)=11.71, P<0.000001; Sex x Genotype Interaction: $F_{1,34}$=0.45, P=0.50; Sex x Trial Interaction: $F_{7,238}$=0.51, P=0.82; Genotype x Trial: $F_{7,238}$=1.60, P=0.13; Sex x Genotype x Trial Interaction: $F_{7,238}$=1.88, P=0.07).

Interestingly, in addition to the main effect of genotype, there was also a gender difference in performance that appeared to be due to the WT females as they were able to stay on the rotarod longer than the WT males (Planned Comparisons: Females, wt vs. *Shank3*$^{\Delta C/\Delta C}$: $P<0.05$; Males, wt vs. *Shank3*$^{\Delta C/\Delta C}$: $P=0.162$; WT, males vs. females: $P<0.05$; *Shank3*$^{\Delta C/\Delta C}$,males vs. females: $P=0.164$).

Shank3 *Mutant Mice Are Hypersensitive in the Hotplate Task*

Some patients with Phelan-McDermid Syndrome or 22q13 Deletion Syndrome are anecdotally said to have increased pain tolerance. We therefore tested the sensitivity of *Shank3*$^{\Delta C/\Delta C}$ mice to pain by testing the latency to lick the hind the paw on the hotplate task and found that it was decreased suggesting a hypersensitivity to heat (Figure 2.4B, 2-way ANOVA; Main effect of Genotype: $F_{1,32}=4.38$, $P<0.05$).

Shank3 *Mutant Mice Exhibit an Avoidance Phenotype Towards Inanimate Objects*

In attempts to measure nest building, marble burying, and in other tasks, we uncovered an interesting avoidance of inanimate objects in the *Shank3*$^{\Delta C/\Delta C}$ mice. When we measured nest building by adding a nestlet to a novel cage following a habituation period, we found that *Shank3*$^{\Delta C/\Delta C}$ mice showed essentially no change in their nestlets while WT littermates readily made nests from the material (Figure 2.4C, 3-way rmANOVA; Main effect of Genotype: $F_{1,34}=17.06$, $P<0.001$; Main effect of Time: $F_{2,68}=7.60$, $P<0.01$; Genotype x Time Interaction: $F_{2,68}=6.00$, $P<0.004$). At first, we interpreted this as deficient nest-building, but later tasks revealed a potential

alternative explanation. Surprisingly similar avoidance behavior was observed in the marble burying task. *Shank3*$^{\Delta C/\Delta C}$ mice showed little to no interest in burying marbles (Figure 2.4D, 2-way ANOVA; Main effect of Genotype: $F_{1,34}$=58.20, P<0.000001). In many instances it appeared as though *Shank3*$^{\Delta C/\Delta C}$ mice did not even touch or walk over the marbles as they appeared completely undisturbed. A related phenotype was observed in the 3-chamber social interaction task wherein the *Shank3*$^{\Delta C/\Delta C}$ mice interacted significantly less with the inanimate object than WT littermate controls (see Figure 2.5B).

We also tested *Shank3*$^{\Delta C/\Delta C}$ mice in anxiety behaviors and found that these mice show a remarkable increase in avoidance of the brightly lit chamber in the dark/light task. *Shank3*$^{\Delta C/\Delta C}$ mice spent almost the entire 10 minutes of this task in the dark chamber, virtually completely avoiding the brightly lit chamber (Figure 2.4E, Time spent in dark side, 2-way ANOVA; Main effect of Genotype: $F_{1,34}$=29.06, P<0.00006; Time spent in light side, 2-way ANOVA; Main effect of Genotype: $F_{1,34}$=29.06, P<0.00006). This avoidance behavior is also evident by the increased latency to enter the brightly lit side of the box (Figure 2.4F, 2-way ANOVA; Main effect of Genotype: $F_{1,34}$=21.08, P<0.00006). Such behavior in this task is typically interpreted as an increase in anxiety-like behavior. To differentiate between increased anxiety-like behavior versus avoidance behavior we tested *Shank3*$^{\Delta C/\Delta C}$ mice in two other standard tests for anxiety, elevated plus maze and open field. We did not observe an increase in anxiety-related behavior in the elevated plus maze as *Shank3*$^{\Delta C/\Delta C}$ mice and their WT littermate counterparts spent equal time in the open

arms (Figure 2.4G, 2-way ANOVA; Main effect of Genotype: $F_{1,32}$=0.12, P=0.73). Similarly, no anxiety-like phenotype was observed in the open field task as the *Shank3*$^{\Delta C/\Delta C}$ mice spent the same amount of time in the center as their WT littermates (Figure 2.4H, 2-way ANOVA; Main effect of Genotype: $F_{1,34}$=0.003, P=0.95). Thus, it appears that *Shank3*$^{\Delta C/\Delta C}$ mice do not have an anxiety phenotype but demonstrate avoidance behavior in multiple tasks including avoiding the brightly lit chamber in the dark/light box test.

Shank3 *Mutant Mice Exhibit Aberrant Locomotor Activity in Response to Novelty*

Curiously, in some tasks, but not others, *Shank3*$^{\Delta C/\Delta C}$ mice demonstrated decreased locomotor activity that can be interpreted as a transiently decreased locomotor response to novel situations. At first glance when examining locomotor activity over 2 hours in a novel home cage, *Shank3*$^{\Delta C/\Delta C}$ mice demonstrated completely normal locomotor activity (Figure 2.4I, 3-way rmANOVA; Main effect of Genotype: $F_{1,34}$=0.49, P=0.48; Main effect of Trial: $F_{7,782}$=41.30, P<0.000001; Genotype x Trial: $F_{7,782}$=1.21, P=0.22). For the first 5 min in this novel home cage situation, however, the *Shank3*$^{\Delta C/\Delta C}$ mice showed a significant decrease in locomotor activity that reverted to the WT level rapidly thereafter (Figure 4J, 2-way ANOVA; Main effect of Genotype: $F_{1,34}$=4.43, P<0.05). Along the same lines, distance travelled in the novel open field arena over 10 min was decreased in *Shank3*$^{\Delta C/\Delta C}$ mice (Figure 2.4K, 2-way ANOVA; Main effect of Genotype: $F_{1,34}$=23.54, P<0.00003), and total number of

photobeams interrupted during the 10 min in the dark/light chamber was decreased in *Shank3*$^{\Delta C/\Delta C}$ mice (Figure 2.4L, 2-way ANOVA; Main effect of Genotype: $F_{1,34}$=35.60, P<0.000002). We interpret these data overall as a decrease in locomotor response to novel environments that reverts rapidly to WT levels.

Shank3 *Mutant Mice Exhibit Minimal Social Interaction Deficits*

Social interaction deficits are one of the three characteristic features of autism (Mahjouri and Lord, 2012; Schreibman, 1988). Therefore we tested social behaviors in *Shank3*$^{\Delta C/\Delta C}$ mice in two separate tasks. Much like their WT littermate pairs, *Shank3*$^{\Delta C/\Delta C}$ mice showed no a priori preference for either side in the three chambered social interaction box prior to introduction of a social target (Figure 2.5A, 3-way rmANOVA: Main effect of Genotype: $F_{1,30}$=1.23, P=0.27; Main effect of Target: $F_{1,30}$=0.01, P=0.90; Genotype x Target Interaction: $F_{1,30}$=0.06, P=0.80). Similarly, in the test for social vs. inanimate preference, both wildtype and *Shank3*$^{\Delta C/\Delta C}$ spent more time interacting with the social target (Figure 2.5B, 3-way rmANOVA: Main effect of Genotype: $F_{1,30}$=2.95, P=0.09; Main effect of Target: $F_{1,30}$=20.81, P<0.0001; Genotype x Target Interaction: $F_{1,30}$=0.36, P=0.54; Planned Comparisons-social vs. Inanimate-WT, P<0.01; *Shank3*$^{\Delta C\square\Delta C}$, P<0.001). However, in the test of preference for social novelty vs. familiarity, *Shank3*$^{\Delta C/\Delta C}$ mice showed no preference for social novelty unlike their WT littermate pairs (Figure 2.5C, 3-way rmANOVA: Main effect of Genotype: $F_{1,30}$=0.56, P=0.45; Main effect of Target: $F_{1,30}$=4.16, P=0.05; Genotype x Target Interaction: $F_{1,30}$=1.68, P=0.20; Planned Comparisons for WT mice: social

vs. inanimate P<0.05; Planned Comparisons for *Shank3*$^{\Delta C/\Delta C}$ mice: social vs. inanimate P=0.23).

No differences were observed in either social interaction or social learning during reciprocal social interaction with a juvenile (Figure 2.5D, 3-way rmANOVA; Main effect of Genotype: $F_{1,32}$=0.502, P=0.48; Main effect of Trial: $F_{1,32}$=138.76, P<0.000001; Genotype x Trial Interaction: $F_{1,32}$=3.88, P=0.05; Planned Comparisons-initial vs. recognition-WT, P<0.00001; *Shank3*$^{\Delta C\square\Delta C}$,P<0.00001).

Shank3 *Mutant Mice Exhibit Normal Startle Response and Pre-pulse Inhibition*

SHANK3 and other autism genes are implicated in schizophrenia (Burbach and van der Zwaag, 2009; Gauthier et al., 2010; Gauthier et al., 2009; Verpelli et al., 2012). Thus, we tested *Shank3*$^{\Delta C/\Delta C}$ mice for pre-pulse inhibition (PPI) deficits and auditory startle responses. We observed no differences in the auditory startle response at the tested sound levels (Figure 2.5E, 3-way rmANOVA; Main effect of Genotype: $F_{1,32}$=0.008, P=0.92; Main effect of Trial: $F_{5,160}$=34.95, P<0.0001; Genotype x Decibel Interaction: $F_{5,160}$=0.03, P=0.99). Similarly, there was no difference in PPI between the WT and *Shank3*$^{\Delta C/\Delta C}$ mice (Figure 2.5F, 3-way rmANOVA; Main effect of Genotype: $F_{1,34}$=3.06, P=0.08; Main effect of Trial: $F_{2,64}$=54.86, P<0.0001; Genotype x Trial Interaction: $F_{2,64}$=0.20, P=0.81). We did find an interaction between Sex and genotype and upon further analysis uncovered that the *Shank3*$^{\Delta C/\Delta C}$ female mice show less pre-pulse inhibition than *Shank3*$^{\Delta C/\Delta C}$ males or WT females (See Table 3).

Shank3 *Mutant Mice Develop Grooming Deficits With Age*

We characterized grooming behavior in *Shank3*$^{\Delta C/\Delta C}$, as a measure of the repetitive, stereotyped behavior core symptom domain of autism. When tested at a younger age (9-18 weeks old), *Shank3*$^{\Delta C/\Delta C}$ mice do not exhibit an increase in total time spent grooming (Figure 2.5G, 2-way ANOVA; Main effect of Genotype: $F_{1,34}$=0.36, P=0.54). Similarly no difference was observed in the time spent per grooming bout (Figure 2.5H, 2-way ANOVA; Main effect of Genotype: $F_{1,34}$=0.44, P=0.50). However, when grooming was tested in older mice (10-13 months old), *Shank3*$^{\Delta C/\Delta C}$ mutants exhibited a significant increase in grooming when compared to WT (Figure 2.5I, 2-way ANOVA; Main effect of Genotype: $F_{1,28}$=4.69, P<0.04). The older *Shank3*$^{\Delta C/\Delta C}$ mutants also showed an increase in time spent per grooming bout (Figure 2.5J, 2-way ANOVA; Main effect of Genotype: $F_{1,28}$=6.00, P<0.03). It is worth mentioning that this significant difference is found due to a decrease in grooming behavior in WT mice as they age whereas it persists in the *Shank3*$^{\Delta C/\Delta C}$ mutants

Shank3 *Mutant Mice Do Not Exhibit Communication Deficits*

Communication deficits are also a hallmark of autism. In order to test communication, *Shank3*$^{\Delta C/\Delta C}$ mutant males were allowed to mate with free roaming females and their ultrasonic vocalizations were recorded. No differences were

observed in the latency to emit the first call or the total number of calls emitted in a 5 minute duration. See Table 1 for results.

Shank3 *Mutant Mice Are Impaired in Hippocampal Synaptic Transmission and Plasticity*

Because *Shank3*$^{\Delta C/\Delta C}$ mice exhibited significant deficits in hippocampus-dependent spatial learning, we examined long-term synaptic plasticity in the hippocampus. Extracellular "field" recordings made in the CA3-CA1 region of the hippocampus revealed a deficit in long-term plasticity (Figure 2.6) that is consistent with the spatial learning deficits in *Shank3*$^{\Delta C/\Delta C}$ mice. Long-term potentiation (LTP) was significantly impaired in *Shank3*$^{\Delta C/\Delta C}$ mice compared to WT mice at 55-60 minutes following a 100Hz, 1s conditioning stimulus (Figure 2.6A, WT: 127.2 ± 3.64 %, N = 8 vs. *Shank3*$^{\Delta C/\Delta C}$: 112.1 ± 4.08 %, N = 6; t (12) = 2.753, P = 0.018).

Shank3 also binds indirectly to Group 1 metabotropic glutamate receptors (mGluRs) through interactions with Homer at the C-terminus proline rich region (Tu et al., 1999). Specifically, Shank3 has been shown to regulate mGluR5 signaling in hippocampal neuronal cultures, and knockdown of Shank3 in cultured neurons causes a decrease in mGluR5 signaling and mEPSC frequency (Verpelli et al., 2011). In our *Shank3*$^{\Delta C/\Delta C}$ homozygous mice, however, we identified a significant increase in mGluR5 in synaptosome and PSDII fractions (Figure 2.2A & C).

To determine whether mGluR5 signaling is altered in *Shank3*$^{\Delta C/\Delta C}$ mice, we induced mGluR-LTD first using a five-minute bath application of the Group I mGluR

agonist DHPG (100 μM) in 6 - 8 week old mice. DHPG was used no more than ten days after stock was prepared, and LTD experiments were carried out with the experimenter blind to genotype and in an interleaved fashion (alternating WT and mutant experiments) with no more than 2 slices per mouse. At 55-60 minutes after washout began (Figure 2.6B), we found that modest LTD was induced in WT mice (90.36 ± 5.73 %, N = 9) and in *Shank3*$^{\Delta C/\Delta C}$ mice (80.24 ± 5.84 %, N = 7), but no difference in % LTD between WT and *Shank3*$^{\Delta C/\Delta C}$ mice was observed (t (18) = 0.996, P = 0.243). To optimize expression of mGluR-LTD, we repeated the experiment in 3-4 week old mice with a 10 minute bath application of DHPG (Figure 2.6C). With a larger sample size and doubling of DHPG application time, we again found no difference in mGluR-LTD between *Shank3*$^{\Delta C/\Delta C}$ mice and WT controls (WT 87.38 ± 4.14 %, N = 9 vs. *Shank3*$^{\Delta C/\Delta C}$ 78.67 ± 7.12 %, N = 11; t (14) = 1.219, P = 0.332).

Since long-term plasticity is dependent on proper function of glutamatergic AMPA and NMDA receptors, and because Shank3 is known to interact indirectly with both types of receptors (Arons et al., 2012; Naisbitt et al., 1999; Uchino et al., 2006), we hypothesized that the relative contributions of AMPA and NMDA receptors to the excitatory postsynaptic current (EPSC) would be altered in *Shank3*$^{\Delta C/\Delta C}$ mice. As predicted, there was a significant decrease in NMDA/AMPA ratio in *Shank3*$^{\Delta C/\Delta C}$ compared to WT mice (Figure 2.7A, WT: 0.91 ± 0.12, N = 22 vs. *Shank3*$^{\Delta C/\Delta C}$: 0.62 ± 0.06, N = 25; t (45) = 2.129, P = 0.039).

In an effort to determine whether the decreased NMDA/AMPA ratio was due to decreased NMDA receptor-mediated synaptic transmission or to increased AMPA receptor-mediated transmission, we examined the amplitude of spontaneous, miniature excitatory postsynaptic currents (mEPSCs) that largely reflect AMPA receptor-mediated responses at individual synapses. Consistent with the NMDA/AMPA ratio decrease being due to decreased NMDA receptor-mediated responses, cumulative frequency of mEPSC amplitudes was not different in *Shank3*$^{\Delta C/\Delta C}$ mice compared to WT (Figure 2.7B, Kolmagorov-Smirnov two-sample test, $P > 0.1$). Similarly, mean mEPSC amplitude was not affected by Shank3 deletion (Figure 2.7C, WT: -9.74 ± 1.19 pA, N = 15 vs. *Shank3*$^{\Delta C \square \Delta C}$: -9.19 ± 0.97 pA, N = 22; $t(35) = 0.364$, $P = 0.718$).

The frequency of miniature EPSCs, however, was significantly decreased in *Shank3*$^{\Delta C/\Delta C}$ mice compared to WT (Figure 2.7D, WT: 1.16 ± 0.11 Hz, N = 15 vs. *Shank3*$^{\Delta C/\Delta C}$: 0.74 ± 0.09 Hz, N = 22; $t(35) = 2.971$, $P = 0.005$). A decrease in mEPSC frequency can be due to a decrease in presynaptic evoked release probability (P_r), decreased synapse number, decreased synaptic release sites, or a selective decrease in spontaneous release probability. To distinguish among these possibilities, we examined both paired pulse ratios (PPR) and baseline synaptic strength via input/output curves. Alterations in PPR often accompany changes in presynaptic release probability (Lauri et al., 2007; Regehr, 2012; Zucker and Regehr, 2002), but we identified no changes in PPR using a broad range of interstimulus intervals (50 - 500 ms) in *Shank3*$^{\Delta C/\Delta C}$ mice compared to WT littermate controls (Figure 2.7E, 2-

Way rmANOVA: Genotype: $F_{1,107} = 0.748$, P = 0.389; Interstimulus Interval: $F_{5,107} = 29.43$, P <0.0001; Genotype X Interstimulus Interval: $F_{5,107} = 0.254$, P = 0.937; WT N = 10, *Shank3*$^{\Delta C/\Delta C}$ N = 10). This finding is consistent with there being no change in evoked synaptic P_r.

The input/output relationship of stimulus intensity to slope of the field excitatory postsynaptic potential (fEPSP), was decreased in *Shank3*$^{\Delta C/\Delta C}$ mice (Figure 2.7F, 2-Way rmANOVA: Genotype: $F_{1,18} = 8.969$, P = 0.008; Intensity: $F_{10,180} = 93.93$, P < 0.0001; Intensity X Genotype: $F_{10,180} = 6.155$, P <0.0001; WT N = 10, *Shank3*$^{\Delta C/\Delta C}$ N = 10). Bonferroni multiple comparisons indicate significant differences between WT and *Shank3*$^{\Delta C/\Delta C}$ mice at stimulus intensities greater than 50 μA, with a maximum fEPSP slope 36.9% greater in WT compared to *Shank3*$^{\Delta C/\Delta C}$ mice (WT: -0.34 ± 0.04 mV/ms; *Shank3*$^{\Delta C/\Delta C}$: -0.22 ± 0.03 mV/ms; Bonferoni multiple comparisons, P < 0.0001). No difference was found between WT and *Shank3*$^{\Delta C/\Delta C}$ mice in the relationship between stimulus intensity and fiber volley amplitude (inset) suggesting no change in presynaptic axonal excitability (2-Way rmANOVA: Intensity: $F_{10,280} = 65.97$, P < 0.0001; Genotype: $F_{2,28} = 0.427$, P = 0.656; Intensity X Genotype: $F_{20,280} = 0.936$, P = 0.542). These alterations in spontaneous and evoked synaptic transmission without changes in mEPSC amplitude suggest a possible decrease in the number of functional CA3-CA1 synapses to account for decreased LTP in *Shank3*$^{\Delta C/\Delta C}$ mice.

To determine whether a change in the number of synaptic spines is contributing to deficits in synaptic transmission and plasticity, we used Golgi-Cox

staining and histology to see if the CA1 neuronal morphology is altered in the *Shank3*$^{\Delta C/\Delta C}$ mice. No differences were observed in the dendritic complexity of the WT and *Shank3*$^{\Delta C/\Delta C}$ mice (Figure 2.8A, 2-way rmANOVA; Main effect of Genotype: $F_{1,8}$=0.75, P=0.41; Main effect of Distance from cell body: $F_{9,74}$=58.82, P<0.0001; Genotype x Distance Interaction: $F_{9,74}$=0.57, P=0.81). Furthermore, no differences were observed in spine density between WT and *Shank3*$^{\Delta C/\Delta C}$ mice (Figure 2.8B and C, rmANOVA; Main effect of Genotype: $F_{1,8}$=1.01, P=0.34; Main effect of Distance from cell body: $F_{3,24}$=32.91, P<0.0001; Genotype x Distance Interaction: $F_{3,24}$=0.70, P=0.56). Therefore, changes in synaptic spine number do not account for alterations in synaptic transmission and plasticity in *Shank3*$^{\Delta C/\Delta C}$ mice. However, we may be underpowered to detect subtle differences in spine density.

Discussion

Role of Shank3 *in Hippocampus-dependent Learning and Memory and Synaptic Transmission*

We have identified multiple abnormalities in hippocampus function in a mouse model lacking major naturally occurring isoforms of Shank3. These mice exhibit decreased NMDA-receptor-dependent synaptic transmission, decreased frequency of spontaneous glutamate release, and decreased evoked excitatory synaptic transmission with no change in short-term plasticity or mEPSC amplitude in area CA1 of the hippocampus. This decrease in NMDA-receptor-mediated synaptic transmission is a likely cause of the observed decrease in long-term potentiation in

the *Shank3*$^{\Delta C/\Delta C}$ mice. In turn, the LTP deficits are one potential explanation for the decreased hippocampus-dependent spatial learning abnormalities.

These abnormalities are most likely due to the loss of multiple, naturally occurring isoforms of Shank3 in the *Shank3*$^{\Delta C/\Delta C}$ mutants. We cannot rule out the possibility, however, that increases in smaller molecular weight forms of Shank3 that appear in the *Shank3*$^{\Delta C/\Delta C}$ mice on Western blot with N-terminal and SH3 antibodies could be contributing to these abnormalities. The additional presence of these smaller molecular weight isoforms in the *Shank3*$^{\Delta C/\Delta C}$ mutants is likely to occur in patients with autism caused by either translocation breakpoints or insertion mutations in exon 21 of *Shank3*, making them of potential relevance to a subset of autism associated with *Shank3* mutations. Furthermore, the presence of additional, novel isoforms of Shank3 has not yet been thoroughly evaluated in other published *Shank3* mutant models (Bozdagi et al., 2010; Peca et al., 2011; Wang et al., 2011b; Yang et al., 2012) and may also account for differences observed in these mutants. Indeed, it is not clear in these other *Shank3* mutant models whether the phenotypes are attributable to loss of particular isoforms of Shank3 or to altered ratios of one isoform to another, much less whether novel isoforms appear as a result of these mutations. Mice lacking the entire *Shank3* gene coding region will be of interest to compare to existing *Shank3* mutant models to resolve these issues and as a model of the 22q13 Deletion Syndrome or Phelan-McDermid Syndrome.

Both spatial learning deficits and decreased LTP in area CA1 of the hippocampus have also been reported in the *Shank3*$^{e4-9}$ homozygous mutant mice.

This model lacks exons 4-9 coding for the ankryin repeat domain resulting in loss of only the largest molecular weight isoform of Shank3 (SHANK3α) (Wang et al., 2011b). This finding suggests that loss of this largest isoform alone may be sufficient to produce altered spatial learning and decreased LTP in *Shank3* mutants. NMDA/AMPA ratio was not reported in the *Shank3*$^{e4-9}$ homozygous mutant mice. Similar to the present findings in *Shank3*$^{\Delta C/\Delta C}$ homozygotes, AMPA-receptor-mediated synaptic transmission was intact in the *Shank3*$^{\Delta C/\Delta C}$ homozygous mutants as supported by no change in whole-cell mEPSC amplitude. It will be of interest to examine NMDA/AMPA ratio directly in the *Shank3*$^{e4-9}$ homozygous mutants to determine if loss of only the largest molecular weight isoform of Shank3 is sufficient to decrease NMDA-receptor-mediated synaptic transmission.

In addition, LTP deficits in area CA1 of hippocampus have been reported in the *Shank3*$^{e4-9}$ heterozygous mouse model (Bozdagi et al., 2010). In this case, however, extracellular field recording suggests no change in NMDA-receptor-mediated synaptic transmission but rather a decrease in AMPA-receptor-mediated transmission. Furthermore, whole-cell recording in the *Shank3*$^{e4-9}$ heterozygotes demonstrated decreased mEPSC amplitude consistent with a decrease in AMPA-mediated transmission as well as a dramatic increase in mEPSC frequency (Yang et al., 2012). The finding of extracellularly recorded decreases in both LTP and input/output curves were reproduced in a follow-up paper by the same group, demonstrating the input/output curve differences in *Shank3*$^{e4-9}$ homozygotes as well as heterozygotes (Yang et al., 2012) in conflict with a prior report (Wang et al.,

2011b). Again, NMDA/AMPA ratio was not measured in whole-cell recordings. Also in Yang et al, behavioral studies of *Shank3*$^{e4-9}$ homozygous and heterozygous mice did not find a statistically significant difference in water maze learning in two, small, male-only cohorts, a finding that contrasts with previously published work on *Shank3*$^{e4-9}$ homozygotes (Wang et al., 2011b). The different findings in *Shank3*$^{e4-9}$ homozygous mice input/output curves using extracellular field recordings (Wang et al., 2011b; Yang et al., 2012) and in *Shank3*$^{e4-9}$ homozygous water maze (Wang et al., 2011b; Yang et al., 2012) remain to be resolved.

In yet another *Shank3* homozygous mutant targeting exons 13-16 that code for the PDZ domain of Shank3 (*Shank3*$^{e13-16}$) leading to loss of the two higher molecular weight isoforms of Shank3 (Shank3α and Shank3ß), the minimal hippocampal electrophysiology performed highlights differences with the present findings in *Shank3*$^{\Delta C/\Delta C}$ homozygotes. This includes normal extracellularly recorded input/output curves measuring population spike amplitude rather than direct measurement of field excitatory postsynaptic potentials (fEPSPs) and no change in the amplitude or frequency of mEPSCs in area CA1 of hippocampus (Peca et al., 2011). Neither NMDA/AMPA ratio nor LTP were measured in the hippocampus of *Shank3*$^{e13-16}$ homozygous mutants (Peca et al., 2011). Curiously, the *Shank3*$^{e13-16}$ homozygotes also did not show altered spatial learning in the water maze task with a small cohort of 4-5 week old male mutants (Peca et al., 2011). This difference could be due to the different *Shank3* mutation, to different ages of mice tested, or to differences in protocols across laboratories. Comparison of the multiple published *Shank3* models

within the same laboratory under the same conditions will be necessary to resolve these issues.

Interestingly, in spite of a dramatic increase mGluR5 in synaptic fractions, we find that mGluR-LTD is not significantly enhanced in *Shank3*$^{\Delta C/\Delta C}$ mice. Because Group I mGluRs are currently being targeted as novel treatments for other mouse models of autism (Bear et al., 2004; Won et al., 2012; Yang et al., 2012), and Shank3 has been shown to regulate mGluR5 expression and signaling in cultured neurons (Verpelli et al., 2011), further functional studies of mGluR function in *Shank3* mutants will be of critical importance.

Shank3 *and Social Behavior*

Social deficits are one of the key diagnostic features of autism (Mahjouri and Lord, 2012; Schreibman, 1988), yet of the two social interaction tests that we administered, we only observed deficits in one trial of the three chambered social interaction test where *Shank3*$^{\Delta C/\Delta C}$ mice failed to show a preference for social novelty. This phenotype has previously been reported in *Shank3*$^{e13\text{-}16}$ homozygotes (Peca et al., 2011) and *Shank3*$^{e4\text{-}9}$ homozygotes (Wang et al., 2011b). In the second test using social interaction with a juvenile, *Shank3*$^{\Delta C/\Delta C}$ mice did not show any deficits in initial interaction with juveniles or in a subsequent test of social memory. Taken together these data suggest largely intact social interaction with only minimal dysfunction in one task relevant to the social domain.

Shank3 *and Associated Features*

Aside from the three core diagnostic features, autism is also associated with motor-coordination impairments (Abu-Dahab et al., 2012; Clarke, 1996) and many patients with 22q13 deletion syndrome exhibit hypotonia and incoordination (Phelan and McDermid, 2012). *Shank3*$^{\Delta C/\Delta C}$ mice also show impairment in motor coordination but not in motor learning.

We also tested *Shank3*$^{\Delta C/\Delta C}$ mice in tests of anxiety as autism can be associated with anxiety disorders (Gillott et al., 2001). Of the three anxiety-related tasks, elevated plus maze, open field and dark/light, we only found abnormalities in the dark/light task. *Shank3*$^{\Delta C/\Delta C}$ mice showed an increased latency to enter the light side and significantly preferred the dark chamber. Generally, this result would lead to a conclusion that *Shank3*$^{\Delta C/\Delta C}$ mice have increased anxiety. However, we did not see any differences in the other two anxiety tests. Thus, we interpret the avoidance of light in the dark/light task not as an increase in anxiety but as hypersensitivity to light or perhaps to novelty avoidance. We also tested *Shank3*$^{\Delta C/\Delta C}$ mice for acoustic startle response but found no differences. This suggests that *Shank3*$^{\Delta C/\Delta C}$ mice have hypersensitivity to only select sensory stimuli.

Some studies report that children with autism respond to novelty with avoidance behaviors (Anckarsater et al., 2006; Kootz et al., 1982). Our *Shank3*$^{\Delta C/\Delta C}$ mice show a marked increase in avoidance of novel inanimate objects as evident in the results from nest building and marble burying behavior. Another aberrant response to novelty in *Shank3*$^{\Delta C/\Delta C}$ mice is decreased initial locomotor response to a

novel environment. This phenotype was only observed in the initial 5 min of exposure with rapid habituation to the locomotor apparatus thereafter. Interestingly, *Shank3*$^{\Delta C/\Delta C}$ mice also show a decreased latency to lick their hind paw on a hot-plate indicating an increase in sensitivity to heat.

Conclusions

Recent studies strongly implicate SHANK3 in autism and Phelan-McDermid Syndrome, making a thorough understanding of SHANK3 function in the central nervous system of critical importance. Our results indicate Shank3 is critically important for normal synaptic transmission in the hippocampus and for normal spatial learning and memory. Loss of Shank3 leads to minimal social deficits but unveils multiple additional behavioral abnormalities including motor coordination impairment, novelty avoidance, hypersensitivity to select sensory stimuli, and aberrant locomotor responses to novelty. Further studies are needed to elucidate the underlying mechanisms of how Shank3 is involved in the above deficits, which brain regions are responsible for such deficits, and whether loss of Shank3 leads to irreversible neurodevelopmental abnormalities or to functional synaptic deficits that can be reversed later in life. Our findings of decreased NMDA/AMPA ratio at hippocampal synapses and a dramatic increase in mGluR5 localization to synaptosome and PSD fractions suggests these as potential therapeutic targets for future preclinical study.

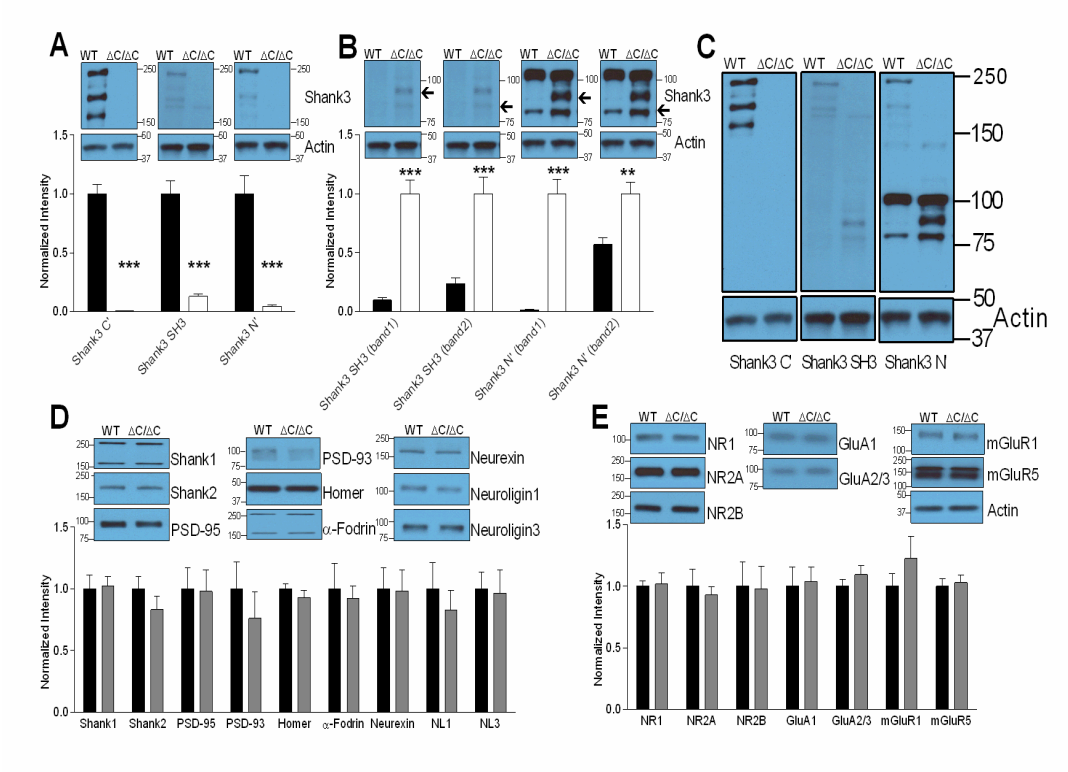

Figure 2.1: Loss of Major, Naturally Occurring Shank3 Proteins in *Shank3*$^{\Delta C/\Delta C}$ mice. A) Quantification and representative Western blot of hippocampal lysates showing loss of the major isoforms of Shank3 with C-terminus (C', JH3025), SH3 domain (SH3, Abcam), and N-terminus (N', P. Worley) antibody. B) Quantification and representative Western blot of lower molecular weight bands that appear or increase in intensity in the *Shank3*$^{\Delta C/\Delta C}$ hippocampal lysates using SH3 domain and N' antibodies. C) Representative, complete Western blots showing the comparison of bands detected by the three Shank3 antibodies. D and E) Quantification and representative blots of whole hippocampus lysates with antibodies against post-synaptic density proteins and receptors that interact directly or indirectly with Shank3. In panels A, D and E, data are normalized to ß-actin control and then to

average of WT levels. In panel B, data are normalized to ß-actin control and then to average of *Shank3*$^{\Delta C/\Delta C}$.

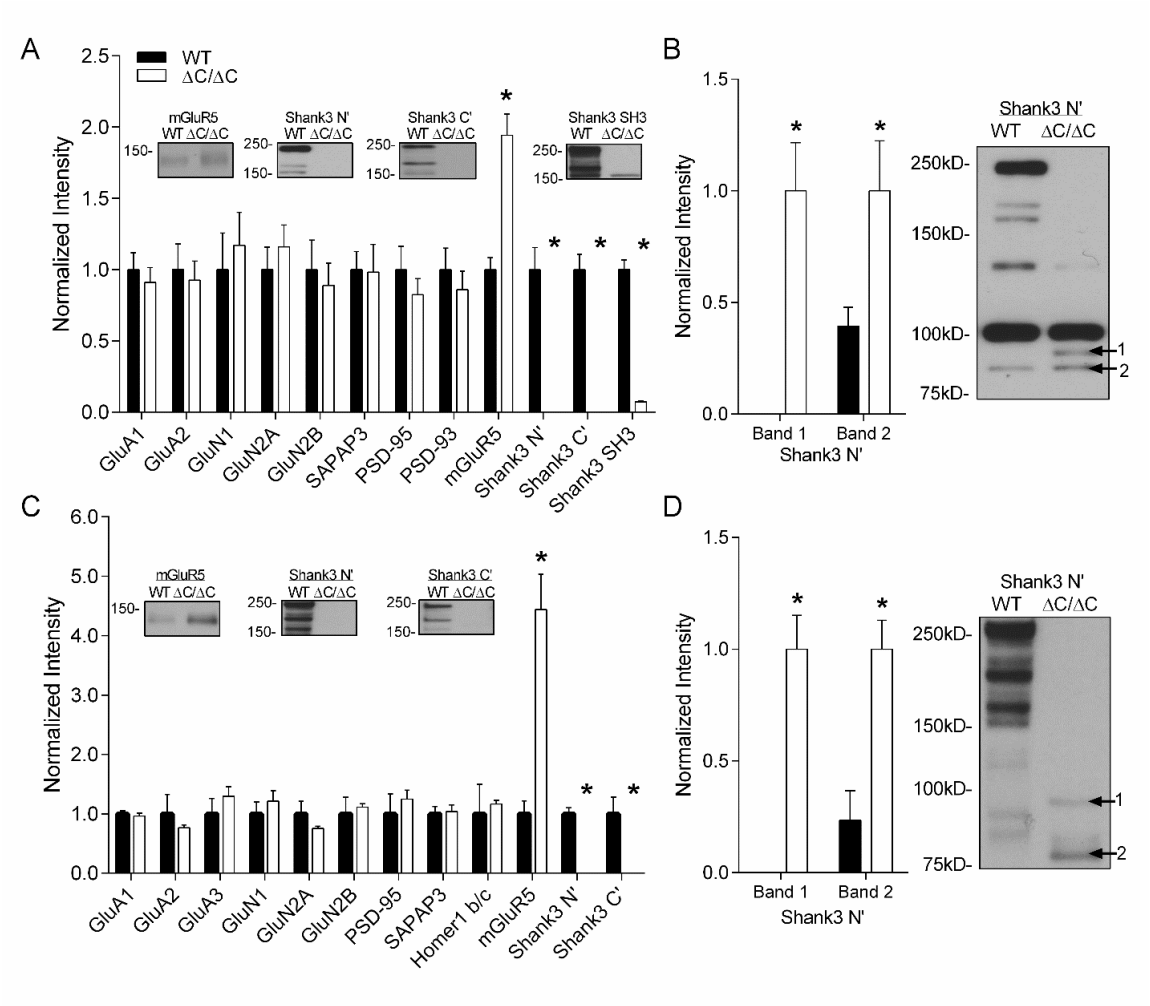

Figure 2.2. Increased mGluR5 Protein Levels in Hippocampal Synaptosome and PSDII Fractions of *Shank3*$^{\Delta C/\Delta C}$ Mice. A) Quantification of PSD proteins in synaptosome fractions of the hippocampus show a complete loss of the major isoforms of Shank3 using the C-terminus, N-terminus, and SH3 domain antibody of Shank3 in *Shank3*$^{\Delta C/\Delta C}$ mice (*P< 0.0001) as well as an increase in mGluR5 (*P<0.0001) compared to WT (WT, N=8; ΔC/ΔC, N=6). Representative blots are shown inset for proteins showing significant differences. B) Quantification of the

<100 kD bands that appear or increase in the hippocampal synaptosomes of *Shank3*$^{\Delta C/\Delta C}$ mice. C) Quantification of PSD proteins in PSDII fractions of the hippocampus shows a complete loss of Shank3 using the C-terminal antibody (*P< 0.05) as well as the N-terminal antibody (*P<0.001) of Shank3 in *Shank3*$^{\Delta C/\Delta C}$ mice as well as a robust increase in mGluR5 (*P<0.01) compared to WT (for each group, N= 3 sets of hippocampi pooled from 2 mice each). D) Quantification of the <100 kD bands that appear or increase in the hippocampal PSDII fraction of *Shank3*$^{\Delta C/\Delta C}$ mice. For A-D data were normalized to β-Actin levels and then to the average of WT (A and C) or ΔC/ΔC (B and D). Data shown as average +/- SEM. Representative blots are shown inset for PSD proteins showing significant differences.

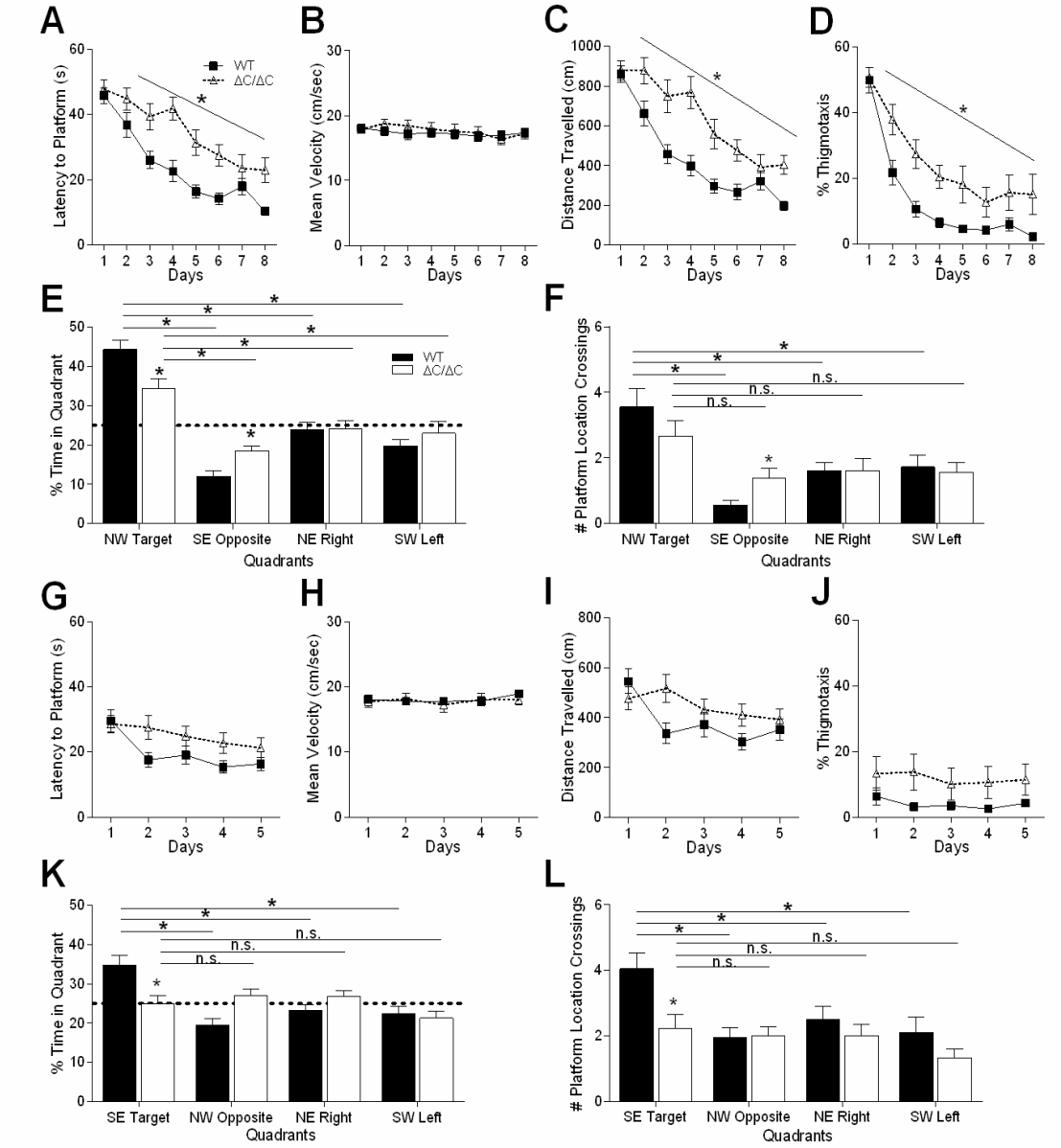

Figure 2.3: *Shank3*$^{\Delta C/\Delta C}$ Mice Exhibit Impaired Spatial Learning. A-D: Training days for the Morris water maze task. For each day of training, data were averaged across four daily trials. A) Latency to reach hidden platform on successive water maze days. *Shank3*$^{\Delta C/\Delta C}$ mice take longer to reach the submerged platform. B) Swim

speed on successive water maze training days. The average swim speed was unchanged in *Shank3*$^{\Delta C/\Delta C}$ mice. C) Distance travelled prior to reaching the hidden platform on successive water maze training days. *Shank3*$^{\Delta C/\Delta C}$ mice travel a more circuitous route (longer distance) before reaching the submerged platform. D) Percent time spent in thigmotaxis on successive water maze training days. E) Time spent in target quadrant and other quadrants during probe trial in which target platform is removed. *Shank3*$^{\Delta C/\Delta C}$ mice spend more time in the target quadrant vs. other quadrants but less time in target quadrant compared to littermate controls. F) Number of target location crossings and corresponding phantom platform location crossings in other quadrants during the probe trial. *Shank3*$^{\Delta C/\Delta C}$ mice fail to show a preference for the target platform location. G-J: Training trials for the Morris water maze reversal task. No differences were observed during training for the Morris water maze reversal learning task in G) latency to platform, H) mean swim speed, I) distance travelled, or J) thigmotaxis. K) On the probe trial for the Morris water maze reversal task, *Shank3*$^{\Delta C/\Delta C}$ mice failed to show preference for the target quadrant and spent equal time in all four quadrants. L) On the probe trial for the Morris water maze reversal task, *Shank3*$^{\Delta C/\Delta C}$ mice did not show preference for the target platform location (N=18 in all panels, data depicted as average +/- S.E.M., *P < 0.05).

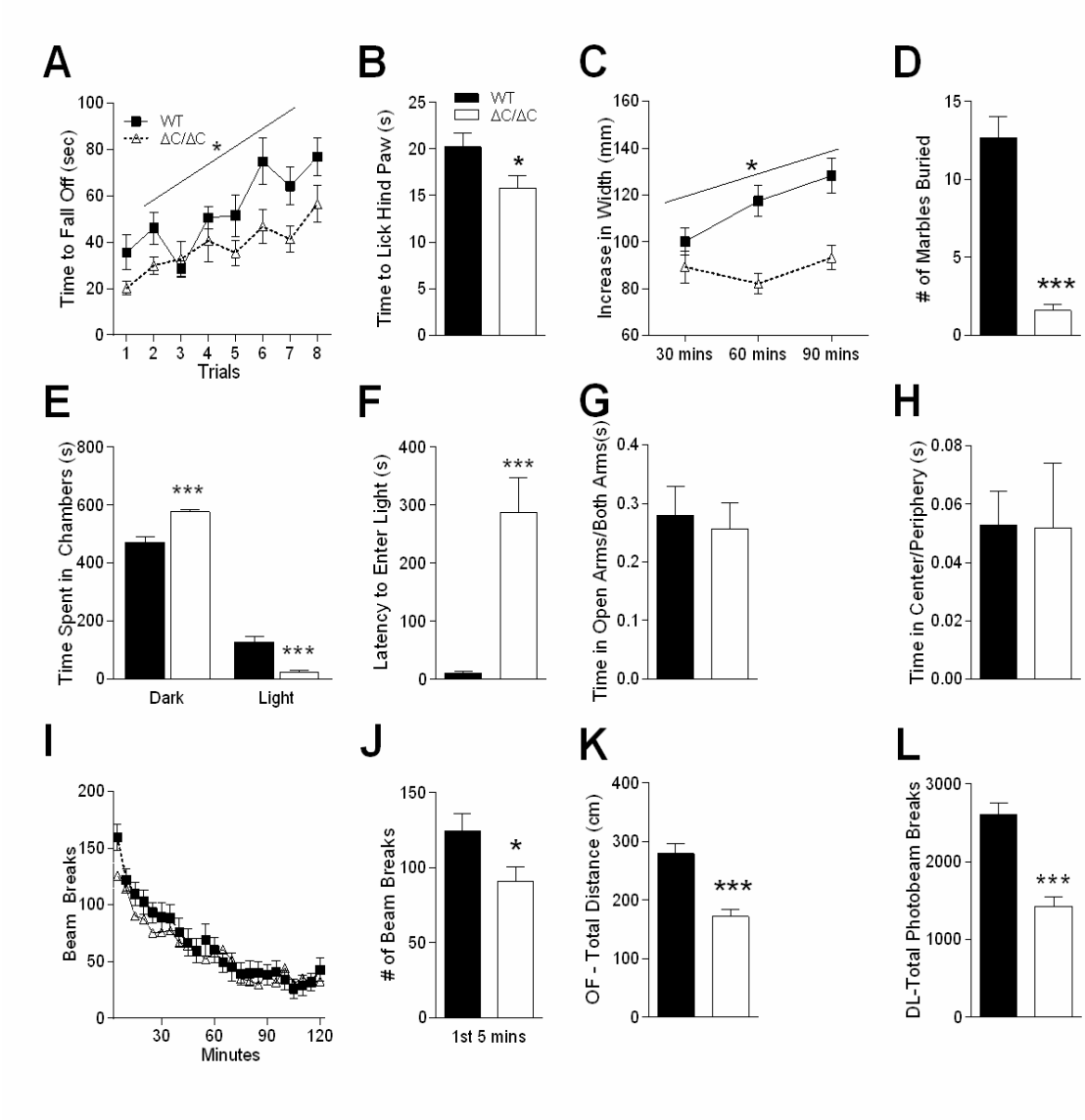

Figure 2.4: *Shank3*$^{\Delta C/\Delta C}$ Mice Exhibit Impairments in Other Behavioral Tasks. A) Latency to fall from or to go one full revolution on the rotarod task. *Shank3*$^{\Delta C/\Delta C}$ mice exhibit motor coordination impairments in 8 trials of rotarod test conducted over two days (N=19). Legend in A applies to C and I. B) Latency to lick hind paw on the hotplate task. *Shank3*$^{\Delta C/\Delta C}$ mice show hypersensitivity to heat on a hot-plate (N=18). Legend in B applies to D-H and J-L. C) Width of nest built as a function of time in a

nest-building task. *Shank3*$^{\Delta C/\Delta C}$ mice exhibit impairments in nest building behavior over a 90 minute period (N=19). D) Number of marbles buried during a 30-min marble-burying task. *Shank3*$^{\Delta C/\Delta C}$ mice show impaired marble burying behavior (N=19). E) Time spent in dark and light chambers during dark/light task. *Shank3*$^{\Delta C/\Delta C}$ mice spend more time in the dark than littermate controls (N=19). F) Latency to enter the light chamber in the dark/light task. *Shank3*$^{\Delta C/\Delta C}$ mice exhibit dramatically increased latency to enter the light side (N=19). G) Fraction of time in the open arms vs. time in other arms in the elevated plus maze task. *Shank3*$^{\Delta C/\Delta C}$ mice spend the same time in open vs. closed arms when compared to littermate controls (N=18). H) Ratio of time spent in the center to time spent in the periphery in an open field task. *Shank3*$^{\Delta C/\Delta C}$ mice behave the same as littermate controls (N=19). I) Locomotor activity as measured by number of photobeam breaks during successive 5-min intervals over a two-hour period. *Shank3*$^{\Delta C/\Delta C}$ mice exhibit normal locomotor habituation over the full 2-hr period (N=19). J) Number of photobeam breaks during the initial 5 min of the locomotor task shown in I. *Shank3*$^{\Delta C/\Delta C}$ mice show decreased activity initially suggesting abnormal locomotor response to novelty (N=19). K) Total distance travelled during the 10-min open field task. *Shank3*$^{\Delta C/\Delta C}$ mice have decreased locomotor activity in the open field (N=19). L) Number of photobeam breaks during the 10-min dark/light task. *Shank3*$^{\Delta C/\Delta C}$ mice have decreased locomotor activity in dark/light (N=19). *$P < 0.05$

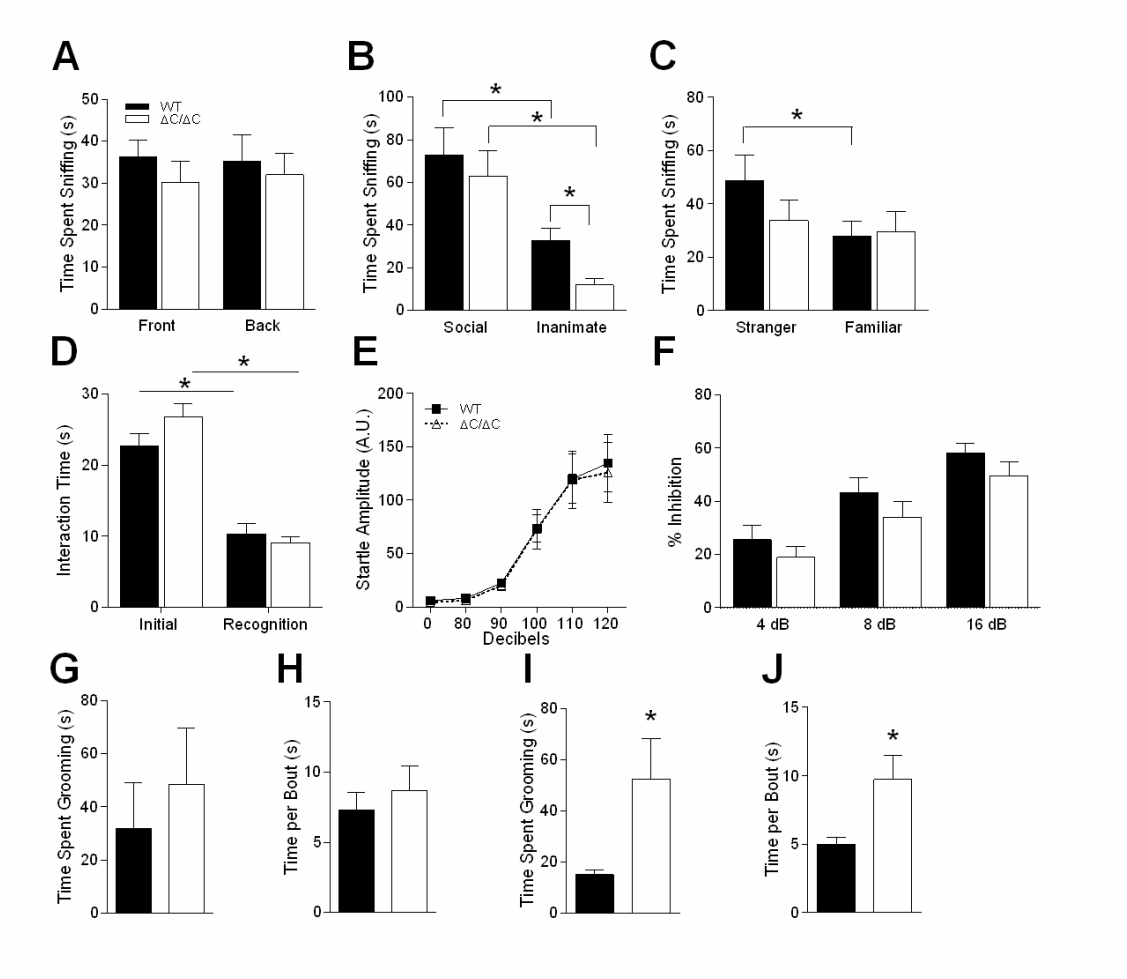

Figure 2.5: *Shank3*$^{\Delta C/\Delta C}$ Mice Exhibit Minimal Social Interaction Deficits and Normal Startle Reactivity and PPI. A) Time spent in chambers with empty cages. For the first trial of three-chambered social interaction test, *Shank3*$^{\Delta C/\Delta C}$ mice were allowed to explore a 3-chambered apparatus and showed no initial preference for either end of the box (N=17). Legend in A applies to B-D and F.B) In the second trial when given a choice between social or inanimate target, both WT and *Shank3*$^{\Delta C/\Delta C}$ mice show a preference for a caged social target vs. inanimate object. *Shank3*$^{\Delta C/\Delta C}$ mice however, avoided the inanimate object and spend less time sniffing it than WT

group (N=17). C) In the third trial, when given a choice between novel social target vs. a familiar social target, *Shank3*$^{\Delta C/\Delta C}$ mice failed to show a preference for the novel social target unlike their WT littermate pairs (N=17). D) *Shank3*$^{\Delta C/\Delta C}$ mice show normal social interaction with a juvenile conspecific mouse and when presented with the same mouse 3 days later, exhibit normal social memory (N=18). E) *Shank3*$^{\Delta C/\Delta C}$ mice exhibit normal response to startle and F) show no deficits in pre-pulse inhibition (N=18). G) *Shank3*$^{\Delta C/\Delta C}$ mice show no change in total time spent in repetitive grooming behavior or H) in time spent grooming per bout (N=19). I)However when tested at an older age *Shank3*$^{\Delta C/\Delta C}$ mice show a significant increase in overall time spent grooming and J) time spent grooming per bout (N=16). *$P < 0.05$

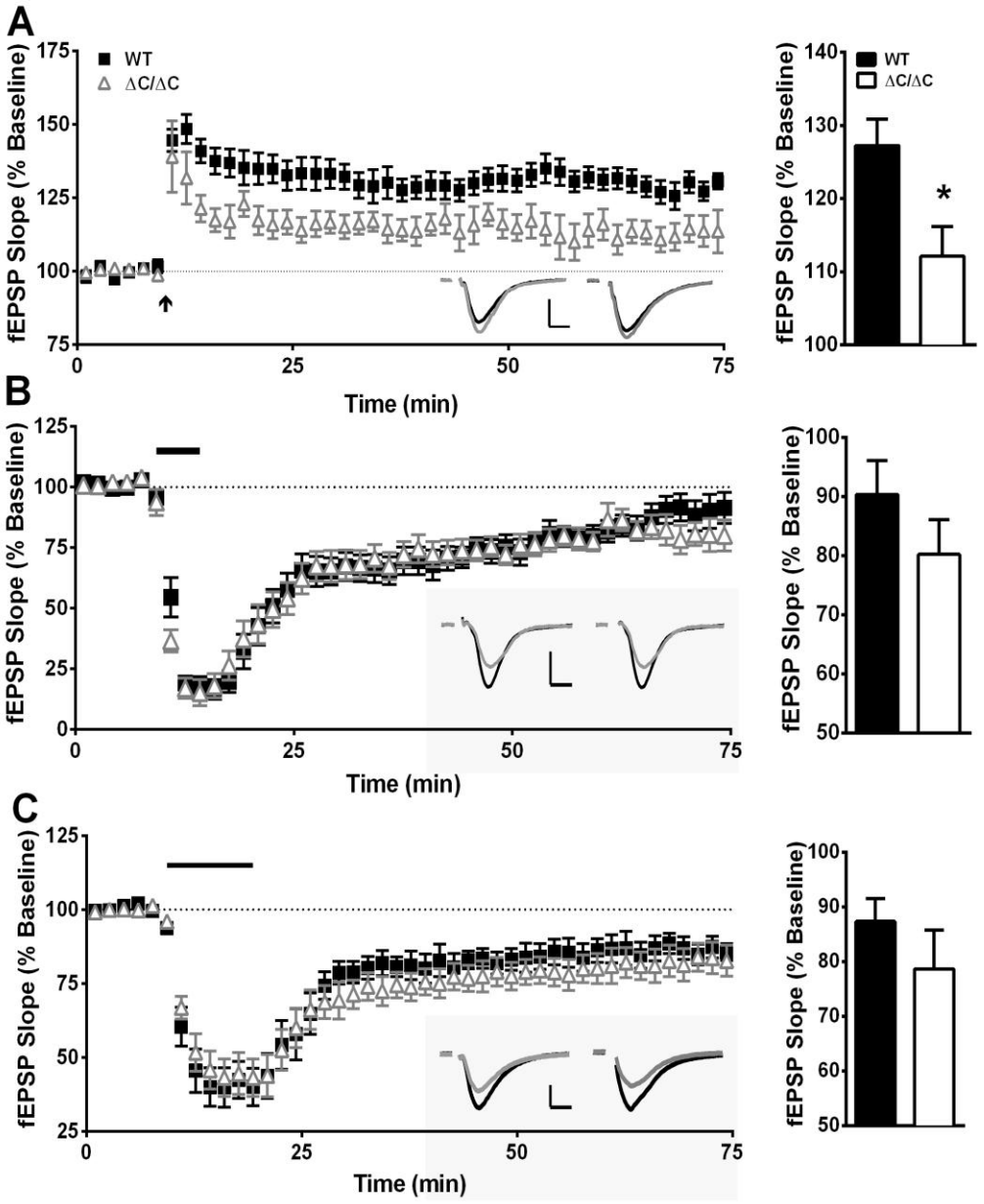

Figure 2.6: Synaptic plasticity at hippocampal CA3-CA1 synapses is altered in *Shank3*$^{\Delta C/\Delta C}$ mice. A) LTP is decreased in *Shank3*$^{\Delta C/\Delta C}$ mice (N = 6) compared to WT controls (N = 8). Arrow indicates onset of 100Hz train for 1s. Inset: Average of 15 consecutive traces immediately before (black) and 60 minutes after (gray) 100 Hz

tetanus. Scale bars: 0.3 mV (WT) or 0.55 mV (*Shank3*$^{\Delta C/\Delta C}$), 5 ms. Legends in A also apply to B and C. B) mGluR-LTD from 6-8 week old mice is not significantly affected by exon 21 deletion (WT N = 9, *Shank3*$^{\Delta C/\Delta C}$ N = 7). Bar indicates 5 minute bath application of DHPG. Inset: Average of 15 consecutive traces immediately before DHPG wash-in (black) and 60 minutes after the start of DHPG washout (gray). Scale bars: 0.3 mV, 5 ms. C) There no significant difference in mGluR-LTD from 3-4 week old *Shank3*$^{\Delta C/\Delta C}$ mice (N = 11) compared to WT (N = 9). Bar indicates 10 minute bath application of DHPG. Inset: Average of 15 consecutive traces immediately before DHPG wash-in (black) and 60 minutes after the start of DHPG washout (gray). Scale bars: 0.3 mV (WT) or 0.22 mV (*Shank3*$^{\Delta C\square\Delta C}$), 5 ms. *P < 0.05

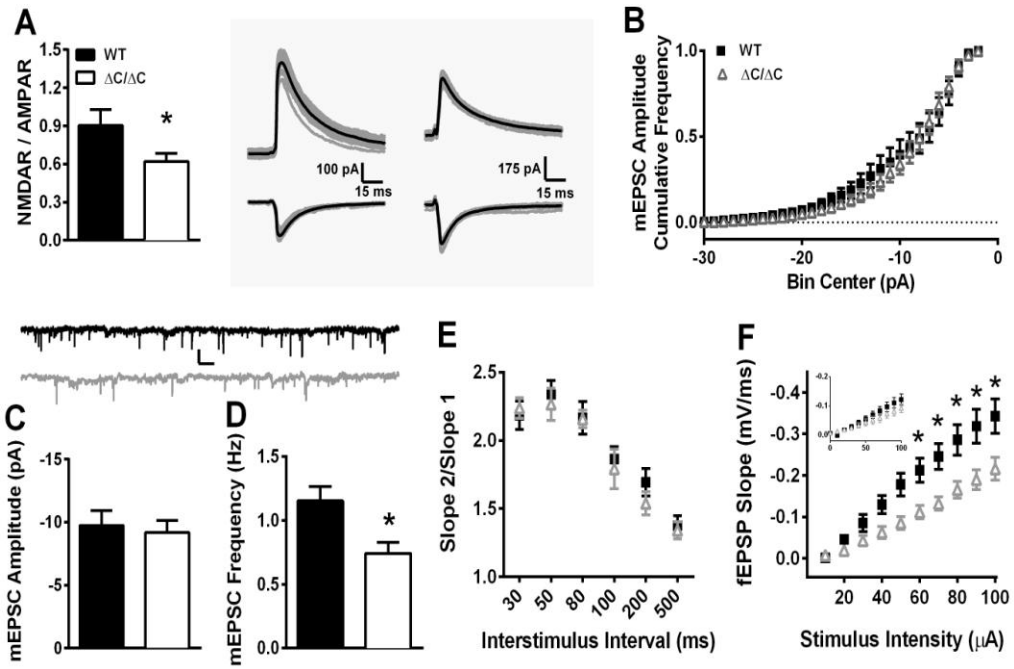

Figure 2.7: Synaptic transmission is altered at hippocampal CA3-CA1 synapses in *Shank3*$^{\Delta C/\Delta C}$ mice. A) NMDA/AMPA ratio is decreased in *Shank3*$^{\Delta C/\Delta C}$ mice (N = 25) compared to WT (N = 22). 15 consecutive traces (gray) and average trace (black) at -70 mV (bottom) and at +40 mV (top) from WT mice (left) and *Shank3*$^{\Delta C/\Delta C}$ mice (right). Legend in A applies to C & D. Cumulative frequency of mEPSC amplitude (B) and mean mEPSC amplitude (C) were unchanged, but mEPSC frequency (D) was significantly decreased in *Shank3*$^{\Delta C/\Delta C}$ compared to WT (WT N = 15, *Shank3*$^{\Delta C/\Delta C}$ N = 22). Inset: 1 minute raw traces from a WT CA1 neuron (black) and a *Shank3*$^{\Delta C/\Delta C}$ CA1 neuron (gray). Scale bar: 10 pA, 2.5 s. Legend in B also applies to E and F. E) Paired-pulse ratio is not different between WT and *Shank3*$^{\Delta C/\Delta C}$ mice at interstimulus intervals 30-500ms. N = 10 for each genotype. F) The relationship of stimulus

intensity to fEPSP slope is decreased in *Shank3*$^{\Delta C/\Delta C}$ mice. Inset: Relationship of fiber volley to fEPSP slope is similar between WT and *Shank3*$^{\Delta C/\Delta C}$ mice. N = 10 for each genotype. *P < 0.05

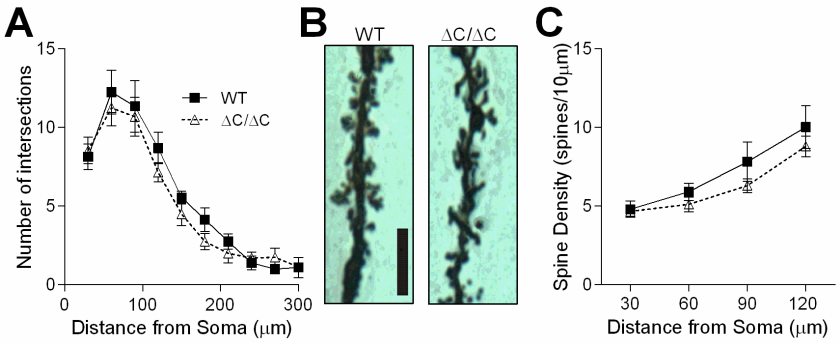

Figure 2.8: No morphological deficits observed in the CA1hippocampal neurons in *Shank3*$^{\Delta C/\Delta C}$ mice. A) No differences between genotypes were observed in quantitative assessment of branching via Sholl analysis. Legend in A also applies to C. B) Representative examples of WT and *Shank3*$^{\Delta C/\Delta C}$ spine density at 90μm from the soma at X100 magnification. Scale bar = 5μm in WT also applies to *Shank3*$^{\Delta C/\Delta C}$ C) No differences between genotype were observed in spine density in the apical dendrites of CA1 hippocampla neurons. N = 20 neurons from 5 mice for each genotype. *P < 0.05.

Table 3: Statistical Analysis of Behavioral Studies		
Parameter	**Comparison**	**Results**
Body Weight N=19	Sex and Genotype	2-way ANOVA; Main effect of Sex: F(1,34)=25.47, P<.00001; Main effect of Genotype: F(1,34)=14.60, P<0.001; Sex x Genotype Interaction: F(1,34)=0.17, P=0.67
Open Field N=19		
Time in Center	Sex & Genotype	2-way ANOVA; Main effect of Sex: F(1,34)=.33, P=0.56; Main effect of Genotype:F(1,34)=0.10, P=0.74; Sex x Genotype Interaction: F(1,34)=4.26, **P<0.4**
Frequency in Center	Sex & Genotype	2-way ANOVA; Main effect of Sex: F(1,34)=0.05, P=0.82 ; Main effect of Genotype: F(1,34)=5.59, P<0.03; Sex x Genotype Interaction: F(1,34)=2.47, P=0.12
Time in periphery	Sex & Genotype	2-way ANOVA; Main effect of Sex: F(1,34)=0.99, P=0.32 ; Main effect of Genotype: F(1,34)=4.44, P<0.05 ; Sex x Genotype Interaction: F(1,34)=0.13, P=0.71
Frequency in Periphery	Sex & Genotype	2-way ANOVA; Main effect of Sex: P<0.0004 F(1,34)=0.86, P=0.36; Main effect of Genotype: F(1,34)=15.83, ; Sex x Genotype Interaction: F(1,34)=1.19, P=0.28
Time in Center / Time in Periphery	Sex & Genotype	2-way ANOVA; Main effect of Sex: F(1,34)=0.14, P=0.70 ; Main effect of Genotype: F(1,34)=0.003, P=0.95; Sex x Genotype Interaction: F(1,34)=3.34, P=0.07
Distance Travelled	Sex & Genotype	2-way ANOVA; Main effect of Sex: F(1,34)=0.02, P=0.88 ; Main effect of Genotype: F(1,34)=23.54, P<0.00003 ; Sex x Genotype Interaction: F(1,34)=0.04, P=0.83
Velocity	Sex & Genotype	2-way ANOVA; Main effect of Sex: F(1,34)=0.02, P=0.88; Main effect of Genotype: F(1,34)=23.42, P<0.00003; Sex x Genotype Interaction: F(1,34)=0.04, P=0.84
Dark/light Box N = 19		
Total Activity	Sex & Genotype	2-way ANOVA; Main effect of Sex: F(1,34)=0.16, P=0.68; Main effect of Genotype: F(1,34)=35.60, **P<0.000002**; Sex x Genotype Interaction: F(1,34)=0.0001, P=0.99
Time in Light Side	Sex & Genotype	2-way ANOVA; Main effect of Sex: F(1,34)=2.32, P=0.13; Main effect of Genotype: F(1,34)=29.06, **P<0.00006**; Sex x Genotype

		Interaction: F(1,34)=3.47, P=0.071
Crosses	Sex & Genotype	2-way ANOVA; Main effect of Sex: F(1,34)=1.55, P=0.22; Main effect of Genotype: F(1,34)=26.83, **P<0.00002**; Sex x Genotype Interaction: F(1,34)=0.71, P=0.40
Latency to Enter Light Side	Sex & Genotype; parametric	2-way ANOVA; Main effect of Sex: F(1,34)=0.002, P=0.96; Main effect of Genotype: F(1,34)=21.08, **P<0.00006**; Sex x Genotype Interaction: F(1,34)=0.006, P=0.93
Time in Dark Side	Sex, Genotype; non-parametric	2-way ANOVA; Main effect of Sex: F(1,34)=2.32, P=0.14; Main effect of Genotype: F(1,34)=29.06, **P<0.00006**; Sex x Genotype Interaction: F(1,34)=3.47, P=0.07
Elevated Plus Maze N = 18		
Distance Travelled	Sex & Genotype	2-way ANOVA; Main effect of Sex: F(1,32)=0.01, P=0.90; Main effect of Genotype: F(1,32)=.05,P=0.82; Sex x Genotype Interaction: F(1,32)=0.01, P=0.91
Velocity	Sex & Genotype	2-way ANOVA; Main effect of Sex: F(1,32)=0.14, P=0.70; Main effect of Genotype: F(1,32)=0.48,P=0.49; Sex x Genotype Interaction: F(1,32)=0.14, P=0.70
Time in Open Arms / Time in Both Arms	Sex & Genotype	2-way ANOVA; Main effect of Sex: F(1,32)=0.50, P=0.48; Main effect of Genotype: F(1,32)=0.12,P=0.73; Sex x Genotype Interaction: F(1,32)=0.06, P=0.79
Entries in Open / Entries in Both	Sex & Genotype	2-way ANOVA; Main effect of Sex: F(1,32)=3.78, P=0.06; Main effect of Genotype: F(1,32)=3.07,P=0.08; Sex x Genotype Interaction: F(1,32)=0.48, P=0.49
Morris Water Maze -Initial Training N = 18		
Latency to Reach Platform	Sex, Genotype & Day	3-way rmANOVA; Main effect of Sex: F(1,32)=0.35, P=0.55; Main effect of Genotype: F(1,32)=13.55, **P<0.001**; Main effect of Day: F(7,224)=36.47, **P<0.000001**; Sex x Genotype Interaction: F(1,32)=0.12, P=0.72; Sex x Day Interaction: F(7,224)=1.58, P=0.14; Genotype x Day Interaction: F(7,224)=2.54, **P<0.05**; Sex x Genotype x Day Interaction: F(7,224)=0.53, P=0.806
% Thigmotaxis	Sex, Genotype & Day	3-way rmANOVA; Main effect of Sex: F(1,32)=0.49, P=0.49; Main effect of Genotype: F(1,32)=7.62, **P<0.01**; Main effect of Day:

		F(7,224)=75.09, **P<0.000001**; Sex x Genotype Interaction: F(1,32)=0.07, P=0.79; Sex x Day Interaction: F(7,224)=5.09, **P<0.0001**; Genotype x Day Interaction: F(7,224)=2.41, **P<0.05**; Sex x Genotype x Day Interaction: F(7,224)=2.10, **P<0.05**
Distance Travelled to Platform	Sex, Genotype & Day	3-way rmANOVA; Main effect of Sex: F(1,32)=0.83, P=0.36; Main effect of Genotype: F(1,32)=17.41, **P<0.001**; Main effect of Day: F(7,224)=41.61, **P<0.000001**; Sex x Genotype Interaction: F(1,32)=2.39, P=0.13; Sex x Day Interaction: F(7,224)=1.02, P=0.41; Genotype x Day Interaction: F(7,224)=3.25, **P<0.005**; Sex x Genotype x Day Interaction: F(7,224)=0.72, P=0.65
Ave. Swim Speed	Sex, Genotype & Day	3-way rmANOVA; Main effect of Sex: F(1,32)=3.51, P=0.07; Main effect of Genotype: F(1,32)=0.5, P=0.48; Main effect of Day: F(7,224)=2.00, P=0.05; Sex x Genotype Interaction: F(1,32)=5.48, **P<0.02**; Sex x Day Interaction: F(7,224)=0.59, P=0.75; Genotype x Day Interaction: F(7,224)=0.92, P=0.48; Sex x Genotype x Day Interaction: F(7,224)=1.12, P=0.34
	WT vs. KO	Planned Comparisons: Females (WTvsKO): P<.05; Males(WTvsKO): P=0.22
	Males vs. Females	Planned Comparisons: WT (MvsF): P= 0.74 KO(MvsF): P<.0006
Morris Water Maze -Probe Trial N = 18		
% Time in Quadrant	Sex, Genotype & Quadrant	3-way rmANOVA; Main effect of Sex: F(1,32)=0.91, P=0.34; Main effect of Genotype: F(1,32)=0.22, P=0.63; Main effect of Quadrant: F(3,96)=33.49, **P<0.000001**; Sex x Genotype Interaction: F(1,32)=3.64, P=0.06; Sex x Quadrant Interaction: F(3,96)=0.51, P=0.67; Genotype x Quadrant Interaction: F(3,96)=4.21, **P<0.01**; Sex x Genotype x Quadrant Interaction: F(3,96)=0.63, P=0.59
	WT vs. KO within Quadrants	Planned Comparisons: Target NW Quad: **P<0.01**; Right NE Quad: P=0.87; Left SW Quad: P=0.40; Opposite SE Quad: **P<0.01**
	Target vs. other Quads within	Planned Comparisons: TargetNW vs. RightNE: **P<0.00001**; TargetNW vs. LeftSW: **P<0.00001**;

	WT	TargetNW vs. OppositeSE: **P<0.00001**
	Target vs. other Platforms KO	Planned Comparisons: TargetNW vs. RightNE: **P<0.02**; TargetNW vs. LeftSW: **P<0.02**; TargetNW vs. OppositeSE: **P<0.0001**
# of Platform Crossings	Sex, Genotype & Platform	3-way rmANOVA; Main effect of Sex: F(1,32)=1.59, P=0.21; Main effect of Genotype: F(1,32)=0.01, P=0.91; Main effect of Quadrant: F(3,96)=13.00, **P<0.000001**; Sex x Genotype Interaction: F(1,32)=8.39, **P<0.01**; Sex x Quadrant Interaction: F(3,96)=1.30, P=0.27; Genotype x Quadrant Interaction: F(3,96)=2.13, P=0.10; Sex x Genotype x Quadrant Interaction: F(3,96)=0.47, P=0.70
	WT vs. KO within Platforms	Planned Comparisons: Target NW Quad: P=0.27; Right NE Quad: P=0.69; Left SW Quad: P=0.83; Opposite SE Quad: **P<0.01**
	Target vs. other Platforms WT	Planned Comparisons: TargetNW vs. RightNE: **P<0.001**; TargetNW vs. LeftSW: **P<0.01**; TargetNW vs. OppositeSE: **P<0.0001**
	Target vs. other Platforms KO	Planned Comparisons: TargetNW vs. RightNE: P=0.08; TargetNW vs. LeftSW: P=0.08; TargetNW vs. OppositeSE: P=0.052
	WT vs. KO	Planned Comparisons: Females (WTvsKO): P=0.05; Males(WTvsKO): P<0.05
	Males vs. Females	Planned Comparisons: WT (MvsF): P= 0.25 KO(MvsF): P<.007
Ave. Swim Speed	Sex & Genotype	2-way ANOVA; Main effect of Sex: F(1,32)=2.51, P=0.12; Main effect of Genotype: F(1,32)=0.03, P=0.84; Sex x Genotype Interaction: F(1,32)=5.17, **P<0.01**
	WT vs. KO	Planned Comparisons: Females (WTvsKO): P=0.10; Males(WTvsKO): P=0.12
	Males vs. Females	Planned Comparisons: WT (MvsF): P= 0.62 KO(MvsF): P<.05
% Thigmotaxis	Sex & Genotype	2-way ANOVA; Main effect of Sex: F(1,32)=1.42, P=0.24; Main effect of Genotype: F(1,32)=5.45, **P<0.01**; Sex x Genotype Interaction: F(1,32)=0.03, P=0.84
Distance travelled	Sex & Genotype	2-way ANOVA; Main effect of Sex: F(1,32)=2.52, P=0.12; Main effect of Genotype: F(1,32)=0.03, P=0.86; Sex x Genotype Interaction: F(1,32)=5.12, **P<0.05**
	WT vs. KO	Planned Comparisons: Females (WTvsKO):

		P=0.11; Males(WTvsKO): P=0.12
	Males vs. Females	Planned Comparisons: WT (MvsF): P= 0.63 KO(MvsF): P<.02
Morris Water Maze -Reversal Training N = 18		
Latency to Reach Platform	Sex, Genotype & Day	3-way rmANOVA; Main effect of Sex: F(1,32)=0.0000041, P=0.99; Main effect of Genotype: F(1,32)=2.63, P=0.11; Main effect of Day: F(4,128)=8.05, **P<0.0009**; Sex x Genotype Interaction: F(1,32)=1.21, P=0.27; Sex x Day Interaction: F(4,128)=0.64, P=0.63; Genotype x Day Interaction: F(4,128)=1.69, P=0.15; Sex x Genotype x Day Interaction: F(4,128)=0.27, P=0.89
% Thigmotaxis	Sex, Genotype & Day	3-way rmANOVA; Main effect of Sex: F(1,32)=0.50, P=0.48; Main effect of Genotype: F(1,32)=2.29, P=0.13; Main effect of Day: F(4,128)=1.50, P=0.20; Sex x Genotype Interaction: F(1,32)=0.39, P=0.53; Sex x Day Interaction: F(4,128)=1.22, P=0.30; Genotype x Day Interaction: F(4,128)=0.57, P=0.68; Sex x Genotype x Day Interaction: F(4,128)=0.77, P=0.54
Distance Travelled to Platform	Sex, Genotype & Day	3-way rmANOVA; Main effect of Sex: F(1,32)=0.44, P=0.51; Main effect of Genotype: F(1,32)=2.08, P=0.15; Main effect of Day: F(4,128)=4.99, **P<0.0009**; Sex x Genotype Interaction: F(1,32)=0.01, P=0.89; Sex x Day Interaction: F(4,128)=0.91, P=0.45; Genotype x Day Interaction: F(4,128)=2.64, **P<0.05**; Sex x Genotype x Day Interaction: F(4,128)=0.65, P=0.62
Ave. Swim Speed	Sex, Genotype & Day	3-way rmANOVA; Main effect of Sex: F(1,32)=2.48, P=0.12; Main effect of Genotype: F(1,32)=0.006, P=0.93; Main effect of Day: F(4,128)=1.08, P=0.36; Sex x Genotype Interaction: F(1,32)=3.05, P=0.09; Sex x Day Interaction: F(4,128)=1.21, P=0.30; Genotype x Day Interaction: F(4,128)=0.68, P=0.60; Sex x Genotype x Day Interaction: F(4,128)=1.84, P=0.12
Morris Water Maze -Reversal Probe N = 18		
% Time in Quadrant	Sex, Genotype & Quadrant	3-way rmANOVA; Main effect of Sex: F(1,32)=0.71, P=0.40; Main effect of Genotype:

		F(1,32)=0.83, P=0.36; Main effect of Quadrant: F(3,96)=5.87, P<0.01; Sex x Genotype Interaction: F(1,32)=0.76, P=0.38; Sex x Quadrant Interaction: F(3,96)=1.76, P=0.15; Genotype x Quadrant Interaction: F(3,96)=6.51, P<0.001; Sex x Genotype x Quadrant Interaction: F(3,96)=0.59, P=0.61
	WT vs. KO within Platforms	Planned Comparisons: Target SE Quad: **P<0.001**; Right NE Quad: P=0.08; Left SW Quad: P=0.76; Opposite NW Quad: **P<0.01**
	Target vs. other Platforms WT	Planned Comparisons: TargetSE vs. RightNE: **P<0.001**; TargetSE vs. LeftSW: **P<0.001**; TargetSE vs. OppositeNW: **P<0.0001**
	Target vs. other Platforms KO	Planned Comparisons: TargetSE vs. RightNE: P=0.55; TargetSE vs. LeftSW: P=0.32 ; TargetSE vs. OppositeNW: P=0.60
# of Platform Crossings	Sex, Genotype & Platform	3-way rmANOVA; Main effect of Sex: F(1,32)=0.003, P=0.95; Main effect of Genotype: F(1,32)=6.11, **P<0.02**; Main effect of Quadrant: F(3,96)=4.93, **P<0.01**; Sex x Genotype Interaction: F(1,32)=0.63, P=0.43; Sex x Quadrant Interaction: F(3,96)=0.35, P=0.78; Genotype x Quadrant Interaction: F(3,96)=1.98, P=0.12; Sex x Genotype x Quadrant Interaction: F(3,96)=0.04, P=0.98
	WT vs. KO within Platforms	Planned Comparisons: Target SE Quad:**P<0.05**; Right NE Quad: P=0.39; Left SW Quad: P=0.19; Opposite NW Quad: P=0.86
	Target vs. other Platforms WT	Planned Comparisons: TargetSE vs. RightNE: **P<0.05**; TargetSE vs. LeftSW: **P<0.01**; TargetSE vs. OppositeNW: **P<0.01**
	Target vs. other Platforms KO	Planned Comparisons: TargetSE vs. RightNE: P=0.66; TargetSE vs. LeftSW: P=0.20; TargetSE vs. OppositeNW: P=0.68
Ave. Swim Speed	Sex & Genotype	2-way ANOVA; Main effect of Sex: F(1,32)=1.67, P=0.20; Main effect of Genotype: F(1,32)=1.16, P=0.28; Sex x Genotype Interaction: F(1,32)=3.13, P=0.08
% Thigmotaxis	Sex & Genotype	2-way ANOVA; Main effect of Sex: F(1,32)=0.49, P=0.48; Main effect of Genotype: F(1,32)=1.32, P=0.25; Sex x Genotype Interaction: F(1,32)=1.04, P=0.31
Distance travelled	Sex & Genotype	2-way ANOVA; Main effect of Sex: F(1,32)=1.72, P=0.19; Main effect of Genotype: F(1,32)=1.12,

		P=0.29; Sex x Genotype Interaction: F(1,32)=3.23, P=0.08
Visible Water Maze N = 18		
Latency to Platform	Sex & Genotype	2-way ANOVA; Main effect of Sex: F(1,32)=0.15, P=0.69; Main effect of Genotype: F(1,32)=2.93, P=0.09; Sex x Genotype: F(1,32)=0.07, P=0.78
% Thigmotaxis	Sex & Genotype	2-way ANOVA; Main effect of Sex: F(1,32)=0.0008, P=0.97; Main effect of Genotype: F(1,32)=0.98, P=0.32; Sex x Genotype: F(1,32)=0.04, P=0.82
Distance Travelled to Platform	Sex & Genotype	2-way ANOVA; Main effect of Sex: F(1,32)=0.82, P=0.36; Main effect of Genotype: F(1,32)=3.34, P=0.07; Sex x Genotype: F(1,32)=0.02, P=0.86
Ave. Swim Speed	Sex & Genotype	2-way ANOVA; Main effect of Sex: F(1,32)=0.89, P=0.35; Main effect of Genotype: F(1,32)=0.34, P=0.56; Sex x Genotype: F(1,32)=0.12, P=0.72
Hot Plate N = 18		
Time to Lick Shake Hind Paw	Sex & Genotype	2-way ANOVA; Main effect of Sex: F(1,32)=0.68, P=0.41; Main effect of Genotype: F(1,32)=4.38, **P<0.05**; Sex x Genotype: F(1,32)=0.97, P=0.33
Nesting Behavior N = 19		
Increase in Nest Height	Sex, Genotype & Time	3-way rmANOVA; Main effect of Sex: F(1,34)=6.004, **P<0.02**; Main effect of Genotype: F(1,34)=17.78, **P<0.001**; Main effect of Trial: F(2,68)=17.44, **P<0.0001**; Sex x Genotype Interaction: F(1,34)=7.57, **P<0.01**; Sex x Trial Interaction: F(2,68)=1.78, P=0.17; Genotype x Trial Interaction: F(2,68)=4.73, **P<0.02**; Sex x Genotype x Trial Interaction: F(4,128)=0.55, P=0.57
Increase in Nest Width	Sex, Genotype & Time	3-way rmANOVA; Main effect of Sex: F(1,34)=3.77, P=0.06; Main effect of Genotype: F(1,34)=17.06, **P<0.001**; Main effect of Trial: F(2,68)=7.60, **P<0.01**; Sex x Genotype Interaction: F(1,34)=3.55, P=0.06; Sex x Trial Interaction: F(2,68)=1.84, P=0.16; Genotype x Trial Interaction: F(2,68)=6.00, **P<0.004**; Sex x Genotype x Trial Interaction: F(4,128)=1.48, P=0.23
3-choice Interaction Test- Baseline N = 17		
Distance Travelled	Sex & Genotype	2-way ANOVA: Main effect of Sex:F(1,30)=0.52, P=0.47 ; Main effect of Genotype: F(1,30)= 2.70, P=0.11; Sex x Genotype Interaction:

		F(1,30)=0.0004, P=0.98
Velocity	Sex & Genotype	2-way ANOVA: Main effect of Sex:F(1,30)=0.43, P=0.51 ; Main effect of Genotype: F(1,30)= 2.36, P=0.13; Sex x Genotype Interaction: F(1,30)=0.0023, P=0.96
Time Spent Sniffing	Sex, Genotype & Interaction Target (front vs. back)	3-way rmANOVA: Main effect of Sex: F(1,30)=0.03, P=0.86; Main effect of Genotype: F(1,30)=1.23, P=0.27; Main effect of Target: F(1,30)=0.01, P=0.90; Sex x Genotype Interaction: F(1,30)=4.01, P=0.05; Sex x Target Interaction: F(1,30)=1.00 P=0.32; Genotype x Target Interaction: F(1,30)=0.06, P=0.80; Sex x Genotype x Target Interaction: F(1,30)=0.20, P=0.65
	Effect of Target (within each genotype	Planned Comparisons; A: P=0.92; B: P=0.79
3-choice Interaction Test- Social Preference N = 17		
Distance Travelled	Sex & Genotype	2-way ANOVA: Main effect of Sex:F(1,30)=3.57, P=0.06 ; Main effect of Genotype: F(1,30)= 2.68, P=0.11; Sex x Genotype Interaction: F(1,30)=0.14, P=0.70
Velocity	Sex & Genotype	2-way ANOVA: Main effect of Sex:F(1,30)=1.30, P=0.26 ; Main effect of Genotype: F(1,30)= 1.53, P=0.22; Sex x Genotype Interaction: F(1,30)=0.55, P=0.46
Interaction Time	Sex, Genotype & Interaction Target (inanimate vs. social)	3-way rmANOVA: Main effect of Sex: F(1,30)=0.23, P=0.63; Main effect of Genotype: F(1,30)=2.95, P=0.09; Main effect of Target: F(1,30)=20.81, **P<0.0001**; Sex x Genotype Interaction: F(1,30)=0.002, P=0.96; Sex x Target Interaction: F(1,30)=1.54 P=0.22; Genotype x Target Interaction: F(1,30)=0.36, P=0.54; Sex x Genotype x Target Interaction: F(1,30)=0.55, P=0.46
	Effect of Target within each Genotype	Planned Comparisons; A: **P<0.01**; B: **P<0.001**
	Effect of Gentoype (WT vs. KO) within each Target	Planned Comparisons; Social Target: P=0.60; Inanimate: **P<0.01**
3-choice Interaction Test- Social Novelty N = 17		
Distance	Sex & Genotype	2-way ANOVA: Main effect of Sex:F(1,30)=

Travelled		14.80, **P<0.0005**; Main effect of Genotype: F(1,30)= 0.87, P=0.35; Sex x Genotype Interaction: F(1,30)=0.13, P=0.71
Velocity	Sex & Genotype	2-way ANOVA: Main effect of Sex:F(1,30)= 15.90, **P<0.0003**; Main effect of Genotype: F(1,30)= 0.45, P=0.50; Sex x Genotype Interaction: F(1,30)=0.007, P=0.93
Interaction Time	Genotype & Interaction Target (familiar vs. stranger)	3-way rmANOVA: Main effect of Sex: F(1,30)=0.004, P=0.94; Main effect of Genotype: F(1,30)=0.56, P=0.45; Main effect of Target: F(1,30)=4.16, P=0.05; Sex x Genotype Interaction: F(1,30)=0.10, P=0.74; Sex x Target Interaction: F(1,30)=3.35, P=0.07; Genotype x Target Interaction: F(1,30)=1.68, P=0.20; Sex x Genotype x Target Interaction: F(1,30)=0.17, P=0.67
	Effect of Target within each Genotype	Planned Comparisons; A: **P<0.05**; B: P=0.60
	Effect of Gentoype (WT vs. KO) within each Target	Planned Comparisons; Familiar Target: P=0.87; Novel: P=0.23
Social Interaction with Juvenile N = 18		
Interaction Time	Sex, Genotype & Trial	3-way rmANOVA; Main effect of Sex: F(1,32)=1.46, P=0.23; Main effect of Genotype: F(1,32)=0.502, P=0.48; Main effect of Trial: F(1,32)=138.76, **P<0.000001**; Sex x Genotype: F(1,32)=1.00, P=0.32; Sex x Trial Interaction: F(1,32)=0.008, P=0.92; Genotype x Trial Interaction: F(1,32)=3.88, P=0.05; Sex x Genotype x Trial Interaction: F(1,32)=1.175, P=0.28
	Trial (Initial vs. Recognition) within each Genotype	Planned Comparisons; A: **P<0.00001**; B: **P<0.00001**
Locomotor Habituation N = 19		
Total Beam Breaks	Sex, Genotype, & Bin	3-way rmANOVA; Main effect of Sex: F(1,34)=0.32, P=0.57; Main effect of Genotype: F(1,34)=0.49, P=0.48; Main effect of Trial: F(7,782)=41.30, **P<0.000001**; Sex x Genotype Interaction: F(1,34)=0.06, P=0.80; Sex x Trial Interaction: F(7,782)=1.09, P=0.34; Genotype x Trial: F(7,782)=1.21, P=0.22; Sex x Genotype x

		Trial Interaction: F(7,782)=0.88, P=0.61
1st bin only	Genotype & Sex	2-way ANOVA; Main effect of Sex: F(1,34)=2.28, P=0.14; Main effect of Genotype: F(1,34)=4.43, **P<0.05**; Sex x Genotype Interaction: F(1,34)=0.09, P=0.76
Stereodypy Beam breaks	Sex, Genotype, & Bin	3-way rmANOVA; Main effect of Sex: F(1,34)=0.45, P=0.50; Main effect of Genotype: F(1,34)=1.99, P=0.16; Main effect of Trial: F(7,782)=21.07, **P<0.000001**; Sex x Genotype Interaction: F(1,34)=1.07, P=0.30; Sex x Trial Interaction: F(7,782)=1.16, P=0.27; Genotype x Trial: F(7,782)=0.72, P=0.81; Sex x Genotype x Trial Interaction: F(7,782)=0.72, P=0.82
Ambulatory Beam Breaks	Sex, Genotype, & Bin	3-way rmANOVA; Main effect of Sex: F(1,34)=1.03, P=0.31; Main effect of Genotype: F(1,34)=2.07, P=0.15; Main effect of Trial: F(7,782)=39.29, **P<0.000001**; Sex x Genotype Interaction: F(1,34)=0.001, P=0.96; Sex x Trial Interaction: F(7,782)=1.07, P=0.36; Genotype x Trial: F(7,782)=1.42, P=0.08; Sex x Genotype x Trial Interaction: F(7,782)=0.89, P=0.60
Rotarod N = 19		
Time to Fall Off	Sex, Genotype & Trial	3-way rmANOVA; Main effect of Sex: F(1,34)=7.17,**P<0.02**; Main effect of Genotype: F(1,34)=6.95, **P<0.02**; Main effect of Trial: F(7,238)=11.71, **P<0.000001**; Sex x Genotype Interaction: F(1,34)=0.45, P=0.50; Sex x Trial Interaction: F(7,238)=0.51, P=0.82; Genotype x Trial: F(7,238)=1.60, P=0.13; Sex x Genotype x Trial Interaction: F(7,238)=1.88, P=0.07
	WT vs. KO within each gender	Planned Comparisons: Within Females: **P<0.05**; Within Males: P=0.162
	Males vs. Females within each genotype	Planned Comparisons: Within WT: **P<0.05**; Within KO: P=0.164
Prepulse Inhibition N = 18		
Initial Startle Response	Sex & Genotype	2-way ANOVA; Main effect of Sex: F(1,32)=0.15, P=0.69**;** Main effect of Genotype: F(1,32)=0.04, P=0.83; Sex x Genotype Interaction: F(1,32)=0.12, P=0.72
Second Set Startle	Sex & Genotype	2-way ANOVA; Main effect of Sex: F(1,32)=0.01, P=0.91 **;** Main effect of Genotype: F(1,32)=0.01,

Response		P=0.89; Sex x Genotype Interaction: F(1,32)=0.08, P=0.77
Third Set Startle Response	Sex & Genotype	2-way ANOVA; Main effect of Sex: F(1,32)=0.002, P=0.95**;** Main effect of Genotype: F(1,32)=0.008, P=0.92; Sex x Genotype Interaction: F(1,32)=0.0, P=0.99
Startle habituation	Sex, Genotype & Trial	3-way rmANOVA; Main effect of Sex: F(1,32)=0.02, P=0.87; Main effect of Genotype: F(1,32)=0.02, P=0.88; Main effect of Trial: F(2,64)=6.16, **P<0.03**; Sex x Genotype Interaction: F(1,32)=0.05, P=0.81; Sex x Decibel Interaction: F(2,64)=1.13, P=0.32; Genotype x Decibel Interaction: F(2,64)=0.09, P=0.90; Sex x Genotype x Decibel Interaction: F(2,64)=0.81, P=0.44
Prepulse Inhibition	Sex, Genotype & Decibel	3-way rmANOVA; Main effect of Sex: F(1,34)=5.85, **P<0.03**; Main effect of Genotype: F(1,34)=3.06, P=0.08; Main effect of Trial: F(2,64)=54.86, **P<0.0001**; Sex x Genotype Interaction: F(1,34)=5.50, **P<0.03**; Sex x Trial Interaction: F(2,64)=0.03, P=0.96; Genotype x Trial Interaction: F(2,64)=0.20, P=0.81; Sex x Genotype x Trial Interaction: F(2,64)=1.14, P=0.32
	WT vs. KO	Planned Comparisons: Females (WTvsKO): P<0.01; Males(WTvsKO): P=0.65
	Males vs. Females	Planned Comparisons: WT (MvsF): P= 0.95 KO(MvsF): P<.01
Startle Threshold N = 18		
Startle Response	Sex, Genotype & Decibel	3-way rmANOVA; Main effect of Sex: F(1,32)=0.19, P=0.65; Main effect of Genotype: F(1,32)=0.008, P=0.92; Main effect of Trial: F(5,160)=34.95, **P<0.0001**; Sex x Genotype Interaction: F(1,32)=0.47, P=0.49; Sex x Decibel Interaction: F(5,160)=0.25 P=0.93; Genotype x Decibel Interaction: F(5,160)=0.03, P=0.99; Sex x Genotype x Decibel Interaction: F(5,160)=0.34, P=0.88
Marble Burying N = 19		
Number of Marbles Buried	Sex & Genotype	2-way ANOVA; Main effect of Sex: F(1,34)=0.01, P=0.90; Main effect of Genotype: F(1,34)=58.20, **P<0.000001**; Sex x Genotype Interaction: F(1,34)=0.19, P=0.66
Grooming (9-18weeks old) N=19		

Time Spent Grooming	Sex and Genotype	2-way ANOVA: Main effect of Sex:F(1,34)=2.04, P=0.16 ; Main effect of Genotype: F(1,34)= 0.36, P=0.54; Sex x Genotype Interaction: F(1,34)=0.03, P=0.85
Number of Bouts	Sex and Genotype	2-way ANOVA: Main effect of Sex:F(1,34)=0.17, P=0.67 ; Main effect of Genotype: F(1,34)= 1.32, P=0.25; Sex x Genotype Interaction: F(1,34)=0.25, P=0.62
Time per Bout	Sex and Genotype	2-way ANOVA: Main effect of Sex:F(1,34)=1.92, P=0.17 ; Main effect of Genotype: F(1,34)= 0.44, P=0.50; Sex x Genotype Interaction: F(1,34)=0.88, P=0.35
Grooming (10-13months old) N=16		
Time Spent Grooming	Sex and Genotype	2-way ANOVA: Main effect of Sex:F(1,28)=0.62, P=0.43 ; Main effect of Genotype: F(1,28)= 4.69, **P<0.04**; Sex x Genotype Interaction: F(1,28)=1.61, P=0.21
Number of Bouts	Sex and Genotype	2-way ANOVA: Main effect of Sex:F(1,28)=1.13, P=0.29 ; Main effect of Genotype: F(1,28)= 1.86, P=0.18; Sex x Genotype Interaction: F(1,28)=0.53, P=0.47
Time per Bout	Sex and Genotype	2-way ANOVA: Main effect of Sex:F(1,28)=1.60, P=0.21 ; Main effect of Genotype: F(1,28)= 6.00, **P<0.03**; Sex x Genotype Interaction: F(1,28)=2.44, P=0.12
Ultrasonic Vocalizations (10-13months old) N=8		
Latency to call	Genotype	1-way ANOVA; Main effect of Genotype: F(1,14)=0.14, P=0.71
Number of calls	Genotype	1-way ANOVA; Main effect of Genotype: F(1,14)=0.40, P=0.52

ANOVA: analysis of variance, WT: wildtype, rmANOVA: ANOVA (between subjects factors are generally sex and genotype) with repeated measures (day, time, or trial). F(x,y): F ratio statistic is used to determine whether the variances in two independent samples are equal, x,y are degrees of freedom (df). Degrees of freedom is a measure of the number of independent pieces of information on which the precision of a parameter estimate is based. x = number of groups-1, y = number of animals per group minus 1, multiplied by the number of groups.

CHAPTER THREE
Results

Autism-associated insertion mutation (InsG) of *Shank3* exon 21 causes impaired synaptic transmission and behavioral deficits

Submitted and In Review: Speed, H.E., Kouser, M., Xuan, Z., Reimers, J.M., Ochoa, C.F., Gupta, N., Liu, S., Powell, C.M. Autism-associated point mutation (InsG) of *Shank3* exon 21 causes impaired synaptic transmission and behavioral deficits. J Neuroscience (In Revision)

Introduction

Shank3 is a postsynaptic scaffolding protein (Boeckers et al., 1999a; Boeckers et al., 2005; Boeckers et al., 1999b) with roles in spine shape/maturation (Durand et al., 2012; Roussignol et al., 2005), localization of glutamate receptors (Naisbitt et al., 1999; Roussignol et al., 2005; reviewed in Sheng and Kim, 2000; Uchino et al., 2006), and growth cone motility (Durand et al., 2012; Naisbitt et al., 1999). Mutations and copy number variants of *SHANK3* have been implicated in patients with idiopathic autism (Chen et al., 2010; Durand et al., 2007; Gauthier et al., 2009; Kolevzon et al., 2011; Moessner et al., 2007; Soorya et al., 2013; reviewed in Uchino and Waga, 2013; Waga et al., 2011) and Phelan-McDermid Syndrome (Bonaglia et al., 2011; Bonaglia et al., 2001; Phelan and McDermid, 2012; Phelan, 2008; Sarasua et al., 2011; Wilson et al., 2003), making *SHANK3* deletion/mutation among the most prevalent genetic causes of autism.

Multiple labs have attempted to delete *SHANK3* in mice by targeting regions of the gene with none deleting all isoforms (Bozdagi et al., 2010; reviewed in Jiang and Ehlers, 2013; Kouser et al., 2013; Peca et al., 2011; Wang et al., 2011b; Yang et

al., 2012). Failure to delete all isoforms of Shank3 is likely due to the presence of multiple promoters and within the gene (Lim et al., 1999; Zhu et al., 2014). While each of these models has some construct validity, none represents an accurate mimic of a human *SHANK3* mutation.

Because of these difficulties, we sought to mimic an autism-associated mutation in the *SHANK3* gene in a mouse model by targeting an autism-associated guanine nucleotide insertion mutation (*Shank3*^{G}) in exon 21 found in two brothers with autism, but not in their unaffected brother (Durand et al., 2007). This mutation causes a frameshift and a premature STOP codon in exon 21, theoretically encoding a truncated Shank3 protein lacking the C-terminal region (Durand et al., 2007; Durand et al., 2012). Overexpression of this theoretical truncated Shank3 has been shown to alter synaptic transmission and dendritic spine morphology in cultured neurons (Durand et al., 2012).

We also sought to create a *Shank3* mutant that might be genetically rescued to wild-type at various times during development and in selected brain regions when crossed with inducible or brain-region-specific cre-recombinase lines. Thus, we knocked in the insertion mutant exon 21 upstream of the wild-type exon 21, inserting a transcriptional STOP (neo-STOP) cassette after the mutant exon 21 to prevent exon skipping or splicing out of the mutant exon 21 (Dragatsis and Zeitlin, 2001; Guy et al., 2007). To make this genetically reversible, loxP sites were inserted on both sides of the insertion mutant exon 21 and Neo-STOP cassette, allowing for deletion of the mutant exon/neo-STOP cassette and reversion to wild-type *Shank3* upon activation of

cre-recombinase. This manuscript focuses on phenotyping this novel mutant, while future studies will be aimed at validating and studying genetic reversal in the model. We have identified behavioral, biochemical, and electrophysiologic phenotypes in this novel autism model. These findings set the stage for future studies designed to define the critical periods and brain regions involved in these *Shank3* insertion mutant phenotypes.

Methods

Construction of genetically reversible exon 21 insertion mutant targeting vector

To create a targeting vector with a single nucleotide insertion mutation in exon 21 of the S*hank3* gene followed by a transcriptional stop (Neo-stop) cassette (Dragatsis and Zeitlin, 2001), the e21-Neo-stop cassette was assembled by combining a wild-type *Shank3* exon 21 and PGK-Neo gene cassette with the His3-SV40 pA sequences in pBluescript II SK (+/-) plasmid (see Figure 3.1) (Dragatsis and Zeitlin, 2001; Guy et al., 2007). Two loxP sequences in the same orientation flanked the e21-Neo-stop sequence. Then, the plasmid was subjected to site-directed mutagenesis *in vitro* using Quick Change XL Site-directed Mutagenesis Kit (Stratagene, La Jolla, CA) with PCR mutation primers of e21PM-sense (PM for point mutant) (CAGCAATGGGCAGGAGCCCAGCAGGCTGGGGGGCTGAAGAGGAGC) and e21PM-antisense (GCTCCTCTTGCAGCCCCCCAGAATGCTGGGCTCCTGCCCATTGCTG) to generate the plasmid containing exon 21 with single nucleotide insertion mutation and Neo-stop cassette (G-Neo-stop cassette). The insertion mutation is designed to

mimic an insertion mutation identified in two brothers with autism with an extra "G" inserted into exon 21 (Durand et al., 2007) and located at position #3728 of mouse mRNA of S*hank3*. This results in a frameshift and premature stop codon downstream of the mutation in exon 21. The G-Neo-stop cassette was inserted into a unique Bgl II site located within intron 20 near exon 21 of a 7.0 kb genomic *Shank3* fragment containing a portion of intron 20, exon 21 and a portion of intron 21 in pBluescript II SK (+/-). This insertion made a 1.3 kb 5' flanking homology fragment and a 5.7 kb 3' flanking homology fragment. To enrich for targeting clones by negative selection, a DT (diphtheria toxin) gene cassette was cloned adjacent to the 5' end of the 5' homology in the plasmid. The Neo portion of the Neo-stop cassette provided a positive selection marker for targeting clones (Dragatsis and Zeitlin, 2001; Guy et al., 2007).

Gene targeting

The targeting vector DNA was linearized by Not1 and introduced by electroporation into SM-1 (129Sv/Evs6) embryonic stem (ES) cells grown on mitomycin-C-treated G418-resistant primary mouse embryonic fibroblasts. DNA was purified from the ES cells and analyzed by Southern blotting with a probe that distinguished between the targeting and wild-type *Shank3* alleles. ES cells from 3 correct clones were injected into the blastocoel cavity of E3.5 C57BL6 embryos using standard procedures. The chimeric males with > 90% agouti coat color on black background were bred with 6 week old females of wild-type C57BL6J. The *Shank3*^{G} mutation mice were crossed with wild-type C57BL6J mice more than 4 times.

Genotyping

Routine genotyping was performed using PCR (4’ min denaturation at 98°C, followed by 25 cycles consisting of 30s denaturation at 98°C, 30s annealing at 69°C and 25s extension at 72°C using iProof kit from Bio-Rad, Hercules, CA) with the following 2 primers: 21M-loxp1-sequence-sense (CTGTTGGTGTCAGTTCTTGCAGATG, in intron 20) and 21M-sequence-loxp2-antisense (CAAGGATGCTGGCCATTGAATGGCTTC, in exon 21). This PCR reaction generated a 596 bp product for wild-type S*hank3* allele, a 638 bp product for Shank3-G-stop allele and a 680 bp product for recombined *Shank3* allele following cre-mediated recombination.

Biochemistry

Western blotting was performed as previously described (Kouser et al., 2013). Synaptic protein levels from 7 littermate triplets (WT/*Shank3*$^{WT/G}$/*Shank3*$^{G/G}$, 5-6 months old) were determined by immunoblotting whole hippocampal tissue homogenized in artificial cerebrospinal fluid, 5mM EDTA, and 1X Halt protease and phosphatase inhibitor cocktail (Thermo Scientific, Waltham, MA) diluted from 100X stock solution. 10 µg of protein were loaded per lane and blotted with antibodies for synaptic proteins and internal loading controls (β-actin). An Image Works film processor was used to develop films and the chemiluminescence signals were quantified, normalized, and analyzed using ImageJ, Image Studio and Microsoft Excel.

For synaptosome preparation, all steps were performed at 4 C° or on ice and all buffers contained protease and phosphatase inhibitors (Thermo Scientific, Waltham, MA), as previously described (Kouser et al., 2013). Mice were sacrificed by live decapitation and rapidly dissected hippocampi were homogenized in Syn-Per (Thermo Scientific, Waltham, MA), ~1 mL/100 mg tissue. Samples were centrifuged at 1,200 x g for 10 min. The resulting supernatant was then centrifuged at 15,000 x g for 20 min. Pellets (synaptosomes) were resuspended in buffer B (3 mM sucrose in 6 mM Tris pH 8.0) with 1% sodium dodecyl sulfate (SDS), briefly sonicated, and flash frozen in liquid nitrogen. Samples were stored long-term at -80°C and protein concentration was quantified by DC Protein Assay (Bio-Rad, Hercules, CA).

Behavioral Overview

Behavioral tests were performed on a cohort of age and sex-matched littermate progeny of heterozygous matings (6 female WT/het/homo, 9 male WT/het/homo, 2 female WT/het, 2 male WT/het, and 4 male WT/homo pairs) (WT: n = 23, $Shank3^{WT/G}$: n = 19, $Shank3^{G/G:}$ n = 19) during the light cycle of the mice. All mice were born within 10 weeks of each other and generally only one pair or triplet came from any given individual litter of mice. Behaviors were tested at 2-6 months of age by an experimenter blind to genotype in the following order: elevated plus maze, dark/light, open field, locomotor, grooming, marble burying, rotarod, nesting behavior, Morris water maze, and visible water maze.

Three-box social interaction test was conducted in a separate cohort of age and sex-matched littermate progeny of heterozygous matings (5 female WT/*Shank3*$^{WT/G}$/*Shank3*$^{G/G}$, 6 male WT/*Shank3*$^{WT/G}$/*Shank3*$^{G/G}$, 2 female WT/*Shank3*$^{WT/G}$ littermate pairs, 2 male WT/*Shank3*$^{WT/G}$ pairs, 3 female WT/*Shank3*$^{G/G}$ pairs and 1 male WT/*Shank3*$^{G/G}$ pair) (WT: n = 19, *Shank3*$^{WT/G}$: n = 15, *Shank3*$^{G/G}$: n = 15).

Behavioral results are described out of the order in which they were tested to simplify presentation of the data. Statistical analyses of behavioral data were conducted using Statistica software (Version 10, Statsoft, Tulsa, OK) using either two-way ANOVAs or three-way repeated measures ANOVA using genotype and sex as the main variables and trial as the repeated measure, where applicable. Post-hoc Tukey's Honest Significant Difference test for unequal N was applied for significant effects and interactions. For detailed numerical statistical results see Table 2.

Elevated Plus Maze

Mice were placed in the center of a white Plexiglas elevated plus maze (each arm 33 cm long and 5 cm wide with 15 cm high black Plexiglas walls on closed arms) and allowed to explore for 5 min (Powell et al., 2004). The test was conducted in dim white light (~7 lux). Mice were monitored using CleverSys TopScan Software (Reston, VA) and time spent in and entries into the open and closed arms were measured. Data were analyzed using two-way ANOVA with genotype and sex as between-subject factors.

Dark-Light

Dark/light test was performed as described previously (Powell et al., 2004). Briefly, the dark/light apparatus consisted of two chambers (each chamber 25 cm x 26 cm), one brightly lit (~1700 lux) and the other kept dark with a small door (7 x 7 cm) separating the two. Mice were habituated for two min in the dark side, the door was opened, and then mice were allowed to move freely between the two sides for 10 min. Time spent in and the number of entries into each side was measured along with locomotor activity using photobeams monitored by Med PC IV data acquisition software (St. Albans, VT). Data were analyzed using two-way ANOVA with genotype and sex as between-subject factors.

Open Field

The open field test was performed as described (Blundell et al., 2009; Powell et al., 2004) with the exception of the data acquisition software. Mice were monitored using CleverSys TopScan Software after being placed in a white plastic arena (48x48x48cm) for 10 min. Time spent in and number of entries into the center of the arena (15 x15 cm) as well as locomotor activity. The test was conducted in dim white light (~7 lux). Data were analyzed using two-way ANOVA with genotype and sex as between-subject factors.

Locomotor

Locomotor activity was tested by placing the mice in a fresh home cage with minimal bedding and monitoring their activity for two hours using photobeams linked to a computer with data acquisition software (San Diego Instruments, San Diego, CA) (Powell et al., 2004). The test was conducted in the dark. Three-way repeated measures ANOVA was used to analyze the data with genotype and sex as between-subject factors and time as a within-subject factor.

Grooming

Mice were placed in a novel home cage without bedding and time spent grooming the face, head, or body was measured for 10 min. Number of grooming bouts that lasted more than 1 s was also recorded. Time per bout was calculated by dividing the total time spent grooming by the number of grooming bouts initiated. Each grooming parameter described above was then analyzed using two-way ANOVA with genotype and sex as between-subject factors.

Marble Burying

As previously described (Blundell et al., 2010a), twenty marbles were evenly placed around the edges of a novel home cage with 5 cm of bedding and mice were given 30 min in the cage. After 30 min the number of marbles buried was recorded. A marble was defined as buried when less than 25% of the marble was visible. The test room was well lit (~80 lux). Data were analyzed using two-way ANOVA with genotype and sex as between-subject factors.

Accelerating Rotarod

Coordination and motor learning were tested using a rotarod as previously described (Powell et al., 2004). Mice were placed on a stationary rotarod (IITC Life Sciences, Woodland Hills, CA) in a well lit room which was then activated and accelerated from 0-45 revolutions per min over 5 min. The latency for mice to fall off the rod or take one revolution was measured. Trials were repeated 4 times with inter-trial intervals of 30 min over a single day. Data were analyzed using three-way repeated measures ANOVA with genotype and sex as between-subject factors and trials as a within-subject factor.

Nesting

Nesting behavior was performed in a well-lit (~80 lux) room by first habituating the mouse to a novel home cage with approximately 1.5 cm of bedding for 15 min, and then a cotton nestlet (5.5 x5.5 x 0.5 cm) was put in the cage. Height and width of the nests were measured at 30 min, 60 min and 90 min (Etherton et al., 2009). Data were analyzed using two-way ANOVA with genotype and sex as between-subject factors.

Morris Water Maze

The Morris water maze task was conducted as previously described (Powell et al., 2004; Tabuchi et al., 2007). Briefly, a white, circular pool 1.2 m in diameter was

filled with water (22^{o}C ± 1^{o}C) made opaque with non-toxic, "gothic white" liquid tempera paint, and a circular platform (10 cm in diameter) was submerged ~1 cm beneath the surface of the water. The testing room was well lit (~80 lux) and filled with a number of extra-maze cues. Training was conducted over 9 consecutive days with 4 trials/day and an inter-trial interval of ~1-1.5 min. Mice were placed pseudo-randomly into each of 4 starting locations for each of 4 daily training trials. In each trial, mice swam until they found the hidden platform or were guided to it by the experimenter if not found within 60 s. Mice remained on the platform for 15 s before being removed to their home cage. Daily data were averaged across the 4 trials. A probe trial was conducted on day 10; the hidden platform was removed, and mice were placed in the pool and allowed to swim for 60 s. For reversal water maze training, training resumed the next day following the probe trial for 5 days with the platform in the opposite quadrant of the maze; on the sixth day, a second probe trial was administered. Data were analyzed using three-way repeated measures ANOVA with genotype and sex as between-subject factors and trial days as a within-subject factor for training. For probe trials, quadrant or platform location was used as the within-subject factor.

Three Chambered Social Approach

Social vs. inanimate object preference and preference for social novelty analyses were performed in a three chambered box with small openings connecting the chambers as described (Blundell et al., 2009) and based to a large extent on the

original descriptions (Moy et al., 2004; Nadler et al., 2004) . The test was conducted in dim white light (~7 lux). The mouse behavior was monitored objectively using CleverSys TopScan Software (Reston, VA). This test consisted of three, 10-min trials. During the first trial, the mouse was allowed to explore the entire apparatus with empty cages in each end chamber. In the second trial, the mouse was given a choice between an inanimate cage and a caged, social target. For the third trial, the mouse was given a choice between a caged, novel social target vs. a caged, familiar social target. Locations of empty cages and social targets were counterbalanced and mice were placed back into their home cage for very brief intervals between trials. Data were analyzed using three-way mixed ANOVA with genotype and sex as between-subject factors and target as a within-subject factor.

Electrophysiology

Male mice (4-6 weeks old) were anaesthetized with 8% chloral hydrate (400 mg/kg) then transcardially perfused with artificial cerebral spinal fluid (ACSF) and the brains rapidly removed and placed in ice-cold dissection ACSF containing sucrose. Acute coronal slices 300-400μm thick were made using a VT1000s Vibratome (Leica Biosystems, Buffalo Grove, IL). Slices containing dorsal hippocampus were allowed to recover at 35°C ± 0.5^{o}C for 30 min in normal ACSF and slowly cooled to room temperature over a 30-45 min period for holding prior to recording. A cut was made between CA3-CA1 to prevent recurrent excitation and epileptiform activity during recordings. All recordings were performed at 32°C ± 0.5^{o}C with a flow rate of 3-5mL/min.

Data were collected using Clampex (pClamp software suite version 10.3; Molecular Devices, Sunnyvale, CA). CA3-CA1 synapses were stimulated by a 100 μs biphasic pulse placed 400–500 μm laterally from the recording electrode. The distance between the recording electrode and the stimulating electrode was kept constant within these bounds.

Extracellular "field" recordings

Field excitatory postsynaptic potentials (fEPSPs) were evoked using a biphasic pulse through a custom-made monopolar nichrome stimulating electrode for highly focal stimulation and a narrow stimulus artifact. Stimulating and recording electrodes (1-3MΩ) were placed in the *stratum radiatum* 400-500 μm apart. All extracellular recordings were performed using dual-well submersion slice electrophysiology chambers (Fine Science Tools, Foster City, CA or Automate Scientific, Berkeley, CA). Data were collected at 10 kHz and filtered at 1 kHz using Model 1800 amplifiers (A-M Systems, Sequim, WA) and Clampex v10.3 data acquisition software (Molecular Devices, Sunnyvale, CA). Stimulation was controlled via Model 2100 stimulus isolators (A-M Systems, Sequim, WA). Sample size (*n*) indicates number of slices, with no more than two slices reported per mouse.

Input/output (I/O) curves were generated by sequential 50 μA steps from 0- 350 μA and the amplitude of the resulting fiber volley (FV), as well as the initial fEPSP slope (10-40 %) were measured. Frequency of stimulation was 0.05 Hz, which does not

induce plasticity. Each data point is the average of five consecutive traces at the same stimulus intensity.

Paired-pulse ratio (PPR) was measured at 0.05 Hz with interstimulus intervals 30-500 ms in pseudo-random order to prevent induction of plasticity (50, 500, 100, 80, 200, 30 ms). Immediately prior to each experiment, stimulus intensity was set at 50 % of the maximum fEPSP and adjusted to prevent epileptiform activity at the shorter interstimulus intervals. Once set, stimulus intensity did not change during the course of the experiment. The average of 5 trials at each interstimulus interval is reported per slice.

Long-term potentiation (LTP) was induced with either 1 train or 4 trains of 100Hz for 1s, separated by 20 s. A 20 min baseline was recorded prior to stimulation and followed by 60 min of 0.05 Hz stimulation. Stimulus intensity was set to generate 50 % of the maximum fEPSP and did not change during the course of the experiment. The average amount of LTP (% LTP) was determined at 55-60 min post-induction, relative to the 10 min immediately preceding LTP induction.

mGluR-LTD was induced by application of 100 μM DHPG for 10 min followed by a 20 min wash-out. Stimulus intensity was set at 75-85 % of the maximum fEPSP slope according to I/O curves performed immediately before each experiment and did not change during the course of the experiment. The mean magnitude of LTD (% LTD) was determined at 55-60 min following the start of DHPG washout and normalized to the last 10 min of the baseline period immediately preceding DHPG application.

Whole-cell patch clamp recordings

Excitatory postsynaptic currents (ESPCs) were recorded in voltage-clamp from CA1 pyramidal neuron cell bodies visually identified at 80X magnification using an AxioExaminer D1 Differential Interference Contrast (DIC) microscope (Zeiss, Thornwood, New York). Borosilicate glass electrodes (4-6 MΩ) were filled with internal pipette solution containing (in mM): 110 CsMethanesulfonate, 15 CsCl, 8 NaCl, 10 TEA-Cl, 2 EGTA, 10 HEPES, 3 QX 314, 2 ATP, 0.3 GTP. Observed junction potential was ~10mV and was compensated in each experiment. Cells with more than 25% change in either access resistance (15-25 MΩ) or holding current were not included in analysis. Data were collected at 10 kHz and filtered at 1-3 kHz using Mutliclamp 700B amplifiers, a Digidata 1440 digitizer, and Clampex v10.3 data acquisition software (Molecular Devices, Sunnyvale, CA). Stimulation was controlled via a Model 2200 stimulus isolator (A-M Systems, Sequim, WA) though a monopolar tungsten microelectrode (FHC, Bowdoin, ME) with a 0.1ms biphasic pulse. All experiments were performed in the presence of 100 μM picrotoxin. Sample size (*n*) indicates number of cells, with no more than 5 cells reported per mouse and 5 or more mice per genotype.

For NMDA/AMPA, stimulus intensity (230-250 μA) was set to generate a 200-500 pA EPSC at -70mV holding potential. Once a stable 5-10 min baseline was achieved, 20 consecutive traces were obtained at -70 mV holding potential and at +40 mV holding potential at 0.1 Hz. The NMDA/AMPA ratio was taken as the ratio of primarily NMDA receptor-mediated EPSCs at 40 s after stimulus onset at +40 mV to

the peak of the primarily AMPA receptor-mediated EPSCs 10-15 ms after stimulus onset at -70 mV.

Miniature spontaneous ESPCs (mEPSCs) were measured at -70 mV holding potential in the presence of picrotoxin and 1 µM TTX 5-10 minutes after break-in. Each cell was recorded for 15-20 min and a 5-min continuous trace was analyzed for frequency and amplitude (≥ 3 pA) using manual and automated analysis in Clampfit v10.3 (Molecular Devices, Sunnyvale, CA).

Raw traces were analyzed with Clampfit v10.3 (Molecular Devices, Sunnyvale, CA). Plotting and statistics were performed in GraphPad v6 (GraphPad Software, San Diego, CA). Results were considered significant if $P < 0.05$.

Solutions

ACSF contained (in mM): 120 NaCl, 3.5 KCl, 1.25 NaH_2PO_4, 1 $MgSO_4$, 26 $NaHCO_3$, 10 dextrose, and 2 $CaCl_2$. Dissection ACSF consisted of (in mM): 75 sucrose, 87 NaCl, 3 KCl, 1.25 NaH_2PO_4, 7 $MgSO_4$, 26 $NaHCO_3$, 20 dextrose, and 0.5 $CaCl_2$. All solutions were adjusted to pH 7.4 and saturated with 95 % O_2/5 % CO_2.

Drugs

Octahydro-12-(hydroxymethyl)-2-imino-5,9:7,10a-dimethano-10aH[1,3]dioxocino[6,5-d]pyrimidine-4,7,10,11,12-pentolTetrodotoxin (TTX, Tetrodotoxin), picrotoxin, N-(2,6-Dimethylphenylcarbamoylmethyl)triethylammonium chloride (QX 314), and (RS)-

3,5-Dihydroxyphenylglycine (DHPG) were obtained from Tocris Bioscience (Minneapolis, MN). CsMethanesulfonate and CsCl were obtained from Sigma-Aldrich (St. Louis, MO). All other reagents were obtained from Fisher Scientific (Waltham, MA).

Results

The Shank3^{G} mutation results in loss of predominant higher molecular weight Shank3 isoforms at hippocampal synapses.

To determine the effect of the *Shank3* mutation on Shank3 protein expression in the hippocampus, synaptosomes were isolated from hippocampus and subjected to Western blot analysis (n = 8 mice per genotype). As expected, there was a roughly 50 % decrease in Shank3 in *Shank3*$^{WT/G}$ mice and complete loss of Shank3 in *Shank3*$^{G/G}$ mice (Figure 3.2A), as identified with Shank3 C-terminal antibody (One-way ANOVA: $F_{2,21}$ = 89.75, P < 0.0001) and Shank3 N-terminal antibody (One-way ANOVA: $F_{2,21}$ = 68.31, P < 0.0001). Western blotting with the Shank3 N-terminal antibody revealed the appearance of a single novel band of ~90 kD (Band 1) in synaptoneurosomes from *Shank3*$^{WT/G}$ and *Shank3*$^{G/G}$ mice (Figure 3.2B. One-way ANOVA: $F_{2,21}$ = 34.92, P < 0.0001), in addition to the smaller ~75 kD band (Band 2) present in WT mice and unchanged in *Shank3*$^{WT/G}$ and *Shank3*$^{G/G}$ mice (Figure 3.2B. One-way ANOVA: $F_{2,21}$ = 1.18, P > 0.05).

Synaptic expression of glutamate receptors and Shank3-associated synaptic proteins in the hippocampus was unchanged in *Shank3*$^{WT/G}$ and *Shank3*$^{G/G}$ mice (Figure 3.2C). By western blot analysis of hippocampal synaptosomes, we found no

change in the expression of AMPA receptor subunits (GluA1 One-way ANOVA: $F_{2,21} = 0.21$, $P > 0.05$; GluA2 One-way ANOVA: $F_{2,21} = 0.26$, $P > 0.05$), or in the expression of NMDA receptor subunits (GluN1 One-way ANOVA: $F_{2,21} = 0.041$, $P > 0.05$; GluN2A One-way ANOVA: $F_{2,21} = 0.19$, $P > 0.05$; GluN2B One-way ANOVA: $F_{2,21} = 0.07$, $P > 0.05$). Expression levels of mGluR5, the primary mediator of mGluR-mediated long-term depression (mGluR-LTD) at CA3-CA1 synapses was also unchanged in *Shank3*$^{WT/G}$ and *Shank3*$^{G/G}$ mice (One-way ANOVA: $F_{2,21} = 0.09$, $P > 0.05$). Similarly, expression of the Shank3-associated postsynaptic proteins Homer1 b/c and PSD95 were not significantly changed in *Shank3*$^{WT/G}$ or *Shank3*$^{G/G}$ mice (Homer1 b/c One-way ANOVA: $F_{2,21} = 1.09$, $P > 0.05$; PSD95 One-way ANOVA: $F_{2,21} = 0.25$, $P > 0.05$).

We also found no change in glutamate receptor or Shank3-associated Homer1b/c expression in whole hippocampal lysates from *Shank3*$^{WT/G}$ or *Shank3*$^{G/G}$ mice (Figure 3.2D. GluA1 One-way ANOVA: $F_{2,21} = 0.59$, $P > 0.05$; GluA2 One-way ANOVA: $F_{2,21} = 0.84$, $P > 0.05$; GluN1 One-way ANOVA: $F_{2,21} = 0.09$, $P > 0.05$; GluN2A One-way ANOVA: $F_{2,21} = 0.23$, $P > 0.05$; GluN2B One-way ANOVA: $F_{2,21} = 2.29$, $P > 0.05$; mGluR5 One-way ANOVA: $F_{2,21} = 1.18$, $P > 0.05$; Homer1 b/c One-way ANOVA: $F_{2,21} = 0.17$, $P > 0.05$; PSD95 One-way ANOVA: $F_{2,21} = 1.29$, $P > 0.05$; $n = 8$ mice per genotype). Therefore, despite a loss of predominant higher molecular weight isoforms of Shank3 at hippocampal synapses, expression and trafficking of glutamate receptors and other scaffolding proteins remain intact.

Homozygous Shank3 mutants have impaired motor learning and coordination

We tested motor learning and coordination in these mice as motor abnormalities are commonly observed in autistic patients (Kopp et al., 2010; Nobile et al., 2011). *Shank3*$^{G/G}$ mice but not the *Shank3*$^{WT/G}$ mice exhibit impaired motor coordination/learning on the accelerating rotarod. *Shank3*$^{G/G}$ mice consistently displayed shorter latencies to fall from the rotarod apparatus and showed little to no improvement in motor learning over the duration of the trials while heterozygous mice were unaffected (Figure 3.3A. Three-way rmANOVA: Main effect of Genotype: $F_{2,55} = 20.37$, $P < 0.001$; Main effect of Trial: $F_{7,385} = 23.36$, $P < 0.001$; Genotype x Trial Interaction: $F_{14,385} = 1.25$, $P > 0.05$).

Homozygous Shank3 mutant mice exhibit an avoidance phenotype toward inanimate objects

We observed a novelty avoidance phenotype in the *Shank3*$^{G/G}$ mice in several behavioral tasks. When we measured nest-building by adding a nestlet to a novel cage following a habituation period, we found that *Shank3*$^{G/G}$ mice showed very little change in their nestlets while WT and *Shank3*$^{WT/G}$ littermates readily made nests from the material (Figure 3B and C. Three-way rmANOVA for Nest Width: Main effect of Genotype: $F_{2,55} = 4.60$, $P < 0.05$; Main effect of Time: $F_{2,110} = 23.64$, $P < 0.001$; Genotype x Time Interaction: $F_{4,110} = 0.71$, $P > 0.05$. Three-way rmANOVA for Nest Height: Main effect of Genotype: $F_{2,55} = 7.19$, $P < 0.05$; Main effect of Time: $F_{2,110} = 21.03$, $P < 0.001$; Genotype x Time Interaction: $F_{4,110} = 1.07$, $P > 0.05$).

Similar avoidance behavior was observed in the marble burying task which further confirmed our explanation that *Shank3*$^{G/G}$ mice have a novelty avoidance phenotype (Figure 3.3D). *Shank3*$^{G/G}$ mice showed little to no interest in burying marbles and in many cases left them undisturbed (Figure 3.3D. Two-way ANOVA: Main effect of Genotype: $F_{2,55} = 9.80$, $P < 0.001$; Tukey's HSD: WT vs. *Shank3*$^{WT/G}$: $P > 0.05$; WT vs. *Shank3*$^{G/G}$: $P < 0.001$) while *Shank3*$^{WT/G}$ mice show a strong trend toward burying less marbles than their WT littermates.

Homozygous Shank3 mutant mice exhibit aberrant locomotor activity in response to novelty

Shank3$^{G/G}$ mice demonstrate decreased locomotor activity in response to novel situations. When examining locomotor activity over 2 hours in a novel home cage, *Shank3*$^{G/G}$ mice demonstrated normal locomotor activity (Figure 3.3E. Three-way rmANOVA: Main effect of Genotype: $F_{2,55} = 0.38$, $P > 0.05$; Main effect of Trial: $F_{23,1265} = 105.79$, $P < 0.001$; Genotype x Trial Interaction: $F_{46,1265} = 1.72$, $P < 0.01$). However, when we analyzed the locomotor activity for the first 5 min in this novel home cage situation, *Shank3*$^{G/G}$ mice showed a significant decrease in locomotor activity that reverted to the WT level rapidly thereafter (Figure 3F. Two-way ANOVA: Main effect of Genotype: $F_{2,55} = 10.85$, $P < 0.001$).

Along the same lines, distance travelled in the novel open field arena over 10 min was decreased in *Shank3*$^{G/G}$ mice compared to WT littermate controls (Figure 3.3G. Two-way ANOVA: Main effect of Genotype: $F_{2,55} = 2.56$, $P > 0.05$; Tukey's

HSD: WT vs. *Shank3*$^{WT/G}$: $P > 0.05$; WT vs. *Shank3*$^{G/G}$: $P < 0.05$; *Shank3*$^{WT/G}$ vs *Shank3*$^{G/G}$: $P > 0.05$) and distance travelled in the elevated plus maze over 5 min was also decreased in the *Shank3*$^{G/G}$ mice (Figure 3.3H. Two-way ANOVA: Main effect of Genotype: $F_{2,55} = 4.83$, $P < 0.05$; Tukey's HSD: WT vs. *Shank3*$^{WT/G}$: $P > 0.05$; WT vs.*Shank3*$^{G/G}$: $P < 0.01$; *Shank3*$^{WT/G}$ vs *Shank3*$^{G/G}$: $P < 0.01$). Similarly, total number of photobeams interrupted during the 10 min in the dark/light chamber was decreased in *Shank3*$^{G/G}$ mice (Figure 3.3I. Two-way ANOVA: Main effect of Genotype: $F_{2,55} = 2.96$, $P > 0.05$; Tukey's HSD: WT vs. *Shank3*$^{WT/G}$: $P > 0.05$; WT vs. *Shank3*$^{G/G}$: $P < 0.05$; *Shank3*$^{WT/G}$ vs *Shank3*$^{G/G}$: $P < 0.05$). We interpret these data overall as a decrease in locomotor response to novel environments as the mutants clearly habituated normally over time (Figure 3.3E).

Shank3 mutant mice do not express an anxiety-like phenotype

Because there are several reports of children with autism suffering from anxiety disorders (Gillott et al., 2001; White et al., 2009a), we also tested *Shank3*^{G} mice in anxiety behaviors and found that these mice do not show an anxiety-like behavior in open field, elevated plus maze or dark light task. No anxiety-like phenotype was observed in the open field task as both *Shank3*$^{WT/G}$ and *Shank3*$^{G/G}$ mice spent the same amount of time in the center as their WT littermates (Figure 3.3J. Two-way ANOVA: Main effect of Genotype: $F_{2,55}=1.20$, $P > 0.05$). We also did not observe an increase in anxiety-related behavior in the elevated plus maze as all three

genotypes spent equal time in the open arms (Figure 3.3K. Two-way ANOVA: Main effect of Genotype: $F_{2,55} = 0.23$, $P > 0.05$).

Interestingly, there was a strong increase in the latency to enter the brightly lit side of the dark/light box for the *Shank3*$^{G/G}$ mice (Figure 3.3L. Two-way ANOVA: Main effect of Genotype: $F_{2,55} = 6.66$, $P < 0.01$). This is typically interpreted as an increase in anxiety-like behavior, however, there is no difference in the total time spent in either dark or light side of the chamber among the three genotypes (Figure 3.3M. Time spent in dark side, two-way ANOVA: Main effect of Genotype: $F_{2,55} = 0.87$, $P > 0.05$; Time spent in light side, two-way ANOVA: Main effect of Genotype: $F_{2,55} = 0.87$, $P > 0.05$), and no other anxiety-related task demonstrated a phenotype. Thus, it appears that *Shank3*$^{G/G}$ mice do not have an anxiety phenotype but may show an avoidance of the novel, brightly lit chamber initially, a finding consistent with their novelty avoidance phenotype observed in other behaviors.

Homozygous Shank3 mutants exhibit minimal spatial learning differences

Because Shank3 mutation/deletion is often associated with intellectual disability (Gong et al., 2012), we tested the *Shank3*^{G} mice in the Morris water maze task, a test of spatial learning and memory. *Shank3*$^{G/G}$ mice were significantly impaired in spatial learning compared to WT littermate controls whereas *Shank3*$^{WT/G}$ mice showed no deficit using latency to reach the hidden platform as a measure (Figure 3.4A. Three-way rmANOVA: Main effect of Genotype: $F_{2,53} = 3.83$, $P < 0.05$; Main effect of Day: $F_{8,424} = 38.03$, $P < 0.001$; Genotype x Day Interaction:

$F_{16,424}$ = 0.76, P < 0.05; see Table 2 for complete statistical results for all experiments). Interestingly, *Shank3*$^{WT/G}$ and *Shank3*$^{G/G}$ mice had significantly higher swim speed during training (Figure 3.4B. Three-way rmANOVA: Main effect of Genotype: $F_{2,53}$ = 36.66, P < 0.001; Main effect of Day: $F_{8,424}$ = 34.05, P < 0.001; Genotype x Day Interaction: $F_{16,424}$ = 9.79, P < 0.001). Using the distance travelled before reaching the hidden platform, a measure that eliminates swim speed as a factor, *Shank3*$^{G/G}$ exhibited significantly decreased learning while *Shank3*$^{WT/G}$ mice did not (Figure 3.4C. Three-way rmANOVA: Main effect of Genotype: $F_{2,53}$ = 5.61, P < 0.01; Main effect of Day: $F_{8,424}$ = 144.53, P < 0.001; Genotype x Day Interaction: $F_{16,424}$ = 5.58, P < 0.001). We also looked at the amount of time spent in thigmotaxis (swimming near the maze walls). Both *Shank3*$^{G/G}$ and *Shank3*$^{WT/G}$ mice spent the same amount of time in thigmotaxis as their WT littermate controls (Figure 3.4D. Three-way rmANOVA: Main effect of Genotype: $F_{2,53}$ = 0.99, P > 0.05; Main effect of Day: $F_{8,424}$ = 44.17, P < 0.001; Genotype x Day Interaction: $F_{16,424}$ = 1.48, P > 0.05). These findings suggest a deficit in spatial learning in the *Shank3*$^{G/G}$ mice.

Although *Shank3*$^{G/G}$ mice were slower to learn the water maze task, their spatial memory performance was unaffected during the initial probe trial. Both *Shank3*$^{G/G}$ and *Shank3*$^{WT/G}$ mice showed a significant preference for the target quadrant compared to the three other quadrants (Figure 3.4E), indicating that these mice were able to recall a previously learned spatial strategy. WT littermate controls showed a significant preference for the target quadrant compared to the opposite quadrant, demonstrating a spatial strategy to some degree as well, although the difference

between the target quadrant and the other two quadrants was not statistically significant (Figure 3.4E.Three-way rmANOVA: Main effect of Genotype: $F_{2,53}$ = $8.4x10^{-8}$, $P > 0.05$; Main effect of Quadrant: $F_{3,159} = 20.62$, $P < 0.001$; Genotype x Quadrant Interaction: $F_{6,159} = 0.89$, $P > 0.05$; Tukey's HSD for WT mice: TargetNW vs. OppositeSE: $P < 0.05$, TargetNW vs. RightNE: $P > 0.05$, TargetNW vs. LeftSW: $P > 0.05$; Tukey's HSD for *Shank3*$^{WT/G}$ mice: TargetNW vs. OppositeSE: $P < 0.001$, TargetNW vs. RightNE: $P < 0.05$,TargetNW vs. LeftSW: $P < 0.001$; Tukey's HSD for *Shank3*$^{G/G}$ mice: TargetNW vs. OppositeSE: $P < 0.001$, TargetNW vs. RightNE: $P < 0.01$, TargetNW vs. LeftSW: $P < 0.001$). Similarly, we analyzed the number of times the mice crossed the exact target platform location and corresponding locations in the other 3 quadrants and found similar results (Figure 3.4F. Three-way rmANOVA: Main effect of Genotype: $F_{2,53} = 1.56$, $P > 0.05$; Main effect of Quadrant: $F_{3,159} = 25.05$, $P < 0.001$; Genotype x Quadrant Interaction: $F_{6,159} = 1.36$, $P > 0.05$; Tukey's HSD for WT mice: TargetNW vs. OppositeSE: $P < 0.01$, TargetNW vs. RightNE: $P > 0.05$; TargetNW vs. LeftSW: $P > 0.05$; Tukey's HSD for *Shank3*$^{WT/G}$ mice: TargetNW vs. OppositeSE: $P < 0.001$, TargetNW vs. RightNE: $P < 0.001$; TargetNW vs. LeftSW: $P < 0.001$; Tukey's HSD for *Shank3*$^{G/G}$ mice: TargetNW vs. OppositeSE: $P < 0.001$, TargetNW vs. RightNE: $P < 0.01$, TargetNW vs. LeftSW: $P < 0.05$). Following the hidden platform water maze task, the mice were tested in a visible platform version of the water maze to rule out visual issues. The latency to reach a visible platform was unchanged in the mutants compared to WT littermate controls suggesting no change in visual acuity (not shown). Taken together,

the training and the probe data suggest that *Shank3*$^{G/G}$ mice are slightly slower to learn the water maze compared to WT littermate controls, but demonstrate significant use of a spatial strategy during subsequent recall.

Shank3 mutant mice do not display social interaction deficits

Social interaction deficits are one of the major characteristic features of autism (Mahjouri and Lord, 2012; Schreibman, 1988). Therefore we tested social behaviors in *Shank3*^{G} mice in the three chambered social interaction task. Much like their WT littermate pairs, *Shank3*$^{WT/G}$ mice, and *Shank3*$^{G/G}$ mice showed no preference for either side in the three chambered social interaction box prior to introduction of a social target (See Table 4). In the test for social vs. inanimate preference, all three genotypes spent more time interacting with the social target (Figure 3.4G. Three-way rmANOVA: Main effect of Genotype: $F_{2,43} = 0.144$, $P > 0.05$; Main effect of Target: $F_{1,43} = 6.01$, $P < 0.05$; Genotype x Target Interaction: $F_{2,43} = 0.02$, $P > 0.05$). Interestingly, none of the three genotypes individually demonstrated a significant preference for the social target (Figure 3.4G. Tukey's HSD for WT mice: $P > 0.05$; Tukey's HSD for *Shank3*$^{WT/G}$ mice: $P > 0.05$; Tukey's HSD for *Shank3*$^{G/G}$ mice: $P > 0.05$), making absolute interpretation of sociability difficult as even the WT mice did not show a preference. Similarly, an overall preference for the novel social target vs. familiar social target was observed in the test of preference for social novelty. Again post hoc tests revealed no significant social novelty preference in the individual groups (Figure 3.4H. Three-way rmANOVA: Main effect

of Genotype: $F_{2,43} = 0.07$, $P > 0.05$; Main effect of Target: $F_{1,43} = 4.52$, $P < 0.05$; Genotype x Target Interaction: $F_{2,43} = 31$, $P > 0.05$; Tukey's HSD for WT mice: $P > 0.05$; Tukey's HSD for *Shank3*$^{WT/G}$ mice: $P > 0.05$; Tukey's HSD for *Shank3*$^{G/G}$ mice: $P > 0.05$) making interpretation of preference for social novelty difficult.

Shank3 mutant mice show normal grooming

We also characterized grooming behavior in *Shank3*^{G} mice as a measure of repetitive, stereotyped behavior. *Shank3*$^{WT/G}$ mice and *Shank3*$^{G/G}$ mice do not exhibit an increase in total time spent grooming when compared to WT mice (Figure 3.4I. Two-way ANOVA: Main effect of Genotype: $F_{2,55} = 0.73$, $P > 0.05$). Similarly, no difference was observed in the number of grooming bouts (Figure 3.3J. Two-way ANOVA: Main effect of Genotype: $F_{2,55} = 0.97$, $P > 0.05$).

Synaptic transmission and plasticity are impaired in mice expressing the Shank3^{G} *mutation.*

We used extracellular (field) electrophysiology to understand how the *Shank3*^{G} mutation disrupts normal synaptic transmission and plasticity at hippocampal CA3-CA1 synapses. For our initial characterization, we focused on the hippocampus for its well-defined structure/function relationship and its role in learning and memory (Wallenstein et al., 1998).

Previously, we found that deletion of exon 21 in the *Shank3*$^{\Delta C/\Delta C}$ mouse causes a decrease in long-term potentiation (LTP) in response to a single 1s train at 100Hz (Kouser et al., 2013), a finding consistent among other Shank3 mutation mouse

models (Bozdagi et al., 2010; Wang et al., 2011a; Yang et al., 2012). We anticipated a similar LTP deficit in *Shank3*$^{G/G}$ mouse which also lacks the Homer binding region and results in loss of major higher molecular weight Shank3 isoforms. On the contrary, we observed a decrease only in the magnitude of post-tetanic potentiation (PTP) in the first five minutes following the conditioning stimulus (Figure 3.5A. One-Way ANOVA: $F_{2,28} = 6.62$, $P < 0.01$; WT $n = 13$, *Shank3*$^{WT/G}$ $n = 9$, *Shank3*$^{G/G}$ $n = 9$), but no change in the mean magnitude of LTP at one hour following the conditioning stimulus (Figure 3.5B. One-Way ANOVA: $F_{2,28} = 1.06$, $P > 0.05$). Believing this alteration in PTP magnitude may indicate a change in threshold for PTP induction, we used a stronger conditioning stimulus of 4 trains at 100Hz for 1s separated by 60 s (Figure 3.5C). In support of this hypothesis, the stronger stimulus elicited LTP that was similar in magnitude across all three genotypes (Figure 3.5D. One-Way ANOVA: $F_{2,22} = 0.09$, $P > 0.05$; WT $n = 7$, *Shank3*$^{WT/G}$ $n = 10$, *Shank3*$^{G/G}$ $n = 8$).

Because Shank3 binds to Homer, linking it to mGluRs, we also investigated the effect of the *Shank3*^{G} mutation on mGluR-LTD, a form of synaptic plasticity known to be disrupted in other mouse models of autism-associated disorders (Bateup et al., 2011; Bear et al., 2004; Bozdagi et al., 2012; Chevere-Torres et al., 2012). Accordingly, *Shank3*$^{G/G}$ mice exhibit a decrease in the magnitude of mGluR-LTD at 55-60 min after DHPG application (Figure 3.5E-F. One-Way ANOVA: $F_{2,25} = 5.35$, $P < 0.05$; WT $n = 7$, *Shank3*$^{WT/G}$ $n = 13$, *Shank3*$^{G/G}$ $n = 8$).

Basal synaptic transmission, in the absence of synaptic plasticity, was also impaired in *Shank3*$^{WT/G}$ and *Shank3*$^{G/G}$ mice. Input/output curves generated from

Shank3$^{WT/G}$ and *Shank3*$^{G/G}$ mice identified a decrease in fEPSP slope compared to WT (Figure 3.6A. Two-Way RM ANOVA: Genotype $F_{2,37} = 6.18$, $P < 0.01$; Stimulus Intensity $F_{7,259} = 98.43$, $P < 0.001$; Stimulus Intensity X Genotype $F_{14,259} = 6.41$, $P < 0.001$; WT $n = 16$, *Shank3*$^{WT/G}$ $n = 12$, *Shank3*$^{G/G}$ $n = 12$). Post-hoc analysis further indicates a significant decrease in fEPSP slope at stimulus intensities greater than 100 µA for both *Shank3*$^{WT/G}$ and *Shank3*$^{G/G}$ mice (Tukey's multiple comparisons, $P < 0.05$). Fiber volley amplitude, however, was not affected by the Shank3^{G} mutation (Two-Way rmANOVA: Genotype $F_{2,37} = 0.19$, $P > 0.05$; Stimulus Intensity $F_{7,259} = 82.61$, $P < 0.0001$; Genotype X Stimulus Intensity $F_{14,259} = 0.61$, $P > 0.05$) suggesting that the decrease in fEPSP slope in *Shank3*$^{WT/G}$ and *Shank3*$^{G/G}$ mice is not due to a decrease in the number of axons activated upon stimulation or in axon excitability.

Consistent with Shank3's postsynaptic locus, we observed similar paired-pulse ratio (PPR) in all three genotypes indicating no change in presynaptic function or short-term plasticity (Figure 3.6B. Two-Way rmANOVA: Genotype $F_{2,32} = 0.02$, $P > 0.05$; Interstimulus Interval $F_{5,160} = 154.4$, $P < 0.0001$; Genotype X Interstimulus Interval $F_{10,160} = 0.56$, $P > 0.05$; WT $n = 12$, *Shank3*$^{WT/G}$ $n = 8$,*Shank3*$^{G/G}$ $n = 15$). When we measured the relative contribution of NMDA and AMPA receptors to the EPSC, NMDA/AMPA ratio was decreased in *Shank3*$^{G/G}$ mice compared to WT (Figure 3.6C. One-Way ANOVA: $F_{2,60} = 4.88$, $P < 0.05$; Tukey's Multiple Comparisons: WT vs. *Shank3*$^{WT/G}$ $P > 0.05$, WT vs *Shank3*$^{G/G}$ $P < 0.01$; WT $n = 22$, *Shank3*$^{WT/G}$ $n = 18$, *Shank3*$^{G/G}$ $n = 23$). Because each experiment was normalized to the AMPA receptor component of the EPSC (200-500 pA), the decrease in

NMDA/AMPA ratio was most likely due to a decrease in the NMDA receptor-mediated component of the EPSC.

Finally, we measured the frequency and amplitude of miniature excitatory postsynaptic currents (mEPSCs) onto CA1 pyramidal neurons in the presence of 1 µM TTX (Figure 3.6D-H). Mean frequency of mEPSCs was decreased in *Shank3*$^{G/G}$ mice (Figure 6E. One-Way ANOVA: $F_{2,47} = 5.19$, $P < 0.01$; Tukey's multiple comparisons $P < 0.01$; WT $n = 15$, *Shank3*$^{WT/G}$ $n = 21$, *Shank3*$^{G/G}$ $n = 14$). The cumulative frequency of inter-event intervals was shifted rightward, also indicating longer periods between mEPSCs in *Shank3*$^{WT/G}$ and *Shank3*$^{G/G}$ mice. Mean amplitude of mEPSCs was unchanged in *Shank3*$^{G/G}$ and *Shank3*$^{G/G}$ mice (Figure 3.6G. One-Way ANOVA: $F_{2,47} = 0.12$, $P > 0.05$; WT $n = 15$, *Shank3*$^{WT/G}$ $n = 21$,*Shank3*$^{G/G}$ $n = 14$), as reflected in the similar cumulative distribution of mEPSC amplitudes (Figure 3.6H). Absence of a change in the largely AMPA receptor-mediated mEPSC amplitude further suggests that the decreased NMDA/AMPA ratio is due to decreased NMDA receptor-mediated responses.

Discussion

The *Shank3*$^{G/G}$ mouse is the first genetically accurate, potentially reversible *Shank3* mouse model of autism. This *Shank3*$^{G/G}$ mouse possesses a single nucleotide insertion that causes a frameshift and subsequent translational STOP codon identified in human idiopathic autism (Durand et al., 2007). The model also incorporates the potential to reverse the genetic mutation in future studies using cre recombinase. We

have identified clear synaptic and behavioral phenotypes in this model, setting the stage for genetic reversal experiments to determine developmental timeframes and brain-region specificity of these phenotypes.

Rather than resulting in a truncated Shank3 protein, the premature stop codon insertion mutation leads to a complete loss of multiple higher molecular weight Shank3 protein isoforms (150 kD and above) using both C-terminal and N-terminal Shank3 antibodies. In addition, there is appearance of a lower molecular weight Shank3 immunoreactive band between 75 and 100 kD that may represent a truncated Shank3 protein that likely starts from an internal promoter or has additional exons spliced out.

These biochemical findings largely mimic alterations in Shank3 isoforms identified in a Shank3 exon 21 deletion mouse model (Kouser et al., 2013). Both the present exon 21 insertion mutant and the exon 21 deletion mutant result in loss of higher molecular weight Shank3 isoforms at 150 kD and above. The exon 21 deletion also resulted in loss of a band between 100 and 150 kD that does not appear to be lost in the exon 21 insertion mutant model (Kouser et al., 2013). This slight difference in Shank3 isoform alteration may account for any phenotypic differences between the two models. We were not able to identify any alterations in multiple Shank3 direct or indirect interacting partners in the hippocampus in either this exon 21 insertion mutant or the previously published exon 21 deletion mutant (Kouser et al., 2013), perhaps due to compensatory action of Shank1 and Shank2 as both are also expressed in hippocampus .

Many aspects of the behavioral phenotypes between the exon 21 insertion mutant and the exon 21 deletion mutant model are strikingly similar, providing a replication of behavioral abnormalities in two similar models (Kouser et al., 2013). Both models demonstrated equivalent altered responses to novelty including avoidance of marbles, and increased initial locomotor response to novelty in locomotor apparatus, open field, and dark/light boxes. Furthermore, both models resulted in unusually long latencies to move from the dark side of dark/light boxes into the novel light side. In addition, both models exhibited significant differences in motor coordination ability on the accelerating rotarod. Finally, while the Morris water maze abnormality was subtle in the Shank3 exon 21 insertion mutation, both models demonstrated abnormalities in this task. Overall there is striking concordance in behavioral measure outcomes across the two models, likely due to the largely overlapping loss of corresponding Shank3 isoforms.

Alterations in nest building could be interpreted as supportive of altered response to novelty or as supporting the decreased motor coordination in the model. Anecdotally, mutant mice often completely avoided the nestlets upon their introduction. However, we cannot rule out the possibility that they were simply less effective nest builders.

Curiously, although the model has high construct validity for a human Shank3 mutation, it does not have complete face validity for every symptom of Phelan-McDermid Syndrome or for patients with autism due to Shank3 mutation/deletion. Behaviorally, the mutant mouse model recapitulates incoordination, intellectual

disability, and to some extent "insistence on sameness" due to abnormal behavior in response to novelty. It does not show abnormalities in social behavior, a core component of an autism diagnosis and a feature of many patients with Phelan-McDermid Syndrome. While it is intellectually satisfying when a genetic mouse model demonstrates strong behavioral face validity with autism or PMS, we do not feel that absence of social behavioral abnormalities in a mouse model provides any information against that gene's involvement in the human disorder. Instead, we use any resulting behavioral abnormality as a viable outcome measure for future studies linking brain function abnormalities to mouse behavior in general.

Shank3 is an integral part of the PSD-95 complex of proteins at excitatory synapses in the hippocampus, yet expression of PSD-95 and Homer in the hippocampus were unaffected in *Shank3*$^{G/G}$ in the present study and in *Shank3*$^{\Delta C/\Delta C}$ mice (Kouser et al., 2013). While other *Shank3* mouse models lacking exons 4-9 (Bozdagi et al., 2010; Wang et al., 2011b) or exon 13 (Peca et al., 2011) have reported decreases in some hippocampal glutamate receptor subunits and other members of the PSD complex, our results are in agreement with Verpelli et al. (2011) in which no change in PSD-95, Homer, AMPA receptor, or NMDA receptor expression was found at hippocampal synapses following Shank3 knock down in neuronal culture.

mGluRs bind to Shank3 indirectly through the Homer binding domain, as well as directly to the PDZ domain (Naisbitt et al., 1999), and Homer binding is required for mGluR-LTD (Ronesi and Huber, 2008). Shank3 has also been shown to regulate

mGluR5 expression and function in cell culture models (Verpelli et al., 2011). However, we did not observe any alteration in mGluR5 expression in the hippocampus of *Shank3*^{G} mice. As a consequence, one of the most striking differences in synaptic protein expression between our two *Shank3* exon 21 models is the unexpected increase in mGluR5 expression at hippocampal synapses in *Shank3*$^{\Delta C/\Delta C}$ mice (Kouser et al., 2013) not present in *Shank3*$^{WT/G}$ or *Shank3*$^{G/G}$ mice. Similarly, mGluR-LTD is abolished in *Shank3*$^{G/G}$ mice, but preserved in *Shank3*$^{\Delta C/\Delta C}$ mice (Kouser et al., 2013). These findings are difficult to reconcile across the two models, though the slight difference in Shank3 isoform alterations may account for these differences.

Perhaps most puzzling is the lack of a decrease in long-term potentiation (LTP) in *Shank3*$^{G/G}$ mice, a surprising finding given that decreased hippocampal LTP has been identified in Shank3 mouse models lacking exons 4-9 (Bozdagi et al., 2010; Wang et al., 2011b; Yang et al., 2012) and exon 21 (Kouser et al., 2013). Incidentally, we do see a significant decrease in post-tetanic potentiation in the first five minutes following a single 1s, 100Hz conditioning stimulus which may result from decreased NMDA receptor contribution to the EPSC, but is still sufficient for maintaining LTP at 60 minutes post-induction. A similar decrease in PTP was observed in homozygous *Shank3*$^{e4\text{-}9}$ mice lacking the ankyrin repeat region, though LTP was also impaired in that mouse (Wang et al., 2011b; Yang et al., 2012). When the experiments were repeated with a much stronger conditioning stimulus (4, 1-s trains at 100 Hz), this difference in PTP was absent and no change in LTP was identified. This suggests that

NMDA receptor function at hippocampal synapses is weaker in *Shank3*$^{WT/G}$ mice and *Shank3*$^{G/G}$ mice than in WT mice, consistent with the role of Shank3 in modulation of NMDA receptors at the synapse (Roussignol et al., 2005), but is not detrimental to LTP induced by stronger tetanic stimulation protocols. We leave open the possibility, however, that an intermediate tetanic stimulation protocols under different conditions could lead to a finding of a decrease in LTP induction.

The most striking synaptic deficits in both *Shank3*$^{G/G}$ and *Shank3*$^{\Delta C/\Delta C}$ mice (Kouser et al., 2013) are impaired basal synaptic transmission measured via input/output curves, decreased mEPSC frequency, and decreased NMDA/AMPA ratio at CA3-CA1 synapses. The alteration in NMDA/AMPA ratio is likely due to a decrease in NMDAR-mediated synaptic responses, which in turn likely contributes to decreased synaptic plasticity in both models. This interpretation is supported by the finding of normal mEPSC amplitude in both models. While at first glance our lack of biochemical alterations in NMDA subunits in hippocampal synaptosomes would seem to contradict this explanation, there are many post-translational mechanisms to decreased NMDA receptor function. Furthermore, synaptosomes are not always perfectly representative of synaptic surface receptors. Synaptosomes made from the entire hippocampus also contain synaptic proteints from many other synapses in addition to the CA1-CA3 synapses studied by electrophysiology.

Interestingly, mEPSC frequency is decreased in *Shank3*$^{G/G}$ and *Shank3*$^{\Delta C/\Delta C}$ mice (Kouser et al., 2013), as was reported in cultured hippocampal neurons expressing the *Shank3*^{G} mutation (Durand et al., 2012). This could indicate a change

in functional synapse number, as levels of Shank3 expression are directly related to mEPSC frequency (Durand et al., 2012; Roussignol et al., 2005; Verpelli et al., 2011) in cultured neurons. Conversely, the decrease in mEPSC frequency could indicate decreased probability of vesicle release, though we observed no changes in PPR to suggest a presynaptic contribution to synaptic deficits in *Shank3*$^{WT/G}$ or *Shank3*$^{G/G}$ mice.

Other regions of the brain may also contribute to behavioral deficits identified in mice lacking the C-terminal region of Shank3. Specifically, the striatum is a promising target for future study because locomotor activity in response to novelty and motor coordination are decreased in *Shank3*$^{G/G}$ mice, as well as *Shank3*$^{\Delta C/\Delta C}$ (Kouser et al., 2013). *Shank3*$^{G/G}$ mice also exhibit impaired motor learning, which may further implicate synaptic abnormalities in the cerebellum or prefrontal cortex.

The *Shank3* exon 21 insertion mutant model highlights a potential pitfall in interpreting and testing functional relevance of human autism mutations. This premature stop codon in exon 21 led to predictions of a truncated Shank3 protein (Durand et al., 2007; Durand et al., 2012). We now see that at least in a mouse model of this mutation, the effects of this insertion mutation are much more complex and lead to a striking loss of multiple higher molecular weight Shank3 isoforms. While the mechanism of this loss remains unclear, the regulation of the *Shank3* gene with its multiple promoters and multiple splice variants is much more complex than originally anticipated (Wang et al., 2011b; Zhu et al., 2014).

In summary, we have generated a genetically accurate and genetically reversible *Shank3* exon 21 insertion mutation mouse model of autism. This model results in significant loss of multiple Shank3 protein isoforms and has significant and robust behavioral and electrophysiological abnormalities that are similar to a previous *Shank3* exon 21 deletion model. We have pinpointed key deficits in mGluR and NMDA receptor-mediated synaptic transmission in $Shank3^{G/G}$ mice, further validating these receptors as potential therapeutic targets in *Shank3* mutant mouse models of autism and related disorders. Our findings suggest NMDA receptors as a potential therapeutic target in these models and set the stage for future studies of region-specific and temporal rescue of this mutant.

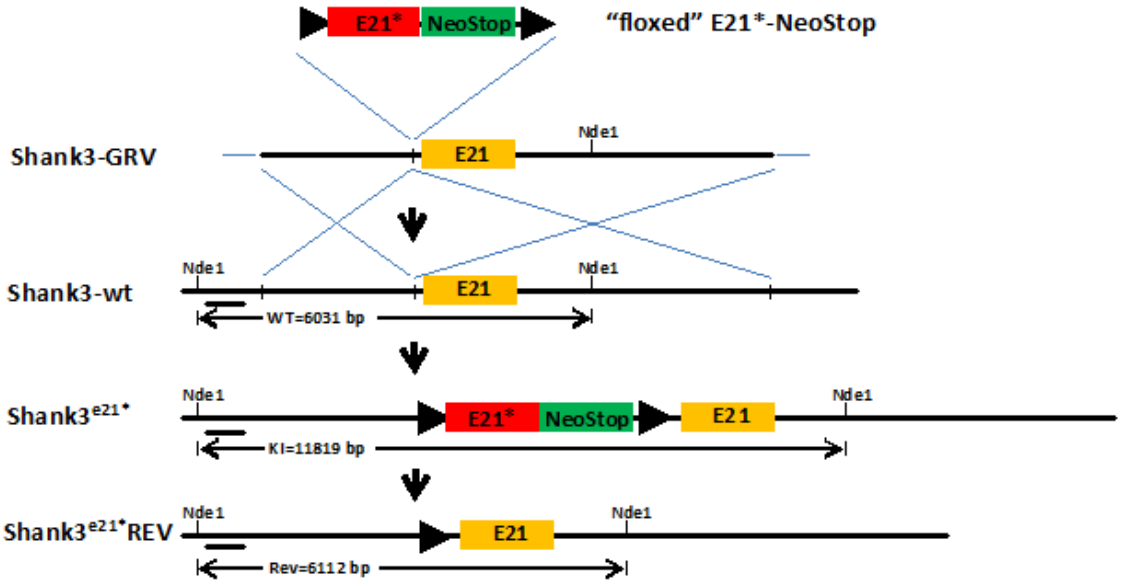

Figure 3.1: Schematic diagram of the exon 21 insertion mutation (insert G) mouse model. A gene repair targeting vector (Shank3-GRV) was created via insertion of an insertion mutant exon 21 followed by a NeoStop Cassette flanked by loxP sites ("floxed" E21^{G}-NeoStop cassette) upstream of the wild-type exon 21. The resulting Shank3-GRV was targeted in mouse ES cells into the wild-type *Shank3* gene (*Shank3-wt*). This resulted in the creation of mice constitutively expressing a human *Shank3* exon 21 insertion mutation associated with autism, the *Shank3*^{G} mouse model. In future experiments, the *Shank3*^{G} mice can be genetically reversed to wild-type *Shank3* whenever and wherever cre-recombinase is activated or expressed. Nde1 denotes restriction sites with size of diagnostic restriction fragments indicated between the Nde1 sites below.

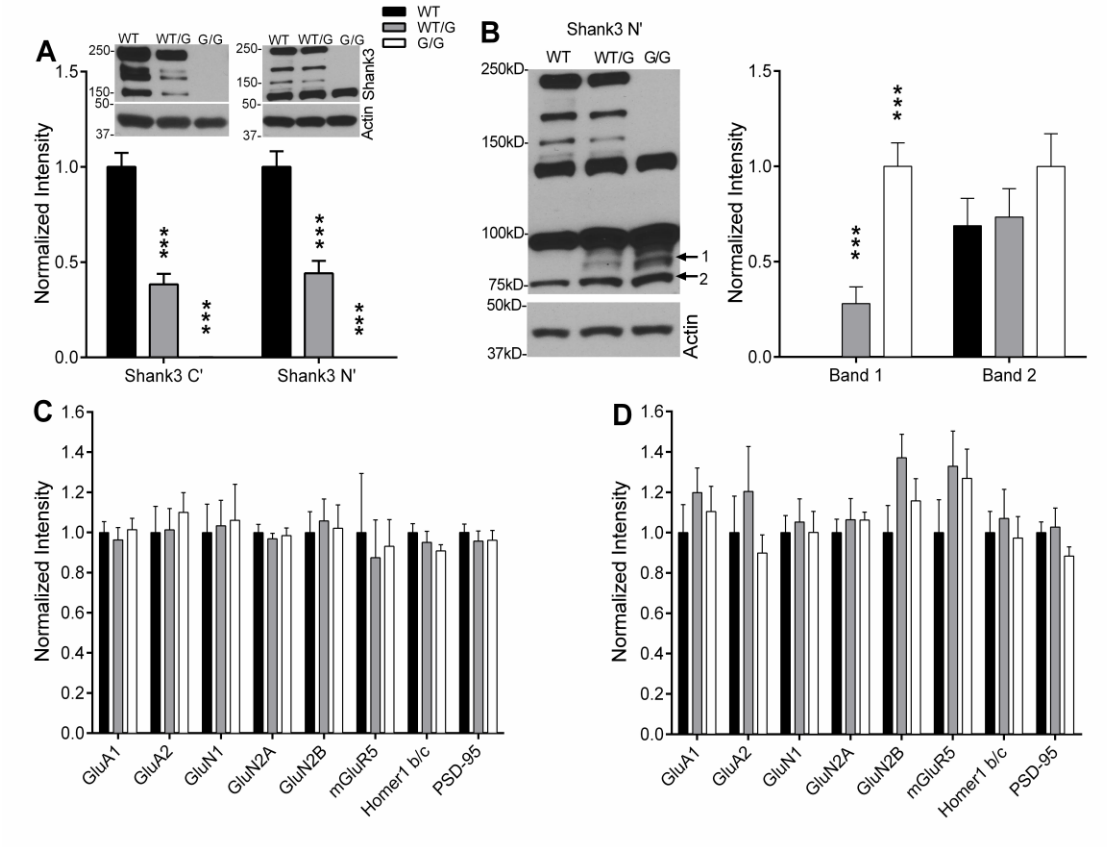

Figure 3.2: Expression of Shank3 and associated proteins at hippocampal synapses. (A) Western blots with both C-terminal and N-terminal Shank3 antibodies reveal that all three major Shank3 isoforms are absent in hippocampal synaptosomes from *Shank3*$^{G/G}$ mice. (B) The Shank3 N-terminal antibody reveals the appearance of one novel Shank3 isoform and a trend toward enhanced expression of another isoform of low molecular weight in *Shank3*$^{G/G}$ mice compared to WT. Expression of synaptic and scaffolding proteins known to associate with Shank3 are unchanged in hippocampal synaptosomes (C) and in whole hippocampal lysates (D) from *Shank3*$^{G/G}$ mice. $n = 8$ mice per genotype. ***$P < 0.001$.

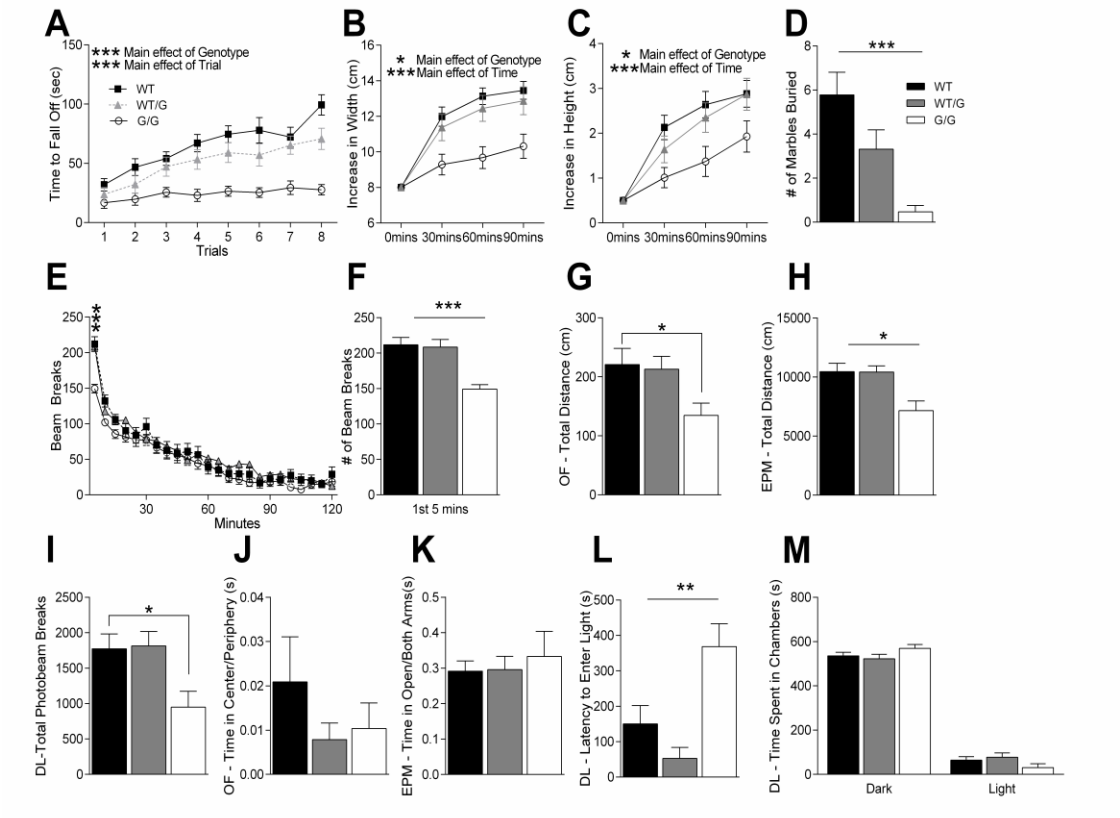

Figure 3.3: *Shank3*$^{G/G}$ Mice Exhibit Impairments in Behavioral Tasks. A) Latency to fall from or to go one full revolution on the rotarod task. *Shank3*$^{G/G}$ mice exhibit motor coordination impairments in 8 trials of rotarod test conducted over two days. Legend in A applies to B and E. B and C) Width and height of nest built as a function of time in a nest-building task. *Shank3*$^{G/G}$ mice exhibit impairments in nest building behavior over a 90-min period. D) Number of marbles buried during a 30-min marble-burying task. *Shank3*$^{G/G}$ mice show impaired marble burying behavior. Legend in D applies to F-M. E) Locomotor activity as measured by number of photobeam breaks during successive 5-min intervals over a two-hour period. *Shank3*$^{G/G}$ mice exhibit normal locomotor habituation over the full 2-h period. F)

Number of photobeam breaks during the initial 5 min of the locomotor task shown in E. *Shank3*$^{G/G}$ mice show decreased activity initially suggesting abnormal locomotor response to novelty. G) Total distance travelled during the 5-min elevated plus maze task. *Shank3*$^{G/G}$ mice have decreased locomotor activity in the elevated plus maze task. H) Total distance travelled during the 10-min open field task. *Shank3*$^{G/G}$ mice have decreased locomotor activity in the open field. I) Number of photobeam breaks during the 10-min dark/light task. *Shank3*$^{G/G}$ mice have decreased locomotor activity in dark/light. J) Ratio of time spent in the center to time spent in the periphery in an open field task. No differences were observed among genotypes. K) Ratio of time in the open arms vs. time in other arms in the elevated plus maze task. *Shank3*$^{G/G}$ mice spend the same time in open vs. closed arms when compared to littermate controls. L) Latency to enter the light side of the dark/light apparatus. *Shank3*$^{G/G}$ mice exhibit an increased latency to enter the light chamber. M) Time spent in dark and light sides of the dark/light apparatus. No difference was observed in the total time spent in the dark versus the light side of the chamber. n = 23 (WT), n = 19 (*Shank3*$^{WT/G}$), n = 19 (*Shank3*$^{G/G}$) for all panels. *P < 0.05, **P < 0.01, ***P < 0.001

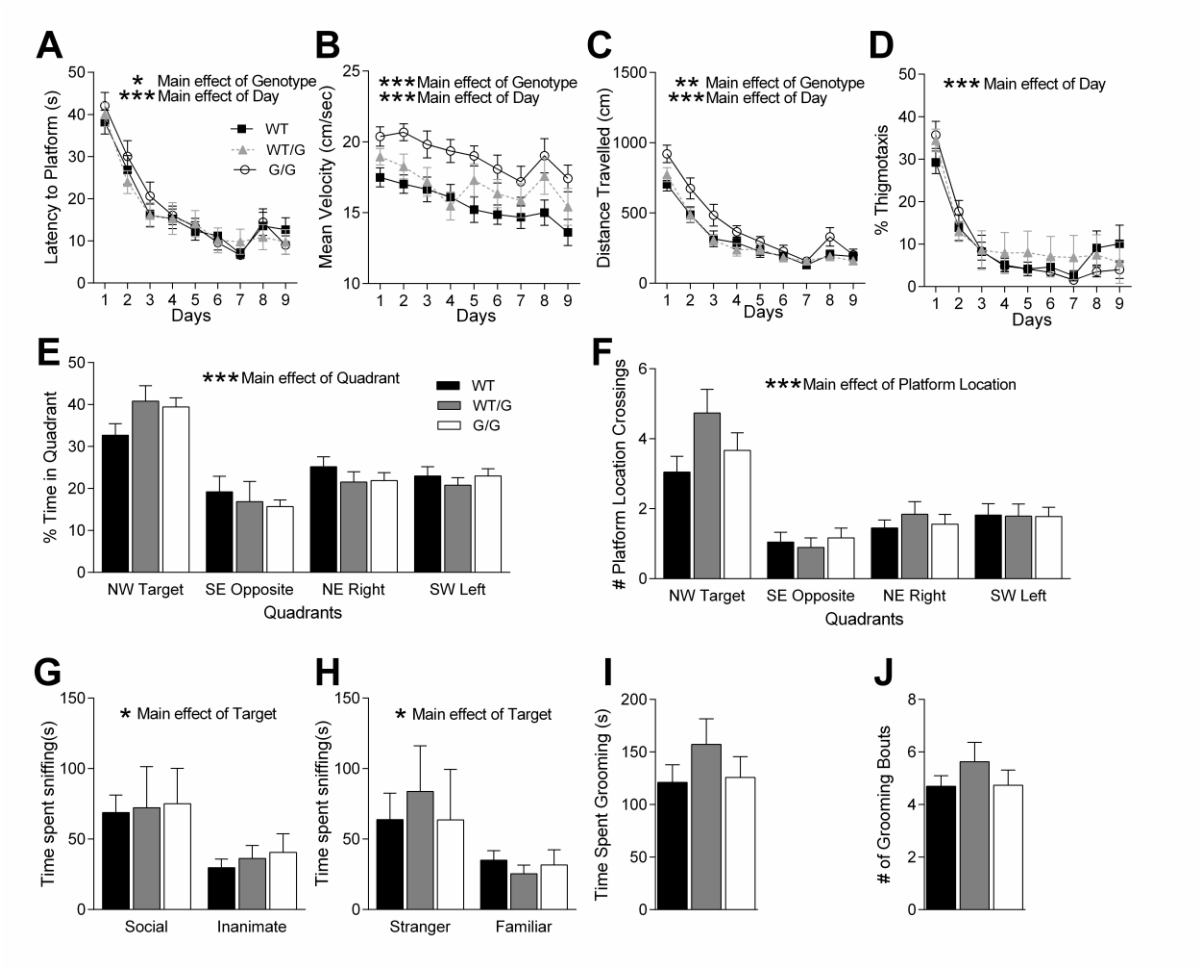

Figure 3.4: *Shank3*$^{G/G}$ Mice Exhibit Mild Spatial Learning Impairment, Normal Social Interaction and Normal Grooming Behavior. A-D: Training days for the Morris water maze task. For each day of training, data were averaged across four daily trials. A) Latency to reach hidden platform on successive water maze days. *Shank3*$^{G/G}$ mice take longer to reach the submerged platform. Legend in A applies to B, C, and D. B) Swim speed on successive water maze training days. *Shank3*$^{G/G}$ mice swim faster in the water maze. C) Distance travelled prior to reaching the hidden platform on successive water maze training days. *Shank3*$^{G/G}$ mice travel a longer distance before reaching the submerged platform. D) Percent time spent in

thigmotaxis on successive water maze training days. *Shank3*$^{G/G}$ mice spend the same amount of time in the thigmotaxis region as their littermate controls. E) Time spent in target quadrant and other quadrants during probe trial in which target platform is removed. *Shank3*$^{G/G}$ mice spend more time in the target quadrant vs. other quadrants. Legend in E applies to F-J. F) Number of target location crossings and corresponding phantom platform location crossings in other quadrants during the probe trial. Shank3$^{E21PM-/-}$ mice show a clear preference for the target platform location (n = 22 (WT), n = 19 (*Shank3*$^{WT/G}$), n = 18 (*Shank3*$^{G/G}$)). G) In the three-chambered social Interaction test, all groups show a normal preference for the social vs. the inanimate target and H) for the stranger mouse vs. the familiar mouse (n = 19 (WT), n = 15(*Shank3*$^{WT/G}$), n = 15 (*Shank3*$^{G/G}$)). I) *Shank3*$^{G/G}$ mice show no change in total time spent grooming or J) number of grooming bouts in a 10-min period (n = 23 (WT), n = 19 (*Shank3*$^{WT/G}$), n = 19 (*Shank3*$^{G/G}$)). *P < 0.05, **P < 0.01, ***P < 0.001

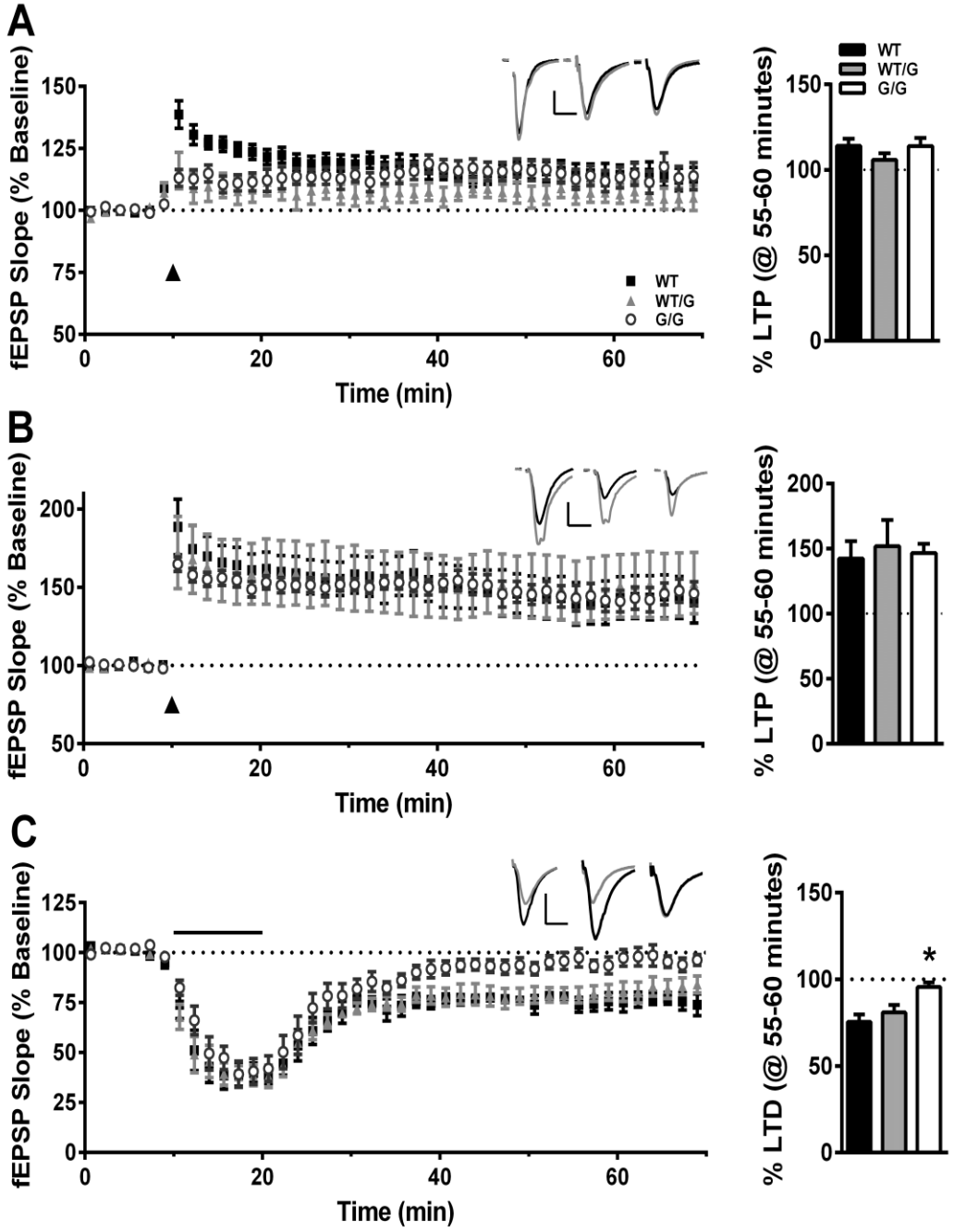

Figure 3.5: Hippocampal synaptic plasticity is impaired in *Shank3*$^{G/G}$ mice. (A) LTP induced by a single 1 s, 100 Hz train (arrow) is normal at 55-60 minutes post-tetanus, though post-tetanic potentiation (PTP) in the first 5 min following

conditioning stimulus is decreased in *Shank3*$^{WT/G}$ and *Shank3*$^{G/G}$ mice (WT n = 13, *Shank3*$^{WT/G}$ n = 9, *Shank3*$^{G/G}$ n = 9). Inset: Average of 10 consecutive raw traces immediately preceding (black) and 60 minutes (gray) after conditioning stimulus for WT (left), *Shank3*$^{WT/G}$ (middle), and *Shank3*$^{G/G}$ (right). Scale bar: 0.25 mV, 10 ms. (B) LTP induced by four, 1-s, 100 Hz trains (arrow) is not affected by the *Shank3*^{G} mutation (WT n = 7, *Shank3*$^{WT/G}$ n = 10, *Shank3*$^{G/G}$ n = 8). Inset: Average of 10 consecutive raw traces immediately preceding (black) and 60 minutes (gray) after conditioning stimulus for WT (left), *Shank3*$^{WT/G}$ (middle), and *Shank3*$^{G/G}$ (right). Scale bar: 0.25 mV, 10 ms. (C) mGluR-LTD induced by 10-min application of 100 μm DHPG (bar) is impaired in *Shank3*$^{G/G}$ mice (WT n = 7, *Shank3*$^{WT/G}$ n = 13, *Shank3*$^{G/G}$ n = 8). Inset: Average of 10 consecutive raw traces immediately preceding (black) and 60 minutes (gray) after DHPG application for WT (left), *Shank3*$^{WT/G}$ (middle), and *Shank3*$^{G/G}$ (right). Scale bar: 0.5 mV, 10 ms. For clarity, scatter plots in A-C are represented as the mean ± SEM of 5 consecutive data points. *$P < 0.05$, **$P < 0.01$.

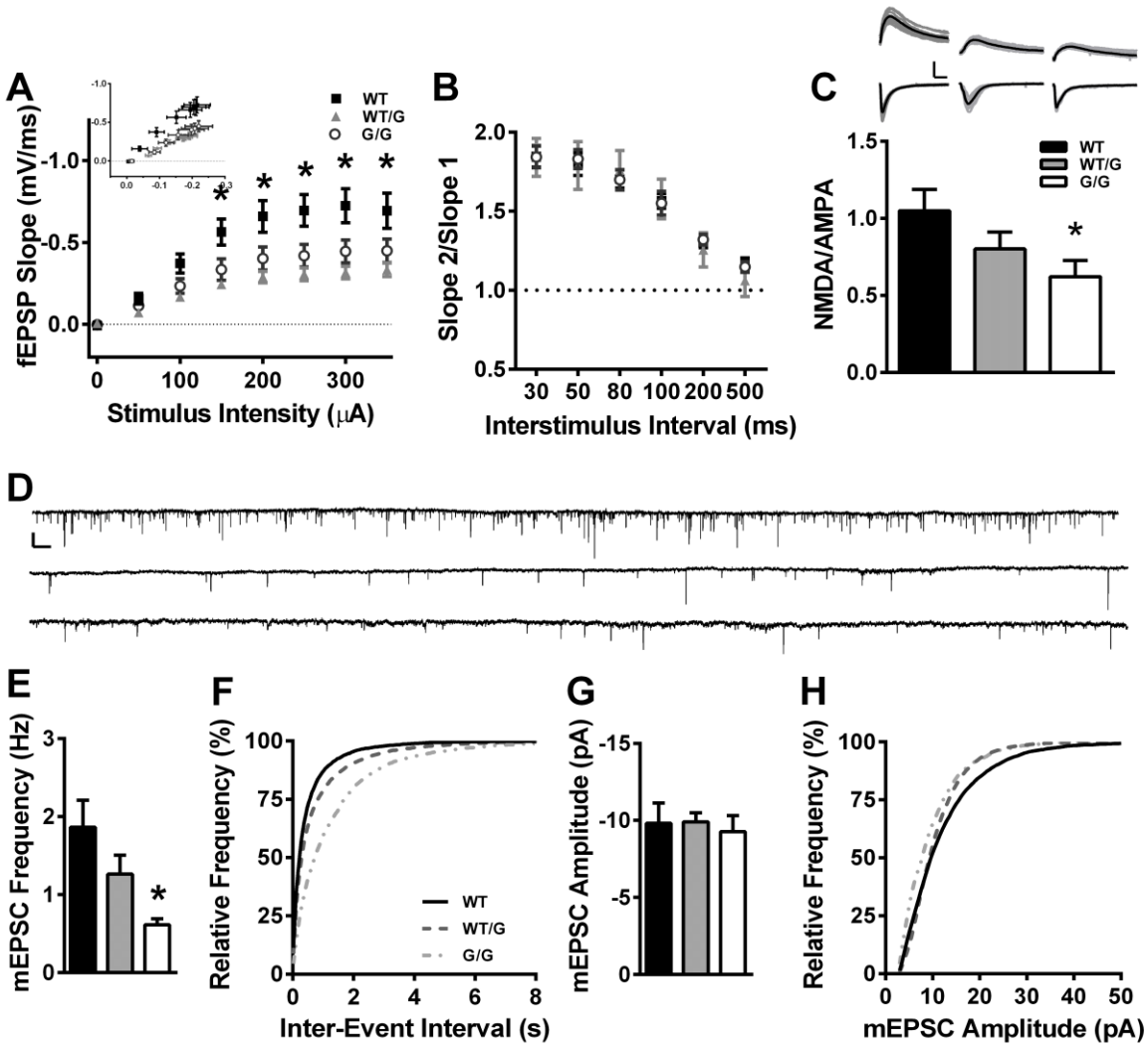

Figure 3.6: Hippocampal synaptic transmission is impaired in *Shank3*$^{WT/G}$ and *Shank3*$^{G/G}$ mice. (A) I/O curves of stimulus intensity versus fEPSP slope indicate a decrease in basal synaptic strength at CA3-CA1 synapses. Inset: fEPSP slope (mV/ms) measured in relation to fiber volley amplitude (mV) (WT *n* = 16, *Shank3*$^{WT/G}$ *n* = 12, *Shank3*$^{G/G}$ *n* = 12). (B) Paired-pulse ratio is not affected by the *Shank3*^{G} mutation at interstimulus intervals 30-500 ms (WT *n* = 12, *Shank3*$^{WT/G}$ *n* = 8, *Shank3*$^{G/G}$ *n* = 15). (C) NMDA/AMPA ratio is decreased in *Shank3*$^{G/G}$ mice (WT *n* =

22, *Shank3*$^{WT/G}$ *n* = 18, *Shank3*$^{G/G}$ *n* = 23). Inset: Average of 10 consecutive traces at -70 mV and at +40 mV holding potential from *Shank3*^{WT} (left), *Shank3*$^{WT/G}$ (middle), and *Shank3*$^{G/G}$ (right). Scale bar: 200 pA, 25 ms. (D) One-min traces of mEPSCs from WT (top), *Shank3*$^{WT/G}$ (middle), and *Shank3*$^{G/G}$ (bottom). Scale bar: 20 pA, 1 s. Mean mEPSC frequency (E) is decreased in CA1 neurons from *Shank3*$^{G/G}$ mice and is reflected in the rightward shift in the distribution of inter-event frequency (F) in *Shank3*$^{G/G}$ mice indicating longer inter-event intervals in *Shank3*$^{G/G}$ mice. Mean mEPSC amplitude (G) and distribution of mEPSC amplitudes (H) is not affected by the *Shank3*^{G} mutation (WT *n* = 15, *Shank3*$^{WT/G}$ *n* = 21, *Shank3*$^{G/G}$ *n* = 14). **P* < 0.05, ***P* < 0.01

Table 4: Statistical Analysis of Behavioral Studies		
Parameter	**Comparison**	**Results**
Body Weight N = (WT:23, Shank3$^{WT/G}$:19, Shank3$^{G/G}$:19)		
Body Weight in grams	Sex & Genotype	2-way ANOVA; Main effect of Sex: $F(1,55)=15.05$, $P<0.001$; Main effect of Genotype: $F(2,55)=4.107$, $P<0.05$; Sex x Genotype Interaction: $F(2,55)=0.117$, $P=0.89$
		Tukey HSD: wt vs. het: $P=0.980$; wt vs. ko: $P=0.060$; het vs ko: $P=0.050$
Open Field N = (WT:23, Shank3$^{WT/G}$:19, Shank3$^{G/G}$:19)		
Time in Center	Sex & Genotype	2-way ANOVA; Main effect of Sex: $F(1,55)=0.01$, $P=0.90$; Main effect of Genotype: $F(2,55)=1.15$, $P=0.32$; Sex x Genotype Interaction: $F(2,55)=0.30$, $P=0.73$
Frequency in Center	Sex & Genotype	2-way ANOVA; Main effect of Sex: $F(1,55)=0.07$, $P=0.78$; Main effect of Genotype: $F(2,55)=1.11$, $P=0.33$; Sex x Genotype Interaction: $F(2,55)=0.67$, $P=0.51$
Time in periphery	Sex & Genotype	2-way ANOVA; Main effect of Sex: $F(1,55)=0.34$, $P=0.55$; Main effect of Genotype: $F(2,55)=0.26$, $P=0.76$; Sex x Genotype Interaction: $F(2,55)=1.41$, $P=0.25$
Frequency in Periphery	Sex & Genotype	2-way ANOVA; Main effect of Sex: $F(1,55)=0.80$, $P=0.37$; Main effect of Genotype: $F(2,55)=1.43$, $P=0.24$; Sex x Genotype Interaction: $F(2,55)=2.47$, $P=0.09$
Time in Center / Time in Periphery	Sex & Genotype	2-way ANOVA; Main effect of Sex: $F(1,55)=0.06$, $P=0.79$; Main effect of Genotype: $F(2,55)=1.20$, $P=0.30$; Sex x Genotype Interaction: $F(2,55)=0.65$, $P=0.52$
Distance Travelled	Sex & Genotype	2-way ANOVA; Main effect of Sex: $F(1,55)=0.01$, $P=0.89$; Main effect of Genotype: $F(2,55)=2.56$, $P=0.08$; Sex x Genotype Interaction: $F(2,55)=2.75$, $P=0.07$
		Tukey HSD: WT vs. Shank3$^{WT/G}$: $P=0.96$; WT vs. Shank3$^{G/G}$: $P<0.05$; Shank3$^{WT/G}$ vs Shank3$^{G/G}$: $P=0.06$
Velocity	Sex & Genotype	2-way ANOVA; Main effect of Sex: $F(1,55)=0.004$, $P=0.94$; Main effect of Genotype: $F(2,55)=2.35$, $P=0.10$; Sex x Genotype Interaction: $F(2,55)=2.90$, $P=0.06$
		Tukey HSD: WT vs. Shank3$^{WT/G}$: $P=0.96$;

		WT vs. Shank3$^{G/G}$: P<0.05; Shank3$^{WT/G}$ vs Shank3$^{G/G}$: P=0.07
Dark/light Box N = (WT:23, Shank3$^{WT/G}$:19, Shank3$^{G/G}$:19)		
Total Activity	Sex & Genotype	2-way ANOVA; Main effect of Sex: F(1,55)=0.15, P=0.69; Main effect of Genotype: F(2,55)=2.96, P=0.059; Sex x Genotype Interaction: F(2,55)=1.48, P=0.23
		Tukey HSD: WT vs. Shank3$^{WT/G}$: P=0.99; WT vs. Shank3$^{G/G}$: P<0.05; Shank3$^{WT/G}$ vs Shank3$^{G/G}$: P<0.05
Time in Light Side	Sex & Genotype	2-way ANOVA; Main effect of Sex: F(1,55)=0.06, P=0.79; Main effect of Genotype: F(2,55)=0.87, P=0.42; Sex x Genotype Interaction: F(2,55)=1.36, P=0.26
Crosses	Sex & Genotype	2-way ANOVA; Main effect of Sex: F(1,55)=0.20, P=0.65; Main effect of Genotype: F(2,55)=0.66, P=0.51; Sex x Genotype Interaction: F(2,55)=2.12, P=0.12
Latency to Enter Light Side	Sex & Genotype; parametric	2-way ANOVA; Main effect of Sex: F(1,55)=0.92, P=0.33; Main effect of Genotype: F(2,55)=6.66, P<0.01; Sex x Genotype Interaction: F(2,55)=0.69, P=0.50
		Tukey HSD: WT vs. Shank3$^{WT/G}$: P=0.38; WT vs. Shank3$^{G/G}$: P<0.05; Shank3$^{WT/G}$ vs Shank3$^{G/G}$: P<0.001
Time in Dark Side	Sex, Genotype; non-parametric	2-way ANOVA; Main effect of Sex: F(1,55)=0.06, P=0.79; Main effect of Genotype: F(2,55)=0.87, P=0.42; Sex x Genotype Interaction: F(2,55)=1.36, P=0.26
Elevated Plus Maze N = (WT:23, Shank3$^{WT/G}$:19, Shank3$^{G/G}$:19)		
Distance Travelled	Sex & Genotype	2-way ANOVA; Main effect of Sex: F(1,55)=0.03, P=0.85; Main effect of Genotype: F(2,55)=4.83, P<0.05; Sex x Genotype Interaction: F(2,55)=1.79, P=0.17
		Tukey HSD: WT vs. Shank3$^{WT/G}$: P=0.99; WT vs. Shank3$^{G/G}$: P<0.01; Shank3$^{WT/G}$ vs Shank3$^{G/G}$: P<0.01
Velocity	Sex & Genotype	2-way ANOVA; Main effect of Sex: F(1,55)=0.03, P=0.85; Main effect of Genotype: F(2,55)=4.83, P<0.05; Sex x Genotype Interaction: F(2,55)=1.79, P=0.17
		Tukey HSD: WT vs. Shank3$^{WT/G}$: P=0.99; WT vs. Shank3$^{G/G}$: P<0.01; Shank3$^{WT/G}$ vs

		Shank3$^{G/G}$: P<0.01
Time in Open Arms / Time in Both Arms	Sex & Genotype	2-way ANOVA; Main effect of Sex: F(1,55)=0.17, P=0.68; Main effect of Genotype: F(2,55)=0.23, P=0.79; Sex x Genotype Interaction: F(2,55)=0.24, P=0.78
Entries in Open / Entries in Both	Sex & Genotype	2-way ANOVA; Main effect of Sex: F(1,55)=3.52, P=0.06; Main effect of Genotype: F(2,55)=0.24, P=0.78; Sex x Genotype Interaction: F(2,55)=0.62, P=0.54
Morris Water Maze -Initial Training N = (WT:22, Shank3$^{WT/G}$:19, Shank3$^{G/G}$:18)		
Latency to Reach Platform	Sex, Genotype & Day	3-way rmANOVA; Main effect of Sex: F(1,53)=0.94, P=0.33; Main effect of Genotype: F(2,53)=3.83, P<0.05; Main effect of Day: F(8,424)=38.03, P<0.001; Sex x Genotype Interaction: F(2,53)=1.07, P=0.34; Sex x Day Interaction: F(8,424)=0.43, P=0.90; Genotype x Day Interaction: F(16,424)=0.76, P=0.73; Sex x Genotype x Day Interaction: F(16,424)=0.80, P=0.67
		Tukey HSD: WT vs. Shank3$^{WT/G}$: P=0.30; WT vs. Shank3$^{G/G}$: P<0.05; Shank3$^{WT/G}$ vs Shank3$^{G/G}$: P=0.49
Distance Travelled to Platform	Sex, Genotype & Day	3-way rmANOVA; Main effect of Sex: F(1,53)=1.22, P=0.27; Main effect of Genotype: F(2,53)=5.61, P<0.01; Main effect of Day: F(8,424)=144.53, P<0.001; Sex x Genotype Interaction: F(2,53)=0.71, P=0.49; Sex x Day Interaction: F(8,424)=0.49, P=0.86; Genotype x Day Interaction: F(16,424)=5.58, P<0.001; Sex x Genotype x Day Interaction: F(16,424)=0.90, P=0.56
		Tukey HSD: WT vs. Shank3$^{WT/G}$: P=0.88; WT vs. Shank3$^{G/G}$: P<0.01; Shank3$^{WT/G}$ vs Shank3$^{G/G}$: P<0.05
Thigmotaxis	Sex, Genotype & Day	3-way rmANOVA; Main effect of Sex: F(1,53)=0.20, P=0.65; Main effect of Genotype: F(2,53)=0.99, P=0.37; Main effect of Day: F(8,424)=44.17, P<0.001; Sex x Genotype Interaction: F(2,53)=0.52, P=0.59; Sex x Day Interaction: F(8,424)=0.21, P=0.98; Genotype x Day Interaction: F(16,424)=1.48, P=0.10; Sex x Genotype x

		Day Interaction: F(16,424)=0.69, P=0.79
Ave. Swim Speed	Sex, Genotype & Day	3-way rmANOVA; Main effect of Sex: F(1,53)=0.78, P=0.37; Main effect of Genotype: F(2,53)=36.66, P<0.001; Main effect of Day: F(8,424)=34.05, P<0.001; Sex x Genotype Interaction: F(2,53)=0.44, P=0.64; Sex x Day Interaction: F(8,424)=0.64, P=0.74; Genotype x Day Interaction: F(16,424)=9.79,P<0.001; Sex x Genotype x Day Interaction: F(16,424)=0.54, P=0.92
		Tukey HSD: WT vs. Shank3$^{WT/G}$: P<0.001; WT vs. Shank3$^{G/G}$: P<0.001 Shank3$^{WT/G}$ vs Shank3$^{G/G}$: P<0.05
Morris Water Maze -Probe Trial N = (WT:22, Shank3$^{WT/G}$:19, Shank3$^{G/G}$:18)		
% Time in Quadrant	Sex, Genotype & Quadrant	3-way rmANOVA; Main effect of Sex: F(1,53)=0.00000001, P=0.99; Main effect of Genotype: F(2,53)=0.00000008, P=0.99; Main effect of Quadrant: F(3,159)=20.621, P<0.001; Sex x Genotype Interaction: F(2,53)=0.0000002, P=0.99; Sex x Quadrant Interaction: F(3,159)=1.91, P=0.13; Genotype x Quadrant Interaction: F(6,159)=0.89,P=0.50; Sex x Genotype x Quadrant Interaction: F(6,159)=1.20, P=0.30
	Target vs. other Quadrants	Tukey HSD: TargetNW vs. RightNE: P<0.001; TargetNW vs. LeftSW: P<0.001; TargetNW vs. OppositeSE: P<0.001
	Target vs. other Quadrants within WT	Tukey HSD: TargetNW vs. RightNE: P=0.78 TargetNW vs. LeftSW: P=0.40; TargetNW vs. OppositeSE: P<0.05
	Target vs. other Quadrants within Shank3$^{WT/G}$	Tukey HSD: TargetNW vs. RightNE: P<0.001; TargetNW vs. LeftSW: P<0.001; TargetNW vs. OppositeSE: P<0.001
	Target vs. other Quadrants within Shank3$^{G/G}$	Tukey HSD: TargetNW vs. RightNE: P<0.01; TargetNW vs. LeftSW: P<0.05; TargetNW vs. OppositeSE: P<0.001
# of Platform Crossings	Sex, Genotype & Platform	3-way rmANOVA; Main effect of Sex: F(1,53)=2.54, P=0.11; Main effect of Genotype: F(2,53)=1.56, P=0.21; Main effect of Quadrant: F(3,159)=25.05, P<0.001; Sex x Genotype Interaction: F(2,53)=0.35, P=0.70;

		Sex x Quadrant Interaction: F(3,159)=2.50, P=0.06; Genotype x Quadrant Interaction: F(6,159)=1.36,P=0.23; Sex x Genotype x Quadrant Interaction: F(6,159)=0.72, P=0.62
	Target vs. other Platforms	Tukey HSD: TargetNW vs. RightNE: P<0.001; TargetNW vs. LeftSW: P<0.001; TargetNW vs. OppositeSE: P<0.001
	Target vs. other Platforms within WT	Tukey HSD: TargetNW vs. RightNE: P=0.06 TargetNW vs. LeftSW: P=0.37; TargetNW vs. OppositeSE: P<0.01
	Target vs. other Platforms within Shank3$^{WT/G}$	Tukey HSD: TargetNW vs. RightNE: P<0.001; TargetNW vs. LeftSW: P<0.001; TargetNW vs. OppositeSE: P<0.001
	Target vs. other Platforms within Shank3$^{G/G}$	Tukey HSD: TargetNW vs. RightNE: P<0.01; TargetNW vs. LeftSW: P<0.05; TargetNW vs. OppositeSE: P<0.001
Ave. Swim Speed	Sex & Genotype	2-way ANOVA; Main effect of Sex: F(1,53)=0.03, P=0.85; Main effect of Genotype: F(2,53)=1.45, P=0.24; Sex x Genotype Interaction: F(2,53)=0.14, P=0.86
% Thigmotaxis	Sex & Genotype	2-way ANOVA; Main effect of Sex: F(1,53)=0.21, P=0.64; Main effect of Genotype: F(2,53)=0.07, P=0.93; Sex x Genotype Interaction: F(2,53)=1.11, P=0.33
Distance travelled	Sex & Genotype	2-way ANOVA; Main effect of Sex: F(1,53)=0.02, P=0.86; Main effect of Genotype: F(2,53)=1.49, P=0.23; Sex x Genotype Interaction: F(2,53)=0.13, P=0.87
Visible Water Maze N = (WT:22, Shank3$^{WT/G}$:19, Shank3$^{G/G}$:18)		
Latency to Platform	Sex & Genotype	2-way ANOVA; Main effect of Sex: F(1,53)=0.30, P=0.58; Main effect of Genotype: F(2,53)=2.87, P=0.06; Sex x Genotype Interaction: F(2,53)=0.71, P=0.49
% Thigmotaxis	Sex & Genotype	2-way ANOVA; Main effect of Sex: F(1,32)=0.0008, P=0.97; Main effect of Genotype: F(1,32)=0.98, P=0.32; Sex x Genotype: F(1,32)=0.04, P=0.82
Distance Travelled to Platform	Sex & Genotype	2-way ANOVA; Main effect of Sex: F(1,53)=0.02, P=0.88; Main effect of Genotype: F(2,53)=9.32, P<0.001; Sex x Genotype Interaction: F(2,53)=0.81, P=0.44
		Tukey HSD: WT vs. Shank3$^{WT/G}$: P=0.70; WT vs. Shank3$^{G/G}$: P<0.01; Shank3$^{WT/G}$ vs

		Shank3$^{G/G}$: P<0.001
Ave. Swim Speed	Sex & Genotype	2-way ANOVA; Main effect of Sex: F(1,53)=0.12, P=0.72; Main effect of Genotype: F(2,53)=5.12, P<0.01; Sex x Genotype Interaction: F(2,53)=0.66, P=0.51
		Tukey HSD: WT vs. Shank3$^{WT/G}$: P=0.10; WT vs. Shank3$^{G/G}$: P<0.01; Shank3$^{WT/G}$ vs Shank3$^{G/G}$: P=0.52
Nesting Behavior N = (WT:23, Shank3$^{WT/G}$:19, Shank3$^{G/G}$:19)		
Increase in Nest Height	Sex, Genotype & Time	3-way rmANOVA; Main effect of Sex: F(1,55)=0.114, P=0.73; Main effect of Genotype: F(2,55)=7.19, P<0.01; Main effect of Time: F(2,110)=21.03, P<0.001; Sex x Genotype Interaction: F(2,55)=2.18, P=0.12; Sex x Time Interaction: F(2,110)=0.39, P=0.67; Genotype x Time Interaction: F(4,110)=1.07, P=0.37; Sex x Genotype x Time Interaction: F(4,110)=0.85, P=0.49
		Tukey HSD: WT vs. Shank3$^{WT/G}$: P=0.37; WT vs. Shank3$^{G/G}$: P<0.01; Shank3$^{WT/G}$ vs Shank3$^{G/G}$: P=0.24
Increase in Nest Width	Sex, Genotype & Time	3-way rmANOVA; Main effect of Sex: F(1,55)=0.71, P=0.40; Main effect of Genotype: F(2,55)=4.60, P<0.05; Main effect of Time: F(2,110)=23.64, P<0.001; Sex x Genotype Interaction: F(2,55)=1.62, P=0.20; Sex x Time Interaction: F(2,110)=1.73, P=0.18; Genotype x Time Interaction: F(4,110)=0.71, P=0.58; Sex x Genotype x Time Interaction: F(4,110)=0.18, P=0.94
		Tukey HSD: WT vs. Shank3$^{WT/G}$: P=0.77; WT vs. Shank3$^{G/G}$: P<0.05; Shank3$^{WT/G}$ vs Shank3$^{G/G}$: P=0.10
3-choice Interaction Test- Baseline N = (WT:19, Shank3$^{WT/G}$:15, Shank3$^{G/G}$:15)		
Distance Travelled	Sex & Genotype	2-way ANOVA: Main effect of Sex:F(1,43)=0.34, P=0.55 ; Main effect of Genotype: F(2,43)= 6.85, P<0.01; Sex x Genotype Interaction: F(2,43)=0.24, P=0.78
		Tukey HSD: WT vs. Shank3$^{WT/G}$: P=0.99; WT vs. Shank3$^{G/G}$: P<0.01; Shank3$^{WT/G}$ vs Shank3$^{G/G}$: P<0.01
Velocity	Sex & Genotype	2-way ANOVA: Main effect of Sex:F(1,43)=0.0007, P=0.97 ; Main effect of

		Genotype: F(2,43)= 6.44, P<0.01; Sex x Genotype Interaction: F(2,43)=0.26, P=0.76
		Tukey HSD: WT vs. Shank3$^{WT/G}$: P=0.99; WT vs. Shank3$^{G/G}$: P<0.01; Shank3$^{WT/G}$ vs Shank3$^{G/G}$: P<0.05
Time Spent Sniffing	Sex, Genotype & Interaction Target (front vs. back)	3-way rmANOVA: Main effect of Sex: F(1,43)=0.0001, P=0.99; Main effect of Genotype: F(2,43)=1.37, P=0.26; Main effect of Target: F(1,43)=1.28, P=0.26; Sex x Genotype Interaction: F(2,43)=0.004, P=0.99; Sex x Target Interaction: F(1,43)=0.14, P=0.70; Genotype x Target Interaction: F(2,43)=0.50, P=0.60; Sex x Genotype x Target Interaction: F(2,43)=0.16, P=0.84
3-choice Interaction Test- Social Preference N = (WT:19, Shank3$^{WT/G}$:15, Shank3$^{G/G}$:15)		
Distance Travelled	Sex & Genotype	2-way ANOVA: Main effect of Sex:F(1,43)=4.59, P<0.05; Main effect of Genotype: F(2,43)= 1.85; P=0.16; Sex x Genotype Interaction: F(2,43)=1.25, P=0.29
Velocity	Sex & Genotype	2-way ANOVA: Main effect of Sex:F(1,43)=3.30, P=0.07 ; Main effect of Genotype: F(2,43)= 1.60; P=0.21; Sex x Genotype Interaction: F(2,43)=1.46, P=0.24
Time Spent Sniffing	Sex, Genotype & Interaction Target (inanimate vs. social)	3-way rmANOVA: Main effect of Sex: F(1,43)=0.001, P=0.96; Main effect of Genotype: F(2,43)=0.144, P=0.86; Main effect of Target: F(1,43)=6.01, P<0.05; Sex x Genotype Interaction: F(2,43)=0.46, P=0.62; Sex x Target Interaction: F(1,43)=0.06, P=0.79; Genotype x Target Interaction: F(2,43)=0.02, P=0.97; Sex x Genotype x Target Interaction: F(2,43)=2.25, P=0.11
	Effect of Target (inanimate vs. social) within each Genotype	Tukey HSD: WT: P=0.60; Shank3$^{WT/G}$: P=0.77; Shank3$^{G/G}$: P=0.80
3-choice Interaction Test- Social Novelty N = (WT:19, Shank3$^{WT/G}$:15, Shank3$^{G/G}$:15)		
Distance Travelled	Sex & Genotype	2-way ANOVA: Main effect of Sex:F(1,43)=4.59, P<0.05 ; Main effect of Genotype: F(2,43)= 1.85; P=0.16; Sex x Genotype Interaction: F(2,43)=1.25, P=0.29

Velocity	Sex & Genotype	2-way ANOVA: Main effect of Sex:F(1,43)=3.30, P=0.07 ; Main effect of Genotype: F(2,43)=1.60; P=0.21; Sex x Genotype Interaction: F(2,43)=1.46, P=0.24
Time Spent Sniffing	Genotype & Interaction Target (familiar vs. stranger)	3-way rmANOVA: Main effect of Sex: F(1,43)=0.257, P=0.61; Main effect of Genotype: F(2,43)=0.07, P=0.93; Main effect of Target: F(1,43)=4.52, P<0.05; Sex x Genotype Interaction: F(2,43)=0.26, P=0.76; Sex x Target Interaction: F(1,43)=1.88, P=0.17; Genotype x Target Interaction: F(2,43)=31, P=0.73; Sex x Genotype x Target Interaction: F(2,43)=0.06, P=0.93
	Effect of Target (Familiar vs. Novel) within each Genotype	Tukey HSD: WT: P=0.91; $Shank3^{WT/G}$: P=0.48; $Shank3^{G/G}$: P=0.92
Locomotor Habituation N = (WT:23, $Shank3^{WT/G}$:19, $Shank3^{G/G}$:19)		
Total Beam Breaks	Sex, Genotype, & Bin	3-way rmANOVA; Main effect of Sex: F(1,55)=0.20, P=0.65; Main effect of Genotype: F(2,55)=0.38, P=0.68; Main effect of Trial: F(23,1265)=105.79, P<0.001; Sex x Genotype Interaction: F(2,55)=2.62, P=0.08; Sex x Trial Interaction: F(23,1265)=0.94, P=0.53; Genotype x Trial: F(46,1265)=1.72, P<0.01; Sex x Genotype x Trial Interaction: F(46,1265)=1.21, P=0.16
		Tukey HSD: WT vs. $Shank3^{WT/G}$: P=0.97; WT vs. $Shank3^{G/G}$: P=0.49; $Shank3^{WT/G}$ vs $Shank3^{G/G}$: P=0.40
1st bin only	Genotype & Sex	2-way ANOVA; Main effect of Sex: F(1,55)=0.38, P=0.53; Main effect of Genotype: F(2,55)=10.85, P<0.001; Sex x Genotype Interaction: F(2,55)=0.50, P=0.60
		Tukey HSD: WT vs. $Shank3^{WT/G}$: P=0.96; WT vs. $Shank3^{G/G}$: P<0.001; $Shank3^{WT/G}$ vs $Shank3^{G/G}$: P<0.001
Stereodypy Beam breaks	Sex, Genotype, & Bin	3-way rmANOVA; Main effect of Sex: F(1,55)=5.95, P<0.05; Main effect of Genotype: F(2,55)=1.18, P=0.31; Main effect of Trial: F(23,1265)=50.59, P<0.001; Sex x Genotype Interaction: F(2,55)=3.78, P<0.05; Sex x Trial Interaction: F(23,1265)=0.70,

		P=0.84; Genotype x Trial: F(46,1265)=0.84, P=0.76 ; Sex x Genotype x Trial Interaction: F(46,1265)=1.30, P=0.08
Ambulatory Beam Breaks	Sex, Genotype, & Bin	3-way rmANOVA; Main effect of Sex: F(1,55)=0.03, P=0.84; Main effect of Genotype: F(2,55)=1.21, P=0.30; Main effect of Trial: F(23,1265)=101.88, P<0.001; Sex x Genotype Interaction: F(2,55)=2.03, P=0.14; Sex x Trial Interaction: F(23,1265)=1.03, P=0.41; Genotype x Trial: F(46,1265)=2.16, P<0.001 ; Sex x Genotype x Trial Interaction: F(46,1265)=0.99, P=0.47
Rotarod N = (WT:23, Shank3$^{WT/G}$:19, Shank3$^{G/G}$:19)		
Time to Fall Off	Sex, Genotype & Trial	3-way rmANOVA; Main effect of Sex: F(1,55)=12.36, P<0.001; Main effect of Genotype: F(2,55)=20.37, P<0.001; Main effect of Trial: F(7,385)=23.36, P<0.001; Sex x Genotype Interaction: F(2,55)=3.73, P<0.05; Sex x Trial Interaction: F(7,238)=0.51, P=0.82; Genotype x Trial: F(14,385)=1.25, P=0.27; Sex x Genotype x Trial Interaction: F(14,385)=0.60, P=0.86
		Tukey HSD: WT vs. Shank3$^{WT/G}$: P=0.10; WT vs. Shank3$^{G/G}$: P<0.001; Shank3$^{WT/G}$ vs Shank3$^{G/G}$: P<0.01
Marble Burying N = (WT:23, Shank3$^{WT/G}$:19, Shank3$^{G/G}$:19)		
Number of Marbles Buried	Sex & Genotype	2-way ANOVA; Main effect of Sex: F(1,55)=1.31, P=0.25; Main effect of Genotype: F(2,55)=9.80, P<0.001; Sex x Genotype Interaction: F(2,55)=0.29, P=0.74
		Tukey HSD: WT vs. Shank3$^{WT/G}$: P=0.10; WT vs. Shank3$^{G/G}$: P<0.001; Shank3$^{WT/G}$ vs Shank3$^{G/G}$: P=0.06
Grooming N = (WT:23, Shank3$^{WT/G}$:19, Shank3$^{G/G}$:19)		
Time Spent Grooming	Sex and Genotype	2-way ANOVA; Main effect of Sex: F(1,55)=0.53, P=0.46; Main effect of Genotype: F(2,55)=0.97, P=0.38; Sex x Genotype Interaction: F(2,55)=1.27, P=0.28
Number of Bouts	Sex and Genotype	2-way ANOVA; Main effect of Sex: F(1,55)=0.004, P=0.94; Main effect of Genotype: F(2,55)=0.73, P=0.48; Sex x Genotype Interaction: F(2,55)=0.09, P=0.91
Time per Bout	Sex and	2-way ANOVA; Main effect of Sex:

	Genotype	F(1,55)=0.12, P=0.72; Main effect of Genotype: F(2,55)=0.69, P=0.50; Sex x Genotype Interaction: F(2,55)=1.25, P=0.29

ANOVA: analysis of variance, WT: wildtype, rmANOVA: ANOVA (between subjects factors are generally sex and genotype) with repeated measures (day, time, or trial). F(x,y): F ratio statistic is used to determine whether the variances in two independent samples are equal, x,y are degrees of freedom (df). Degrees of freedom is a measure of the number of independent pieces of information on which the precision of a parameter estimate is based. x = number of groups-1, y = number of animals per group minus 1, multiplied by the number of groups.

CHAPTER FOUR
Results

Rescue of Biochemical and Behavioral Phenotypes Observed in Autism Relevant Mutation of *Shank3* in Rodents

Introduction

Shank3 is a multi domain post-synaptic scaffolding protein that plays a critical role in forming the post-synaptic density by connecting the necessary excitatory machinery together with each of its functional domains (Naisbitt et al., 1999; Roussignol et al., 2005; reviewed in Sheng and Kim, 2000; Uchino et al., 2006). *SHANK3* mutations and deletions has been strongly implicated in human autism (Boccuto et al., 2012; Durand et al., 2007; Gauthier et al., 2009; Moessner et al., 2007). *SHANK3* is also considered as one of the causative genes for Phelan-McDermid Syndrome (22q13 Deletion Syndrome, intellectual disability with autism or autistic features) (Boccuto et al., 2012; Bonaglia et al., 2001; Bonaglia et al., 2006; Dhar et al., 2010; Wilson et al., 2003). In addition, children with 22q13 Deletion Syndrome (also known as Phelan-McDermid Syndrome) exhibit autistic behavior, absent to severely delayed speech along with global developmental delay. In these patients, deletion of the *SHANK3* gene is most closely associated with neurobehavioral symptoms in affected individuals (Bonaglia et al., 2001; Wilson et al., 2003). These studies strongly link *SHANK3* deletion/mutation and autism spectrum disorders.

We have successfully created and characterized a mouse model which directly mimics a human autism associated guanine nucleotide insertion mutation (*Shank3*^{G}) in exon 21 (Durand et al., 2007). This insertion mutation induces a frameshift causing a premature STOP codon in exon 21, resulting in truncated Shank3 protein. (Durand et al., 2007; Durand et al., 2012). This mutation also causes loss of all major higher molecular weight isoforms of shank3 protein (Speed et al., 2015). Extensive behavioral characterization showed that *Shank3*$^{G/G}$ mice exhibit impairments in motor coordination, altered response to novelty, and sensory processing deficits (Speed et al., 2015).

Although classically autism is defined as neurodevelopmental disorder, recent studies have suggested feasibility of rescue of the autism phenotypic characteristics after neurodevelopment is complete (Dragatsis and Zeitlin, 2001; Guy et al., 2007). To study the reversibility in *Shank3*^{G} mutation mice, we designed them with genetic rescue in mind. The construction of these mice is explained in detail in Chapter 3. Briefly, the mice express a point mutation (insG) in exon 21 of *Shank3* gene causing a premature stop codon followed by a transcriptional neo-STOP cassette that results in a truncated shank3 protein. This mutated region is flanked by *loxp* sites and is followed by a WT exon 21 allowing us temporal and spatial control over the reversibility (Dragatsis and Zeitlin, 2001; Guy et al., 2007). For this study, we focused on ubiquitous rescue of *Shank3*^{G} mutation and looked at rescue of Shank3 protein and robust behavioral impairments in the adult *Shank3*^{G} mutation mice.

Methods

Breeding Strategy

The *Shank3*^{G} mutation mice were crossed with wild-type C57BL6J mice more than 4 times. The progeny from the final backcross with the wild-type C57BL6J mice was then crossed with a tamoxifen-inducible CreESRT transgenic mouse line driven by chicken beta actin promoter that is expressed ubiquitously from the Jackson Laboratory (Strain:B6.Cg-Tg(CAG-cre/Esr1*)5Amc/J)(Hayashi and McMahon, 2002). This cross produced *Shank3*^{G} mutation mice with and without the CreESRT (Cre+ and Cre- respectively). The mice with the heterozygous *Shank3*^{G} mutation with CreESRT (*Reversible-Shank3*$^{GCre+}$) were then crossed with heterozygous *Shank3*^{G} mutation without CreESRT(*Irreversible-Shank3*$^{GCre-}$). This final cross yielded all the mice to be used in this study. In the *Reversible-Shank3*$^{GCre+}$mice, tamoxifen administration will allow the Cre recombinase to be transported inside the nucleus and excise out the mutated region of the S*hank3* gene resulting in WT shank3 to be expressed, effectively reversing the mutation. The *Irreversible-Shank3*$^{GCre-}$ mice also went under extensive behavioral testing to tease out any off target effects of tamoxifen.

Tamoxifen Dosing

The *Reversible-Shank3*$^{GCre+}$ and *Irreversible-Shank3*$^{GCre-}$ mutation mice were then randomly assigned to the Regular Diet group or the Tamoxifen Diet group. The tamoxifen food was ordered from Harlan (TD.130857, TAM Diet, 500, 2016). To

optimize the duration for tamoxifen food, mice were given tamoxifen food for 1, 2, or 4 weeks. We also compared 4-hydroxytamoxifen (Sigma-T176) injection treatment (66.67mg/kg of body weight, subcutaneous injections everyday for 15 days) with the food. After optimization, mice generated for behavior were treated with tamoxifen food for 6 weeks after reaching adulthood (8 weeks). Then the mice were switched back to regular 18% protein food for two weeks before being used for experiments. The Regular Diet group received regular 18% protein mouse food (Vehicle) for the whole duration.

Biochemistry

Western blotting was performed as previously described (Kouser et al., 2013). Synaptic protein levels from 7 littermate triplets ($WT^{(Cre+)}$/$Shank^{+/G(Cre+)}$/$Shank3^{G/G(Cre+)}$, 3-4 months old) at each treatment time point were determined by immunoblotting whole brain tissue homogenized in artificial cerebrospinal fluid, 5mM EDTA, and 1X Halt protease and phosphatase inhibitor cocktail (Thermo Scientific, Waltham, MA) diluted from 100X stock solution. 10 µg of protein were loaded per lane and blotted with a Shank3 antibody and internal loading controls (β-actin). An Image Works film processor was used to develop films and the chemiluminescence signals were quantified, normalized, and analyzed using Image Studi, Microsoft Excel and StatSoft software (Version 10, Statsoft, Tulsa, OK).

Behavioral Overview

Behavioral tests were performed on 4 cohorts (2 cohorts for *Reversible-Shank3*$^{GCre+}$ and 2 cohorts for *Irreversible-Shank3*$^{G/Cre-}$) of age and sex-matched littermate progeny of heterozygous matings (*Reversible-Shank3*$^{GCre+:}$ WT-Vehicle: *n* = 26, *Reversible-Shank3*$^{+/G}$-Vehicle: *n* = 21, *Reversible-Shank3*$^{G/G}$-Vehicle: *n* = 15, WT-Tamoxifen: *n* = 23, *Reversible-Shank3*$^{+/G}$- Tamoxifen: *n* = 15, *Reversible-Shank3*$^{G/G}$- Tamoxifen: *n* = 18; *Irreversible-Shank3*$^{GCre-:}$ WT-Vehicle: *n* = 27, *Irreversible-Shank3*$^{+/G}$-Vehicle: *n* = 18, *Irreversible-Shank3*$^{G/G}$-Vehicle: *n* = 19, WT-Tamoxifen: *n* = 25, *Irreversible-Shank3*$^{+/G}$- Tamoxifen: *n* = 19, *Irreversible-Shank3*$^{G/G}$- Tamoxifen: *n* = 16) during the light cycle of the mice (Table 5). All mice in each cohort were born within 12 weeks of each other. Tamoxifen dosing for the cohort began when the youngest pair or triplet was 8 weeks of age. Behaviors were tested at 4-6 months of age by an experimenter blind to genotype in the following order: locomotor, marble burying, rotarod, and nesting behavior. Behavioral results are described not in the order in which they were tested to simplify presentation of the data. One *Reversible-Shank3*$^{+/GCre+}$-Tamoxifen mouse was found dead in cage before marble burying behavior so it's littermate paired WT was also excluded from the future experiments. Statistical analyses of behavioral data were conducted using Statistica software using either three-way ANOVAs or four-way repeated measures ANOVA using genotype, sex and treatment as the main variables and trial as the repeated measure, where applicable. For detailed numerical statistical results see Table 6.

Locomotor

Locomotor activity was tested by placing the mice in a fresh home cage with minimal bedding and monitoring their activity for two hours using photobeams linked to a computer with data acquisition software (San Diego Instruments, San Diego, CA) (Powell et al., 2004). The test was conducted in the dark. Four-way repeated measures ANOVA was used to analyze the data with treatment, genotype and sex as between-subject factors and time as a within-subject factor.

Marble Burying

As previously described (Blundell et al., 2010a), twenty marbles were evenly placed around the edges of a novel home cage with 5 cm of bedding and mice were given 30 min in the cage. After 30 min the number of marbles buried was recorded. A marble was defined as buried when less than 25% of the marble was visible. The test room was well lit (~80 lux). Data were analyzed using three-way ANOVA with treatment, genotype and sex as between-subject factors.

Accelerating Rotarod

Coordination and motor learning were tested using a rotarod as previously described (Powell et al., 2004). Mice were placed on a stationary rotarod (IITC Life Sciences, Woodland Hills, CA) in a well lit room which was then activated and accelerated from 0-45 revolutions per min over 5 min. The latency for mice to fall off the rod or take one revolution was measured. Trials were repeated 4 times with inter-

trial intervals of 30 min over a single day. Data were analyzed using four-way repeated measures ANOVA with treatment, genotype and sex as between-subject factors and trials as a within-subject factor.

Nesting

Nesting behavior was performed in a well-lit (~80 lux) room by first habituating the mouse to a novel home cage with approximately 1.5 cm of bedding for 15 min, and then a cotton nestlet (5.5 x5.5 x 0.5 cm) was put in the cage. Height and width of the nests were measured at 30 min, 60 min and 90 min (Etherton et al., 2009). Data were analyzed using three-way ANOVA with treatment, genotype and sex as between-subject factors.

Results

Treatment with Tamoxifen food results in biochemical rescue of the Shank3 protein in whole brain lysates

Shank3^{G} mutation results in loss of predominant higher molecular weight isoforms of Shank3 protein using C-terminus antibody (Figure 4.1) and N-terminus antibody (Figure 3.2). To test if this loss is rescuable in the adulthood, we subjected whole brain lysates from mice treated with tamoxifen food for 1, 2, or 4 weeks to Western blot analysis (n = 7 per genotype and group) and compared them to the lysates from age and sex matched mice that had been treated with regular diet. We saw highest rescue at the 4 week treatment at which *Shank3*$^{+/G}$ mice showed almost

30% more Shank3 protein when compared to the untreated *Shank3*$^{+/G}$ mice. We also saw a rescue of Shank3 protein in the *Shank3*$^{G/G}$ mice upto 55-60% of the WT level after 4 weeks of tamoxifen food treatment which is the same Shank3 protein levels as the *Shank3*$^{+/G}$ mice in the untreated group (Figure 4.1. Two-way ANOVA: Main effect of Genotype: $F_{2,36} = 13.70$, $P < 0.001$; Main effect of Treatment: $F_{1,36} = 5.72$, $P < 0.05$; Genotype x Treatment Interaction: $F_{2,36} = 1.54$, $P > 0.05$). Lesser degree of rescue was also achieved by tamoxifen treatment for 2 weeks (Figure 4.1. Two-way ANOVA: Main effect of Genotype: $F_{2,36} = 18.63$, $P < 0.001$; Main effect of Treatment: $F_{1,36} = 4.92$, $P < 0.05$; Genotype x Treatment Interaction: $F_{2,36} = 1.49$, $P > 0.05$) and 1 week time (Figure 4.1. Two-way ANOVA: Main effect of Genotype: $F_{2,36} = 25.49$, $P < 0.001$; Main effect of Treatment: $F_{1,36} = 1.77$, $P > 0.05$; Genotype x Treatment Interaction: $F_{2,36} = 0.44$, $P > 0.05$). We also administered 4-hydroxytamoxifen injections for 15 days and compared them to the lysates from age and sex matched mice that had been given vehicle injections for fifteen days. We saw modest rescue of Shank3 protein using the injection method (Figure 4.1. Two-way ANOVA: Main effect of Genotype: $F_{2,36} = 20.97$, $P < 0.001$; Main effect of Treatment: $F_{1,36} = 1.60$, $P > 0.05$; Genotype x Treatment Interaction: $F_{2,36} = 0.48$, $P > 0.05$). These data suggest that duration of tamoxifen administration has a direct impact on the degree of rescue. We saw the highest degree of rescue with a 4 week long tamoxifen food treatment in these mice. Therefore we decided on a 6 week long tamoxifen food treatment for the behavioral experiments.

Effect of Tamoxifen food treatment on the avoidance phenotype of Irreversible-Shank3^{GCre-} and Reversible-Shank3^{GCre+} mice

As discussed in Chapter 3, *Shank3*$^{G/G}$ mice show a robust novelty avoidance phenotype in the nest building task. Therefore we tested the *Irreversible-Shank3*$^{G/GCre-}$ mice in the nest building task by adding a nestlet to a novel cage after a brief habituation period. As expected, vehicle treated *Irreversible-Shank3*$^{G/GCre-}$ mice exhibit impairment in nest building skills whereas their WT counterparts outperformed them by making nests readily. Likewise, tamoxifen treated *Irreversible-Shank3*$^{G/GCre-}$ mice also show poor nest building skills compared to the vehicle-treated WT (Figure 4.2A through D. Four-way rmANOVA for Nest Height: Main effect of Genotype: $F_{(2,112)}=5.08$, $P<0.01$; Main effect of Treatment: $F_{(1,112)}=0.11$, $P=0.73$; Main effect of Time: $F_{(2,224)}=72.37$, $P<0.001$; Treatment x Genotype Interaction: $F_{(2,112)}=0.73$, $P=0.48$; Four-way rmANOVA for Nest Width: Main effect of Genotype: $F_{(2,112)}=9.14$, $P<0.001$; Main effect of Treatment: $F_{(1,112)}=0.001$, $P=0.96$; Main effect of Time: $F_{(2,224)}=73.95$, $P<0.001$; Treatment x Genotype Interaction: $F_{(2,112)}=0.09$, $P=0.91$). We see the same novelty avoidance phenotype in the vehicle treated *Reversible-Shank3*$^{G/GCre+}$ mice but to a much lesser degree not yielding a significant result. This lack of significance makes the interpretation of the tamoxifen treated *Reversible-Shank3*$^{G/GCre+}$ mice data difficult as we do not see a difference among genotypes. (Figure 4.2E through H. Four-way rmANOVA for Nest Height: Main effect of Genotype: $F_{(2,106)}=2.151$, $P=0.12$; Main effect of Treatment: $F_{(1,\ 106)}=1.22$, $P=0.27$; Main effect of Time: $F_{(2,212)}=62.86$, $P<0.001$; Treatment x

Genotype Interaction: $F_{(2, 106)}$=0.48, P=0.61 ; Four-way rmANOVA for Nest Width: Main effect of Genotype: $F_{(2,106)}$=1.65, P=0.19; Main effect of Treatment: $F_{(1, 106)}$=0.25, P=0.61; Main effect of Time: $F_{(2,212)}$=101.07, P<0.001; Treatment x Genotype Interaction: $F_{(2,106)}$=0.83, P=0.43)

In order to shed more light on this observation, we administered the marble burying task. Similar to our previous findings both vehicle and tamoxifen treated *Irreversible-Shank3*$^{G/GCre-}$ mice expressed no interest in the marbles and barely buried any marbles compared to vehicle treated WT (Figure 4.2I. Three-way ANOVA: Main effect of Genotype: $F_{(2,112)}$=32.72, P<0.001; Main effect of Treatment: $F_{(1,112)}$=0.55, P=0.45; Treatment x Genotype Interaction: $F_{(2, 112)}$=0.40, P=0.66) More importantly, same avoidance phenotype was observed in both vehicle and tamoxifen treated *Reversible-Shank3*$^{G/GCre+}$ mice (Figure 4.2J. Three-way ANOVA: Main effect of Genotype: $F_{(2,104)}$=14.26, P<0.001; Main effect of Treatment: $F_{(1, 104)}$=0.006; Treatment x Genotype Interaction: $F_{(2, 104)}$=1.15, P=0.76).

Effect of Tamoxifen food treatment on the locomotor activity of Irreversible-Shank3^{GCre-} *and Reversible-Shank3*$^{GCre+}$ *mice*

In accordance with their novelty avoidance phenotype, the *Irreversible-Shank3*$^{G/GCre-}$ mice are also hypoactive in a novel environment. We observed the locomotor activity of vehicle treated *Irreversible-Shank3*$^{G/GCre-}$ mice by measuring photobeam breaks in a novel home cage for 2 hours and found that they have aberrant response to a novel environment. Tamoxifen treated *Irreversible-Shank3*$^{G/GCre-}$ mice

also show the same phenotype (Figure 4.3A and B. Four-way rmANOVA: Main effect of Genotype: $F_{(2,112)}$=5.13, P<0.01; Main effect of Treatment: $F_{(1,112)}$=0.27, P=0.60; Main effect of Time: $F_{(23,2576)}$=199.36, P<0.001; Treatment x Genotype Interaction: $F_{(2,112)}$=2.34, P=0.67). This hypoactive response is particularly noticeable in the first 5 minutes of the locomotor task. (Figure 4.3E. Three-way ANOVA: Main effect of Genotype: $F_{(2,112)}$=22.20, P<0.001; Main effect of Treatment: $F_{(1,112)}$=2.05; Treatment x Genotype Interaction: $F_{(2, 112)}$=2.8, P=0.06). As observed in previous behaviors, *Reversible-Shank3*$^{G/GCre+}$ mice do not exhibit the differences found in the *Irreversible-Shank3*$^{G/GCre-}$ mice and their WT counterparts. *Reversible-Shank3*$^{G/GCre+}$ mice show no effect of genotype for the 2 hour locomotor test. (Figure 4.3C and D. Four-way rmANOVA: Main effect of Genotype: $F_{(2,106)}$=1.92, P=0.15; Main effect of Treatment: $F_{(1, 106)}$=8.56, P<0.01; Main effect of Time: $F_{(23,2438)}$=199.94, P<0.001). Curiously, in the first five minutes of the task, the *Reversible-Shank3*$^{G/GCre+}$ mice do exhibit a main effect of genotype but as the Figure4.3F shows it is due to decreased activity in vehicle and tamoxifen treated WT mice and not the *Reversible-Shank3*$^{G/GCre+}$ mice as we would have expected (Figure 4.3F. Three-way ANOVA: Main effect of Genotype: $F_{(2,106)}$=14.35, P<0.001; Main effect of Treatment: $F_{(1, 106)}$=2.78, P=0.09; Treatment x Genotype Interaction: $F_{(2, 106)}$=0.81, P=0.10).

Effect of Tamoxifen food treatment on the motor coordination of Irreversible-Shank3^{GCre-} *and Reversible-Shank3*$^{GCre+}$ *mice*

We also tested these mice for motor coordination and learning impairments. Consistent with previous findings described in chapter 3, both vehicle and tamoxifen treated *Irreversible-Shank3*$^{G/GCre-}$ mice show poor motor performance by having shorter latencies to fall off the rotarod over eight trials (Figure 4.4A and B. Four-way rmANOVA: Main effect of Genotype: $F_{(2,112)}$=18.48, P<0.001; Main effect of Treatment: $F_{(1, 112)}$=1.07, P=0.30; Main effect of Trial: $F_{(7,784)}$=30.07, P<0.001; Treatment x Genotype Interaction: $F_{(2, 112)}$=0.80, P=0.44). The *Reversible-Shank3*$^{G/GCre+}$ mice, on the other hand, show no difference in genotypes in vehicle or tamoxifen treated groups which is consistent with our findings in the nesting behavior and the locomotor task (Figure 4.4C and D. Four-way rmANOVA: Main effect of Genotype: $F_{(2,106)}$=1.91, P=0.15; Main effect of Treatment: $F_{(1, 106)}$=3.45, P=0.06; Main effect of Trial: $F_{(7,742)}$=39.08, P<0.001; Treatment x Genotype Interaction: $F_{(2, 106)}$=1.29, P=0.27).

Discussion

The *Reversible-Shank3*$^{GCre+}$ mice are the first reversible *Shank3* mouse model of autism. The *Shank3*^{G} mice express a point mutation (insG) in exon 21 of the *Shank3* gene causing a premature stop codon followed by a transcriptional neo-STOP cassette that results in a truncated Shank3 protein. This mutated region is flanked by *loxp* sites and is followed by a WT exon 21 allowing us temporal and spatial control over the reversibility (Dragatsis and Zeitlin, 2001; Guy et al., 2007). After crossing The *Shank3*^{G} mice with the tamoxifen driven inducible CreESRT line, we get

Irreversible-Shank3^{GCre-} and *Reversible-Shank3*$^{GCre+}$ mice. The *Reversible-Shank3*$^{GCre+}$ mice upon treatment with tamoxifen food show a dose dependent restoration of the Shank3 protein expression. The best rescue is achieved by tamoxifen food administration for 4 weeks as we see the shank3 protein levels in the *Reversible-Shank3*$^{+/GCre+}$ mice rescue up to 90% and in the *Reversible-Shank3*$^{G/GCre+}$ mice rescue up to the 55% (similar to *Reversible-Shank3*$^{+/GCre+}$ mice on regular food) when compared to the WT mice on regular food.

The *Irreversible-Shank3*$^{GCre-}$ and *Reversible-Shank3*$^{GCre+}$ mice were then tested in behavioral assays in which the *Shank3*^{G} mice showed a robust phenotype. The *Shank3*^{G} mice expressed a novelty avoidance, hypoactivity, and motor incoordination phenotype. We have successfully replicated each of these phenotypes in the *Irreversible-Shank3*$^{GCre-}$ mice with and without tamoxifen. This suggests that these behaviors are robust, reproducible, and can provide viable outcome measures for testing future behavioral therapies and pharmaceutical agents. This also provides an important control for the off-target effects of tamoxifen, indicating that tamoxifen is not having any influence on behavior.

At first glance, in the *Reversible-Shank3*$^{GCre+}$ mice the tamoxifen treatment looks like it "rescued" the novelty avoidance phenotype of the *Reversible-Shank3*$^{G/GCre+}$ mice as there is no difference among genotypes in the nest building task. However, in the *Reversible-Shank3*$^{GCre+}$ mice, it is the WT who are building smaller nests when compared to the *Irreversible-Shank3*$^{G/GCre-}$ cohorts. Of course, we cannot statistically compare the *Irreversible-Shank3*$^{GCre-}$ vs. *Reversible-Shank3*$^{GCre+}$

mice as they were tested in different cohorts and differences beyond our control may be affecting the outcome of the behavior in each different cohort (Yang et al., 2012). This decrease in the WT performance of the *Reversible-Shank3*$^{GCre+}$ mice is further supported by the results of the marble burying task, in which we do not see rescue of the marble burying phenotype. In fact, we see a decrease in the number of marbles buried by the tamoxifen treated *Reversible-Shank3*$^{GCre+}$ WT group when compared to the vehicle treated *Reversible-Shank3*$^{GCre+}$ WT group. Similarly, we do not see a difference among genotypes in tamoxifen treated *Reversible-Shank3*$^{GCre+}$ mice in the locomotor and rotarod test, suggesting rescue. However, the controls (vehicle treated *Reversible-Shank3*$^{GCre+}$ mice) also do not show a difference among genotypes making these data hard to interpret. Since all of the mice used in these experiments are progeny of the same breeding cross (*Reversible-Shank3*$^{+/GCre+}$ x *Irreversible-Shank3*$^{+/GCre-}$), genetic background variation can be ruled out as a possible confound. One explanation for this result is that the presence of Cre is affecting behavior in the *Reversible-Shank3*$^{GCre+}$ mice. In order to test this hypothesis, we will need to test *Irreversible-Shank3*$^{GCre-}$ and *Reversible-Shank3*$^{GCre+}$ mice in the same cohort.

Another explanation for the lack of clear rescue of the behavioral phenotype in the *Reversible-Shank3*$^{GCre+}$ mice could be mosaicism in the Cre expression. We do not know if the *Shank3*^{G} mutation is reversed ubiquitously in the brain or is localized to specific brain regions and cell types. Immunohistochemistry studies need to be conducted to distinguish between these possibilities. Alternatively, we could cross the *Reversible-Shank3*$^{G/GCre+}$ with a fluorescent reporter mouse line to show the activity

of the Cre. One more possibility could be that restoration to 55% of WT Shank3 protein in *Reversible-Shank3*$^{G/GCre+}$ mice compared to WT controls after the completion of neurodevelopment simply may not be sufficient to rescue the behavioral phenotype which will further support the presence of critical windows in development. In the absence of critical periods, one would expect that the restoration to 55% of WT Shank3 protein in *Reversible-Shank3*$^{G/GCre+}$ mice compared to WT controls should be sufficient as the untreated *Reversible-Shank3*$^{WT/GCre+}$ mice do not have an impaired phenotype. In order to test that hypothesis, we will need to either use a more stringent tamoxifen dosing regimen to increase rescue levels or use a different Cre recombinase promoter line. As briefly mentioned previously, another likely scenario is the presence of developmental critical periods after which rescue of behavioral abnormalities cannot be achieved. We might have to target at an earlier time point in neurodevelopment to achieve not just biochemical but behavioral rescue as well. Overall, these experiments have demonstrated the feasibility of biochemical rescue of Shank3 in adult animals. Further experimentation is needed before we can draw any meaningful conclusions about the rescue of behavioral phenotype observed in the *Shank3*^{G} mice.

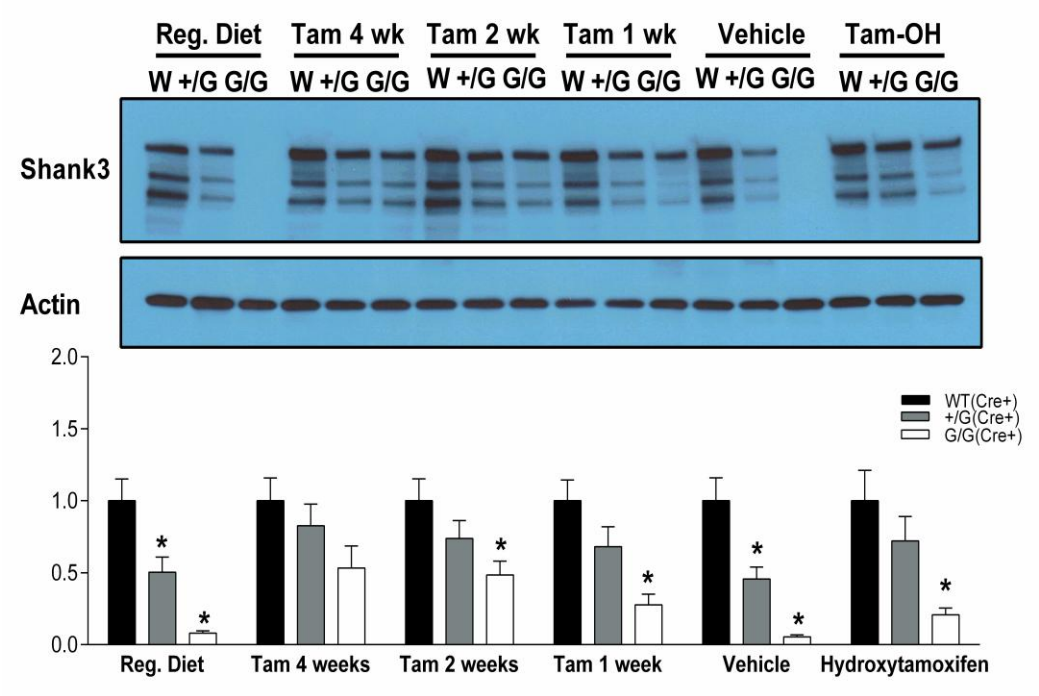

Figure 4.1: Treatment with Tamoxifen Food Results in Biochemical Rescue of the Shank3 protein in the *Reversible-Shank3*$^{GCre+}$ mice: Quantification and representative Western blot of whole brain lysates showing varying degrees of rescue of Shank 3 protein with C-terminus antibody (JH3025) after varying duration of tamoxifen food or 4-Hydroxytamoxifen (Tam-OH) injection treatment. Data are normalized to the ß- Actin control and then to the average of WT levels (n = 7). *P < 0.05

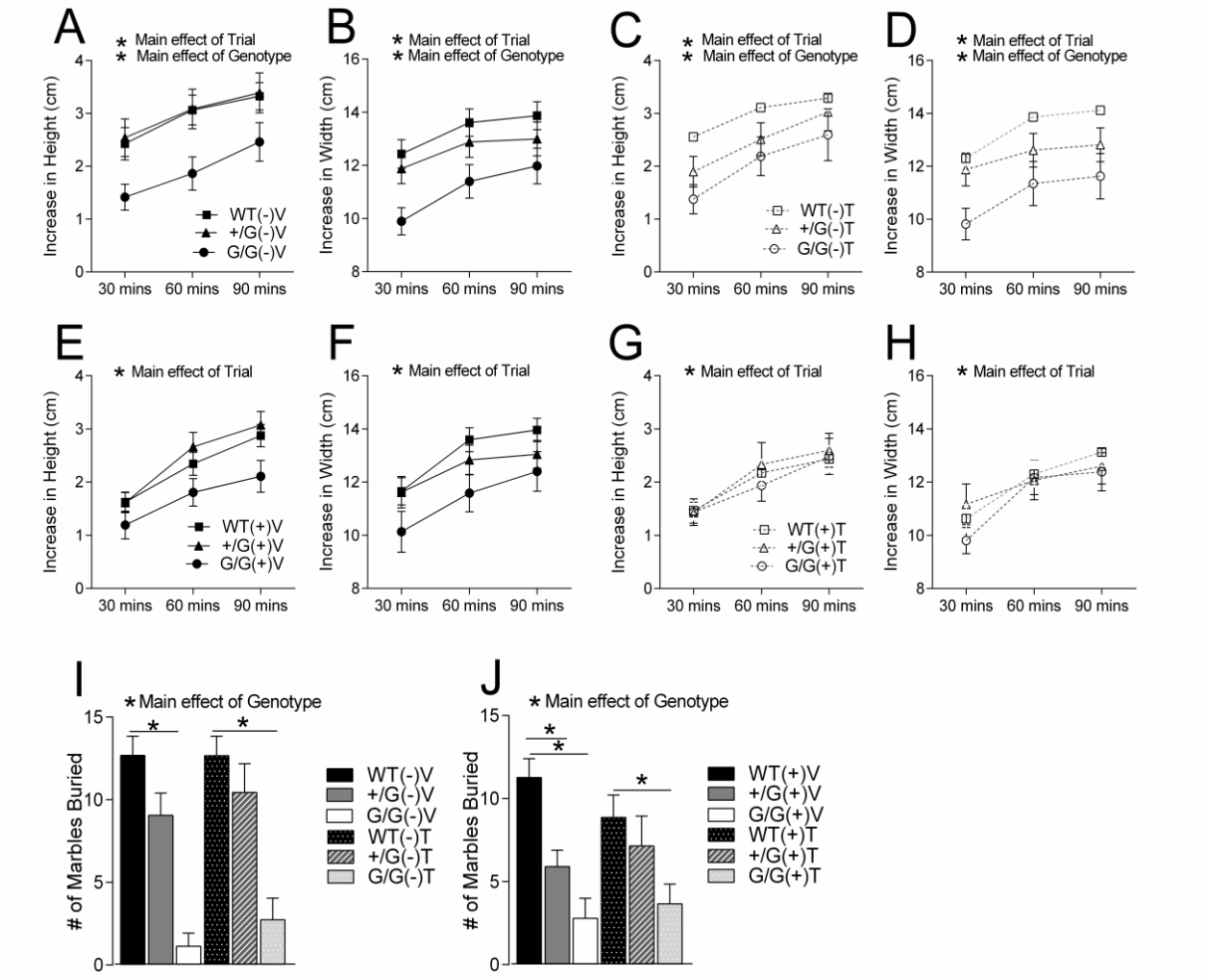

Figure 4.2: *Irreversible-Shank3*$^{GCre-}$ Mice Exhibit Novelty Avoidance Behaviors.

A-H) Height and Width of nest built as a function of time in nest building task. A-D) *Irreversible-Shank3*$^{G/G-}$ mice exhibit nest building deficits over a period of 90 minutes. As expected this deficit is impervious to the tamoxifen treatment. Legend in A and C applies to B and D respectively. (*Irreversible-Shank3*$^{GCre-:}$ WT-Vehicle: *n* = 27, *Irreversible-Shank3*$^{+/G}$-Vehicle: *n* = 18, *Irreversible-Shank3*$^{G/G}$-Vehicle: *n* = 19, WT-Tamoxifen: *n* = 25, *Irreversible-Shank3*$^{+/G}$- Tamoxifen: *n* = 19, *Irreversible-*

Shank3$^{G/G}$- Tamoxifen: *n* = 16). E-H) *Irreversible-Shank3*$^{G/G+}$ mice do not show a nest building deficit in the vehicle treated or tamoxifen treated group. Legend in E and G applies to F and H respectively. (*Reversible-Shank3*$^{GCre+:}$ WT-Vehicle: *n* = 26, *Reversible-Shank3*$^{+/G}$-Vehicle: *n* = 21, *Reversible-Shank3*$^{G/G}$-Vehicle$^{:}$ *n* = 15, WT-Tamoxifen: *n* = 23, *Reversible-Shank3*$^{+/G}$- Tamoxifen: *n* = 15, *Reversible-Shank3*$^{G/G}$-Tamoxifen$^{:}$ *n* = 18). I-J) Number of marbles buried in 30 minute duration. Both *Irreversible-Shank3*$^{G/GCre-}$ and *Reversible-Shank3*$^{G/GCre+}$mice exhibit marble burying deficits irrespective of the tamoxifen treatment. (*Irreversible-Shank3*$^{GCre-:}$ WT-Vehicle: *n* = 27, *Irreversible-Shank3*$^{+/G}$-Vehicle: *n* = 18, *Irreversible-Shank3*$^{G/G}$-Vehicle$^{:}$ *n* = 19, WT-Tamoxifen: *n* = 25, *Irreversible-Shank3*$^{+/G}$- Tamoxifen: *n* = 19, *Irreversible-Shank3*$^{G/G}$- Tamoxifen: *n* = 16 *Reversible-Shank3*$^{GCre+:}$ WT-Vehicle: *n* = 26, *Reversible-Shank3*$^{+/G}$-Vehicle: *n* = 21, *Reversible-Shank3*$^{G/G}$-Vehicle$^{:}$ *n* = 15, WT-Tamoxifen: *n* = 22, *Reversible-Shank3*$^{+/G}$- Tamoxifen: *n* = 14, *Reversible-Shank3*$^{G/G}$- Tamoxifen$^{:}$ *n* = 18). *P < 0.05

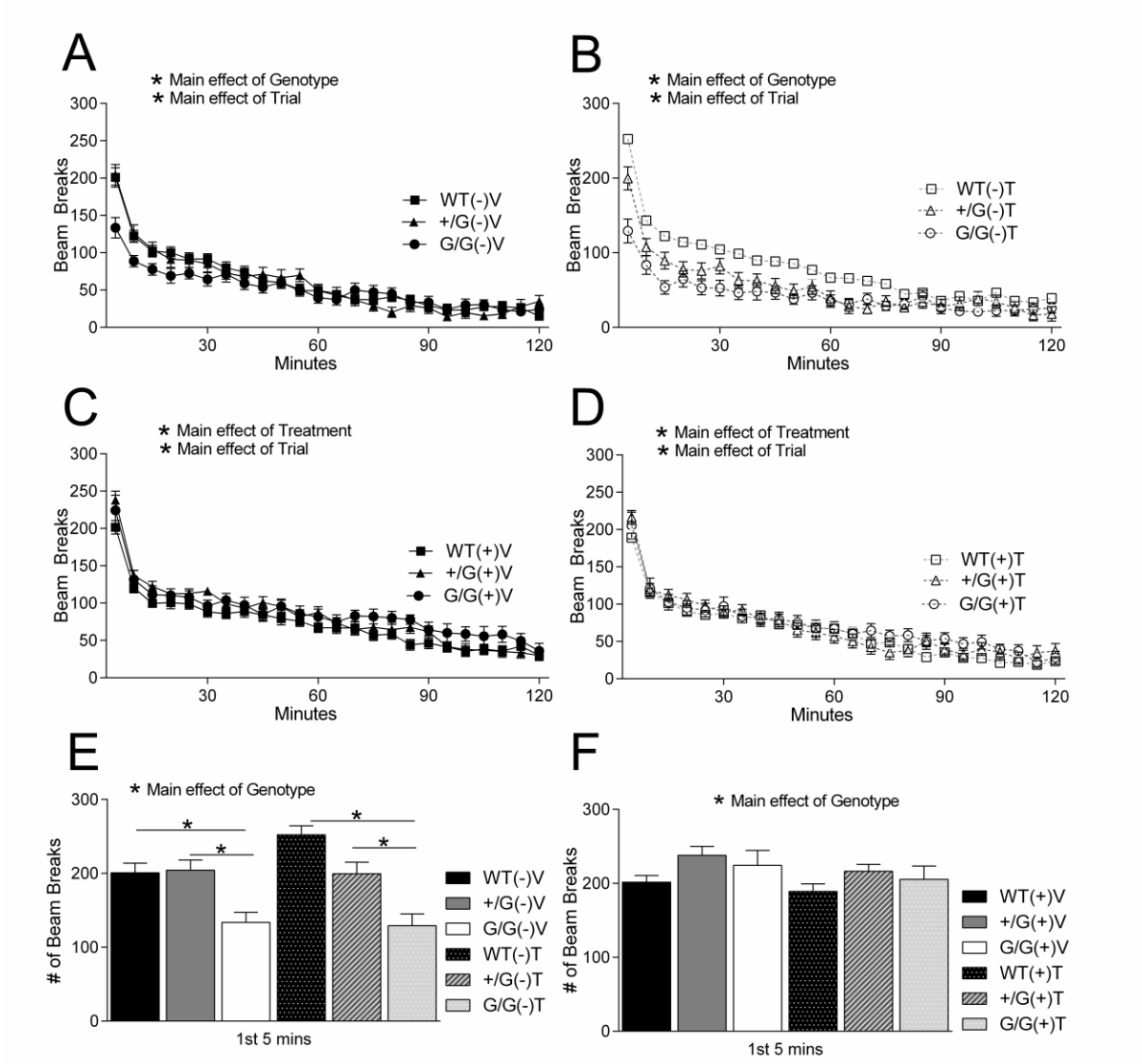

Figure 4.3: *Irreversible-Shank3*$^{G/GCre-}$ and *Reversible-Shank3*$^{G/GCre+}$ Mice Exhibit Mild Impairments in Locomotor Habituation Task. A-D) Locomotor activity was measured by number of photobeam breaks during successive 5-min intervals over a two-hour period. A-B) *Irreversible-Shank3*$^{+/GCre-}$ and *Irreversible-Shank3*$^{G/GCre-}$ mice exhibit slightly less locomotor activity in both Vehicle and Tamoxifen treated groups. C-D) *Reversible-Shank3*$^{+/GCre+}$ and *Reversible-Shank3*$^{G/GCre+}$ mice do not exhibit the

same hypoactive phenotype in neither vehicle nor tamoxifen treated group. E-F) Photobeam breaks in the first 5 minute interval of the locomotor task. E) *Irreversible-Shank3*$^{G/GCre-}$ mice are significantly hypoactive in the first 5 minutes of the locomotor task. F) *Reversible-Shank3*$^{GCre+}$ mice display a main effect of genotype among groups in the first 5 minutes of the locomotor task. (*Irreversible-Shank3*$^{GCre-:}$ WT-Vehicle: *n* = 27, *Irreversible-Shank3*$^{+/G}$-Vehicle: *n* = 18, *Irreversible-Shank3*$^{G/G}$-Vehicle$^{:}$ *n* = 19, WT-Tamoxifen: *n* = 25, *Irreversible-Shank3*$^{+/G}$- Tamoxifen: *n* = 19, *Irreversible-Shank3*$^{G/G}$- Tamoxifen: *n* = 16 *Reversible-Shank3*$^{GCre+:}$ WT-Vehicle: *n* = 26, *Reversible-Shank3*$^{+/G}$-Vehicle: *n* = 21, *Reversible-Shank3*$^{G/G}$-Vehicle$^{:}$ *n* = 15, WT-Tamoxifen: *n* = 23, *Reversible-Shank3*$^{+/G}$- Tamoxifen: *n* = 15, *Reversible-Shank3*$^{G/G}$-Tamoxifen$^{:}$ *n* = 18). *P < 0.05

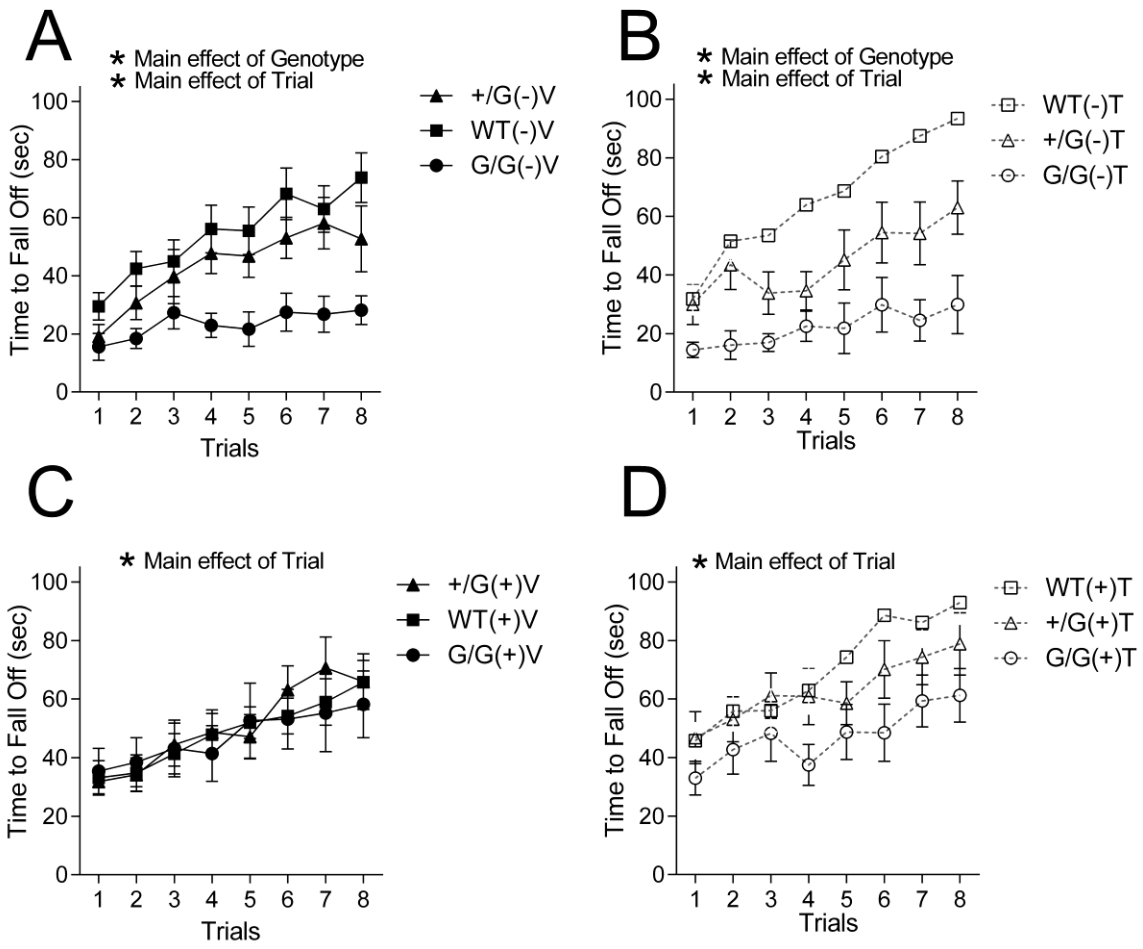

Figure 4.4: *Irreversible-Shank3*$^{G/GCre-}$ Mice Display Impairments in Motor Coordination. A-D) Latency to fall off or go one revolution on the rotarod. A-B) Both Vehicle and tamoxifen treated *Irreversible-Shank3*$^{G/GCre-}$ mice exhibit poor performance on the rotarod. C-D) *Reversible-Shank3*$^{G/GCre+}$ mice exhibit normal motor coordination and learning in vehicle and tamoxifen treated group. (*Irreversible-Shank3*$^{GCre-:}$ WT-Vehicle: *n* = 27, *Irreversible-Shank3*$^{+/G}$-Vehicle: *n* = 18, *Irreversible-Shank3*$^{G/G}$-Vehicle$^{:}$ *n* = 19, WT-Tamoxifen: *n* = 25, *Irreversible-Shank3*$^{+/G}$- Tamoxifen: *n* = 19, *Irreversible-Shank3*$^{G/G}$- Tamoxifen: *n* = 16

Reversible-Shank3$^{GCre+:}$ WT-Vehicle: *n* = 26, *Reversible-Shank3*$^{+/G}$-Vehicle: *n* = 21, *Reversible-Shank3*$^{G/G}$-Vehicle: *n* = 15, WT-Tamoxifen: *n* = 23, *Reversible-Shank3*$^{+/G}$-Tamoxifen: *n* = 15, *Reversible-Shank3*$^{G/G}$- Tamoxifen: *n* = 18). *P < 0.05

Table 5: Experimental Groups		
Strain	**Treatment**	**Genotype (N)**
IRREVERSIBLE -Shank3^{GCre-}	**Vehicle**	**WT (27)** ***Shank3$^{+/G}$*** **(18)** ***Shank3$^{G/G}$*** **(19)**
	Tamoxifen	**WT (25)** ***Shank3$^{+/G}$*** **(19)** ***Shank3$^{G/G}$*** **(16)**
REVERSIBLE - Shank3^{GCre+}	**Vehicle**	**WT (26)** ***Shank3$^{+/G}$*** **(21)** ***Shank3$^{G/G}$*** **(15)**
	Tamoxifen	**WT (23)** ***Shank3$^{+/G}$*** **(15)** ***Shank3$^{G/G}$*** **(18)**

Table 6: Statistical Analysis of Behavioral Studies		
Parameter	**Comparison**	**Results**
Nesting Behavior		
***Irreversible-Shank3^{GCre-}* Vehicle - N= WT:27, Shank3$^{+/G}$:18, Shank3$^{G/G}$:19**		
Tamoxifen - N= WT:25, Shank3$^{+/G}$:19, Shank3$^{G/G}$:16		
Increase in Nest Height	Sex, Genotype, Treatment & Time	4-way rmANOVA; Main effect of Sex: $F(1,112)=0.0006$, $P=0.98$; Main effect of Genotype: $F(2,112)=5.08$, $P<0.01$; Main effect of Treatment: $F(1,112)=0.11$, $P=0.73$; Main effect of Time: $F(2,224)=72.37$, $P<0.001$; Sex x Genotype Interaction: $F(2,112)=0.69$, $P=0.50$; Sex x Treatment Interaction: $F(1,112)=0.02$, $P=0.88$; Treatment x Genotype Interaction: $F(2,112)=0.73$, $P=0.48$
		Tukey HSD: WT-Vvs. WT-T: P=0.99; Shank3$^{+/G}$-V vs Shank3$^{+/G}$-T: P=0.84; Shank3$^{G/G}$-V vs. Shank3$^{G/G}$-T: P=0.99
Increase in Nest Width	Sex, Genotype, Treatment & Time	4-way rmANOVA; Main effect of Sex: $F(1,112)=0.57$, $P=0.45$; Main effect of Genotype: $F(2,112)=9.14$, $P<0.001$; Main effect of Treatment: $F(1,112)=0.001$, $P=0.96$; Main effect of Time: $F(2,224)=73.95$, $P<0.001$; Sex x Genotype Interaction: $F(2,112)=0.65$, $P=0.52$; Sex x Treatment Interaction: $F(1,112)=0.002$, $P=0.96$; Treatment x Genotype Interaction: $F(2,112)=0.09$, $P=0.91$
		Tukey HSD: WT-Vvs. WT-T: P=0.99; Shank3$^{+/G}$-V vs Shank3$^{+/G}$-T: P=0.99; Shank3$^{G/G}$-V vs. Shank3$^{G/G}$-T: P=0.99
***Reversible-Shank3^{GCre+}* Vehicle - N= WT:26, Shank3$^{+/G}$:21, Shank3$^{G/G}$:15**		
Tamoxifen - N= WT:23, Shank3$^{+/G}$:15, Shank3$^{G/G}$:18		
Increase in Nest Height	Sex, Genotype, Treatment & Time	4-way rmANOVA; Main effect of Sex: $F(1,106)=0.01$, $P=0.89$; Main effect of Genotype: $F(2,106)=2.151$, $P=0.12$; Main effect of Treatment: $F(1, 106)=1.22$, $P=0.27$; Main effect of Time: $F(2,212)=62.86$, $P<0.001$; Sex x Genotype Interaction: $F(2, 106)=1.50$, $P=0.22$; Sex x Treatment Interaction: $F(1, 106)=1.06$, $P=0.30$; Treatment x Genotype Interaction: $F(2, 106)=0.48$, $P=0.61$
Increase in Nest	Sex, Genotype,	4-way rmANOVA; Main effect of Sex:

Width	Treatment & Time	F(1,106)=0.007, P=0.93; Main effect of Genotype: F(2,106)=1.65, P=0.19; Main effect of Treatment: F(1, 106)=0.25, P=0.61; Main effect of Time: F(2,212)=101.07, P<0.001; Sex x Genotype Interaction: F(2, 106)=0.78, P=0.46; Sex x Treatment Interaction: F(1, 106)=1.17, P=0.28; Treatment x Genotype Interaction: F(2, 106)=0.83, P=0.43
Marble Burying		
***Irreversible-Shank3^{GCre-}* Vehicle - N= WT:27, Shank3$^{+/G}$:18, Shank3$^{G/G}$:19**		
Tamoxifen - N= WT:25, Shank3$^{+/G}$:19, Shank3$^{G/G}$:16		
Number of Marbles Buried	Sex , Genotype & Treatment	3-way ANOVA; Main effect of Sex: F(1,112)=0.75, P=0.38; Main effect of Genotype: F(2,112)=32.72, P<0.001; Main effect of Treatment: F(1,112)=0.55, P=0.45; Sex x Genotype Interaction: F(2,112)=1.06, P=0.34; Treatment x Genotype Interaction: F(2, 112)=0.40, P=0.66
		Tukey HSD: WT-Vvs. WT-T: P=0.99; Shank3$^{+/G}$-V vs Shank3$^{+/G}$-T: P=0.97; Shank3$^{G/G}$-V vs. Shank3$^{G/G}$-T: P=0.98
***Reversible-Shank3^{GCre+}* Vehicle - N= WT:26, Shank3$^{+/G}$:21, Shank3$^{G/G}$:15**		
Tamoxifen - N= WT:22, Shank3$^{+/G}$:14, Shank3$^{G/G}$:18		
Number of Marbles Buried	Sex , Genotype & Treatment	3-way ANOVA; Main effect of Sex: F(1,104)=0.45, P=0.50; Main effect of Genotype: F(2,104)=14.26, P<0.001; Main effect of Treatment: F(1, 104)=0.006, P=0.93; Sex x Genotype Interaction: F(2, 104)=0.09, P=0.90; Sex x Treatment Interaction: F(1, 104)=0.36, P=0.54; Treatment x Genotype Interaction: F(2, 104)=1.15, P=0.76
		Tukey HSD: WT-Vvs. WT-T: P=0.72; Shank3$^{+/G}$-V vs Shank3$^{+/G}$-T: P=0.99; Shank3$^{G/G}$-V vs. Shank3$^{G/G}$-T: P=0.99
Locomotor Habituation		
***Irreversible-Shank3^{GCre-}* Vehicle - N= WT:27, Shank3$^{+/G}$:18, Shank3$^{G/G}$:19**		
Tamoxifen - N= WT:25, Shank3$^{+/G}$:19, Shank3$^{G/G}$:16		
Total Beam Breaks	Sex, Genotype, Treatment & Time	4-way rmANOVA; Main effect of Sex: F(1,112)=0.007, P=0.93; Main effect of Genotype: F(2,112)=5.13, P<0.01; Main effect of Treatment: F(1,112)=0.27, P=0.60; Main effect of Time: F(23,2576)=199.36, P<0.001; Sex x Genotype Interaction: F(2,112)=0.006,

		P=0.99; Sex x Treatment Interaction: F(1,112)=1.30, P=0.25; Treatment x Genotype Interaction: F(2,112)=2.34, P=0.67
		Tukey HSD: WT-Vvs. WT-T: P=0.30; $Shank3^{+/G}$-V vs $Shank3^{+/G}$-T: P=0.99; $Shank3^{G/G}$-V vs. $Shank3^{G/G}$-T: P=0.97
1st bin only	Sex , Genotype & Treatment	3-way ANOVA; Main effect of Sex: F(1,112)=0.23, P=0.63; Main effect of Genotype: F(2,112)=22.20, P<0.001; Main effect of Treatment: F(1,112)=2.05, P=0.15; Sex x Genotype Interaction: F(2,112)=0.31, P=0.72; Treatment x Genotype Interaction: F(2, 112)=2.8, P=0.06
		Tukey HSD: WT-Vvs. WT-T: P=0.06; $Shank3^{+/G}$-V vs $Shank3^{+/G}$-T: P=0.99; $Shank3^{G/G}$-V vs. $Shank3^{G/G}$-T: P=0.99
***Reversible-Shank3^{GCre+}* Vehicle - N= WT:26, $Shank3^{+/G}$:21, $Shank3^{G/G}$:15**		
Tamoxifen - N= WT:23, $Shank3^{+/G}$:15, $Shank3^{G/G}$:18		
Total Beam Breaks	Sex, Genotype, Treatment & Time	4-way rmANOVA; Main effect of Sex: F(1,106)=2.18, P=0.14; Main effect of Genotype: F(2,106)=1.92, P=0.15; Main effect of Treatment: F(1, 106)=8.56, P<0.01; Main effect of Time: F(23,2438)=199.94, P<0.001; Sex x Genotype Interaction: F(2, 106)=0.10, P=0.90; Sex x Treatment Interaction: F(1, 106)=0.20, P=0.65; Treatment x Genotype Interaction: F(2, 106)=2.29, P=0.10
		Tukey HSD: WT-Vvs. WT-T: P=0.55; $Shank3^{+/G}$-V vs $Shank3^{+/G}$-T: 0.99; $Shank3^{G/G}$-V vs. $Shank3^{G/G}$-T: P<0.05
1st bin only	Sex , Genotype & Treatment	3-way rmANOVA; Main effect of Sex: F(1,106)=9.11, P<0.001; Main effect of Genotype: F(2,106)=14.35, P<0.001; Main effect of Treatment: F(1, 106)=2.78, P=0.09; Sex x Genotype Interaction: F(2, 106)=0.84, P=0.43; Sex x Treatment Interaction: F(1, 106)=1.98, P=0.16; Treatment x Genotype Interaction: F(2, 106)=0.81, P=0.10
		Tukey HSD: WT-Vvs. WT-T: P=0.94; $Shank3^{+/G}$-V vs $Shank3^{+/G}$-T: 0.99; $Shank3^{G/G}$-V vs. $Shank3^{G/G}$-T: P=0.46
Rotarod		
***Irreversible-Shank3^{GCre-}* Vehicle - N= WT:27, $Shank3^{+/G}$:18, $Shank3^{G/G}$:19**		

Tamoxifen - N= WT:25, Shank3$^{+/G}$:19, Shank3$^{G/G}$:16		
Time to Fall Off	Sex, Genotype, Treatment & Trial	4-way rmANOVA; Main effect of Sex: $F(1,112)=19.01$, $P<0.001$; Main effect of Genotype: $F(2,112)=18.48$, $P<0.001$; Main effect of Treatment: $F(1, 112)=1.07$, $P=0.30$; Main effect of Trial: $F(7,784)=30.07$, $P<0.001$; Sex x Genotype Interaction: $F(2, 112)=2.31$, $P=0.10$; Sex x Treatment Interaction: $F(1, 112)=1.85$, $P=0.17$; Treatment x Genotype Interaction: $F(2, 112)=0.80$, $P=0.44$
		Tukey HSD: WT-Vvs. WT-T: P=0.60; Shank3$^{+/G}$-V vs Shank3$^{+/G}$-T: 0.99; Shank3$^{G/G}$-V vs. Shank3$^{G/G}$-T: P=0.99
Reversible-Shank3^{GCre+} **Vehicle - N= WT:26, Shank3$^{+/G}$:21, Shank3$^{G/G}$:15**		
Tamoxifen - N= WT:23, Shank3$^{+/G}$:15, Shank3$^{G/G}$:18		
Time to Fall Off	Sex, Genotype, Treatment & Trial	4-way rmANOVA; Main effect of Sex: $F(1,106)=13.32$, $P<0.001$; Main effect of Genotype: $F(2,106)=1.91$, $P=0.15$; Main effect of Treatment: $F(1, 106)=3.45$, $P=0.06$; Main effect of Trial: $F(7,742)=39.08$, $P<0.001$; Sex x Genotype Interaction: $F(2, 106)=0.94$, $P=0.39$; Sex x Treatment Interaction: $F(1, 106)=0.27$, $P=0.60$; Treatment x Genotype Interaction: $F(2, 106)=1.29$, $P=0.27$
		Tukey HSD: WT-Vvs. WT-T: P=0.13; Shank3$^{+/G}$-V vs Shank3$^{+/G}$-T: 0.99; Shank3$^{G/G}$-V vs. Shank3$^{G/G}$-T: P=0.86

ANOVA: analysis of variance, WT: wildtype, rmANOVA: ANOVA (between subjects factors are generally sex and genotype) with repeated measures (day, time, or trial). F(x,y): F ratio statistic is used to determine whether the variances in two independent samples are equal, x,y are degrees of freedom (df). Degrees of freedom is a measure of the number of independent pieces of information on which the precision of a parameter estimate is based. x = number of groups-1, y = number of animals per group minus 1, multiplied by the number of groups.

CHAPTER FIVE
Conclusions and Recommendations

Here we have validated a human associated autism relevant mutation in two different mouse models using two different approaches. One is deletion of exon 21 *(Shank3*$^{\Delta C}$*)* and the other is directly mimicking a human mutation by inserting a guanine nucleotide creating a premature stop codon in exon 21 *(Shank3*^{G}*).* Both of these mutations results in a similar biochemical, behavioral, and electrophysiological phenotype yet there are subtle differences between the two mouse models that remind us of the heterogeneity that we observe in the human patients of autism spectrum disorder.

The first mouse model described is a *Shank3*$^{\Delta C}$ deletion mutation targeting the homer binding region. This mutation results in loss of all major naturally occurring higher molecular weight isoforms of Shank3 in the *Shank3*$^{\Delta C/\Delta C}$ mice using a C-terminal targeting antibody. We also noticed the appearance of smaller molecular weight isoforms of Shank3 in the *Shank3*$^{\Delta C/\Delta C}$ mice on Western blot with N-terminal and SH3 antibodies. The second mouse model mimics a guanine nucleotide insertion (insG) mutation in exon 21 of *Shank3* found is human idiopathic autism (Durand et al., 2007). This insG mutation (*Shank3*^{G}) causes a frameshift creating a pre-mature translation STOP codon in exon 21 of *Shank3* predicting a truncated Shank3 protein (Durand et al., 2007; Durand et al., 2012). Consistent with the phenotype observed in *Shank3*$^{\Delta C}$ mice, Western blot data show that the homozygous *Shank3*^{G} mutation

causes loss of multiple higher molecular weight isoforms of Shank3 (Kouser et al., 2013) and appearance of smaller molecular weight isoforms in *Shank3*$^{G/G}$ mice. Curiously though an immunoreactive band between 100 and 150 kD seems to persist in *Shank3*$^{G/G}$ mice but is lost in the *Shank3*$^{\Delta C/\Delta C}$ mice. Interestingly, other published mutant mouse models of *Shank3* did not examine the appearance of the novel lower molecular weight isoforms of Shank3 and may account for the heterogeneity in observed phenotype of these mutant mouse models (Bozdagi et al., 2010; Peca et al., 2011; Wang et al., 2011b; Yang et al., 2012). It is also unclear, if these novel lower molecular weight isoforms also appear in the ASD patients that carry deletions or mutations in exon 21 of *SHANK3.*

Shank3 is a critical part of glutamatergic synapses and interacts with multiple cytoskeletal proteins, scaffolding complexes, receptors, ion channels, and signaling molecules. We looked at alterations in several of these direct and indirect Shank3 binding partners in the hippocampus of the *Shank3*$^{\Delta C/\Delta C}$ and *Shank3*$^{G/G}$ mice and found a significant increase only in the mGluR5 levels in synaptic fractions isolated from *Shank3*$^{\Delta C/\Delta C}$ mice but not in the *Shank3*$^{G/G}$ mice. This along with the differences in the Shank3 isoforms may be responsible for any behavioral and physiological differences observed between the two models. Two already published *Shank3* exon$^{4\text{-}9}$ mouse models report a reduction in GluA1, GluN2, GKAP, and Homer 1b/c (Bozdagi et al., 2010; Wang et al., 2011b). Reduction in GKAP, Homer1, PSD-93, GluA2, GluN2A, and GluN2B levels has been reported in *Shank3* exon$^{13\text{-}16}$ mouse model (Peca et al., 2011). All three of these mouse models target the ANK (exon$^{4\text{-}9}$) or PDZ

(exon$^{13\text{-}16}$) domain of Shank3. Verpelli et al. (2011) show a decrease in mGluR5 and no change in any other Shank3 interacting protein in neuronal culture following Shank3 knock down targeting exon 21. This is interesting because on the one hand, like Verpelli et al. (2011) we report alterations only in mGluR5 levels in *Shank3*$^{\Delta C/\Delta C}$ mice but on the other hand, we report an increase and they report a decrease. One could argue that this difference could be due to the fact that one study is conducted in neuronal cultures and the other uses mice but the underlying mechanism for this difference is yet to be elucidated.

Behaviorally, both *Shank3*$^{\Delta C/\Delta C}$ and *Shank3*$^{G/G}$ mice show striking similarities to one another which may be attributed to the loss of overlapping Shank3 isoforms which are directly compared in Table 7. As many patients with ASD and PMS suffer from motor coordination deficits, we administered the accelerating rotarod test to the *Shank3*$^{\Delta C/\Delta C}$ and *Shank3*$^{G/G}$ mice (Abu-Dahab et al., 2012; Clarke, 1996; Phelan and McDermid, 2012). Both mutant mouse models show significantly poorer performance on this task when compared to WT suggesting motor coordination impairments. *Shank3*$^{G/G}$ mice also exhibited poor motor learning whereas the *Shank3*$^{\Delta C/\Delta C}$ mice appeared to only have poor motor coordination. *Shank3*$^{\Delta C\ \Delta C}$ and *Shank3*$^{G/G}$ mice demonstrated similar aberrant response to novelty as they exhibit decreased locomotor activity initially when placed in a novel environment. This was observed only in the first 5 minutes of exposure to the locomotor chamber after which they show normal habituation. Both *Shank3*$^{\Delta C/\Delta C}$ and *Shank3*$^{G/G}$ mice also show decreased locomotor activity in open field and dark/light boxes, further supporting this

hypoactive response to novelty. These mice exhibit no difference in the anxiety measures of the open field and dark/light tests when compared to their WT counterparts. Novelty avoidance phenotype was also observed in the marble burying and nest building task as both *Shank3*$^{\Delta C/\Delta C}$ and *Shank3*$^{G/G}$ mice avoided these inanimate objects for the duration of the task.

Social interaction and communication deficits are integral diagnostic criteria for ASD (Mahjouri and Lord, 2012; Schreibman, 1988). Previously, *Shank3*$^{e4\text{-}9}$ homozygotes (Wang et al., 2011b) and *Shank3*$^{e13\text{-}16}$ homozygotes (Peca et al., 2011) have reported impaired social interaction deficits. We also found social interaction deficits but only in *Shank3*$^{\Delta C/\Delta C}$ mice and not in *Shank3*$^{G/G}$ mice. *Shank3*$^{\Delta C/\Delta C}$ mice did not show a preference for social novelty in the classic three chambered social interaction test. Another diagnostic measure for ASD is an increase in repetitive behaviors (Mahjouri and Lord, 2012; Schreibman, 1988). Both *Shank3*$^{e4\text{-}9}$ homozygotes (Wang et al., 2011b) and *Shank3*$^{e13\text{-}16}$ homozygotes (Peca et al., 2011) exhibit increased repetitive self grooming behavior. Both *Shank3*$^{\Delta C/\ \Delta C}$ and *Shank3*$^{G/G}$ mice did not display an increase in grooming behavior. Interestingly, when we tested *Shank3*$^{\Delta C/\Delta C}$ mice at an older age (10-13 months old), they showed a significant increase in time spent grooming compared to their WT littermate pairs. We did not conduct this test with *Shank3*$^{G/G}$ mice. It will be interesting to see if they also develop an increase in repetitive grooming behavior at an older age. It will be even more interesting if other behavioral phenotypes observed in the *Shank3* mutant mice also change with age.

Hippocampus-dependent spatial learning abnormalities are also observed in *Shank3*$^{\Delta C/\Delta C}$ mice and to a lesser degree in *Shank3*$^{G/G}$ mice in the Morris water maze task. Further supporting this phenotype are the hippocampal area CA1 synaptic transmission and plasticity abnormalities found in the *Shank3*$^{\Delta C/\Delta C}$ and *Shank3*$^{G/G}$ mice. In the *Shank3*$^{\Delta C/\Delta C}$ mice, we show decreased LTP in area CA1 of the hippocampus which offer a potential explanation for the decreased hippocampus dependent spatial learning impairments. The LTP deficits in the *Shank3*$^{\Delta C/\Delta C}$ mice are likely due to the decreased NMDA-receptor-dependent synaptic transmission observed in these mice. *Shank3*$^{\Delta C/\Delta C}$ mice also exhibit decreased frequency of spontaneous glutamate release, and decreased evoked excitatory synaptic transmission with no change in short-term plasticity or mEPSC amplitude in area CA1 of the hippocampus. As previously mentioned, we see a significant increase of mGluR5 in the hippocampal synaptic fractions of these mice. Also mGlurRs bind to Shank3 indirectly via Homer binding domain (Naisbitt et al., 1999). Therefore we expected to see aberrant Group I mGluR dependent LTD in the *Shank3*$^{\Delta C/\Delta C}$ mice but we do not see any changes in Group I mGluR dependent LTD. Curiously, we do see attenuation of mGluR dependent LTD in the *Shank3*$^{G/G}$ mice despite normal levels of mGluRs in the hippocampal synaptic fraction. Additional functional studies are needed to understand the underlying mechanisms and consequences of this mGluR dependent LTD in *Shank3*$^{\Delta C/\Delta C}$ and *Shank3*$^{G/G}$ mice.

Another difference between the *Shank3*$^{\Delta C/\Delta C}$ and *Shank3*$^{G/G}$ mice is the absence of decreased hippocampal LTP in *Shank3*$^{G/G}$ mice. We see a significant post-tetanic

potentiation in the first five minutes after the conditioning stimulus but no difference among genotypes in the remaining 60 minutes of the LTP. The decrease in post-tetanic potentiation may be explained by the decreased NMDA-receptor-dependent synaptic transmission observed in these mice. We repeated the LTP experiment with a stronger conditioning stimulus and still found no significant difference among genotypes. Despite the differences, it could be concluded that both *Shank3*$^{\Delta C/\Delta C}$ and *Shank3*$^{G/G}$ mice show synaptic plasticity differences. In terms of basal synpatic transmission, like the *Shank3*$^{\Delta C/\Delta C}$ mice, *Shank3*$^{G/G}$ mice also exhibit decreased NMDA/AMPA ratio at CA3-CA1 synapses, decrease mEPSC frequency and decreased evoked excitatory synaptic responses measured by input/output curves. As we see no biochemical changes in NMDAR subunits in the hippocampus but we do see a decrease in NMDAR-mediated synaptic responses, we hypothesize that NMDAR function is being modulated at the synapse via post-translational mechanisms.

Recent studies in rodents have suggested that certain neurodevelopmental phenotypes may be reversed in the adulthood using pharmacological and/or genetic tools (Dragatsis and Zeitlin, 2001; Guy et al., 2007; Silva and Ehninger, 2009). These studies have mostly focused on syndromic neurodevelopmental disorders with a clear genetic origin such as tuberous sclerosis, Rett syndrome, neurofibromatosis, and Fragile-X syndrome. Not only is the *Shank3*^{G} mouse model the first genetically accurate autism mouse model for Shank3 mutations, but also the first fully reversible one. The *Shank3*^{G} mice express a point mutation in exon 21 of *Shank3* gene causing a

premature stop codon followed by a transcriptional neo-STOP cassette that results in a truncated shank3 protein. This mutated region is flanked by *loxp* sites and is followed by a WT exon 21 allowing us temporal and spatial control over the reversibility (Dragatsis and Zeitlin, 2001; Guy et al., 2007). We crossed these mice with a tamoxifen inducible Cre recombinase line and reversed the mutation after the completion of neurodevelopment (8weeks). We successfully reversed the Shank3 protein in the tamoxifen treated *Reversible-Shank3*$^{G/GCre+}$ mice to the same amount of Shank3 protein found in vehicle treated *Reversible-Shank3*$^{+/GCre+}$ mice. We tested both *Irreversible-Shank3*$^{GCre-}$ and *Reversible-Shank3*$^{GCre+}$ mice for behaviors which yielded a robust and significant phenotype in *Shank3*$^{G/G}$ mice. Both vehicle and tamoxifen treated *Irreversible-Shank3*$^{G/GCre-}$ mice also showed impaired motor coordination in the rotarod test, novelty avoidance in marble burying and nest building tasks and hypoactivity in response to novel environments, validating our findings in the *Shank3*$^{G/G}$ mice. We also tested the vehicle and tamoxifen treated *Reversible-Shank3*$^{GCre+}$ mice in the same behavioral tasks. Unfortunately, we were not able to recapitulate the *Shank3*$^{G/G}$ mouse model behavioral phenotype in the vehicle treated *Reversible-Shank3*$^{GCre+}$ mice. We also cannot directly compare the *Irreversible-Shank3*$^{GCre-}$ and *Reversible-Shank3*$^{GCre+}$ mice as they were tested in separate behavioral cohorts. Therefore we cannot draw any meaningful conclusions from the tamoxifen treated *Reversible-Shank3*$^{GCre+}$ mice. One possible explanation for the failure to recapitulate the *Shank3*$^{G/G}$ mouse model behavioral phenotype could be that Cre is somehow affecting the outcome. Another possible reason for the

altered phenotype observed in and *Reversible-Shank3*$^{GCre+}$ mice could be that the inserted mutated region is disrupting the intronic splice region and the rescued Shank3 is not exactly like the WT Shank3. In order to test this hypothesis, we will need to rescue the *Shank3*^{G} mutation using a germline Cre- to ensure there the mutation is rescued from the beginning of life and then comparing the behavioral phenotype of WT and rescued *Shank3*$^{GCre+}$ mice mutant mice.

As mentioned in the introduction, Shank3 and Neuroligin are part of the excitatory/inhibitory transmission imbalance hypothesis of ASD. Interestingly, like the *Shank3*$^{\Delta C/\Delta C}$ mice and *Shank3*$^{G/G}$ mice the Neuroligin 1 deficient (NL1 KO) mice exhibit an impairment in spatial learning and memory and also a decrease in NMDA/AMPA ratio in the area CA1 of the hippocampus (Blundell et al., 2010a; Chubykin et al., 2007). This supports the proposed convergent mechanism of the excitatory/inhibitory synaptic transmission deficit that maybe found in other genetic mutations targeting the synaptic proteins and provides therapeutic targets, NMDAR subunits that can be pharmacologically manipulated to modulate synaptic transmission to normal levels. In order to test this hypothesis, an NMDA receptor coagonist D-Cycloserine, which enhances NMDAR transmission by affecting the glycine-binding sites, was administered to NL1 KO mice and their increased grooming behavior was used as an outcome measure when compared to WT (Blundell et al., 2010a). Just one time administration of D-Cycloserine, was sufficient to significantly reduce the grooming behavior in the NL1 KO mice when compared to vehicle treated NL1 KO mice. Interestingly, there was no difference in the vehicle or

D-Cycloserine treated WT or the D-Cycloserine treated NL1 KO mice suggesting no observable effect of D-Cycloserine on the WT mice. NMDAR function can also be enhanced by inhibition of the glycine transporter-1 and inhibitors for glycine transporter-1 are being proposed as potential therapeutic target in Schizophrenia (Hashimoto, 2010). Interestingly, many ASD risk genes, including Shank3 have also been implicated in Schizophrenia suggesting a biological overlap between these neurological disorder (Murdoch and State, 2013). This further supports the NMDAR subunits as valid pharmacological targets for potential treatment of ASD phenotypes.

In summary, I have described three novel mutant mouse models (*Shank3*$^{\Delta C}$, *Shank3*^{G}, *Irreversible-Shank3*$^{GCre-}$) that model or directly mimic a human autism mutation. Although they may not show impairments in the core diagnostic ASD behaviors, they do show abnormalities in associated symptoms. Moreover, these abnormalities are persistent across these different mouse models and multiple cohorts providing valid outcome measures for developing and testing cures and pharmaceutical agents for autism spectrum disorder.

Table 7: Detailed Comparison of *Shank3*$^{\Delta C/\Delta C}$ and *Shank3*$^{G/G}$ Mice.			
BEHAVIOR	**Behavioral Parameter**	**Shank3E21Worley wt/homo**	**Shank3E21PM wt/homo**
Body Weight	Body weight in grams	↓	↓
Open Field	Time in Center/Time in Periphrey	—	—
	Distance Travelled	↓	↓
	Velocity	↓	↓
Dark/Light	Time Spent in Dark Chamber	↑	—
	Time Spent in Light Chamber	↓	—
	Latency to Enter Light Chamber	↑	↑
	Distance Travelled	↓	↓
Elevated Plus Maze	Time in Open arms/both arms	—	—
	Distance Travelled	—	↓
	Velocity	—	↓
Morris Water Maze	Training - Latency to Platform	↑	↑
	Training - Distance Travelled	↑	↑
	Training - Thigmotaxis	↑	—
	Training - Velocity	—	↑
	Probe - % Time in Target Quadrant	↓	—
	Probe - Frequency of Target Platform Location Crossing	—	—
	Probe - Thigmotaxis	↑	—
	Probe - Velocity	—	—
Nesting	Nest Width	↓	↓
	Nest Height	↓	↓

3-Choice Social Interaction Test	Front vs. Back Target	—	—
	Social vs. Inanimate Target	—	—
	Familiar vs. Novel Target	↓	—
Locomotor Test	Two hours	—	—
	First 5 minutes	↓	↓
Rotarod	Motor Learning	—	↓
	Motor Coordination	↓	↓
Marble Burying	Number of Buried Marbles	↓	↓
Grooming	Time Spent Grooming	—	—
	No. of Bouts	—	—
	Time Per Bout	—	—
ELECTROPHYSIOLOGY			
	Input/Output Curves	↓	↓
	PPR	—	—
	LTP	↓	—
	mGluR-LTD	—	↓
	mEPSC Amplitude	—	—
	mEPSC Frequency	↓	↓
	NMDA/AMPA	↓	↓

BIBLIOGRAPHY

Abrahams, B.S., and Geschwind, D.H. (2008). Advances in autism genetics: on the threshold of a new neurobiology. Nature reviews Genetics *9*, 341-355.

Abu-Dahab, S.M., Skidmore, E.R., Holm, M.B., Rogers, J.C., and Minshew, N.J. (2012). Motor and Tactile-Perceptual Skill Differences Between Individuals with High-Functioning Autism and Typically Developing Individuals Ages 5-21. Journal of autism and developmental disorders.

Accardo, J.A., and Malow, B.A. (2014). Sleep, epilepsy, and autism. Epilepsy & behavior : E&B.

Anckarsater, H., Stahlberg, O., Larson, T., Hakansson, C., Jutblad, S.B., Niklasson, L., Nyden, A., Wentz, E., Westergren, S., Cloninger, C.R., Gillberg, C., and Rastam, M. (2006). The impact of ADHD and autism spectrum disorders on temperament, character, and personality development. The American journal of psychiatry *163*, 1239-1244.

Arons, M.H., Thynne, C.J., Grabrucker, A.M., Li, D., Schoen, M., Cheyne, J.E., Boeckers, T.M., Montgomery, J.M., and Garner, C.C. (2012). Autism-associated mutations in ProSAP2/Shank3 impair synaptic transmission and neurexin-neuroligin-mediated transsynaptic signaling. The Journal of neuroscience : the official journal of the Society for Neuroscience *32*, 14966-14978.

Bailey, A., Le Couteur, A., Gottesman, I., Bolton, P., Simonoff, E., Yuzda, E., and Rutter, M. (1995). Autism as a strongly genetic disorder: evidence from a British twin study. Psychological medicine *25*, 63-77.

Baio, J. (2014). Prevalence of Autism Spectrum Disorder Among Children Aged 8 Years — Autism and Developmental Disabilities Monitoring Network, 11 Sites, United States, 2010 (USA: CDC).

Bateup, H.S., Takasaki, K.T., Saulnier, J.L., Denefrio, C.L., and Sabatini, B.L. (2011). Loss of Tsc1 in vivo impairs hippocampal mGluR-LTD and increases excitatory synaptic function. The Journal of neuroscience : the official journal of the Society for Neuroscience *31*, 8862-8869.

Bear, M.F., Huber, K.M., and Warren, S.T. (2004). The mGluR theory of fragile X mental retardation. Trends Neurosci *27*, 370-377.

Beri, S., Tonna, N., Menozzi, G., Bonaglia, M.C., Sala, C., and Giorda, R. (2007). DNA methylation regulates tissue-specific expression of Shank3. Journal of neurochemistry *101*, 1380-1391.

Betancur, C. (2011). Etiological heterogeneity in autism spectrum disorders: more than 100 genetic and genomic disorders and still counting. Brain Res *1380*, 42-77.

Bishop, N., Aziz, A., and Barth, C. (2014). Phenotypic Variation in Autism Spectrum Disorder: Insights from Syndromic Forms of Autism. In Comprehensive Guide to Autism, V.B. Patel, V.R. Preedy, and C.R. Martin, eds. (Springer New York), pp. 1715-1735.

Blundell, J., Blaiss, C.A., Etherton, M.R., Espinosa, F., Tabuchi, K., Walz, C., Bolliger, M.F., Sudhof, T.C., and Powell, C.M. (2010a). Neuroligin-1 deletion results in impaired spatial memory and increased repetitive behavior. The Journal of neuroscience : the official journal of the Society for Neuroscience *30*, 2115-2129.

Blundell, J., Kaeser, P.S., Sudhof, T.C., and Powell, C.M. (2010b). RIM1alpha and interacting proteins involved in presynaptic plasticity mediate prepulse inhibition and additional behaviors linked to schizophrenia. The Journal of neuroscience : the official journal of the Society for Neuroscience *30*, 5326-5333.

Blundell, J., Tabuchi, K., Bolliger, M.F., Blaiss, C.A., Brose, N., Liu, X., Sudhof, T.C., and Powell, C.M. (2009). Increased anxiety-like behavior in mice lacking the inhibitory synapse cell adhesion molecule neuroligin 2. Genes Brain Behav *8*, 114-126.

Boccuto, L., Lauri, M., Sarasua, S.M., Skinner, C.D., Buccella, D., Dwivedi, A., Orteschi, D., Collins, J.S., Zollino, M., Visconti, P., Dupont, B., Tiziano, D., Schroer, R.J., Neri, G., Stevenson, R.E., Gurrieri, F., and Schwartz, C.E. (2012). Prevalence of SHANK3 variants in patients with different subtypes of autism spectrum disorders. Eur J Hum Genet.

Boccuto, L., Lauri, M., Sarasua, S.M., Skinner, C.D., Buccella, D., Dwivedi, A., Orteschi, D., Collins, J.S., Zollino, M., Visconti, P., Dupont, B., Tiziano, D., Schroer, R.J., Neri, G., Stevenson, R.E., Gurrieri, F., and Schwartz, C.E.

(2013). Prevalence of SHANK3 variants in patients with different subtypes of autism spectrum disorders. Eur J Hum Genet *21*, 310-316.

Bockers, T.M., Mameza, M.G., Kreutz, M.R., Bockmann, J., Weise, C., Buck, F., Richter, D., Gundelfinger, E.D., and Kreienkamp, H.J. (2001). Synaptic scaffolding proteins in rat brain. Ankyrin repeats of the multidomain Shank protein family interact with the cytoskeletal protein alpha-fodrin. J Biol Chem *276*, 40104-40112.

Bodfish, J.W., Symons, F.J., Parker, D.E., and Lewis, M.H. (2000). Varieties of repetitive behavior in autism: comparisons to mental retardation. Journal of autism and developmental disorders *30*, 237-243.

Boeckers, T.M., Kreutz, M.R., Winter, C., Zuschratter, W., Smalla, K.H., Sanmarti-Vila, L., Wex, H., Langnaese, K., Bockmann, J., Garner, C.C., and Gundelfinger, E.D. (1999a). Proline-rich synapse-associated protein-1/cortactin binding protein 1 (ProSAP1/CortBP1) is a PDZ-domain protein highly enriched in the postsynaptic density. The Journal of neuroscience : the official journal of the Society for Neuroscience *19*, 6506-6518.

Boeckers, T.M., Liedtke, T., Spilker, C., Dresbach, T., Bockmann, J., Kreutz, M.R., and Gundelfinger, E.D. (2005). C-terminal synaptic targeting elements for postsynaptic density proteins ProSAP1/Shank2 and ProSAP2/Shank3. Journal of neurochemistry *92*, 519-524.

Boeckers, T.M., Winter, C., Smalla, K.H., Kreutz, M.R., Bockmann, J., Seidenbecher, C., Garner, C.C., and Gundelfinger, E.D. (1999b). Proline-rich

synapse-associated proteins ProSAP1 and ProSAP2 interact with synaptic proteins of the SAPAP/GKAP family. Biochem Biophys Res Commun *264*, 247-252.

Bonaglia, M.C., Giorda, R., Beri, S., De Agostini, C., Novara, F., Fichera, M., Grillo, L., Galesi, O., Vetro, A., Ciccone, R., Bonati, M.T., Giglio, S., Guerrini, R., Osimani, S., Marelli, S., Zucca, C., Grasso, R., Borgatti, R., Mani, E., Motta, C., Molteni, M., Romano, C., Greco, D., Reitano, S., Baroncini, A., Lapi, E., Cecconi, A., Arrigo, G., Patricelli, M.G., Pantaleoni, C., D'Arrigo, S., Riva, D., Sciacca, F., Dalla Bernardina, B., Zoccante, L., Darra, F., Termine, C., Maserati, E., Bigoni, S., Priolo, E., Bottani, A., Gimelli, S., Bena, F., Brusco, A., di Gregorio, E., Bagnasco, I., Giussani, U., Nitsch, L., Politi, P., Martinez-Frias, M.L., Martinez-Fernandez, M.L., Martinez Guardia, N., Bremer, A., Anderlid, B.M., and Zuffardi, O. (2011). Molecular mechanisms generating and stabilizing terminal 22q13 deletions in 44 subjects with Phelan/McDermid Syndrome. PLoS Genet *7*, e1002173.

Bonaglia, M.C., Giorda, R., Borgatti, R., Felisari, G., Gagliardi, C., Selicorni, A., and Zuffardi, O. (2001). Disruption of the ProSAP2 gene in a t(12;22)(q24.1;q13.3) is associated with the 22q13.3 deletion syndrome. Am J Hum Genet *69*, 261-268.

Bonaglia, M.C., Giorda, R., Mani, E., Aceti, G., Anderlid, B.M., Baroncini, A., Pramparo, T., and Zuffardi, O. (2006). Identification of a recurrent breakpoint

within the SHANK3 gene in the 22q13.3 deletion syndrome. J Med Genet *43*, 822-828.

Bourgeron, T. (2009). A synaptic trek to autism. Current opinion in neurobiology *19*, 231-234.

Bozdagi, O., Sakurai, T., Dorr, N., Pilorge, M., Takahashi, N., and Buxbaum, J.D. (2012). Haploinsufficiency of Cyfip1 produces fragile X-like phenotypes in mice. PloS one *7*, e42422.

Bozdagi, O., Sakurai, T., Papapetrou, D., Wang, X., Dickstein, D.L., Takahashi, N., Kajiwara, Y., Yang, M., Katz, A.M., Scattoni, M.L., Harris, M.J., Saxena, R., Silverman, J.L., Crawley, J.N., Zhou, Q., Hof, P.R., and Buxbaum, J.D. (2010). Haploinsufficiency of the autism-associated Shank3 gene leads to deficits in synaptic function, social interaction, and social communication. Mol Autism *1*, 15.

Buescher, A.V., Cidav, Z., Knapp, M., and Mandell, D.S. (2014). Costs of autism spectrum disorders in the United Kingdom and the United States. JAMA pediatrics *168*, 721-728.

Burbach, J.P., and van der Zwaag, B. (2009). Contact in the genetics of autism and schizophrenia. Trends Neurosci *32*, 69-72.

Chen, C.P., Lin, S.P., Chern, S.R., Tsai, F.J., Wu, P.C., Lee, C.C., Chen, Y.T., Chen, W.L., and Wang, W. (2010). A de novo 7.9 Mb deletion in 22q13.2-->qter in a boy with autistic features, epilepsy, developmental delay, atopic dermatitis and abnormal immunological findings. Eur J Med Genet *53*, 329-332.

Chevere-Torres, I., Kaphzan, H., Bhattacharya, A., Kang, A., Maki, J.M., Gambello, M.J., Arbiser, J.L., Santini, E., and Klann, E. (2012). Metabotropic glutamate receptor-dependent long-term depression is impaired due to elevated ERK signaling in the DeltaRG mouse model of tuberous sclerosis complex. Neurobiol Dis *45*, 1101-1110.

Chubykin, A.A., Atasoy, D., Etherton, M.R., Brose, N., Kavalali, E.T., Gibson, J.R., and Sudhof, T.C. (2007). Activity-dependent validation of excitatory versus inhibitory synapses by neuroligin-1 versus neuroligin-2. Neuron *54*, 919-931.

Clarke, A. (1996). Rett syndrome. J Med Genet *33*, 693-699.

Cohen, R.S., Blomberg, F., Berzins, K., and Siekevitz, P. (1977). The structure of postsynaptic densities isolated from dog cerebral cortex. I. Overall morphology and protein composition. The Journal of cell biology *74*, 181-203.

Craig, A.M., and Kang, Y. (2007). Neurexin-neuroligin signaling in synapse development. Current opinion in neurobiology *17*, 43-52.

Devlin, B., Melhem, N., and Roeder, K. (2011). Do common variants play a role in risk for autism? Evidence and theoretical musings. Brain Res *1380*, 78-84.

Devlin, B., and Scherer, S.W. (2012). Genetic architecture in autism spectrum disorder. Current opinion in genetics & development *22*, 229-237.

Dhar, S.U., del Gaudio, D., German, J.R., Peters, S.U., Ou, Z., Bader, P.I., Berg, J.S., Blazo, M., Brown, C.W., Graham, B.H., Grebe, T.A., Lalani, S., Irons, M., Sparagana, S., Williams, M., Phillips, J.A., 3rd, Beaudet, A.L., Stankiewicz,

P., Patel, A., Cheung, S.W., and Sahoo, T. (2010). 22q13.3 deletion syndrome: clinical and molecular analysis using array CGH. Am J Med Genet A *152A*, 573-581.

Dragatsis, I., and Zeitlin, S. (2001). A method for the generation of conditional gene repair mutations in mice. Nucleic Acids Res *29*, E10.

Durand, C.M., Betancur, C., Boeckers, T.M., Bockmann, J., Chaste, P., Fauchereau, F., Nygren, G., Rastam, M., Gillberg, I.C., Anckarsater, H., Sponheim, E., Goubran-Botros, H., Delorme, R., Chabane, N., Mouren-Simeoni, M.C., de Mas, P., Bieth, E., Roge, B., Heron, D., Burglen, L., Gillberg, C., Leboyer, M., and Bourgeron, T. (2007). Mutations in the gene encoding the synaptic scaffolding protein SHANK3 are associated with autism spectrum disorders. Nat Genet *39*, 25-27.

Durand, C.M., Perroy, J., Loll, F., Perrais, D., Fagni, L., Bourgeron, T., Montcouquiol, M., and Sans, N. (2012). SHANK3 mutations identified in autism lead to modification of dendritic spine morphology via an actin-dependent mechanism. Molecular psychiatry *17*, 71-84.

Etherton, M.R., Blaiss, C.A., Powell, C.M., and Sudhof, T.C. (2009). Mouse neurexin-1alpha deletion causes correlated electrophysiological and behavioral changes consistent with cognitive impairments. Proc Natl Acad Sci U S A *106*, 17998-18003.

Ey, E., Leblond, C.S., and Bourgeron, T. (2011). Behavioral profiles of mouse models for autism spectrum disorders. Autism research : official journal of the International Society for Autism Research *4*, 5-16.

Folstein, S., and Rutter, M. (1977). Infantile autism: a genetic study of 21 twin pairs. Journal of child psychology and psychiatry, and allied disciplines *18*, 297-321.

Fombonne, E. (2005). Epidemiology of autistic disorder and other pervasive developmental disorders. The Journal of clinical psychiatry *66 Suppl 10*, 3-8.

Freitag, C.M. (2007). The genetics of autistic disorders and its clinical relevance: a review of the literature. Molecular psychiatry *12*, 2-22.

Garner, C.C., Nash, J., and Huganir, R.L. (2000). PDZ domains in synapse assembly and signalling. Trends in cell biology *10*, 274-280.

Gauthier, J., Champagne, N., Lafreniere, R.G., Xiong, L., Spiegelman, D., Brustein, E., Lapointe, M., Peng, H., Cote, M., Noreau, A., Hamdan, F.F., Addington, A.M., Rapoport, J.L., Delisi, L.E., Krebs, M.O., Joober, R., Fathalli, F., Mouaffak, F., Haghighi, A.P., Neri, C., Dube, M.P., Samuels, M.E., Marineau, C., Stone, E.A., Awadalla, P., Barker, P.A., Carbonetto, S., Drapeau, P., and Rouleau, G.A. (2010). De novo mutations in the gene encoding the synaptic scaffolding protein SHANK3 in patients ascertained for schizophrenia. Proc Natl Acad Sci U S A *107*, 7863-7868.

Gauthier, J., Spiegelman, D., Piton, A., Lafreniere, R.G., Laurent, S., St-Onge, J., Lapointe, L., Hamdan, F.F., Cossette, P., Mottron, L., Fombonne, E., Joober,

R., Marineau, C., Drapeau, P., and Rouleau, G.A. (2009). Novel de novo SHANK3 mutation in autistic patients. Am J Med Genet B Neuropsychiatr Genet *150B*, 421-424.

Gillott, A., Furniss, F., and Walter, A. (2001). Anxiety in high-functioning children with autism. Autism *5*, 277-286.

Goldberg, W.A., Osann, K., Filipek, P.A., Laulhere, T., Jarvis, K., Modahl, C., Flodman, P., and Spence, M.A. (2003). Language and other regression: assessment and timing. Journal of autism and developmental disorders *33*, 607-616.

Gong, X., Jiang, Y.W., Zhang, X., An, Y., Zhang, J., Wu, Y., Wang, J., Sun, Y., Liu, Y., Gao, X., Shen, Y., Wu, X., Qiu, Z., Jin, L., Wu, B.L., and Wang, H. (2012). High proportion of 22q13 deletions and SHANK3 mutations in Chinese patients with intellectual disability. PloS one *7*, e34739.

Grabrucker, A.M., Schmeisser, M.J., Schoen, M., and Boeckers, T.M. (2011). Postsynaptic ProSAP/Shank scaffolds in the cross-hair of synaptopathies. Trends in cell biology *21*, 594-603.

Greaves, N., Prince, E., Evans, D.W., and Charman, T. (2006). Repetitive and ritualistic behaviour in children with Prader-Willi syndrome and children with autism. J Intellect Disabil Res *50*, 92-100.

Grossman, R.B., Edelson, L.R., and Tager-Flusberg, H. (2013). Emotional facial and vocal expressions during story retelling by children and adolescents with high-

functioning autism. Journal of speech, language, and hearing research : JSLHR *56*, 1035-1044.

Guy, J., Gan, J., Selfridge, J., Cobb, S., and Bird, A. (2007). Reversal of neurological defects in a mouse model of Rett syndrome. Science *315*, 1143-1147.

Hansen, S.N., Schendel, D.E., and Parner, E.T. (2015). Explaining the increase in the prevalence of autism spectrum disorders: the proportion attributable to changes in reporting practices. JAMA pediatrics *169*, 56-62.

Hashimoto, K. (2010). Glycine transport inhibitors for the treatment of schizophrenia. The open medicinal chemistry journal *4*, 10-19.

Hayashi, S., and McMahon, A.P. (2002). Efficient recombination in diverse tissues by a tamoxifen-inducible form of Cre: a tool for temporally regulated gene activation/inactivation in the mouse. Developmental biology *244*, 305-318.

Hazlett, H.C., Poe, M.D., Lightbody, A.A., Gerig, G., Macfall, J.R., Ross, A.K., Provenzale, J., Martin, A., Reiss, A.L., and Piven, J. (2009). Teasing apart the heterogeneity of autism: Same behavior, different brains in toddlers with fragile X syndrome and autism. Journal of neurodevelopmental disorders *1*, 81-90.

Jamain, S., Quach, H., Betancur, C., Rastam, M., Colineaux, C., Gillberg, I.C., Soderstrom, H., Giros, B., Leboyer, M., Gillberg, C., Bourgeron, T., and Paris Autism Research International Sibpair, S. (2003). Mutations of the X-linked genes encoding neuroligins NLGN3 and NLGN4 are associated with autism. Nat Genet *34*, 27-29.

Jeffries, A.R., Curran, S., Elmslie, F., Sharma, A., Wenger, S., Hummel, M., and Powell, J. (2005). Molecular and phenotypic characterization of ring chromosome 22. Am J Med Genet A *137*, 139-147.

Jensen, F.E. (2011). Epilepsy as a spectrum disorder: Implications from novel clinical and basic neuroscience. Epilepsia *52 Suppl 1*, 1-6.

Jiang, Y.H., and Ehlers, M.D. (2013). Modeling autism by SHANK gene mutations in mice. Neuron *78*, 8-27.

Kanner, L. (1943). Autistic Disturbances of Affective Contact Nervous Child, 217-250.

Kelleher, R.J., 3rd, and Bear, M.F. (2008). The autistic neuron: troubled translation? Cell *135*, 401-406.

Kim, H.G., Kishikawa, S., Higgins, A.W., Seong, I.S., Donovan, D.J., Shen, Y., Lally, E., Weiss, L.A., Najm, J., Kutsche, K., Descartes, M., Holt, L., Braddock, S., Troxell, R., Kaplan, L., Volkmar, F., Klin, A., Tsatsanis, K., Harris, D.J., Noens, I., Pauls, D.L., Daly, M.J., MacDonald, M.E., Morton, C.C., Quade, B.J., and Gusella, J.F. (2008). Disruption of neurexin 1 associated with autism spectrum disorder. Am J Hum Genet *82*, 199-207.

Kim, Y.S., Leventhal, B.L., Koh, Y.J., Fombonne, E., Laska, E., Lim, E.C., Cheon, K.A., Kim, S.J., Kim, Y.K., Lee, H., Song, D.H., and Grinker, R.R. (2011). Prevalence of autism spectrum disorders in a total population sample. The American journal of psychiatry *168*, 904-912.

Kolevzon, A., Cai, G., Soorya, L., Takahashi, N., Grodberg, D., Kajiwara, Y., Willner, J.P., Tryfon, A., and Buxbaum, J.D. (2011). Analysis of a purported SHANK3 mutation in a boy with autism: clinical impact of rare variant research in neurodevelopmental disabilities. Brain Res *1380*, 98-105.

Kootz, J.P., Marinelli, B., and Cohen, D.J. (1982). Modulation of response to environmental stimulation in autistic children. Journal of autism and developmental disorders *12*, 185-193.

Kopp, S., Beckung, E., and Gillberg, C. (2010). Developmental coordination disorder and other motor control problems in girls with autism spectrum disorder and/or attention-deficit/hyperactivity disorder. Research in developmental disabilities *31*, 350-361.

Kouser, M., Speed, H.E., Dewey, C.M., Reimers, J.M., Widman, A.J., Gupta, N., Liu, S., Jaramillo, T.C., Bangash, M., Xiao, B., Worley, P.F., and Powell, C.M. (2013). Loss of predominant shank3 isoforms results in hippocampus-dependent impairments in behavior and synaptic transmission. The Journal of neuroscience : the official journal of the Society for Neuroscience *33*, 18448-18468.

Kwon, C.H., Luikart, B.W., Powell, C.M., Zhou, J., Matheny, S.A., Zhang, W., Li, Y., Baker, S.J., and Parada, L.F. (2006). Pten regulates neuronal arborization and social interaction in mice. Neuron *50*, 377-388.

Lam, K.S., Bodfish, J.W., and Piven, J. (2008). Evidence for three subtypes of repetitive behavior in autism that differ in familiality and association with

other symptoms. Journal of child psychology and psychiatry, and allied disciplines *49*, 1193-1200.

Lauri, S.E., Palmer, M., Segerstrale, M., Vesikansa, A., Taira, T., and Collingridge, G.L. (2007). Presynaptic mechanisms involved in the expression of STP and LTP at CA1 synapses in the hippocampus. Neuropharmacology *52*, 1-11.

Lichtenstein, P., Carlstrom, E., Rastam, M., Gillberg, C., and Anckarsater, H. (2010). The genetics of autism spectrum disorders and related neuropsychiatric disorders in childhood. The American journal of psychiatry *167*, 1357-1363.

Lim, S., Naisbitt, S., Yoon, J., Hwang, J.I., Suh, P.G., Sheng, M., and Kim, E. (1999). Characterization of the Shank family of synaptic proteins. Multiple genes, alternative splicing, and differential expression in brain and development. J Biol Chem *274*, 29510-29518.

Lord, C. (1995). Follow-up of two-year-olds referred for possible autism. Journal of child psychology and psychiatry, and allied disciplines *36*, 1365-1382.

Mahjouri, S., and Lord, C.E. (2012). What the DSM-5 Portends for Research, Diagnosis, and Treatment of Autism Spectrum Disorders. Curr Psychiatry Rep.

Marshall, C.R., Noor, A., Vincent, J.B., Lionel, A.C., Feuk, L., Skaug, J., Shago, M., Moessner, R., Pinto, D., Ren, Y., Thiruvahindrapduram, B., Fiebig, A., Schreiber, S., Friedman, J., Ketelaars, C.E., Vos, Y.J., Ficicioglu, C., Kirkpatrick, S., Nicolson, R., Sloman, L., Summers, A., Gibbons, C.A., Teebi, A., Chitayat, D., Weksberg, R., Thompson, A., Vardy, C., Crosbie, V.,

Luscombe, S., Baatjes, R., Zwaigenbaum, L., Roberts, W., Fernandez, B., Szatmari, P., and Scherer, S.W. (2008). Structural variation of chromosomes in autism spectrum disorder. Am J Hum Genet *82*, 477-488.

Moessner, R., Marshall, C.R., Sutcliffe, J.S., Skaug, J., Pinto, D., Vincent, J., Zwaigenbaum, L., Fernandez, B., Roberts, W., Szatmari, P., and Scherer, S.W. (2007). Contribution of SHANK3 mutations to autism spectrum disorder. Am J Hum Genet *81*, 1289-1297.

Moruzzi, S., Ogliari, A., Ronald, A., Happe, F., and Battaglia, M. (2011). The nature of covariation between autistic traits and clumsiness: a twin study in a general population sample. Journal of autism and developmental disorders *41*, 1665-1674.

Moy, S.S., Nadler, J.J., Perez, A., Barbaro, R.P., Johns, J.M., Magnuson, T.R., Piven, J., and Crawley, J.N. (2004). Sociability and preference for social novelty in five inbred strains: an approach to assess autistic-like behavior in mice. Genes Brain Behav *3*, 287-302.

Murdoch, J.D., and State, M.W. (2013). Recent developments in the genetics of autism spectrum disorders. Current opinion in genetics & development *23*, 310-315.

Nadler, J.J., Moy, S.S., Dold, G., Trang, D., Simmons, N., Perez, A., Young, N.B., Barbaro, R.P., Piven, J., Magnuson, T.R., and Crawley, J.N. (2004). Automated apparatus for quantitation of social approach behaviors in mice. Genes Brain Behav *3*, 303-314.

Naisbitt, S., Kim, E., Tu, J.C., Xiao, B., Sala, C., Valtschanoff, J., Weinberg, R.J., Worley, P.F., and Sheng, M. (1999). Shank, a novel family of postsynaptic density proteins that binds to the NMDA receptor/PSD-95/GKAP complex and cortactin. Neuron *23*, 569-582.

Nobile, M., Perego, P., Piccinini, L., Mani, E., Rossi, A., Bellina, M., and Molteni, M. (2011). Further evidence of complex motor dysfunction in drug naive children with autism using automatic motion analysis of gait. Autism *15*, 263-283.

Okamoto, N., Kubota, T., Nakamura, Y., Murakami, R., Nishikubo, T., Tanaka, I., Takahashi, Y., Hayashi, S., Imoto, I., Inazawa, J., Hosokai, N., Kohsaka, S., and Uchino, S. (2007). 22q13 Microduplication in two patients with common clinical manifestations: a recognizable syndrome? Am J Med Genet A *143A*, 2804-2809.

Ozonoff, S., Iosif, A.M., Baguio, F., Cook, I.C., Hill, M.M., Hutman, T., Rogers, S.J., Rozga, A., Sangha, S., Sigman, M., Steinfeld, M.B., and Young, G.S. (2010). A prospective study of the emergence of early behavioral signs of autism. Journal of the American Academy of Child and Adolescent Psychiatry *49*, 256-266 e251-252.

Ozonoff, S., and Jensen, J. (1999). Brief report: specific executive function profiles in three neurodevelopmental disorders. Journal of autism and developmental disorders *29*, 171-177.

Palomo, R., Belinchon, M., and Ozonoff, S. (2006). Autism and family home movies: a comprehensive review. Journal of developmental and behavioral pediatrics : JDBP *27*, S59-68.

Peca, J., Feliciano, C., Ting, J.T., Wang, W., Wells, M.F., Venkatraman, T.N., Lascola, C.D., Fu, Z., and Feng, G. (2011). Shank3 mutant mice display autistic-like behaviours and striatal dysfunction. Nature *472*, 437-442.

Phelan, K., and McDermid, H.E. (2012). The 22q13.3 Deletion Syndrome (Phelan-McDermid Syndrome). Molecular syndromology *2*, 186-201.

Phelan, K., and Rogers, R.C. (1993). Phelan-McDermid Syndrome. In GeneReviews(R), R.A. Pagon, M.P. Adam, H.H. Ardinger, T.D. Bird, C.R. Dolan, C.T. Fong, R.J.H. Smith, and K. Stephens, eds. (Seattle (WA)).

Phelan, M.C. (2008). Deletion 22q13.3 syndrome. Orphanet J Rare Dis *3*, 14.

Pinto, D., Pagnamenta, A.T., Klei, L., Anney, R., Merico, D., Regan, R., Conroy, J., Magalhaes, T.R., Correia, C., Abrahams, B.S., Almeida, J., Bacchelli, E., Bader, G.D., Bailey, A.J., Baird, G., Battaglia, A., Berney, T., Bolshakova, N., Bolte, S., Bolton, P.F., Bourgeron, T., Brennan, S., Brian, J., Bryson, S.E., Carson, A.R., Casallo, G., Casey, J., Chung, B.H., Cochrane, L., Corsello, C., Crawford, E.L., Crossett, A., Cytrynbaum, C., Dawson, G., de Jonge, M., Delorme, R., Drmic, I., Duketis, E., Duque, F., Estes, A., Farrar, P., Fernandez, B.A., Folstein, S.E., Fombonne, E., Freitag, C.M., Gilbert, J., Gillberg, C., Glessner, J.T., Goldberg, J., Green, A., Green, J., Guter, S.J., Hakonarson, H., Heron, E.A., Hill, M., Holt, R., Howe, J.L., Hughes, G., Hus,

V., Igliozzi, R., Kim, C., Klauck, S.M., Kolevzon, A., Korvatska, O., Kustanovich, V., Lajonchere, C.M., Lamb, J.A., Laskawiec, M., Leboyer, M., Le Couteur, A., Leventhal, B.L., Lionel, A.C., Liu, X.Q., Lord, C., Lotspeich, L., Lund, S.C., Maestrini, E., Mahoney, W., Mantoulan, C., Marshall, C.R., McConachie, H., McDougle, C.J., McGrath, J., McMahon, W.M., Merikangas, A., Migita, O., Minshew, N.J., Mirza, G.K., Munson, J., Nelson, S.F., Noakes, C., Noor, A., Nygren, G., Oliveira, G., Papanikolaou, K., Parr, J.R., Parrini, B., Paton, T., Pickles, A., Pilorge, M., Piven, J., Ponting, C.P., Posey, D.J., Poustka, A., Poustka, F., Prasad, A., Ragoussis, J., Renshaw, K., Rickaby, J., Roberts, W., Roeder, K., Roge, B., Rutter, M.L., Bierut, L.J., Rice, J.P., Salt, J., Sansom, K., Sato, D., Segurado, R., Sequeira, A.F., Senman, L., Shah, N., Sheffield, V.C., Soorya, L., Sousa, I., Stein, O., Sykes, N., Stoppioni, V., Strawbridge, C., Tancredi, R., Tansey, K., Thiruvahindrapduram, B., Thompson, A.P., Thomson, S., Tryfon, A., Tsiantis, J., Van Engeland, H., Vincent, J.B., Volkmar, F., Wallace, S., Wang, K., Wang, Z., Wassink, T.H., Webber, C., Weksberg, R., Wing, K., Wittemeyer, K., Wood, S., Wu, J., Yaspan, B.L., Zurawiecki, D., Zwaigenbaum, L., Buxbaum, J.D., Cantor, R.M., Cook, E.H., Coon, H., Cuccaro, M.L., Devlin, B., Ennis, S., Gallagher, L., Geschwind, D.H., Gill, M., Haines, J.L., Hallmayer, J., Miller, J., Monaco, A.P., Nurnberger, J.I., Jr., Paterson, A.D., Pericak-Vance, M.A., Schellenberg, G.D., Szatmari, P., Vicente, A.M., Vieland, V.J., Wijsman, E.M., Scherer, S.W., Sutcliffe, J.S., and Betancur, C.

(2010). Functional impact of global rare copy number variation in autism spectrum disorders. Nature *466*, 368-372.

Powell, C.M., Schoch, S., Monteggia, L., Barrot, M., Matos, M.F., Feldmann, N., Sudhof, T.C., and Nestler, E.J. (2004). The presynaptic active zone protein RIM1alpha is critical for normal learning and memory. Neuron *42*, 143-153.

Qualmann, B., Boeckers, T.M., Jeromin, M., Gundelfinger, E.D., and Kessels, M.M. (2004). Linkage of the actin cytoskeleton to the postsynaptic density via direct interactions of Abp1 with the ProSAP/Shank family. The Journal of neuroscience : the official journal of the Society for Neuroscience *24*, 2481-2495.

Regehr, W.G. (2012). Short-term presynaptic plasticity. Cold Spring Harbor perspectives in biology *4*, a005702.

Richler, J., Bishop, S.L., Kleinke, J.R., and Lord, C. (2007). Restricted and repetitive behaviors in young children with autism spectrum disorders. Journal of autism and developmental disorders *37*, 73-85.

Rogers, S.J., and Ozonoff, S. (2005). Annotation: what do we know about sensory dysfunction in autism? A critical review of the empirical evidence. Journal of child psychology and psychiatry, and allied disciplines *46*, 1255-1268.

Ronesi, J.A., and Huber, K.M. (2008). Homer interactions are necessary for metabotropic glutamate receptor-induced long-term depression and translational activation. The Journal of neuroscience : the official journal of the Society for Neuroscience *28*, 543-547.

Roussignol, G., Ango, F., Romorini, S., Tu, J.C., Sala, C., Worley, P.F., Bockaert, J., and Fagni, L. (2005). Shank expression is sufficient to induce functional dendritic spine synapses in aspiny neurons. The Journal of neuroscience : the official journal of the Society for Neuroscience *25*, 3560-3570.

Sacco, R., Militerni, R., Frolli, A., Bravaccio, C., Gritti, A., Elia, M., Curatolo, P., Manzi, B., Trillo, S., Lenti, C., Saccani, M., Schneider, C., Melmed, R., Reichelt, K.L., Pascucci, T., Puglisi-Allegra, S., and Persico, A.M. (2007). Clinical, morphological, and biochemical correlates of head circumference in autism. Biological psychiatry *62*, 1038-1047.

Samadi, S.A., McConkey, R., and Bunting, B. (2014). Parental wellbeing of Iranian families with children who have developmental disabilities. Research in developmental disabilities *35*, 1639-1647.

Sappok, T., Bergmann, T., Kaiser, H., and Diefenbacher, A. (2010). [Autism in adults with intellectual disabilities]. Der Nervenarzt *81*, 1333-1345.

Sarasua, S.M., Dwivedi, A., Boccuto, L., Rollins, J.D., Chen, C.F., Rogers, R.C., Phelan, K., DuPont, B.R., and Collins, J.S. (2011). Association between deletion size and important phenotypes expands the genomic region of interest in Phelan-McDermid syndrome (22q13 deletion syndrome). J Med Genet *48*, 761-766.

Scattoni, M.L., Ricceri, L., and Crawley, J.N. (2010). Unusual repertoire of vocalizations in adult BTBR T+tf/J mice during three types of social encounters. Genes Brain Behav.

Scherer, S.W., and Dawson, G. (2011). Risk factors for autism: translating genomic discoveries into diagnostics. Human genetics *130*, 123-148.

Schreibman, L. (1988). Diagnostic features of autism. J Child Neurol *3 Suppl*, S57-64.

Sheng, M., and Kim, E. (2000). The Shank family of scaffold proteins. J Cell Sci *113 (Pt 11)*, 1851-1856.

Silva, A.J., and Ehninger, D. (2009). Adult reversal of cognitive phenotypes in neurodevelopmental disorders. Journal of neurodevelopmental disorders *1*, 150-157.

Soorya, L., Kolevzon, A., Zweifach, J., Lim, T., Dobry, Y., Schwartz, L., Frank, Y., Wang, A.T., Cai, G., Parkhomenko, E., Halpern, D., Grodberg, D., Angarita, B., Willner, J.P., Yang, A., Canitano, R., Chaplin, W., Betancur, C., and Buxbaum, J.D. (2013). Prospective investigation of autism and genotype-phenotype correlations in 22q13 deletion syndrome and SHANK3 deficiency. Mol Autism *4*, 18.

Speed, H.E., Kouser, M., Xuan, Z., Reimers, J.M., Ochoa, C.F., Gupta, N., Liu, S., and Powell, C.M. (2015). Autism-associated insertion mutation (InsG) of Shank3 exon 21 causes impaired synaptic transmission and behavioral deficits. . J Neurosci (In Review).

Tabuchi, K., Blundell, J., Etherton, M.R., Hammer, R.E., Liu, X., Powell, C.M., and Sudhof, T.C. (2007). A neuroligin-3 mutation implicated in autism increases inhibitory synaptic transmission in mice. Science *318*, 71-76.

Taniai, H., Nishiyama, T., Miyachi, T., Imaeda, M., and Sumi, S. (2008). Genetic influences on the broad spectrum of autism: study of proband-ascertained twins. Am J Med Genet B Neuropsychiatr Genet *147B,* 844-849.

Thurm, A., and Swedo, S.E. (2012). The importance of autism research. Dialogues in clinical neuroscience *14*, 219-222.

Toro, R., Konyukh, M., Delorme, R., Leblond, C., Chaste, P., Fauchereau, F., Coleman, M., Leboyer, M., Gillberg, C., and Bourgeron, T. (2010). Key role for gene dosage and synaptic homeostasis in autism spectrum disorders. Trends in genetics : TIG *26*, 363-372.

Tu, J.C., Xiao, B., Naisbitt, S., Yuan, J.P., Petralia, R.S., Brakeman, P., Doan, A., Aakalu, V.K., Lanahan, A.A., Sheng, M., and Worley, P.F. (1999). Coupling of mGluR/Homer and PSD-95 complexes by the Shank family of postsynaptic density proteins. Neuron *23*, 583-592.

Uchino, S., Wada, H., Honda, S., Nakamura, Y., Ondo, Y., Uchiyama, T., Tsutsumi, M., Suzuki, E., Hirasawa, T., and Kohsaka, S. (2006). Direct interaction of post-synaptic density-95/Dlg/ZO-1 domain-containing synaptic molecule Shank3 with GluR1 alpha-amino-3-hydroxy-5-methyl-4-isoxazole propionic acid receptor. Journal of neurochemistry *97,* 1203-1214.

Uchino, S., and Waga, C. (2013). SHANK3 as an autism spectrum disorder-associated gene. Brain Dev *35,* 106-110.

Verhoeven, W.M., Egger, J.I., Willemsen, M.H., de Leijer, G.J., and Kleefstra, T. (2012). Phelan-McDermid syndrome in two adult brothers: atypical bipolar

disorder as its psychopathological phenotype? Neuropsychiatric disease and treatment *8*, 175-179.

Verpelli, C., Dvoretskova, E., Vicidomini, C., Rossi, F., Chiappalone, M., Schoen, M., Di Stefano, B., Mantegazza, R., Broccoli, V., Bockers, T.M., Dityatev, A., and Sala, C. (2011). Importance of Shank3 protein in regulating metabotropic glutamate receptor 5 (mGluR5) expression and signaling at synapses. J Biol Chem *286*, 34839-34850.

Verpelli, C., Schmeisser, M.J., Sala, C., and Boeckers, T.M. (2012). Scaffold proteins at the postsynaptic density. Adv Exp Med Biol *970*, 29-61.

Waga, C., Okamoto, N., Ondo, Y., Fukumura-Kato, R., Goto, Y., Kohsaka, S., and Uchino, S. (2011). Novel variants of the SHANK3 gene in Japanese autistic patients with severe delayed speech development. Psychiatr Genet *21*, 208-211.

Wallenstein, G.V., Eichenbaum, H., and Hasselmo, M.E. (1998). The hippocampus as an associator of discontiguous events. Trends Neurosci *21*, 317-323.

Wang, X., McCoy, P., Rodriguiz, R.M., Pan, Y., Je, H.S., Roberts, A., Kim, C., Berrios, J., Colvin, J.S., Bousquet-Moore, D., Lorenzo, I., Wu, G., Weinberg, R.J., Ehlers, M.D., Philpot, B.D., Beaudet, A.L., Wetsel, W.C., and Jiang, Y.H. (2011a). Synaptic dysfunction and abnormal behaviors in mice lacking major isoforms of Shank3. Human molecular genetics.

Wang, X., McCoy, P.A., Rodriguiz, R.M., Pan, Y., Je, H.S., Roberts, A.C., Kim, C.J., Berrios, J., Colvin, J.S., Bousquet-Moore, D., Lorenzo, I., Wu, G., Weinberg,

R.J., Ehlers, M.D., Philpot, B.D., Beaudet, A.L., Wetsel, W.C., and Jiang, Y.H. (2011b). Synaptic dysfunction and abnormal behaviors in mice lacking major isoforms of Shank3. Human molecular genetics *20*, 3093-3108.

Werner, E., Dawson, G., Osterling, J., and Dinno, N. (2000). Brief report: Recognition of autism spectrum disorder before one year of age: a retrospective study based on home videotapes. Journal of autism and developmental disorders *30*, 157-162.

White, S.W., Ollendick, T., Scahill, L., Oswald, D., and Albano, A.M. (2009a). Preliminary efficacy of a cognitive-behavioral treatment program for anxious youth with autism spectrum disorders. Journal of autism and developmental disorders *39*, 1652-1662.

White, S.W., Oswald, D., Ollendick, T., and Scahill, L. (2009b). Anxiety in children and adolescents with autism spectrum disorders. Clinical psychology review *29*, 216-229.

Williams, C.A., Dagli, A., and Battaglia, A. (2008). Genetic disorders associated with macrocephaly. Am J Med Genet A *146A*, 2023-2037.

Wilson, H.L., Crolla, J.A., Walker, D., Artifoni, L., Dallapiccola, B., Takano, T., Vasudevan, P., Huang, S., Maloney, V., Yobb, T., Quarrell, O., and McDermid, H.E. (2008). Interstitial 22q13 deletions: genes other than SHANK3 have major effects on cognitive and language development. Eur J Hum Genet *16*, 1301-1310.

Wilson, H.L., Wong, A.C., Shaw, S.R., Tse, W.Y., Stapleton, G.A., Phelan, M.C., Hu, S., Marshall, J., and McDermid, H.E. (2003). Molecular characterisation of the 22q13 deletion syndrome supports the role of haploinsufficiency of SHANK3/PROSAP2 in the major neurological symptoms. J Med Genet *40*, 575-584.

Wingate M, M.B., Kirby RS, Pettygrove S, Cunniff C, Meaney F, Schulz E, Miller L, Robinson C, Quintana G, Kaiser MY, Lee LC, Landa R, Newschaffer C, Constantino J, Fitzgerald R, Zahorodny W, Daniels J, Giarelli E, Pinto-Martin J, Levy SE, Nicholas J, Charles J, Zimmerman J, Maenner MJ, Durkin M, Rice C, Baio J, Van Naarden Braun K, Phillips K, Doernberg N, Yeargin-Allsopp M. (2012). Prevalence of autism spectrum disorders--Autism and Developmental Disabilities Monitoring Network, 14 sites, United States, 2008. MMWR Surveill Summ *61*, 1-19.

Wisessathorn, M., Chanuantong, T., and Fisher, E.B. (2013). The impact of child's severity on quality-of-life among parents of children with autism spectrum disorder: the mediating role of optimism. Journal of the Medical Association of Thailand = Chotmaihet thangphaet *96*, 1313-1318.

Won, H., Lee, H.R., Gee, H.Y., Mah, W., Kim, J.I., Lee, J., Ha, S., Chung, C., Jung, E.S., Cho, Y.S., Park, S.G., Lee, J.S., Lee, K., Kim, D., Bae, Y.C., Kaang, B.K., Lee, M.G., and Kim, E. (2012). Autistic-like social behaviour in Shank2-mutant mice improved by restoring NMDA receptor function. Nature *486*, 261-265.

Yang, M., Bozdagi, O., Scattoni, M.L., Wohr, M., Roullet, F.I., Katz, A.M., Abrams, D.N., Kalikhman, D., Simon, H., Woldeyohannes, L., Zhang, J.Y., Harris, M.J., Saxena, R., Silverman, J.L., Buxbaum, J.D., and Crawley, J.N. (2012). Reduced excitatory neurotransmission and mild autism-relevant phenotypes in adolescent Shank3 null mutant mice. The Journal of neuroscience : the official journal of the Society for Neuroscience *32*, 6525-6541.

Zhu, L., Wang, X., Li, X.L., Towers, A., Cao, X., Wang, P., Bowman, R., Yang, H., Goldstein, J., Li, Y.J., and Jiang, Y.H. (2014). Epigenetic dysregulation of SHANK3 in brain tissues from individuals with autism spectrum disorders. Human molecular genetics *23*, 1563-1578.

Zucker, R.S., and Regehr, W.G. (2002). Short-term synaptic plasticity. Annual review of physiology *64*, 355-405.